

Université de Montréal

**Mutagenèse semi-aléatoire et analyse dynamique de la  
β-lactamase TEM-1 de *Escherichia coli***

par  
Nicolas Doucet

Département de biochimie  
Faculté de médecine

Thèse présentée à la Faculté des études supérieures  
en vue de l'obtention du grade de *Philosophiae Doctor*  
en biochimie

Décembre, 2006

© Nicolas Doucet, 2006

Université de Montréal  
Faculté des études supérieures

Cette thèse intitulée :

Mutagenèse semi-aléatoire et analyse dynamique de la  $\beta$ -lactamase TEM-1 de *Escherichia coli*

présentée par :  
Nicolas Doucet

a été évaluée par un jury composé des personnes suivantes :

Dr James G. Omichinski, président-rapporteur  
Dr Joelle N. Pelletier, directrice de recherche  
Dr Robert Lortie, membre du jury  
Dr Patrick Lagüe, examinateur externe  
Dr Roland Brousseau, représentant du doyen

## Résumé

La  $\beta$ -lactamase TEM-1 de *Escherichia coli* est le principal représentant des  $\beta$ -lactamases de classe A, une famille d'enzymes responsables du plus important mécanisme de défense utilisé par les bactéries pour hydrolyser les antibiotiques à noyau  $\beta$ -lactame. En se basant sur des études préliminaires ayant suggéré son importance dans la reconnaissance des substrats, nous avons entrepris une analyse détaillée du résidu du site actif Tyr105 à l'aide de techniques de mutagenèse dirigée par saturation, de cinétique enzymatique, de modélisation moléculaire et de RMN des protéines dans le but de déterminer son rôle au niveau de la discrimination et de la stabilisation des ligands chez TEM-1. Nos résultats suggèrent que ce résidu adopte deux rotamères énergétiquement favorables au site actif de TEM-1 et que son comportement dynamique sur diverses échelles de temps influence la discrimination des ligands. De surcroît, une analyse de divers mutants de Tyr105 par RMN multidimensionnelle démontre l'existence d'effets à courte et à longue portée dont la magnitude est corrélée de manière négative avec l'efficacité catalytique de chaque variant enzymatique. Par ailleurs, des expériences de relaxation RMN entreprises sur le mutant Y105D révèlent une altération significative des motions moléculaires de certains résidus du site actif sur une échelle de temps correspondant à celle de la catalyse, offrant ainsi une explication quant à la diminution d'affinité observée chez ce mutant. Globalement, nos résultats démontrent que l'effet dynamique causé par le remplacement de ce résidu du site actif ne se limite pas à son environnement immédiat et suggèrent l'existence d'un réseau complexe de motions moléculaires liées à la catalyse parmi les résidus du site actif de TEM-1.

À titre de complément à ces travaux, une approche de mutagenèse semi-aléatoire fut appliquée à l'étude de divers résidus du site actif de cette enzyme dans le but d'étudier l'effet combinatoire de leur remplacement simultané sur la sélectivité des substrats. Nos résultats démontrent que la résistance au céfotaxime acquise chez certains variants s'effectue aux dépens de l'activité sur les substrats pénicillines et n'a que peu d'effet sur les

céphalosporines classiques. Ces études contribuent à la compréhension de la spécificité de reconnaissance chez les  $\beta$ -lactamases de classe A et fournissent des indices quant à la prédiction de mutations futures responsables de l'émergence de résistances aux antibiotiques chez de multiples organismes pathogènes.

**Mots-clés :** résistance aux antibiotiques, catalyse enzymatique, mutagenèse, modélisation moléculaire, recuit simulé, résonance magnétique nucléaire, évolution dirigée, analyse structure-fonction, structure des protéines, cinétique enzymatique

## Abstract

TEM-1 is the prevalent member of class A  $\beta$ -lactamases, a family of enzymes responsible for the primary defensive measure used by bacteria to hydrolyse the clinically-relevant  $\beta$ -lactam antibiotics. Based on previous reports suggesting its importance in substrate recognition, we have performed a detailed structural and functional analysis of the active-site residue Tyr105 using a combination of site-saturation mutagenesis, enzyme kinetics, molecular modelling and protein NMR experiments in order to decipher its precise role in enzyme catalysis as well as in ligand discrimination and stabilization in TEM-1. In addition to showing that this residue is directly implicated in substrate recognition, our results suggest that it can also adopt two energetically-favoured rotameric conformations in the active-site of this enzyme and that its dynamical behaviour on various time scales may influence ligand discrimination. In addition, our investigation of a variety of Tyr105 mutants by protein NMR demonstrates the existence of a number of short- and long-range effects with a magnitude inversely correlated with the catalytic efficiencies of each enzymatic variant. NMR relaxation experiments performed on the Y105D mutant reveal that it also displays significantly altered motions of various active-site residues on the time scale of catalysis, which may account for its observed decrease in affinity. Overall, our results demonstrate that the effects of mutation at this active-site position are not confined to its local environment and imply the existence of an intricate network of functionally-relevant molecular motions among active-site residues in TEM-1  $\beta$ -lactamase.

In an extension of this work, a semi-random mutagenesis approach was conducted on a number of active-site residues of this enzyme in order to investigate the combinatorial effects of their simultaneous replacement on substrate selectivity. Upon antibiotic selection with the oxyiminocephalosporin cefotaxime, our results yielded multiple variants that conferred high cephalosporin but decreased penicillin hydrolysis. Overall, our work contributes to the better understanding of substrate specificity in class A  $\beta$ -lactamases and

provides information regarding future mutations responsible for the emergence of antibiotic resistance in several infectious agents.

**Keywords :** antibiotic resistance, enzyme catalysis, mutagenesis, molecular modelling, simulated annealing, nuclear magnetic resonance, directed evolution, structure-function relationship, protein structure, enzyme kinetics

## Table des matières

Résumé .....	iii
Abstract .....	v
Table des matières .....	vii
Liste des tableaux .....	x
Liste des figures .....	xii
Liste des abréviations .....	xv
Remerciements .....	xx
Préface au chapitre 1 .....	1
<b>CHAPITRE 1 – Introduction .....</b>	<b>2</b>
1.0 – La problématique des résistances bactériennes aux antibiotiques .....	4
1.1 – Les classes d’antibiotiques et les mécanismes de résistance .....	6
1.2 – Les antibiotiques à noyau $\beta$ -lactame .....	7
1.2.1 – Mode d’action .....	9
1.3 – Les $\beta$ -lactamases .....	11
1.3.1 – TEM-1 et les enzymes de classe A .....	12
1.3.2 – Structure moléculaire .....	13
1.3.3 – Mécanisme catalytique et controverse entourant l’étape d’acylation .....	14
1.3.4 – Topologie du site actif et motifs conservés .....	16
1.3.5 – Les $\beta$ -lactamases ESBL et IRT .....	18
1.3.6 – Spécificité de reconnaissance .....	20
1.4 – Objectifs du projet de recherche et justification des méthodes employées .....	21
1.4.1 – Biologie moléculaire et cinétique enzymatique .....	23
1.4.2 – Modélisation <i>in silico</i> par dynamique moléculaire .....	24
1.4.3 – Modélisation <i>in silico</i> par recuit simulé .....	25
1.4.4 – Résonance magnétique nucléaire (RMN) .....	27

1.4.5 – Mutagenèse semi-aléatoire du site actif de TEM-1.....	28
FIGURES .....	30
Préface au chapitre 2 .....	37
<b>CHAPITRE 2.....</b>	39
Mutagenèse par saturation à la position 105 de la $\beta$ -lactamase TEM-1 : Importance de la tyrosine dans la stabilisation et la discrimination des substrats .....	39
<b>2.1 Article 1.</b> <i>Site-saturation mutagenesis of Tyr-105 reveals its importance in substrate stabilization and discrimination in TEM-1 <math>\beta</math>-lactamase.....</i>	39
Préface au chapitre 3 .....	76
<b>CHAPITRE 3.....</b>	78
Exploration par recuit simulé d'une tyrosine au site actif de la $\beta$ -lactamase TEM-1 : Existence potentielle de conformères alternatifs.....	78
<b>3.1 Article 2.</b> <i>Simulated annealing exploration of an active-site tyrosine in TEM-1 <math>\beta</math>-lactamase suggests the existence of alternate conformations .....</i>	78
Préface au chapitre 4 .....	105
<b>CHAPITRE 4.....</b>	107
Analyse RMN de mutants Y105X de la $\beta$ -lactamase TEM-1 : Corrélation entre dynamique et fonction.....	107
<b>4.1 Article 3.</b> <i>NMR investigation of Tyr-105 mutants in TEM-1 <math>\beta</math>-lactamase: Dynamics are correlated with function.....</i>	107
Préface au chapitre 5 .....	149
<b>CHAPITRE 5.....</b>	151
Ingénierie enzymatique par mutagenèse semi-aléatoire : Combiner les avantages de l'évolution dirigée à ceux du design rationnel .....	151

<b>5.1 Article 4.</b> <i>Semi-rational approaches to engineering enzyme activity: Combining the benefits of directed evolution and rational design .....</i>	151
Préface au chapitre 6 .....	175
<b>CHAPITRE 6.....</b>	176
Analyse de la coopérativité au site actif de la $\beta$ -lactamase TEM-1 par mutagenèse combinatoire semi-aléatoire .....	176
<b>6.1 Article 5.</b> <i>Combinatorial active-site mutations in TEM-1 <math>\beta</math>-lactamase provide more generalized drug recognition.....</i>	176
<b>CHAPITRE 7 – Conclusions et perspectives .....</b>	213
7.0 – Conclusions générales.....	214
7.1 – Perspectives.....	216
7.1.1 – Inhibition et études cristallographiques .....	216
7.1.2 – Analyse <i>in silico</i> en présence de ligands.....	218
7.1.3 – Analyse RMN en présence de ligands .....	219
7.1.4 – Études dynamiques de $\beta$ -lactamases chimériques .....	220
FIGURE .....	224
Bibliographie.....	225
Annexe 1 – Numérotation de la $\beta$ -lactamase TEM-1 .....	238
Annexe 2 – Enzymologie : Détail des méthodes de régression employées .....	242
Annexe 3 – Survol de la RMN des protéines.....	247
Annexe 4 – Matériel supplémentaire (chapitres 3 et 4) .....	257
Annexe 5 – Réponse aux questions et commentaires des membres du jury .....	280

## Liste des tableaux

### CHAPITRE 2

<b>Table 2.1.</b> MICs of <i>E. coli</i> XL1-Blue cells expressing TEM-1 $\beta$ -lactamase with Tyr-105 replacements.....	69
<b>Table 2.2.</b> Sequence alignment of residues 103–107 for major representatives of Class-A $\beta$ -lactamase .....	70
<b>Table 2.3.</b> Kinetic parameters for wild-type TEM-1 $\beta$ -lactamase and Y105X mutant derivatives .....	71

### CHAPITRE 4

<b>Table 4.1.</b> Distribution of $^1\text{H}$ - $^{15}\text{N}$ backbone chemical shift differences ( $\Delta\delta_{\text{HN}}$ ) for residues affected by the Y105X mutation .....	138
<b>Table 4.2.</b> Backbone $^1\text{H}$ - $^{15}\text{N}$ chemical shift differences ( $\Delta\delta_{\text{HN}}$ ) between Y105X mutants and wild-type TEM-1 for selected active-site residues.....	140
<b>Table 4.3.</b> Average backbone relaxation and model-free parameters for wild-type TEM-1 and mutant Y105D .....	141
<b>Table 4.4.</b> Active-site wall and invariant residues displaying significant relaxation parameter variation between wild-type TEM-1 and mutant Y105D .....	142

### CHAPITRE 5

<b>Table 5.1.</b> Comparison of approaches for engineering enzyme activity .....	172
--	-----

### CHAPITRE 6

<b>Table 6.1.</b> Identification of TEM-1 $\beta$ -lactamase mutants selected on media containing 250 ng/mL CTX .....	207
---	-----

<b>Table 6.2.</b> Minimum inhibitory concentrations of <i>E. coli</i> XL1-Blue cells containing wild-type or mutant $\beta$ -lactamases.....	208
<b>Table 6.3.</b> Kinetic parameters for wild-type TEM-1 $\beta$ -lactamase and the combinatorial mutants .....	209
 <b>ANNEXES</b>	
<b>Table S3.1.</b> Residue geometry of Glu104, Tyr105, Met129 and Asn132 analyzed by MolProbity for each minimized simulated annealing conformer obtained in the present study .....	257
<b>Table S4.1.</b> R <sub>1</sub> , R <sub>2</sub> , and { <sup>1</sup> H}- <sup>15</sup> N NOE values for TEM-1 WT and the Y105D mutant at 600 MHz .....	263
<b>Table S4.2.</b> Model-free Parameters .....	270
<b>Table S4.3.</b> Residues displaying significant variation between wild-type TEM-1 and mutant Y105D .....	277
<b>Table A5.1.</b> Comparison of $\Delta\delta_{\text{HN}}$ relative to WT for mutants Y105N and Y105D .....	290

# Liste des figures

## CHAPITRE 1

<b>Figure 1.1.</b> Structure chimique de la benzylpénicilline et de la portion C-terminale des chaînes N-acétyleglucosamine des peptidoglycanes .....	30
<b>Figure 1.2.</b> Structure chimique des principales classes et composés antibiotiques à noyau $\beta$ -lactame.....	31
<b>Figure 1.3.</b> Structure moléculaire de la $\beta$ -lactamase TEM-1 de <i>Escherichia coli</i> .....	32
<b>Figure 1.4.</b> Représentation schématique du mécanisme catalytique de la $\beta$ -lactamase TEM-1 .....	33
<b>Figure 1.5.</b> Principaux résidus du site actif de la $\beta$ -lactamase TEM-1 .....	34
<b>Figure 1.6.</b> Échelle de temps de divers événements dynamiques internes des protéines....	35
<b>Figure 1.7.</b> Schéma théorique de l'espace conformationnel énergétique adopté par divers conformères d'une protéine.....	36

## CHAPITRE 2

<b>Figure 2.1.</b> Structures of $\beta$ -lactam antibiotics used in this study .....	72
<b>Figure 2.2.</b> Superimposition of residues 104–107 of 5 Class A $\beta$ -lactamases crystal structures .....	73
<b>Figure 2.3.</b> Superimpositions of snapshots from a 200-ps molecular dynamics simulation of various Y105X mutants of TEM-1, shown in stereo.....	74
<b>Figure 2.4.</b> Conformation of benzylpenicillin in the active site of wild-type TEM-1 and mutant Y105G at the end of a 200-ps dynamics trajectory.....	75

## CHAPITRE 3

<b>Figure 3.1.</b> Representation of Tyr105 rotamers in TEM-1 $\beta$ -lactamase .....	100
--	-----

<b>Figure 3.2.</b> Electron density surrounding residue Tyr105 in the apoenzyme structure of TEM-1 $\beta$ -lactamase (PDB coordinates 1BTL) .....	102
<b>Figure 3.3.</b> $\chi_1/\chi_2$ distribution of Tyr105 for the 260 1-ps simulated annealing snapshots generated in this study.....	103
 <b>CHAPITRE 4</b>	
<b>Figure 4.1.</b> Structural mapping of $^1\text{H}$ - $^{15}\text{N}$ backbone chemical shift differences ( $\Delta\delta_{\text{HN}}$ ) (Hz) calculated between wild-type TEM-1 and mutants a) Y105W, b) Y105G, c) Y105N and d) Y105D.....	143
<b>Figure 4.2.</b> Sequence mapping of $^1\text{H}$ - $^{15}\text{N}$ backbone chemical shift differences ( $\Delta\delta_{\text{HN}}$ ) (Hz) calculated between wild-type TEM-1 and mutants Y105W, Y105G, Y105N and Y105D .....	144
<b>Figure 4.3.</b> Solvent-accessible surface representation of the active-site walls in TEM-1 $\beta$ -lactamase .....	145
<b>Figure 4.4.</b> $R_1$ , $R_2$ and $\{^1\text{H}\}$ - $^{15}\text{N}$ NOE relaxation parameters and the model-free-calculated order ( $S^2$ ) and $R_{\text{ex}}$ parameters plotted on the sequence of TEM-1 $\beta$ -lactamase .....	146
<b>Figure 4.5.</b> Y105D/WT ratios for the relaxation parameters ( $R_1$ , $R_2$ , and $\{^1\text{H}\}$ - $^{15}\text{N}$ NOE) .....	147
 <b>CHAPITRE 5</b>	
<b>Figure 5.1.</b> Selection of the preferred experimental approach for enzyme engineering based on the availability of experimental tools and prior knowledge of structure and function .....	173
<b>Figure 5.2.</b> Residues in or near the enzyme active site that were targeted for semi-rational combinatorial mutagenesis.....	174
 <b>CHAPITRE 6</b>	
<b>Figure 6.1.</b> Structure of the $\beta$ -lactam antibiotics used in this study.....	211

**Figure 6.2.** Schematic representation of the active site of TEM-1  $\beta$ -lactamase ..... 212

## CHAPITRE 7

**Figure 7.1.** Représentation schématique de trois chimères de TEM-1 et PSE-4 actuellement à l'étude ..... 224

## ANNEXES

**Figure A3.1.** Spectroscopie RMN multidimensionnelle ..... 255

**Figure A3.2.** Représentation schématique de la corrélation entre les noyaux atomiques de trois spectres RMN tridimensionnels ..... 256

**Figure S4.1.** Main area of the 2D  $^1\text{H}$ - $^{15}\text{N}$  HSQC spectra of TEM-1 Y105X at pH 6.6, and 30°C ..... 262

**Figure 4.2 (Alternate Version).** Sequence mapping of  $^1\text{H}$ - $^{15}\text{N}$  backbone chemical shift differences ( $\Delta\delta_{\text{HN}}$ ) (Hz) calculated between wild-type TEM-1 and mutants Y105W, Y105G, Y105N and Y105D ..... 293

## Liste des abréviations

A	<i>Alanine</i>
Å	<i>Ångström (10<sup>-10</sup> mètre)</i>
Ala	<i>Alanine</i>
AMP	<i>Ampicilline</i>
Arg	<i>Arginine</i>
Asn	<i>Asparagine</i>
Asp	<i>Acide aspartique (Aspartate)</i>
bp	<i>Base Pair (Paire de base)</i>
BZ	<i>Benzylpénicilline (Pénicilline G)</i>
C	<i>Cystéine</i>
<sup>13</sup> C	<i>Carbone-13</i>
CAZ	<i>Ceftazidime</i>
CF	<i>Céphalothine</i>
CTX	<i>Céfotaxime</i>
CVFF	<i>Constant Valence Force Field</i>
CZ	<i>Céfazoline</i>
Chl	<i>Chloramphénicol</i>
Cys	<i>Cystéine</i>
D	<i>Acide aspartique (Aspartate)</i>
δ	<i>Déplacement chimique</i>
Δδ	<i>Variation du déplacement chimique</i>
D <sub>  </sub> /D <sub>⊥</sub>	<i>Anisotropie axiale</i>
Da	<i>Dalton (1 g/mol)</i>
DD	<i>D-Ala-D-Ala</i>
DM	<i>Dynamique moléculaire (in silico)</i>
DNA	<i>Acide désoxyribonucléique (ADN)</i>

E	<i>Acide glutamique (Glutamate)</i>
$\epsilon$	<i>Coefficient d'extinction molaire</i>
E.C.	<i>Enzyme Commission Number (numéro de classification des enzymes)</i>
<i>E. coli</i>	<i>Escherichia coli</i>
epPCR	<i>Error-prone PCR</i>
ESBL	<i>Extented-Spectrum <math>\beta</math>-Lactamase (<math>\beta</math>-Lactamase à large spectre de reconnaissance)</i>
F	<i>Phénylalanine</i>
FACS	<i>Fluorescence-Activated Cell Sorting</i>
fs	<i>Femtoseconde (<math>10^{-15}</math> s)</i>
G	<i>Glycine</i>
Glu	<i>Acide glutamique (Glutamate)</i>
Gln	<i>Glutamine</i>
Gly	<i>Glycine</i>
H	<i>Histidine</i>
$^1\text{H}$	<i>Proton (atome d'hydrogène)</i>
His	<i>Histidine</i>
HSQC	<i>Heteronuclear Single Quantum Correlation (Spectre <math>^1\text{H}</math>-<math>^{15}\text{N}</math> à deux dimensions)</i>
Hz	<i>Hertz</i>
I	<i>Isoleucine</i>
Ile	<i>Isoleucine</i>
IPTG	<i>Isopropyl 1-thio-<math>\beta</math>-D-galactopyranoside</i>
IRT	<i>Inhibitor-Resistant TEM (<math>\beta</math>-lactamase) (<math>\beta</math>-Lactamase résistante à l'action des inhibiteurs)</i>
K	<i>Lysine</i>
Kan	<i>Kanamycine</i>
L	<i>Leucine</i>

LB	<i>Luria-Bertani</i>
LC/MS/ESI	<i>Liquid Chromatography-Mass Spectrometry-Electro-Spray Ionisation</i>
Leu	<i>Leucine</i>
Lys	<i>Lysine</i>
M	<i>Méthionine</i>
Met	<i>Méthionine</i>
MIC	<i>Minimum Inhibitory Concentration (Concentration minimale inhibitrice)</i>
mM	<i>Millimolaire</i>
µs	<i>Microseconde (<math>10^{-6}</math> s)</i>
ms	<i>Milliseconde (<math>10^{-3}</math> s)</i>
N	<i>Asparagine</i>
<sup>15</sup> N	<i>Azote-15</i>
nm	<i>Nanomètre</i>
NOE	<i>Nuclear Overhauser Effect</i>
ns	<i>Nanoseconde (<math>10^{-9}</math> s)</i>
OXA	<i><math>\beta</math>-lactamases « Oxacillin-resistant » de <i>Pseudomonas aeruginosa</i></i>
P	<i>Proline</i>
PBP	<i>Penicillin Binding Proteins (synonyme de D-Ala-D-Ala transpeptidase)</i>
PCR	<i>Polymerase Chain Reaction (Réaction de polymérisation en chaîne)</i>
PDA	<i>Protein Design Automation</i>
PDB	<i>Protein Data Bank</i>
Phe	<i>Phénylalanine</i>
Pro	<i>Proline</i>
ps	<i>Picoseconde (<math>10^{-12}</math> s)</i>
Q	<i>Glutamine</i>
R	<i>Arginine</i>
R <sub>1</sub>	<i>Relaxation longitudinale</i>
R <sub>2</sub>	<i>Relaxation transversale</i>

$R_{ex}$	<i>Paramètre d'échange conformationnel (motions <math>\mu s-ms</math>)</i>
RMN	<i>Résonance magnétique nucléaire</i>
RMSD	<i>Root Mean Square Deviation</i>
S	<i>Sérine</i>
$S^2$	<i>Paramètre d'ordre (motions <math>ps-ns</math>)</i>
SDS-PAGE	<i>Électrophorèse sur gel de polyacrylamide en présence de dodécylsulfate de sodium</i>
Ser	<i>Sérine</i>
SHV	<i><math>\beta</math>-lactamases « Sulphydryl Variable » retrouvées chez Klebsiella pneumoniae et Escherichia coli</i>
T	<i>Thréonine</i>
$\tau_e$	<i>Temps de corrélation des motions internes</i>
$\tau_m$	<i>Temps de corrélation global</i>
TEM-1	<i><math>\beta</math>-lactamase TEM-1 de Escherichia coli</i>
Thr	<i>Thréonine</i>
Tris	<i>Tris(hydroxyméthyl)méthane</i>
Trp	<i>Tryptophane</i>
Tyr	<i>Tyrosine</i>
UV	<i>Ultraviolet</i>
V	<i>Valine</i>
Val	<i>Valine</i>
W	<i>Tryptophane</i>
Xaa	<i>Acide aminé</i>
Y	<i>Tyrosine</i>

*Seuls l'art et la science élèvent l'Homme jusqu'à la divinité.*

*– Ludwig van Beethoven*

## Remerciements

Plus qu'un simple cheminement académique, les années passées aux cycles supérieurs à l'Université de Montréal auront été parmi les plus belles de ma vie et je ne saurais passer sous silence l'importante contribution de plusieurs individus dans ce cheminement personnel et professionnel.

J'aimerais en premier lieu offrir toute ma gratitude et mon énorme appréciation à ma directrice de recherche, Joelle Pelletier, sans qui rien de tout cela n'aurait été accompli. Joelle, je garderai pour toujours des souvenirs exemplaires de ton exceptionnelle supervision, de tes constants encouragements, de ton incroyable capacité à corriger un manuscrit en quelques jours (!), de ta disponibilité quasi infinie et de ta grande ouverture d'esprit m'ayant notamment permis de « faire-autre-chose-que-juste-de-la-biomol ! ». Merci de nous avoir permis d'expérimenter avec le « *dry lab* » et de nous avoir ouvert les portes des congrès internationaux, sans lesquels l'ampleur du projet et les collaborations n'auraient pas été ce qu'elles furent. Ensemble, j'ose croire que nous aurons fait un bon bout de chemin depuis ce fameux jour de février 2000, où tu m'as montré pour la première fois ton lugubre « labo » tout poussiéreux qui tombait pratiquement en ruines... Merci sincèrement pour tout Joelle, ce fut un plaisir et un honneur.

En second lieu, j'aimerais offrir mon appréciation personnelle aux comparses avec lesquels nous aurons su créer un vocabulaire, un mode de vie et même un univers personnel : Roberto Chica (*la route des CD/DVD, les nombreuses rencontres à Boston et San Diego*), Jordan Volpato (*l'artisan de notre carrière cinématographique et le rassembleur de tout ce beau monde...*), Pierre-Yves De Wals (*le seul bon stagiaire... ☺*) et Félix Doyon (*le chialeux de la gang !*). En plus des nombreuses discussions scientifiques ayant fait partie intégrante de notre cheminement commun, je n'oublierai jamais notre amitié et notre complicité ayant donné lieu à tant d'événements à la fois grandioses et loufoques. Merci aussi aux autres membres du laboratoire ainsi qu'à tous ceux ayant

contribué à la création du mythe de l'aile F-500, qu'ils soient encore présents ou qu'ils soient venus et repartis au fil des ans. En ordre chronologique approximatif : Jeff Keillor (*I'll always remember meeting you for the first time with that HUGE hockey bag in your office! I hope to see you again in the future, whether in Montréal or in Edinburgh! Your only mistake was to introduce me to Joelle... ☺*), Jean-François St-Amant (*la muse*), Jean-Louis Cabral (*les insolences du téléphone et le manque de classe*), Andreea Schmitzer (*les bons souvenirs du début*), la vieille gang de chez Michnick (Jof, Duracell, Dimitri, Martin, André, FX, Alexis), Roselyne Castonguay (*enzymologue devant l'éternel...*), Christian Lherbet, Stéphane Girouard (*les BBQ à Longueuil*), Michael Shirm (*Comment va ton travail monsieur ?*), Carl Hémond, Georgios Lappas (*Lappas has one foot in the door!*), Patrick Sénéchal (*l'explosion dans le E-800*), Nicolas Lahaie (*Ah, pour de vrai ? C'est pas sérieux, sauf !*), Marie-Ève Beaudoin (*le lavage des vitres à la moppe*), Audrey Tousignant (*Sainte-Julie !!!*), Dany Halim (*Halawa !*), Steve Gillet (*Sting man !*), Farah-Jade Dryburgh, Tan Wang (*Usually, dosen't work, you know?*), Audrey Nisole, Christophe Pardin, Natalhie Campos-Reales, Nicolas Chabot, Elena Fosatti (*Bah !*), Jessica Laroche (*les rires et les tours de char*), Lucie Poulin (*Oh yeah Lucie ! Merci pour la révision, Lucie ! Longue vie à Raphaël !*), Krista Morley, Jonathan Blanchet (*la relève*), Valerio Vinci et Alieh Kazemeini. Merci aussi aux biochimistes qui nous croient chimistes et aux chimistes qui nous croient biochimistes, car sans vous la biologie structurale et l'ingénierie enzymatique n'existeraient pas...

Une partie importante des travaux de cette thèse n'auraient pu voir le jour sans l'apport extraordinaire de nos collaborateurs scientifiques, que je remercie sincèrement pour leur fidèle intérêt. Un merci particulier à Stéphane M. Gagné (Université Laval, Québec) pour m'avoir si gentiment accueilli dans son laboratoire et pour avoir plongé sans hésitation dans l'étude RMN de nos mutants. Je remercie également Pierre-Yves Savard pour son aide extraordinaire en RMN et sa complicité dévouée dans ce qui fut notre projet commun pour plus de deux ans (*« Solide » PY ! On en déménagera tant que tu voudras des laveuses ! ☺ Longue vie à Raphaëlle !*). Merci aussi à Olivier Fisette pour ses précieux

conseils Linux et à Sébastien Morin pour son intérêt grandissant dans le projet des chimères. I'd also like to extend my thanks to Michelle M. Meyer (currently at Yale University, New Haven, Connecticut) and Frances H. Arnold (California Institute of Technology, Pasadena, California) for sharing their  $\beta$ -lactamase chimeras with us and for stimulating helpful discussions regarding our current collaboration.

Par ailleurs, je ne saurais passer sous silence l'important support moral et psychologique offert par tous mes amis et les membres de ma famille à travers ces années. À leur façon, ils auront tous participé de près ou de loin à mon développement personnel ainsi qu'à mon cheminement scientifique. Je tiens particulièrement à remercier mon père, André Doucet, ainsi que sa conjointe, Denise Proteau, pour leur appui et leur support inconditionnel à bien des niveaux. Finalement, pour la fine lueur dans ses yeux, son sourire et son émerveillement infini face aux petits détails de la vie, je tiens également à remercier affectueusement ma copine Nadia, qui aura fait tout ce bout de chemin avec moi et qui aura toujours su allumer chez moi cette petite flamme qui rend son émerveillement contagieux. Le bonheur que tu me procures m'est immensément précieux.

Cette thèse est dédiée à la mémoire de ma mère, Jocelyne Saucier (1944-1980), qui m'aura transmis bien malgré elle cet amour des études et des sciences...

## Préface au chapitre 1

L'objectif de la présente thèse fut d'entreprendre une étude moléculaire détaillée entre la structure et la fonction de divers mutants d'une enzyme de résistance bactérienne aux antibiotiques, la  $\beta$ -lactamase TEM-1 de *Escherichia coli*, et certains substrats à noyau  $\beta$ -lactame qu'elle inactive par hydrolyse. Sur la base de sa proximité des substrats au site actif, une attention particulière fut portée à l'étude mutationnelle et dynamique détaillée du résidu Tyr105 ainsi que sur celle de certains résidus de la cavité du site actif permettant l'apparition de  $\beta$ -lactamases à large spectre de reconnaissance (ESBL) (notamment Glu104, Gly238 et Glu240). Nous avons accompli ces analyses dans le but d'améliorer la compréhension que nous avons de la reconnaissance et de la discrimination de certains  $\beta$ -lactames par TEM-1 ainsi que pour explorer en plus de détails certains aspects du mécanisme catalytique de cette enzyme, qui demeure à ce jour controversé. Ainsi, l'objectif général de cette étude vise à fournir des indices quant à la prédiction de mutations futures responsables de l'émergence de résistances aux antibiotiques chez de multiples organismes pathogènes.

À titre d'introduction aux sections expérimentales exposées dans les chapitres subséquents, le présent chapitre propose une mise en contexte de la problématique des mécanismes de résistance bactérienne aux antibiotiques en mettant particulièrement l'emphase sur les  $\beta$ -lactamases de classe A, des enzymes inactivant les différentes classes d'antibiotiques à noyau  $\beta$ -lactame. En plus d'exposer brièvement la structure moléculaire de ces enzymes ainsi que leur mécanisme catalytique, une section est également consacrée à la description de l'état actuel des connaissances par rapport aux résidus du site actif responsables de la discrimination et de la stabilisation des ligands. Finalement, les différentes méthodes expérimentales utilisées tout au long de cette thèse sont également présentées à titre de complément.

# **CHAPITRE 1**

## **Introduction**

*“...experts agree that by year 2000, viral, and bacterial diseases will have been eliminated.”*

*– Time Magazine, 1966*

*“It is time to close the book on infectious diseases.”*

*– William H. Stewart, US Surgeon General, 1969*

*“Development of resistance is not a matter of if but only a matter of when.”*

*– Christopher Walsh, 2000*

## 1.0 – La problématique des résistances bactériennes aux antibiotiques

C'est en 1928, en examinant par accident un pétri contenant une culture lysée de *Staphylococcus aureus* contaminée avec une moisissure (*Penicillium chrysogenum*), que Alexander Fleming se rendit compte de la production par ce champignon d'une substance bactéricide qui allait dès lors révolutionner le monde de la médecine moderne [1]. Cette substance antibactérienne, la benzylpénicilline, qui sera synthétisée *de novo* et cristallisée dans les années 1940, sera le premier antibiotique naturel à être introduit dans le milieu clinique et servira de base à la révolution antibiotique de la deuxième moitié du vingtième siècle. Avec la benzylpénicilline comme figure de proue [2, 3], cet « âge d'or » de la découverte des antibiotiques (1940-1962) [4] donnera ainsi naissance à plusieurs générations subséquentes d'antibiotiques similaires, dont les effets bénéfiques sur la santé humaine se font encore ressentir de nos jours.

Si la mention de diverses classes d'antibiotiques ne fait que suggérer l'existence de cibles différentes et de modes d'action distincts, la simple suggestion de l'existence de « générations subséquentes » d'antibiotiques soulève néanmoins les interrogations fondamentales suivantes : pourquoi a-t-on besoin d'améliorer les antibiotiques déjà connus et comment se fait-il que nous soyons mis dans une situation nous obligeant à en découvrir de nouveaux ? L'unique réponse à ces deux questions se retrouve dans l'idée fondamentale de la théorie de l'évolution de Charles Darwin et s'explique par le principe de la sélection naturelle. Ainsi, une population bactérienne soumise à une pression sélective causée par l'introduction d'un bactéricide dans son environnement de croissance (dans ce cas-ci l'être humain) sera indubitablement affectée et la grande majorité de ses représentants sera éliminée. En revanche, sur les bases évolutives de l'apparition aléatoire de mutations définissant la diversité génétique d'une population, certaines cellules bactériennes possèderont des traits physiologiques qui s'avéreront avantageux dans cette situation

particulière et qui permettront leur survie en présence de cet antibiotique. Étant sélectionnées, ces cellules auront ainsi une meilleure chance de reproduction et transmettront ces traits génétiques à leur progéniture, qui possédera également la capacité de survivre en présence de ce même antibiotique. En raison de la pression sélective constante offerte par ce médicament, ces traits génétiques se transmettront désormais de génération en génération en tant que caractère essentiel à la survie cellulaire, jusqu'au point où l'antibiotique en question n'aura plus aucun effet sur la population bactérienne en entier.

Ce phénomène particulier donne lieu à ce que l'on nomme la résistance bactérienne aux antibiotiques, un problème sérieux et bien connu des milieux hospitaliers [5, 6]. En effet, du point de vue de l'être humain, cette résistance aux antibiotiques permet la recrudescence contemporaine d'infections bactériennes jusqu'alors traitées de manière efficace par divers antibiotiques. À titre d'exemple, alors que plus de 90 % des souches de *Staphylococcus aureus* étaient sensibles à la benzylpénicilline lors de son introduction clinique au début des années 1940, 50 % de ces souches étaient devenues résistantes à cet antibiotique au courant des années 1950, et plus de 90 % l'étaient dans les années 1990 [7, 8]. Ironiquement, bien que ce problème soit aujourd'hui d'une importance critique au niveau clinique, la résistance bactérienne aux antibiotiques demeure un phénomène connu depuis la découverte de la benzylpénicilline et son importance fut simplement négligée pendant de nombreuses années [9]. Or, au courant des années 1960 et 1970, la résurgence de nombreuses infections bactériennes couplée à la piètre performance antimicrobienne de nombreux antibiotiques dits « classiques » permit le développement de nouvelles classes d'antibiotiques ainsi que la modification chimique des molécules préexistantes [10].

## 1.1 – Les classes d’antibiotiques et les mécanismes de résistance

Il existe présentement sept classes majeures d’antibiotiques bactériens utilisés en milieu clinique : les  $\beta$ -lactames, les glycopeptides, les aminoglycosides, les tétracyclines, les macrolides, les quinolones et les sulfonamides [8]. Toutes ces classes de composés chimiques tirent profit de la différence physiologique intrinsèque existant entre les cellules procaryotes et eucaryotes en inhibant exclusivement des voies métaboliques essentielles à la survie et/ou à la reproduction de leurs cibles bactériennes, n’ayant que peu d’effets sur les cellules eucaryotes. Ainsi, les  $\beta$ -lactames et les glycopeptides sont impliquées dans l’inhibition de la synthèse de la paroi cellulaire bactérienne alors que les aminoglycosides, les tétracyclines et les macrolides se fixent au ribosome et inhibent la traduction [4, 11]. En revanche, les quinolones et les sulfonamides inhibent respectivement des enzymes essentielles à la réPLICATION de l’ADN et à la synthèse de la voie métabolique des folates [4, 11].

Puisque l’exposition à ces divers types d’antibiotiques donne lieu à de multiples conditions de sélection différentes, il n’est pas surprenant de constater l’émergence de mécanismes de résistance variés dont les cellules bactériennes tirent profit pour contrer l’action néfaste de ces molécules. La résistance bactérienne aux antibiotiques peut ainsi se manifester sous la forme de trois mécanismes généraux : 1) la modification des cibles moléculaires des antibiotiques [12] ; 2) la modification de la perméabilité cellulaire et/ou l’utilisation de pompes à efflux [13] ; et 3) la modification et/ou la dégradation enzymatique des antibiotiques [14]. En réponse à l’énorme utilisation clinique des trois principaux types d’antibiotiques dont la résistance apparaît *via* l’hydrolyse ou la modification covalente (les  $\beta$ -lactames, les macrolides et les fluoroquinolones) [15], cette dernière stratégie semble aujourd’hui être la plus efficace et la plus répandue chez les bactéries [16]. Ainsi, en tirant profit du transfert génétique par conjugaison, les bactéries acquièrent de multiples enzymes qui inactivent les antibiotiques avant qu’ils ne puissent

atteindre leur cible. Par exemple, *via* l'action de kinases et d'acétyletransférases, les aminoglycosides sont modifiés chimiquement par divers groupements acétyle ou phosphate, les rendant conséquemment trop volumineux pour permettre leur fixation appropriée au ribosome [14]. Ce transfert génétique d'enzymes de résistance entre cellules bactériennes, qui s'effectue majoritairement par conjugaison de plasmides et/ou de transposons [17], n'est pas exclusivement observé entre les membres d'une même souche, mais peut également se transmettre entre les membres de diverses espèces [18]. De surcroît, certains organismes (notamment les streptocoques), possèdent la capacité d'acquérir des éléments génétiques contenant des gènes de résistance entiers directement à partir de leur environnement de croissance [15].

Dès lors, la facilité déconcertante avec laquelle les bactéries acquièrent ces enzymes de résistance aux antibiotiques accentue l'ampleur du problème observé de nos jours en milieu clinique [19]. En soi, bien que la résistance aux antibiotiques soit un phénomène évolutif ancien observé depuis longtemps en laboratoire entre diverses souches bactériennes en compétition pour la même niche écologique [15], la perturbation de cet équilibre naturel par l'être humain au courant des 60 dernières années [20] force désormais ces organismes à lutter directement contre nous et pousse vers la découverte et le développement constants de nouvelles substances antibactériennes.

## 1.2 – Les antibiotiques à noyau $\beta$ -lactame

En raison de leur importance historique et de l'ajout de nombreuses modifications synthétiques à leur noyau de base, les antibiotiques à noyau  $\beta$ -lactame (aussi appelés  $\beta$ -lactamines) composent encore aujourd'hui environ 55 % de tous les antibiotiques prescrits en milieu clinique [15]. D'un point de vue chimique, la structure de ces molécules se rapproche grandement de la conformation rigide d'un tripeptide dont les groupements

fonctionnels possèdent la capacité d'effectuer l'acylation de divers nucléophiles (Figure 1.1) [15]. Ces molécules sont d'ailleurs considérées comme des mimes de peptides, sans quoi leur action bactéricide ne pourrait être accomplie. En effet, les propriétés chimiques et structurelles intrinsèques des composés  $\beta$ -lactames sont directement liées à leur action antibactérienne. Leur fonction est de mimer un motif peptidique retrouvé dans les parois cellulaires de ces organismes procaryotes dans le but de confondre une réaction d'acylation essentielle au maintien de l'homéostasie cellulaire (voir section 1.2.1).

La benzylpénicilline (historiquement appelée tout simplement pénicilline, ou pénicilline G) fut ainsi le premier représentant clinique de la grande famille des pénicillines. Ces molécules sont constituées d'un amide cyclique à quatre membres (le noyau  $\beta$ -lactame 2-azétidinone) couplé à un cycle thiazolidine à cinq membres (Figure 1.2). Développées entre 1940 et 1978 [21], ces antibiotiques se caractérisent par la présence d'un seul substituant sur le noyau  $\beta$ -lactame (la chaîne latérale R<sub>1</sub>), dont la modification synthétique donna notamment lieu à l'ampicilline (Figure 2.1) et à la méthicilline.

En raison de l'importance croissante de la résistance à ces antibiotiques *via* l'acquisition microbienne de  $\beta$ -lactamases (voir section 1.3), les pénicillines furent progressivement remplacées entre 1960 et 1978 par plusieurs générations de céphalosporines [21]. Très similaires aux pénicillines, ces composés se distinguent néanmoins par la présence d'un cycle dihydrothiazine à six membres, sur lequel peut se greffer un second substituant (la chaîne latérale R<sub>2</sub>, Figure 1.2). À l'instar des pénicillines, ces composés possédaient historiquement une plus grande efficacité à traverser la membrane cellulaire des bactéries gram-négatives et résistaient mieux à l'action de l'hydrolyse par les  $\beta$ -lactamases [21]. Or, tout comme les pénicillines quelques années auparavant, les céphalosporines devinrent rapidement obsolètes pour cause de résistance et durent être modifiés de manière synthétique pour améliorer leur effet antibactérien. Ces modifications donnèrent ainsi naissance à la vaste gamme de composés à noyau  $\beta$ -lactame que nous connaissons aujourd'hui. Entre 1978 et 1995, les chimistes organiciens ajoutèrent

notamment des groupements  $7\alpha$ -méthoxy au noyau  $\beta$ -lactame des céphalosporines (céphamycines) et à sa chaîne R<sub>1</sub> (oxyiminocéphalosporines), modifièrent l'atome de soufre du cycle dihydrothiazine par un oxygène (oxacéphèmes), ou encore changèrent l'atome de soufre du cycle thiazolidine des pénicillines par un atome de carbone (carbapénèmes) [21, 22] (Figure 1.2). En raison de leur action antibiotique améliorée, tous ces composés permirent de contourner légèrement la menace grandissante de l'apparition de nouvelles  $\beta$ -lactamases à large spectre de reconnaissance (voir section 1.3.5).

La découverte dans les années 1980 de nouveaux composés naturels synthétisés par certaines bactéries et mycètes (les monobactames) permit également l'allègement du fardeau de la résistance aux antibiotiques à noyau  $\beta$ -lactame [21]. En revanche, l'un des plus grands avancements des 30 dernières années fut la découverte du clavulanate, un composé naturel produit par *Streptomyces clavuligerus*, qui possède la capacité d'agir à titre d'inhibiteur des  $\beta$ -lactamases [23]. À défaut d'inhiber les D-Ala-D-Ala-transpeptidases comme tous les autres antibiotiques à noyau  $\beta$ -lactame (voir section 1.2.1), son administration en présence d'un antibiotique classique permet l'inactivation des  $\beta$ -lactamases et empêche ainsi l'hydrolyse de l'antibiotique classique. L'apparition de résistances bactériennes au clavulanate au début des années 1990 fut partiellement compensée par la modification chimique de ce composé, qui donna lieu à l'apparition clinique de deux de ses analogues semi-synthétiques : le sulbactame et le tazobactame (Figure 1.2), dont l'action inhibitrice demeure encore partiellement efficace aujourd'hui [17].

### 1.2.1 – Mode d'action

À l'exception des inhibiteurs de  $\beta$ -lactamases, le mécanisme d'action des antibiotiques à noyau  $\beta$ -lactame est similaire pour tous les membres de cette famille de

composés et demeure à ce jour relativement bien caractérisé [15, 24]. Pour accomplir son action, l'antibiotique à noyau  $\beta$ -lactame doit tout d'abord frayer son chemin à travers la membrane extracellulaire de sa cible bactérienne, qu'il traverse par diffusion à l'aide de canaux protéiques nommés « porines » (voir [24] pour un schéma). Toujours par diffusion, l'antibiotique traverse ensuite la couche de peptidoglycane de la membrane externe pour finalement se retrouver dans l'espace périplasmique de la cellule bactérienne. Située entre la membrane interne et la membrane externe, cette région contient un nombre important d'enzymes impliquées dans le maintien de l'homéostasie de la cellule bactérienne, parmi lesquelles se retrouvent la cible de choix des antibiotiques à noyau  $\beta$ -lactame : les D-Ala-D-Ala-transpeptidases (ou DD-transpeptidases) [15]. Étant impliquées au niveau de la dernière étape de l'assemblage des chaînes de peptidoglycane de la paroi cellulaire, ces enzymes sont responsables du clivage du terminus D-Ala-D-Ala d'une chaîne de peptidoglycane à base de *N*-acétylglucosamine (avec relâchement du D-Ala terminal lors de l'acylation, Figure 1.1) et du transfert de cette chaîne sur le groupement amine d'une autre chaîne *N*-acétylglucosamine de peptidoglycane avoisinante lors de la désacylation [15].

En raison de la très forte similarité entre le groupement D-Ala-D-Ala terminal des chaînes *N*-acétylglucosamine et la structure des antibiotiques à noyau  $\beta$ -lactame (Figure 1.1) [25], les DD-transpeptidases reconnaissent à tort ces antibiotiques en tant que substrats, permettant ainsi la formation d'un intermédiaire acyl-enzyme dont la demi-vie excède largement le temps de dédoublement de la cellule bactérienne [15]. Les antibiotiques à noyau  $\beta$ -lactame agissent donc à titre d'inhibiteurs suicides de ces enzymes et sont si efficaces que les DD-transpeptidases sont souvent tout simplement appelées « *Penicillin Binding Proteins* » (ou PBP). Cette réaction d'inhibition est donc à la base de l'action antibactérienne des antibiotiques à noyau  $\beta$ -lactame : l'inactivation des PBP empêche l'organisation appropriée des peptidoglycanes de la bactérie, ce qui mène à la formation d'anomalies dans l'assemblage des membranes cellulaires. Puisque la cellule bactérienne ne possède pas de mécanisme intrinsèque de contrôle de son osmolarité, elle se retrouve

conséquemment dans l'impossibilité de maintenir l'intégrité de ses parois cellulaires et ne peut donc pas se reproduire.

### 1.3 – Les $\beta$ -lactamases

Le mécanisme de résistance privilégié par les cellules bactériennes pour contrer l'action des antibiotiques à noyau  $\beta$ -lactame demeure à ce jour l'acquisition plasmidique d'enzymes de résistances qui modifient la structure de ces molécules, les rendant ainsi biologiquement inactives [26, 27]. Puisque l'intégrité chimique du noyau  $\beta$ -lactame est à la base de son activité antibactérienne, plusieurs enzymes de résistance ont ainsi évolué pour cliver le lien amide tendu et réactif de ces noyaux  $\beta$ -lactames [14]. Découvertes il y a plus de 60 ans [9], ces hydrolases d'amides cycliques (E.C. 3.5.2.6) forment une vaste famille d'enzymes à large spectre de reconnaissance appelées  $\beta$ -lactamases, dont les membres particuliers sont aussi connus sous le nom de leur cible antibiotique de choix (pénicillinase, céphalosporinase, carbénicillase, etc.). En raison de leur forte similarité structurelle avec les DD-transpeptidases, il est probable que les  $\beta$ -lactamases soient en fait des DD-transpeptidases ayant acquis la capacité de désacyler les antibiotiques à noyau  $\beta$ -lactame [15, 17].

Bien que de multiples systèmes de classification de ces enzymes aient été proposés, le plus répandu demeure à ce jour celui basé sur la classification originale de Ambler [28], dans laquelle les  $\beta$ -lactamases sont séparées en quatre classes (A, B, C et D) en fonction de leur homologie de séquence et de leur mécanisme catalytique. Il existe deux stratégies moléculaires principales utilisées par ces enzymes pour inactiver les antibiotiques à noyau  $\beta$ -lactame : les enzymes de classes A, C et D utilisent un résidu sérine agissant comme nucléophile au site actif [15, 27] alors que les enzymes de classe B sont des métallo- $\beta$ -lactamases qui activent une molécule d'eau *via* la coordination d'un cation divalent au site

actif (typiquement  $Zn^{2+}$ ) [29]. Les  $\beta$ -lactamases à sérine (particulièrement celles des classes A et C) demeurent aujourd’hui les plus répandues alors que les métallo- $\beta$ -lactamases furent longtemps considérées en tant que groupe marginal [27]. En revanche, la dissémination de ces enzymes semble avoir été accélérée au courant des 5 à 10 dernières années dans plusieurs pays, où 20 à 60 % des souches nosocomiales contiennent désormais divers types de métallo- $\beta$ -lactamases [30]. Ces statistiques sont particulièrement inquiétantes puisque la structure moléculaire des métallo- $\beta$ -lactamases est considérablement différente de celle des  $\beta$ -lactamases à sérine, rendant ces enzymes résistantes à presque tous les inhibiteurs des  $\beta$ -lactamases de classes A, C et D connus [30].

### 1.3.1 – TEM-1 et les enzymes de classe A

De loin les plus répandues et les mieux caractérisées, les  $\beta$ -lactamases de classe A possèdent une forte homologie structurelle entre elles. Encore aujourd’hui, ces enzymes sont à la base de la grande majorité des résistances aux composés  $\beta$ -lactames [16]. Synthétisées au cytoplasme de la cellule en tant que précurseurs, ces enzymes d’environ 29 kDa sont exportées au périplasme de la cellule, où elles exercent leur action hydrolytique sous forme mature suite au clivage de la séquence signal de localisation périplasmique [31, 32]. En plus d’être produites en des quantités pouvant excéder 65 000 molécules par cellule bactérienne [24], plusieurs  $\beta$ -lactamases de classe A sont reconnues pour être des enzymes extrêmement efficaces, permettant l’hydrolyse des antibiotiques à des vitesses se rapprochant de la limite de diffusion des molécules en solution [15, 27].

Isolée de *Escherichia coli* il y a plus de 40 ans à partir d’une patiente grecque nommée Temoniera [33, 34], la  $\beta$ -lactamase TEM-1 demeure à ce jour l’un des représentants les mieux caractérisés de cette classe d’enzymes et constitue le membre le plus communément retrouvé chez les bactéries Gram-négatives [17]. En plus des

nombreuses structures cristallines disponibles sous sa forme native [35-37] (dont une à très haute résolution [38]), il existe plusieurs structures de mutants de TEM-1 [35, 37, 39-43] ainsi que de divers complexes enzyme-substrat [44] et enzyme-inhibiteur [43, 45-51] de ce représentant classique des  $\beta$ -lactamases de classe A.

### 1.3.2 – Structure moléculaire

La  $\beta$ -lactamase TEM-1 est une enzyme monomérique globulaire de forme ellipsoïdale dont les dimensions moléculaires approximatives sont de 30 Å × 40 Å × 50 Å [36]. L’enzyme mature est constituée de 263 résidus acides aminés dont les éléments de structure secondaire forment deux domaines structuraux tertiaires (un domaine tout  $\alpha$  et un autre  $\alpha/\beta$ ) à l’interstice desquels se retrouve la crevasse formant le site actif (Figure 1.3). La numérotation séquentielle de la forme mature de TEM-1 (26 à 290) exclut les premiers acides aminés de la séquence de localisation périplasmique et ne contient pas de numéro correspondant aux positions 239 et 253 en raison de la nomenclature des  $\beta$ -lactamases de classe A utilisée depuis le début des années 1990 [52] (voir Annexe 1). Le premier domaine de l’enzyme ( $\alpha/\beta$ ) est constitué d’un feuillet  $\beta$  à cinq brins antiparallèles sur lequel sont empaquetées les hélices  $\alpha$ 1,  $\alpha$ 10 et  $\alpha$ 11 (Figure 1.3). Deux régions charnières (composées des résidus 60-68 et 212-222) relient le domaine  $\alpha/\beta$  au domaine tout  $\alpha$ , composé de huit hélices ( $\alpha$ 2 à  $\alpha$ 9) et situé de l’autre côté du feuillet  $\beta$  central [36].

### 1.3.3 – Mécanisme catalytique et controverse entourant l'étape d'acylation

Le mécanisme catalytique des  $\beta$ -lactamases de classe A demeure à ce jour un sujet de vive controverse en raison des multiples données mécanistiques contradictoires publiées à propos des nombreux résidus catalytiques impliqués dans la réaction. Les prémisses de cette réaction catalytique demeurent malgré tout bien caractérisées et se résument en un mécanisme d'acylation et de désacylation en deux étapes similaire à celui des protéases à sérine [53]. Initialement, le nucléophile de la réaction (Ser70) est déprotoné par une base générale lors de l'attaque nucléophilique de l'oxygène de Ser70 sur le carbonyle du noyau 2-azétidinone du substrat (Figure 1.4B ou C). Cette étape d'acylation mène à la formation d'un intermédiaire acyl-enzyme stable (Figure 1.4F) suite au transfert du proton de Ser130 à l'azote du noyau lactame lors de la décomposition de l'intermédiaire tétraédrique préalablement formé entre l'enzyme et le substrat (Figure 1.4D-F). Finalement, la désacylation de ce lien ester est accomplie *via* un mécanisme d'hydrolyse impliquant Glu166 et une molécule d'eau strictement conservée, ayant pour conséquence le relâchement du substrat hydrolysé (biologiquement inactif) et la régénération de l'enzyme libre (Figure 1.4F-E-G).

Bien que le rôle de Glu166 dans l'étape de désacylation de ce mécanisme catalytique soit généralement accepté [16, 54, 55], la nature de la base générale dans l'étape d'acylation demeure néanmoins nébuleuse. Cette controverse provient de multiples études démontrant que Glu166 [38, 56-61] ou Lys73 [44, 62-65] peuvent efficacement activer Ser70 lors de l'étape d'acylation, menant à de multiples confusions expérimentales et suggérant que ces deux résidus puissent agir de manière concomitante à titre de base générale pour déprotoner Ser70. En apparence contradictoires, les trois conclusions expérimentales suivantes renforcent néanmoins ce débat :

1) *Lys73 et Glu166 sont les deux seuls candidats pouvant agir à titre de base générale au site actif de TEM-1.* En effet, les mutants simples de Lys73 et de Glu166 affectent l'étape d'acylation de manière significative [54, 66-70] alors qu'un mutant double Lys73-Glu166 l'inactive presque entièrement [68]. Ces résultats suggèrent qu'aucun autre résidu du site actif de TEM-1 puisse agir à titre de base générale dans l'étape d'acylation.

2) *Dans l'enzyme libre à pH physiologique, Lys73 est protoné, empêchant ainsi ce résidu d'agir à titre de base générale.* Bien qu'il fut suggéré que l'environnement électrostatique du site actif de TEM-1 puisse réduire le  $pK_a$  de Lys73 pour lui permettre d'adopter sa forme active déprotonée [44, 65], des données expérimentales et théoriques suggèrent que Lys73 est bien protoné à pH physiologique [57, 71, 72], malgré que son  $pK_a$  semble être inférieur à celui des autres résidus lysine de l'enzyme ( $pK_a = 8.0-8.5$ ) [69].

3) *Glu166 n'est pas essentiel à l'étape d'acylation.* Malgré le fait que les mutants de Glu166 réduisent la vitesse d'acylation par un facteur de 2 à 3 ordres de grandeur [54, 68], des structures cristallines d'intermédiaires acyl-enzyme de mutants Glu166 inaptes à servir de base générale furent obtenues à maintes reprises [43-51], démontrant que l'acylation demeure possible en absence de Glu166.

Ces apparentes contradictions expérimentales furent néanmoins récemment réconciliées par une étude du mécanisme d'acylation de TEM-1 par modélisation QM/MM [73]. Dans cette étude, les auteurs démontrent que les deux mécanismes d'acylation de Lys73 et de Glu166 sont énergétiquement favorables, confirmant que ces deux résidus peuvent agir de manière concertée à titre de base générale. Dans le but de réconcilier les données expérimentales controversées décrites ci haut, les auteurs proposent un mécanisme de déprotonation de Lys73 via Ser70, Glu166 et une molécule d'eau strictement conservée (Figure 1.4A-B). En argumentant que la présence du substrat au site actif soit suffisante pour blinder du solvant la paire d'ions 'Glu166 protoné/Lys73 déprotoné', ils offrent ainsi une explication quant aux variations observées pour les différents  $pK_a$  calculés pour Lys73

chez l'enzyme libre. De plus, leur hypothèse unifie les nombreuses études de mutagenèse suggérant que Lys73 et Glu166 agissent tous les deux de manière concertée dans l'étape d'acylation du mécanisme catalytique (Figure 1.4, parcours A-B-D et C-D).

### 1.3.4 – Topologie du site actif et motifs conservés

Une analyse détaillée des séquences en acides aminés ainsi que des structures des  $\beta$ -lactamases de classe A permet de déceler plusieurs motifs structuraux et fonctionnels conservés dans l'environnement du site actif de ces enzymes. Ces motifs définissent plusieurs résidus de la cavité du site actif, qui ont une importance primordiale à la fois dans la reconnaissance et/ou dans la catalyse des substrats [16]. Bien que similaires chez toutes les  $\beta$ -lactamases à sérine, ces motifs possèdent néanmoins quelques différences entre les classes A, C et D et sont ici présentés pour TEM-1, et par extension pour les  $\beta$ -lactamases de classe A (Figure 1.5).

Le premier élément structurel d'importance des  $\beta$ -lactamases de classe A est composé de la portion  $3_{10}$  de l'hélice  $\alpha 2$ , qui se retrouve toujours sous la forme de la séquence primaire Ser70-Xaa-Xaa-Lys73 [16]. Cet élément structurel contient deux résidus catalytiques essentiels : Ser70, impliqué dans l'attaque nucléophile sur le carbone du carbonyle de l'anneau  $\beta$ -lactame des ligands [74]; et Lys73, formant un pont hydrogène avec Ser70 et jouant partiellement le rôle de base générale dans son activation (voir section 1.3.3) [73, 74].

Pratiquement invariable chez toutes les  $\beta$ -lactamases de classe A, le second élément structurel est caractérisé par la triade de résidus Ser130-Asp131-Asn132 et se fait communément appeler « boucle SDN » en raison des acides aminés qui le composent [16]. Comme son nom l'indique, cet élément fonctionnel est situé sur une petite boucle entre les hélices  $\alpha 4$  et  $\alpha 5$  et forme une partie importante d'une paroi du site actif (Figures 1.5 et 4.3).

Ne pointant pas vers la cavité du site actif, Asp131 ne possède pas de rôle catalytique, mais sa conservation semble être reliée à la stabilisation de la boucle SDN ainsi qu'à celle de la protéine en général [75]. En revanche, Ser130 et Asn132 pointent tous les deux vers l'intérieur de la cavité du site actif et sont positionnés de manière appropriée pour jouer des rôles catalytiques essentiels. En effet, en plus d'être un membre important du réseau de ponts hydrogènes qui maintient la géométrie du site actif et qui est impliqué dans la stabilisation des ligands, Ser130 est un résidu essentiel à l'étape d'acylation puisqu'il transfère son proton à l'azote du noyau  $\beta$ -lactame lors de la réaction catalytique (voir section 1.3.3) [74]. Quant au résidu Asn132, il serait impliqué dans la stabilisation de l'antibiotique à l'état de transition en formant un pont hydrogène avec le carbonyle de la chaîne latérale des substrats [74, 75].

Le troisième élément structurel conservé chez les  $\beta$ -lactamases de classe A est situé sur la face opposée du site actif (brin  $\beta$ 3) et se compose des résidus Lys234-Ser/Thr235-Gly236 (triade KTG) (Figure 1.5). À l'exception des carbénicillases (qui possèdent une arginine à cette position) [76], Lys234 est un résidu strictement conservé chez les enzymes de la classe A et son rôle demeure à ce jour controversé [73]. En plus d'avoir été suggéré comme étant la source de proton qui fournit Ser130 lors de l'acylation (hypothèse récemment remise en question au profit de Lys73 [73]), la stricte conservation d'un résidu à charge positive à cet endroit suggère que Lys234 est impliqué dans la reconnaissance et dans la stabilisation des substrats à l'état de transition en formant une interaction électrostatique avec le carboxylate (C3/C4) du noyau thiazolidine/dihydrothiazine des ligands [76]. Cette hypothèse fut toutefois remise en question en raison de la distance relativement élevée entre ces deux charges opposées (3.5 Å) [44]. En second lieu, l'importance de Thr235/Ser235 demeure à ce jour peu connue. En revanche, la présence d'un groupement hydroxyle possédant la capacité de former un pont hydrogène avec le carboxylate des substrats demeure un atout qui ne s'avère toutefois pas strictement essentiel [74]. Par contre, la perte de ce résidu hydroxyle semble clairement plus désavantageuse

pour les céphalosporines que pour les pénicillines [77, 78]. Finalement, la stricte conservation de Gly236 semble exclusivement liée aux contraintes stériques du site actif, puisque le remplacement de cette petite chaîne latérale aurait des conséquences dévastatrices au niveau de l'approche et du positionnement des substrats, en plus d'affecter la géométrie du site actif [16, 74].

Le quatrième et dernier élément structurel conservé chez les  $\beta$ -lactamases de classe A est situé sur une boucle de 16 à 19 résidus communément appelée la « boucle  $\Omega$  » en raison de sa ressemblance avec la lettre grecque du même nom (Arg161 à Asn170 chez TEM-1). Dans la plupart des cas, cette boucle contient l'élément de séquence primaire Glu166-Xaa-Glu168-Leu169-Asn170, dont deux résidus (Glu166 et Asn170) sont essentiels à la catalyse enzymatique [16]. En effet, Glu166 est un résidu catalytique primordial puisqu'il est directement impliqué dans l'acylation et la désacylation des substrats (voir section 1.3.3). Quant à Asn170, sa conservation semble liée au maintien du positionnement approprié de la molécule d'eau catalytique servant à faire le pont entre Glu166 et Ser70 [16].

### 1.3.5 – Les $\beta$ -lactamases ESBL et IRT

L'alignement de séquence de toutes les  $\beta$ -lactamases de classe A semble à ce jour démontrer qu'il n'existe que neuf résidus strictement conservés parmi tous les membres connus de cette famille d'enzymes [16]. Quatre d'entre eux semblent clairement conservés en raison de leur importance catalytique (Ser70, Lys73, Ser130 et Glu166) alors que les cinq autres apparaissent essentiels pour des raisons structurelles (Gly45, Pro107, Asp131, Ala134 et Gly236) [27]. De plus, tel que décrit à la section 1.3.4, certains résidus de la cavité du site actif semblent fortement conservés en raison de leur importance au niveau de la reconnaissance et de la stabilisation des substrats (notamment Asn132, Lys/Arg234, et

Ser/Thr235). En revanche, bien qu'ils contribuent d'une manière ou d'une autre à la stabilisation des substrats *via* des interactions hydrophiles ou hydrophobes, tous les autres résidus de cet environnement local démontrent un potentiel de variabilité et peuvent ainsi être mutés lorsque l'enzyme est soumise à une pression sélective donnée. Le rôle individuel joué par chacun de ces résidus variables impliqués dans la reconnaissance pourra donc être modifié en présence d'antibiotiques différents, permettant ainsi la sélection d'une vaste gamme de mutants possédant une efficacité catalytique distincte d'un substrat à l'autre.

Dans les années 1970 et 1980, l'introduction de cette variabilité est apparue sous la forme des multiples structures chimiques des antibiotiques à noyau  $\beta$ -lactame (voir section 1.2) et favorisa l'apparition de mutants naturels de  $\beta$ -lactamases possédant la capacité d'hydrolyser plusieurs de ces antibiotiques, donnant ainsi naissance aux  $\beta$ -lactamases à large spectre de reconnaissance (nommées ESBL pour « *Extended-Spectrum  $\beta$ -Lactamases* »). Ces ESBL se caractérisent par leur capacité à hydrolyser les pénicillines ainsi que les céphalosporines des 1<sup>ère</sup>, 2<sup>e</sup> et 3<sup>e</sup> générations, mais elles demeurent néanmoins sensibles à l'action des inhibiteurs tel le clavulanate [19]. Les ESBL possèdent toutes un faible nombre de mutations bénéfiques [79] et sont pour la plupart dérivées des parents enzymatiques TEM ou SHV (pour « *Sulphydryl Variable* », retrouvés chez *K. pneumoniae* et *E. coli*), dont près de 250 variants naturels sont connus à ce jour (voir <http://www.lahey.org/Studies/>). Initialement issus de TEM-1, certains mutants naturels possédant une résistance intrinsèque aux inhibiteurs clavulanate et sulbactame furent également découverts au début des années 1990 et furent nommés IRT (pour « *Inhibitor-Resistant TEM* », et par extension « *Inhibitor-Resistant  $\beta$ -lactamases* ») [17]. Certains variants enzymatiques résistants aux inhibiteurs furent également découverts chez les membres SHV et OXA (pour « *Oxacillin-resistant* », en raison de la forte activité que possède cette famille de  $\beta$ -lactamases pour ce substrat), mais la plupart des enzymes IRT demeurent à ce jour sensibles au tazobactame [17].

### 1.3.6 – Spécificité de reconnaissance

La quantité importante de résidus variables dans l'environnement du site actif de TEM-1 fait en sorte que leur mutation individuelle ou combinatoire donne souvent lieu à l'apparition de phénotypes de résistance inattendus et difficilement prévisibles. Ainsi, certaines positions sont reconnues pour conférer un avantage phénotypique particulier lorsque mutées individuellement ou en combinaison. Chez TEM-1, les mutations du site actif responsables de l'apparition du phénotype ESBL sont habituellement retrouvées aux positions Glu104, Gly238 et Glu240 (Figure 1.5). Ces trois résidus pointent vers la même extrémité du site actif et font face au substituant R<sub>1</sub> des substrats. À cet effet, les mutants individuels E104K et E240K sont très régulièrement retrouvés chez les variants de TEM-1 hydrolysant les céphalosporines de troisième génération (*e.g.* cefotaxime et ceftazidime). Le remplacement du glutamate par une lysine à l'une de ces deux positions permet la formation d'une interaction électrostatique favorable avec le substituant oxyimino de ces substrats et améliore ainsi leur affinité pour l'enzyme [79]. Également retrouvée chez de nombreux variants ESBL, la mutation G238S induit un changement conformationnel local chez les résidus 238 à 242 et déplace le brin β3 d'environ 3 Å, ayant ainsi pour effet de permettre l'agrandissement de cette extrémité du site actif [15, 39]. Cette modification structurelle permet de conserver l'orientation appropriée des résidus catalytiques et favorise la reconnaissance de substrats contenant de plus gros substituants R<sub>1</sub> (notamment les oxyiminocéphalosporines).

Des remplacements similaires sont également retrouvés chez les enzymes responsables de l'apparition du phénotype IRT, pour lequel les positions du site actif les plus souvent affectées sont Met69, Ser130 et Arg244 (Figure 1.5) [80]. La mutation M69L ne change à peu près pas la structure de l'enzyme ni son activité pour les substrats classiques, mais semble affecter la dynamique locale de certains résidus importants pour la stabilisation du clavulanate au site actif (réduisant ainsi son énergie de liaison et causant le

phénotype IRT) [81]. Un phénomène similaire est également observé pour la mutation S130G [15]. En revanche, située sur le brin  $\beta$ 4 et pointant vers l'autre extrémité du site actif, la longue chaîne latérale de Arg244 fait partie d'un réseau d'interactions électrostatiques et de ponts hydrogènes essentiels à la stabilisation du carboxylate (C3/C4) du noyau thiazolidine/dihydrothiazine des divers ligands. En plus de Arg244, ce réseau d'interactions implique la chaîne latérale de Lys234, le carbonyle du squelette peptidique de Val216 ainsi qu'une molécule d'eau conservée (Figure 4.6) [42]. Puisque cette molécule d'eau est essentielle à l'inactivation de l'enzyme par les inhibiteurs, son élimination est accomplie par l'introduction de la mutation R244S, qui confère ainsi le phénotype IRT en permettant l'hydrolyse des inhibiteurs de manière similaire à celle des substrats classiques.

Bien que les mutations donnant lieu à l'apparition des phénotypes ESBL et IRT au site actif des  $\beta$ -lactamases de classe A aient été étudiées de manière ponctuelle ou en paire, leur effet combinatoire à plus de deux positions demeure encore relativement obscur. Ainsi, l'apparition de variantes enzymatiques possédant plusieurs de ces mutations synergiques demeure une inquiétude dont les effets en milieu clinique pourraient s'avérer catastrophiques. De plus, la combinaison de ces « *hot spots* » avec d'autres mutations concentrées à des positions en contact direct avec les ligands est également peu connue et mérite une attention particulière (notamment l'effet du remplacement de la chaîne latérale hydroxyphényle de Tyr105).

## 1.4 – Objectifs du projet de recherche et justification des méthodes employées

La découverte de nouvelles  $\beta$ -lactamases à large spectre de reconnaissance causant de graves problèmes de résistance bactérienne en milieu clinique nous force ainsi à examiner et à développer de nouvelles solutions antibiotiques ciblant particulièrement ces

enzymes de résistance retrouvées chez la grande majorité de ces pathogènes opportunistes. Une avenue encourageante dans la synthèse de nouveaux composés  $\beta$ -lactames demeure aujourd’hui la possibilité de prédire l’effet de ces mutations en laboratoire avant d’avoir à subir les conséquences dévastatrices de leur apparition en milieu clinique. En effet, depuis les travaux classiques de la fin des années 1970 ayant démontré la capacité qu’ont les  $\beta$ -lactamases d’acquérir de nouvelles spécificités [82], la synthèse moderne de nouveaux antibiotiques et d’inhibiteurs à noyau  $\beta$ -lactame bénéficie de l’énorme avantage que procurent désormais les outils de la biologie moléculaire. De surcroît, le développement de méthodes *in vitro* d’évolution moléculaire accélérée (évolution dirigée) permet désormais la prédiction en laboratoire de mutations qui pourraient s’avérer catastrophiques en milieu hospitalier [39, 83]. En plus d’avoir prédit correctement l’apparition de mutations d’importance clinique chez diverses  $\beta$ -lactamases [39], ces techniques d’évolution dirigée ont aussi permis d’identifier des exemples où le phénotype de résistance n’apparaîtrait statistiquement pas dans la nature, réfutant ainsi la présomption grandement répandue voulant que les gènes de résistance peuvent évoluer à l’infini pour éventuellement inactiver n’importe quel nouveau composé [84]. Le contournement des mécanismes de résistance et le développement de nouveaux agents antibactériens passent donc désormais par une analyse structure-fonction détaillée de la reconnaissance et de l’inactivation des composés  $\beta$ -lactames par les  $\beta$ -lactamases. Ainsi, la caractérisation détaillée de ces interactions moléculaires et la connaissance des limites de l’adaptation évolutive des  $\beta$ -lactamases sont désormais des étapes essentielles au développement de nouveaux antibiotiques.

Le but du présent projet de recherche fut donc d’entreprendre une étude structure-fonction détaillée entre des mutants d’une enzyme  $\beta$ -lactamase et certains antibiotiques à noyau  $\beta$ -lactame qu’elle inactive par hydrolyse. Le modèle enzymatique utilisé est la  $\beta$ -lactamase TEM-1 de la bactérie Gram-négative *Escherichia coli*, responsable pour plus de 90 % des résistances à l’ampicilline retrouvées chez cet organisme [17, 85] et dont la structure cristallographique en présence et en absence de nombreux ligands est connue.

Nous avons entrepris ces études dans le but d'améliorer la compréhension que nous avons de la reconnaissance et de la discrimination de certains substrats par TEM-1 ainsi que pour explorer en plus de détails certains aspects du mécanisme catalytique de cette enzyme, qui demeure à ce jour controversé (voir section 1.3.3). À cet effet, plusieurs méthodes expérimentales et théoriques complémentaires furent utilisées pour répondre aux objectifs spécifiques du projet.

### **1.4.1 – Biologie moléculaire et cinétique enzymatique**

Le premier objectif spécifique du projet de recherche fut d'étudier l'importance du résidu tyrosine retrouvé en position 105 chez la  $\beta$ -lactamase TEM-1. Partie intégrante de l'une des parois de la cavité du site actif de cette enzyme, l'identité de séquence et la conservation structurelle de cette position demeure très forte chez toutes les  $\beta$ -lactamases de classe A et son importance était peu connue dans la reconnaissance et la discrimination des substrats. Pour ce faire, nous avons utilisé une technique de mutagenèse par saturation dans le but d'obtenir les 20 variantes correspondant à toutes les possibilités d'acides aminés naturels à cette position. L'activité de ces mutants fut ensuite déterminée *in vivo* par des tests de survie cellulaire en présence de divers antibiotiques, permettant ainsi le calcul de concentrations minimales inhibitrices (MIC). Bien que cette technique permette la comparaison rapide de l'activité de chacun des mutants dans leur environnement cellulaire naturel, elle ne donne pas d'information précise quant aux paramètres cinétiques de ces mutants et elle est tributaire de facteurs cellulaires à la base de diverses variations clonales incontrôlables (niveaux d'expression distincts, systèmes alternatifs de résistance, etc.).

Pour pallier les limites de cette technique, les mutants Y105X d'intérêt furent exprimés et purifiés dans le but de calculer leurs paramètres cinétiques *in vitro*. Les paramètres  $k_{cat}$  et  $K_m$  de chacun des mutants d'intérêt furent ainsi déterminés pour plusieurs

substrats antibiotiques en condition de vitesse initiale à l'état stable et dans des conditions de température et de pH identiques. Le calcul de ces paramètres cinétiques révèle la constante de liaison productive que possèdent chacun des mutants pour un substrat donné ( $K_m$ ) ainsi que de la vitesse à laquelle ils catalysent la réaction d'hydrolyse ( $k_{cat}$ ) (voir Annexe 2 pour une explication plus détaillée des méthodes expérimentales employées). Les informations cinétiques ainsi obtenues permirent la démonstration de l'importance de Tyr105 dans la reconnaissance et la discrimination des substrats chez TEM-1 et les détails de cette étude sont présentés au chapitre 2.

#### **1.4.2 – Modélisation *in silico* par dynamique moléculaire**

Dans le but de mieux définir l'importance structurelle de ce résidu dans la reconnaissance et la discrimination des substrats, le deuxième objectif spécifique du projet de recherche fut de complémenter notre analyse expérimentale par une étude de dynamique moléculaire sur divers mutants Y105X d'intérêt. À partir de structures cristallines préétablies et en utilisant des champs de forces décrivant les interactions moléculaires atomiques, les simulations par dynamique moléculaire permettent de créer des modèles structuraux qui capturent les caractéristiques importantes des motions moléculaires des protéines [86-88]. Leur utilité est d'autant plus intéressante que ces méthodes permettent de corréler l'observation visuelle d'un phénomène dynamique avec les données expérimentales obtenues, assurant ainsi l'amélioration de l'interprétation et de la compréhension des résultats expérimentaux. De plus, en permettant l'analyse d'une structure moléculaire en mouvement sur une certaine échelle de temps, la dynamique moléculaire permet l'observation de changements conformationnels locaux dont l'importance dans la fonction de la région d'intérêt à l'étude peut s'avérer cruciale.

Bien que l'un des objectifs avoué des théoriciens ayant développé les méthodes de dynamique moléculaire soit leur acceptation et leur adoption en tant que technique

routinière utilisée par les scientifiques dans l'analyse de leurs données expérimentales [88], il n'en demeure pas moins qu'il s'agit d'un outil dont les résultats doivent être interprétés avec prudence en tenant compte de ses limites intrinsèques. À ce jour, la principale limite de la dynamique moléculaire demeure l'échelle de temps qu'il nous est permis d'étudier par cette méthode (Figure 1.6). Publiée il y a près de 30 ans, la première étude de dynamique moléculaire fut entreprise *in vacuo* sur un système de 500 atomes et sur une échelle de temps inférieure à 10 ps [89]. Depuis ce temps, l'amélioration de la puissance de calcul informatique ainsi que le perfectionnement des champs de forces atomiques ont permis l'analyse de systèmes de plus en plus gros (jusqu'à  $10^4$ - $10^6$  atomes), qu'il est actuellement possible d'étudier sur une échelle de temps jusqu'à 1000 fois plus longue (10 ns) [88]. En revanche, la dynamique moléculaire classique demeure néanmoins confinée à l'étude d'événements dynamiques de l'ordre de la ps-ns et ne permet pas encore l'investigation de mouvements moléculaires plus lents, notamment les mouvements critiques observés à l'échelle de temps de la catalyse (souvent de l'ordre de la  $\mu$ s et de la ms, voir Figure 1.6). Or, cette technique s'avère néanmoins tout à fait appropriée à l'étude de mouvements moléculaires rapides et locaux qui peuvent avoir une implication majeure dans la stabilisation de divers ligands. Présentée au chapitre 2, cette analyse fut ici appliquée à l'étude de divers intermédiaires enzyme-substrat entre TEM-1 et la benzylpénicilline dans le contexte de l'introduction de mutations en position 105. Nos résultats suggèrent que l'effet des mutations en position 105 serait en lien avec la dynamique de ces résidus.

### 1.4.3 – Modélisation *in silico* par recuit simulé

De nos jours, la grande majorité des systèmes enzymatiques étudiés par dynamique moléculaire impliquent l'ajout d'un solvant aqueux explicite, ce qui a pour effet d'améliorer le réalisme du système à l'étude. Ainsi, une couche ou une sphère d'eau est ajoutée à la protéine pour simuler le milieu aqueux dans lequel elle se trouve naturellement

en solution. En entreprenant une solvatation explicite des résidus de la protéine, cette technique permet ainsi la formation de ponts hydrogène avec les molécules d'eau en plus de simuler de manière plus réaliste la polarité du milieu. Or, cet ajout de solvant a néanmoins l'effet pervers d'augmenter significativement le nombre total de molécules composant le système, alourdissant ainsi de manière significative le temps de calcul nécessaire pour accomplir une tâche informatique identique sans solvant. Conséquemment, en raison du nombre de mutants étudiés *in silico* ainsi que de la puissance de calcul limitée à notre disposition, les études de dynamique moléculaire susmentionnées furent entreprises sur une échelle de temps de seulement 200 ps, réduisant ainsi la portée de l'analyse des mouvements d'intérêt adoptés par les chaînes latérales des résidus à l'étude.

Pour pallier cette limite et en utilisant un système similaire à celui employé pour la dynamique moléculaire, le troisième objectif spécifique du projet de recherche fut d'entreprendre une étude de modélisation par recuit simulé sur la  $\beta$ -lactamase TEM-1 dans le but d'analyser l'espace conformationnel adopté par la chaîne latérale de Tyr105 en absence de substrat. Contrairement à la dynamique moléculaire classique, cette procédure implique l'ajout d'énergie au système dans le but de permettre à certains résidus de la protéine de surmonter des barrières énergétiques locales qui ne pourraient être franchies qu'en étudiant le même système sur une échelle de temps beaucoup plus longue (Figure 1.7). En effet, en utilisant la température pour effectuer des cycles de réchauffement et de refroidissement ainsi qu'en validant les conformères locaux obtenus suite à une minimisation énergétique, ce protocole possède l'avantage de permettre l'observation de rotamères alternatifs pouvant être adoptés par les résidus à l'étude. Présenté au chapitre 3, ce protocole fut appliqué à l'étude de Tyr105 et permit l'observation de conformères alternatifs stables de ce résidu chez TEM-1. Ces résultats suggèrent la possibilité que la chaîne latérale de Tyr105 puisse alterner d'un rotamère à l'autre sur une échelle de temps plus longue que celle précédemment étudiée par dynamique moléculaire et propose une explication partielle quant aux différences d'affinité calculées entre divers substrats pénicillines et céphalosporines.

#### 1.4.4 – Résonance magnétique nucléaire (RMN)

Dans le but de vérifier les hypothèses structurales suggérées par nos études de modélisation ainsi que pour vérifier la relation entre la dynamique et les données cinétiques précédemment calculées, le quatrième objectif spécifique du projet de recherche fut d'entreprendre une caractérisation structurelle expérimentale sur divers mutants Y105X de TEM-1. Puisque notre intérêt principal demeurait la caractérisation dynamique des motions observées dans l'environnement de la position 105 mutée, nous avons entrepris des études de résonance magnétique nucléaire sur divers mutants Y105X d'intérêt. Tout comme la cristallographie par diffraction aux rayons-X, la RMN est une technique qui permet l'obtention de la structure des protéines, mais elle possède l'avantage d'être effectuée en solution (un environnement similaire à celui de la protéine dans son milieu naturel) en plus de fournir une quantité importante d'informations sur la dynamique interne des protéines (voir Annexe 3). En effet, puisque cette méthode est basée sur l'analyse des spins nucléaires et que ceux-ci sont sensibles aux mouvements des noyaux avoisinants, l'étude de leur relaxation par RMN permet de caractériser les motions atomiques sur une vaste gamme d'échelles de temps, recouvrant ainsi les motions moléculaires importantes à la fonction des protéines [90]. Ainsi, le développement de diverses techniques employées en RMN et l'analyse théorique des données expérimentales permettent d'extraire des informations de dynamique moléculaire couvrant des motions allant de la picoseconde à plusieurs secondes [91].

Présentés au chapitre 4, les résultats de cette étude nous ont permis de corrélérer les effets de déplacements chimiques du squelette peptidique observés en RMN avec l'efficacité catalytique précédemment calculée pour chacun des mutants Y105X d'intérêt. De plus, des études de relaxation comparatives sur l'enzyme native et le mutant peu actif Y105D ainsi que l'analyse théorique des paramètres calculés nous ont permis d'observer

d'importantes différences dynamiques sur deux échelles de temps : ps-ns et  $\mu$ s-ms. Cette dernière revêt un intérêt particulier en raison de sa pertinence par rapport à l'activité catalytique. Bien que toutes les études de RMN présentées dans ce chapitre se concentrent sur l'analyse de la relaxation du vecteur amide ( $^1\text{H}-^{15}\text{N}$ ) du squelette peptidique, les informations dynamiques calculées furent néanmoins suffisantes pour soulever des hypothèses quant aux mouvements possibles des chaînes latérales des résidus affectés. En effet, bien qu'il soit possible d'entreprendre une analyse détaillée de la dynamique de certaines chaînes latérales d'intérêt en étudiant la relaxation d'isotropomères des groupements méthyles deutérés sur les chaînes latérales [92], les études RMN des protéines démontrent néanmoins que les chaînes latérales sont généralement toujours plus mobiles que les atomes du squelette peptidique [93, 94]. Conséquemment, l'observation de différences significatives affectant les motions du squelette peptidique d'un résidu en particulier suggère que sa chaîne latérale est également affectée.

#### **1.4.5 – Mutagenèse semi-aléatoire du site actif de TEM-1**

Le cinquième et dernier objectif spécifique du projet de recherche fut d'étendre notre analyse structure-fonction de TEM-1 dans le but d'introduire des mutations combinatoires à diverses positions dans l'environnement du site actif pour en étudier l'effet sur l'activité catalytique et sur la spécificité de reconnaissance des substrats. Depuis maintenant un quart de siècle, les études mutationnelles entreprises sur TEM-1 tirent profit de deux techniques principales de mutagenèse : le design rationnel et l'évolution dirigée. Dans le but de guider notre choix, le premier objectif de cette section du projet de recherche fut d'entreprendre une revue exhaustive de la littérature, nous permettant ainsi de faire ressortir les avantages et les inconvénients de chacune de ces deux techniques. Suite à cette analyse, il nous apparut évident que la combinaison des avantages de chacune de ces deux méthodes optimiserait nos chances d'obtenir le plus grand nombre de mutants actifs. Ainsi,

en se basant sur divers systèmes enzymatiques similaires, nous avons compilé les méthodes de mutagenèse ‘semi-aléatoire’ (aussi nommée ‘semi-rationnelle’) et exposé leurs avantages dans un article de revue présenté au chapitre 5.

Finalement, sur la base d’études précédentes ayant démontré l’importance individuelle de nombreux résidus de la cavité du site actif chez TEM-1, nous avons entrepris une étude semi-aléatoire en ciblant simultanément plusieurs des positions impliquées dans l’apparition de variantes ESBL de cette enzyme. Puisque l’importance de l’effet combinatoire des résidus Glu104, Gly238, Gly240 et Arg244 n’avait jamais été vérifiée en ce qui a trait à la reconnaissance des substrats, nous avons entrepris une étude de mutagenèse par saturation à ces quatre positions en les combinant de manière simultanée aux 20 mutants de Tyr105 obtenus précédemment. Le but de cette étude visait à complémer les informations partielles relatives à l’apparition de mutations combinatoires au site actif de TEM-1 et de vérifier si l’effet combiné des mutations à la base du phénotype ESBL s’avérait être synergique, additif ou antagoniste [95]. La technique de mutagenèse employée dans cette étude est une application directe de la méthode semi-aléatoire présentée au chapitre 5 et tire à la fois profit des avantages conférés par les techniques de mutagenèse aléatoire (évolution dirigée) et du design rationnel. En effet, la combinaison de mutations aléatoires couplée à une méthode de sélection efficace permet d’optimiser les chances de trouver des mutants actifs alors que le choix rationnel des positions à muter sur la base d’études précédentes ayant démontré l’importance de ces divers « *hot spots* » améliore les chances de trouver de tels mutants. Présentés au chapitre 6, les résultats de cette étude nous ont permis de découvrir de nouvelles variantes combinatoires de TEM-1 hydrolysant notamment le céfotaxime (une céphalosporine de troisième génération) et permirent la démonstration de l’existence d’une certaine plasticité au site actif de cette enzyme.

## FIGURES

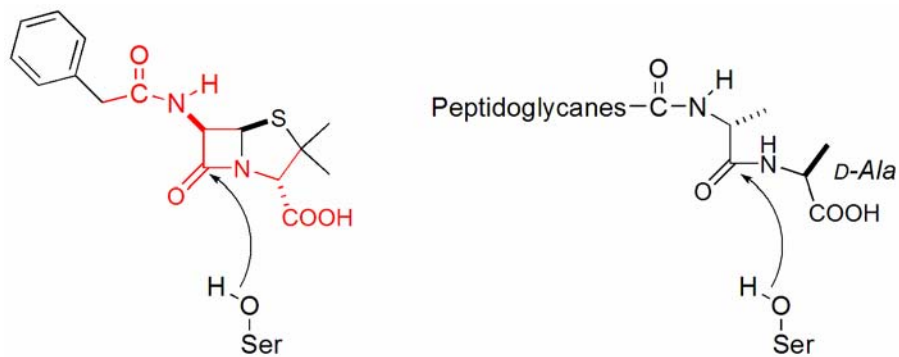


**Figure 1.1.** Structure chimique de la benzylpénicilline (à gauche) et de la portion C-terminale des chaînes *N*-acétylglucosamine des peptidoglycanes (à droite). La représentation schématique de la benzylpénicilline démontre la similarité structurelle (représentée en rouge) entre cet antibiotique et la portion C-terminale des peptidoglycanes. Le site de l’attaque nucléophilique de la sérine des PBP est représenté par une flèche sur les deux structures. Figure adaptée de [96].

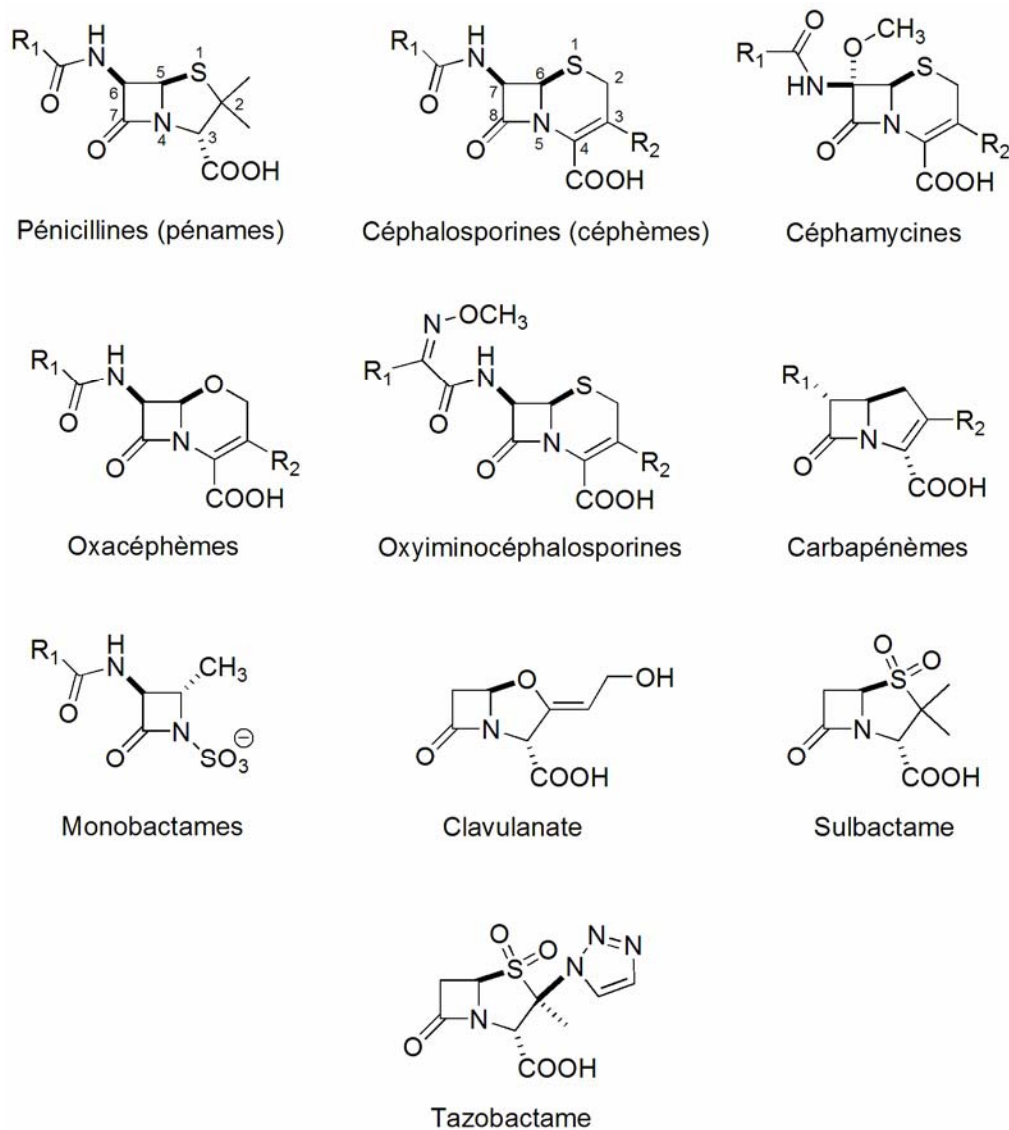


**Figure 1.2.** Structure chimique des principales classes et composés antibiotiques à noyau  $\beta$ -lactame.

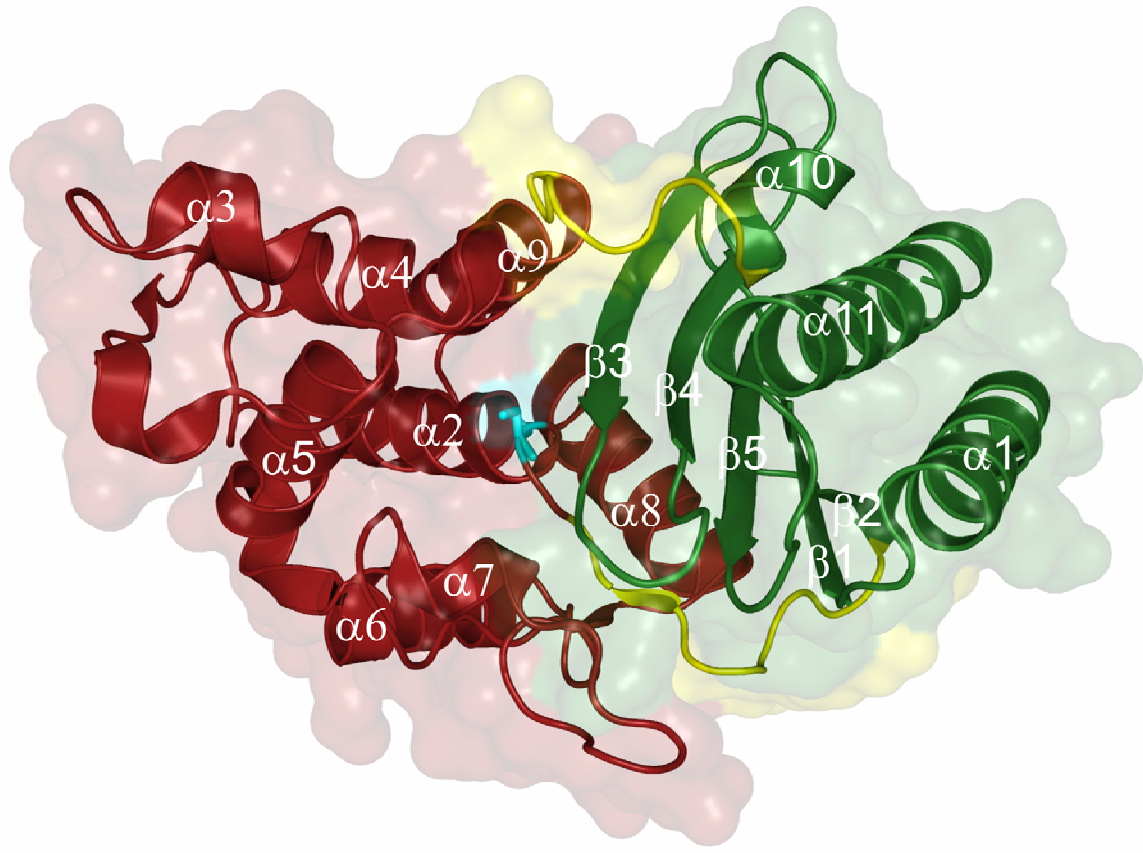


**Figure 1.3.** Structure moléculaire de la  $\beta$ -lactamase TEM-1 de *Escherichia coli*. TEM-1 est un monomère globulaire de 263 acides aminés composé de deux domaines structuraux ( $\alpha/\beta$  en vert et tout  $\alpha$  en rouge), qui sont séparés par deux régions charnières (résidus 60-68 et 212-222, de couleur jaune). Le site actif de l'enzyme est situé dans une crevasse à l'interface des deux domaines et son point central est ici représenté par le résidu catalytique Ser70 (en cyan). Les hélices  $\alpha$  et des brins  $\beta$  sont numérotés en fonction de la séquence primaire et selon la convention définie par Jelsch *et al.* [36].

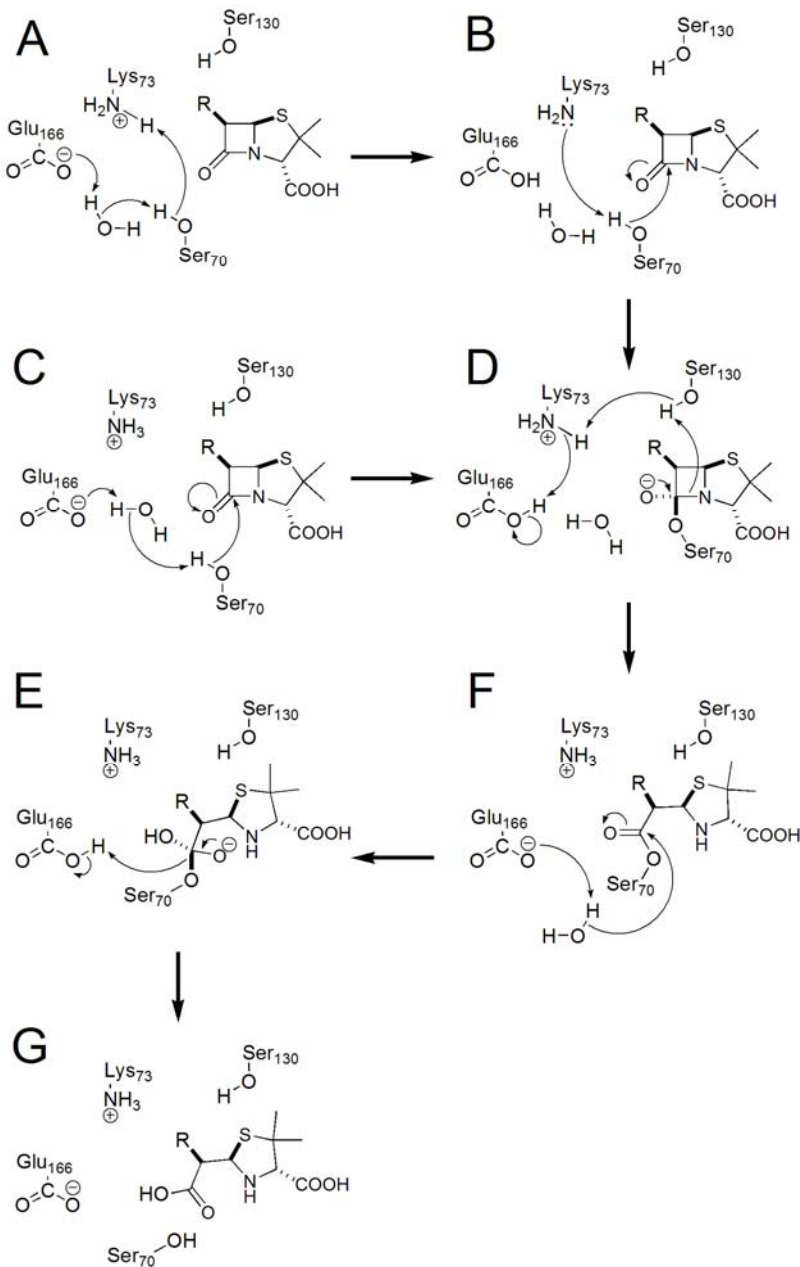


**Figure 1.4.** Représentation schématique du mécanisme catalytique de la  $\beta$ -lactamase TEM-1. Les deux hypothèses d'acylation par Lys73 et Glu166 sont représentées par les parcours A-B-D et C-D, respectivement. Données compilées à partir de [73].

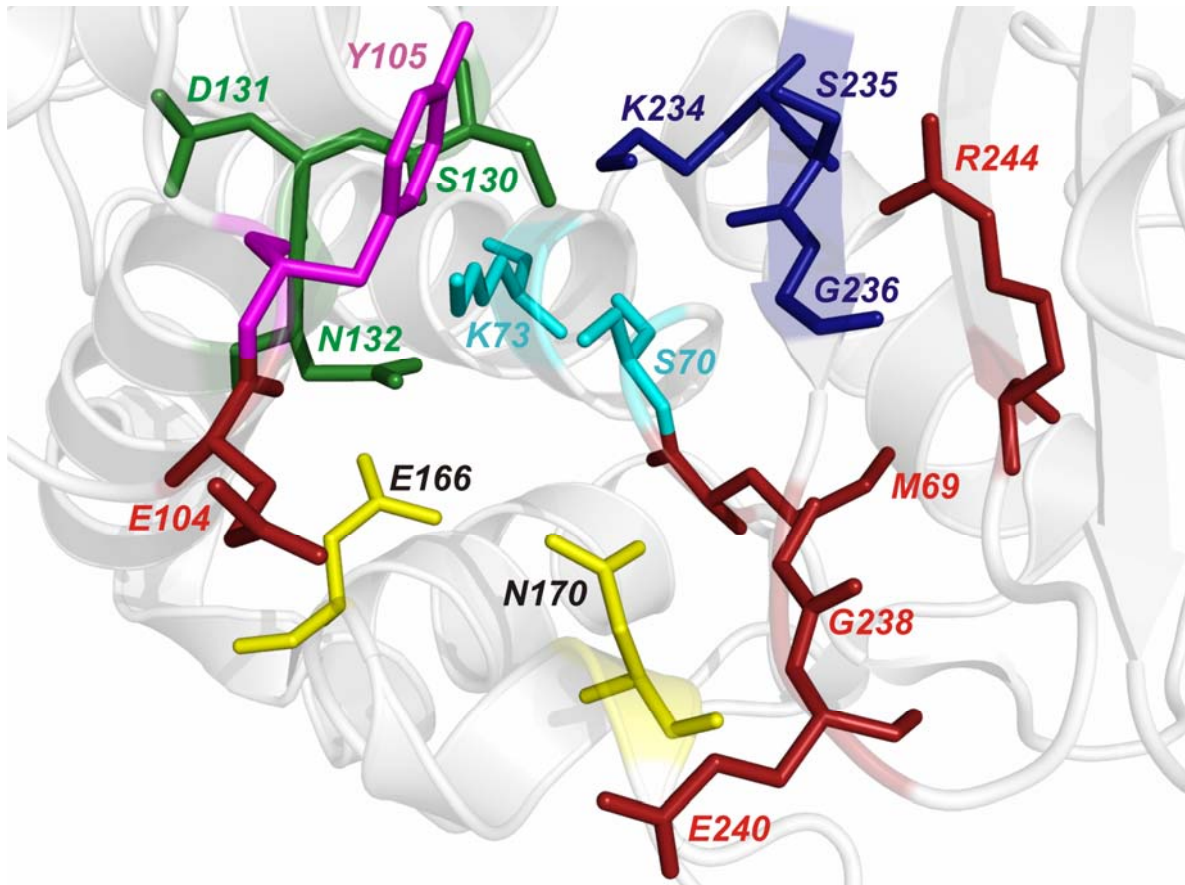


**Figure 1.5.** Principaux résidus du site actif de la  $\beta$ -lactamase TEM-1. Les résidus essentiels aux quatre éléments fonctionnels définis à la section 1.3.4 sont respectivement colorés comme suit : premier élément, S70 et K73 (cyan) ; deuxième élément, S130, D131 et N132 (vert) ; troisième élément, K234, S235 et G236 (bleu) ; quatrième élément, E166 et N170 (jaune). Les résidus de la cavité du site actif dont la mutation donne lieu à l'apparition des phénotypes ESBL ou IRT sont colorés en rouge et le résidu Tyr105 est coloré en magenta.

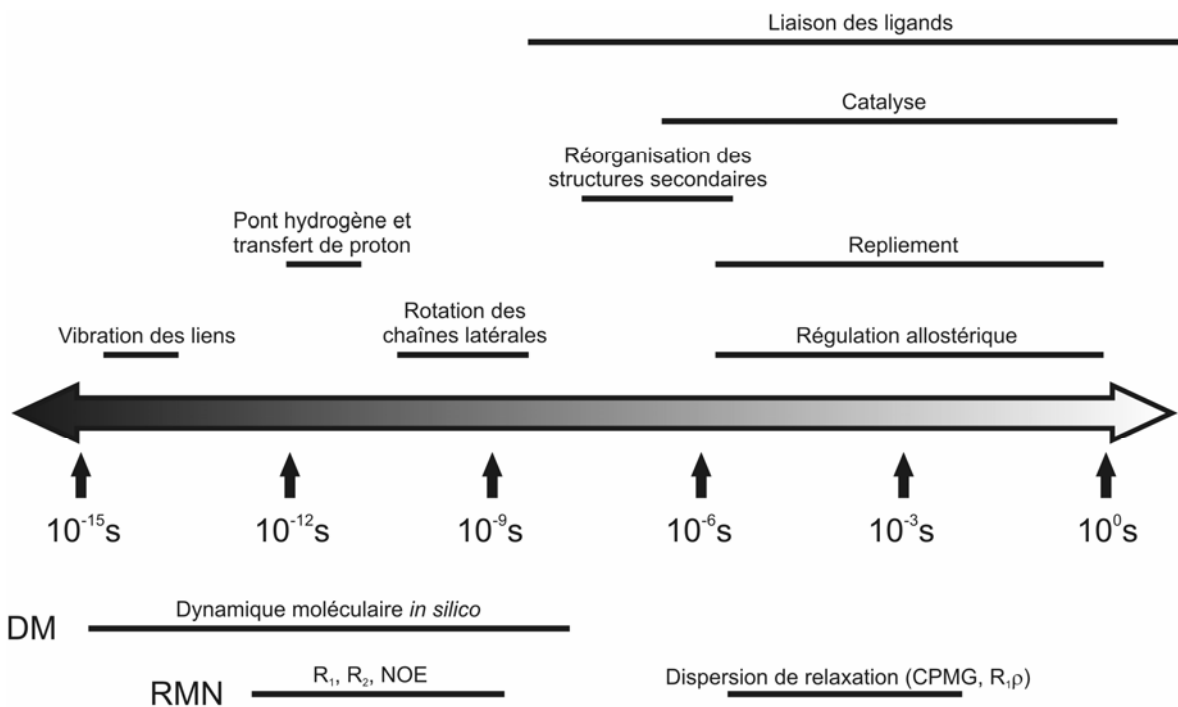


**Figure 1.6.** Échelle de temps de divers événements dynamiques internes des protéines.  
Données compilées à partir de [92, 97-99].

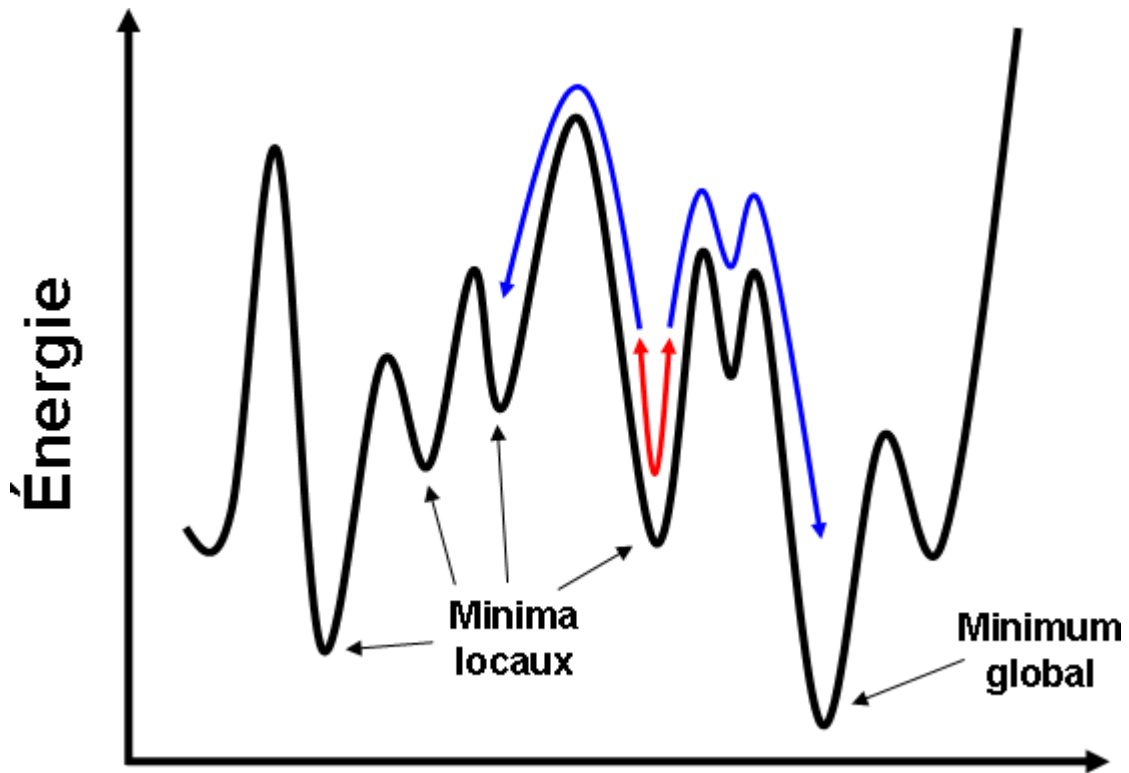


**Figure 1.7.** Schéma théorique de l'espace conformationnel énergétique adopté par divers conformères d'une protéine. Une ronde de dynamique moléculaire classique à courte échelle (flèche rouge) permet l'exploration d'un nombre restreint de conformères, conservant ainsi la protéine dans un minimum énergétique local. Dans une ronde de recuit simulé (flèches bleues), l'ajout d'énergie par l'augmentation de la température permet au système de surmonter des barrières énergétiques locales et d'explorer des conformères alternatifs stables situés dans d'autres minima énergétiques. En dynamique moléculaire classique, l'atteinte de ces minima énergétiques ne serait possible que par l'étude du même système sur une échelle de temps beaucoup plus longue.

## Préface au chapitre 2

Sur la base d'études préliminaires ayant suggéré son importance dans la reconnaissance des ligands chez les  $\beta$ -lactamases de classe A, nous avons entrepris une mutagenèse par saturation à la position Tyr105 chez TEM-1 dans le but de clarifier le rôle de ce résidu au niveau de la stabilisation et de la discrimination des substrats. Les tests de survie cellulaire entrepris sur chacun des mutants Y105X ont démontré que seuls les résidus aromatiques et l'asparagine confèrent de fortes résistances aux substrats pénicillines et céphalosporines testés. De plus, les différences de survie cellulaire observées pour les mutants Y105A et Y105G démontrent que cette position est également impliquée dans la discrimination des substrats. Par ailleurs, la cinétique enzymatique entreprise sur les mutants Y105D, Y105G, Y105N, Y105R et Y105W illustre l'importance de ce résidu au niveau de la stabilisation des substrats au site actif en raison de l'effet significatif observé sur le paramètre cinétique  $K_m$ . À la lumière de ces résultats expérimentaux et de la dynamique moléculaire *in silico* entreprise, nous suggérons que la forte conservation d'un résidu aromatique à cette position chez les  $\beta$ -lactamases de classe A soit attribuable à une nécessité structurelle qui favorise l'adoption d'une conformation stable et planaire qui conserve l'intégrité de cette paroi du site actif sur une courte échelle de temps (ps).

Les résultats de ce chapitre sont présentés sous la forme d'un article scientifique publié dans la revue *The Journal of Biological Chemistry* en octobre 2004. Ayant été impliqué dans tous les aspects de la recherche expérimentale et théorique de cette étude ainsi que dans la rédaction du manuscrit, ma contribution à ce projet est majeure. Une aide technique offerte par Pierre-Yves De Wals au niveau du sous-clonage de certains mutants ainsi que pour les tests de concentrations minimales inhibitrices justifie sa présence en tant que deuxième auteur.

Il est à noter que le terme « apoenzyme », qui signifie spécifiquement la partie protéique et enzymatiquement inactive d'un complexe holoenzyme [100], est utilisé tout au long de ce chapitre pour désigner l'enzyme *active* et *sans substrat* (sous forme libre). Bien que régulièrement utilisée dans la littérature, cette définition n'en demeure pas moins

erronée puisque les  $\beta$ -lactamases n'utilisent pas de cofacteur et ne forment pas de complexe holoenzyme. Par souci de précision, le lecteur substituera volontiers ce terme par «*free form*» ou encore «*unbound form*» lors de la lecture de ce chapitre publié.

## **CHAPITRE 2**

### **Mutagenèse par saturation à la position 105 de la $\beta$ -lactamase TEM-1 : Importance de la tyrosine dans la stabilisation et la discrimination des substrats**

#### **2.1 Article 1. Site-saturation mutagenesis of Tyr-105 reveals its importance in substrate stabilization and discrimination in TEM-1 $\beta$ -lactamase**

“Reprinted with permission from: Nicolas Doucet, Pierre-Yves De Wals and Joelle N. Pelletier. “Site-saturation mutagenesis of Tyr-105 reveals its importance in substrate stabilization and discrimination in TEM-1  $\beta$ -lactamase.” *J. Biol. Chem.*, 279 (44), 46295-46303 (2004). ©2004, *The American Society for Biochemistry and Molecular Biology, Inc.* Reprinted with permission from *The American Society for Biochemistry and Molecular Biology, Inc.*”

**Site-saturation mutagenesis of Tyr-105 reveals its  
importance in substrate stabilization and discrimination  
in TEM-1  $\beta$ -lactamase**

Nicolas Doucet<sup>1</sup>, Pierre-Yves De Wals<sup>1</sup> & Joelle N. Pelletier<sup>1,2</sup>

<sup>1</sup>*Département de biochimie and* <sup>2</sup>*Département de chimie*

*Université de Montréal*

*C.P. 6128, Succursale Centre-ville*

*Montréal (Québec)*

*H3C 3J7 CANADA*

*J. Biol. Chem.*, 2004, 279 (44), 46295-46303

## ABSTRACT

The conserved Class A  $\beta$ -lactamase active site residue Tyr-105 was substituted by saturation mutagenesis in TEM-1  $\beta$ -lactamase from *Escherichia coli* in order to clarify its role in enzyme activity and in substrate stabilization and discrimination. Minimum inhibitory concentrations were calculated for *E. coli* cells harboring each Y105X mutant in the presence of various penicillin and cephalosporin antibiotics. We found that only aromatic residues as well as asparagine replacements conferred high *in vivo* survival rates for all substrates tested. At position 105, the small residues alanine and glycine provide weak substrate discrimination as evidenced by the difference in benzylpenicillin hydrolysis relative to cephalothin, two typical penicillin and cephalosporin antibiotics. Kinetic analyses of mutants of interest revealed that the Y105X replacements have a greater effect on  $K_m$  than  $k_{cat}$ , highlighting the importance of Tyr-105 in substrate recognition. Finally, by performing a short molecular dynamics study on a restricted set of Y105X mutants of TEM-1, we found that the strong aromatic bias observed at position 105 in Class A  $\beta$ -lactamases is primarily defined by a structural requirement, selecting planar residues that form a stabilizing wall to the active site. The adopted conformation of residue 105 prevents detrimental steric interactions with the substrate molecule in the active site cavity and provides a rationalization for the strong aromatic bias found in nature at this position among Class A  $\beta$ -lactamases.

## INTRODUCTION

During the past decades,  $\beta$ -lactamase production (EC 3.5.2.6) has become a significant problem in bacterial strain resistance to widely used clinical antibiotics. Among these enzymes, the prevalent type has always been the Class A active site serine hydrolase  $\beta$ -lactamases, which have become model enzymes extensively studied by protein

engineering with respect to site-directed or combinatorial mutagenesis (1-5), structure determination (6-10), and molecular simulations (11-13). Over the years *Escherichia coli* TEM-1  $\beta$ -lactamase has become an impressive example of the rapid evolution rate of proteins occurring within natural bacterial isolates subjected to selective pressure. Ever since the clinical introduction of  $\beta$ -lactam compounds and the discovery of TEM-1  $\beta$ -lactamase, both in the 1940s (14), natural mutations have generated a large number of single and multiple mutants of this enzyme (for an extensive list see [www.lahey.org/Studies/temtable.asp](http://www.lahey.org/Studies/temtable.asp)).

The high rate of occurrence of mutated enzymes capable of hydrolyzing higher generation cephalosporins has stimulated research of  $\beta$ -lactamase adaptation to these new substrates in order to understand the molecular basis of this evolutionary chain of events. Consequently, a number of studies have successfully predicted the *in vitro* appearance of new mutations conferring resistance before their appearance in natural isolates (for an overall view, see Ref 1). To provide more information regarding these mutations in enzyme catalysis and/or substrate stabilization, multiple mutagenesis replacements have been undertaken in Class A  $\beta$ -lactamases to residues in close proximity to the active site cavity that are most likely to be in direct contact with the substrate, allowing for modified catalytic parameters (2-4). In conjunction with the SDN loop (3), the Class A conserved residue Tyr-105 delineates one of the edges of the active site cavity of TEM-1 as a result of the position of its side chain near the thiazolidine ring of penicillin substrates and the dihydrothiazine ring of cephalosporin substrates. To date, two independent mutagenesis studies were performed to modify Tyr-105 to Phe and Cys on the Class A  $\beta$ -lactamases of *Bacillus licheniformis* and *Bacillus cereus*, respectively (15, 16). The *B. licheniformis* Y105F mutant displayed a 52% catalytic efficiency toward benzylpenicillin compared with its corresponding wild-type enzyme. Based on these results, the Y105F mutation rules out a critical role of the hydroxyl group of the wild-type Tyr residue toward enzyme activity or stability. Moreover, the *B. cereus* Y105C mutant displayed native-like catalytic activity

under standard nitrocefin assay conditions, demonstrating that the aromatic moiety at this position is not essential for enzyme activity or stability.

On the other hand, the location and the strong conservation of aromatic character of this residue among Class A  $\beta$ -lactamases suggest that residue 105 may play a role in substrate recognition and/or stabilization. This hypothesis is based on crystallographic data of many Class A enzymes showing that the Tyr-105 side chain is significantly displaced upon binding of substrates or mechanism-based inhibitors as a result of a flipping motion (7, 17–21). In fact, it has been suggested that the Tyr-105 side chain may “stack” with the thiazolidine ring of penicillins (21, 22) as well as form van der Waals and hydrophobic interactions with the benzyl side chains of substrates (7, 12) or inhibitors (18, 19), suggestive of its active participation in substrate and inhibitor positioning at the active site. As a result of this characteristic, residue 105 has been considered a determinant of susceptibility to mechanism-based inhibitors (23).

To our knowledge, apart from the Y105F and Y105C mutations (15, 16), no further site-directed mutagenesis studies have been undertaken specifically at this critical active site position. Huang *et al.* (24) previously reported a three-codon-based combinatorial mutagenesis for the entire gene of TEM-1 but conducted no detailed analysis of residue 105 with respect to substrate recognition. Nevertheless, their results suggest that only the Y105H mutant is able to confer wild-type activity for ampicillin upon selecting for survival in the presence of 1 mg/ml antibiotic. However, these Y105X mutations were performed only with other simultaneous mutations at positions 103 and 104. Although the high activities observed with the Y105F and Y105C mutants suggest that hydrophobicity may be a determining factor at this active-site position, the effects of variables such as side-chain volume, polarity, and flexibility at this position have not been specifically addressed.

Thus, the importance of sequence conservation at position 105 is unclear, and the role of residue 105 has yet to be elucidated in detail with respect to enzyme stability and

substrate stabilization and discrimination for Class A  $\beta$ -lactamases. Consequently, to clarify the importance of residue 105 in TEM-1  $\beta$ -lactamase as well as its potential role in other Class A  $\beta$ -lactamases, we performed saturation mutagenesis at position 105 on TEM-1. *In vivo* antibiotic susceptibility tests and *in vitro* kinetic studies were carried out using penicillin as well as first- and third-generation cephalosporin substrates to assess the impact of the mutations on substrate recognition and enzyme catalysis. Finally, molecular modeling studies of mutants of interest were undertaken to evaluate the structural importance of residue 105 in substrate stabilization. Our results identify residue 105 as a weak substrate determinant of TEM-1  $\beta$ -lactamase.

## EXPERIMENTAL PROCEDURES

*Reagents*—Restriction and DNA-modifying enzymes were purchased from MBI Fermentas (Burlington, ON) and New England Biolabs, Ltd. (Mississauga, ON). Ampicillin was obtained from BioShop Canada, Inc. (Burlington, ON), and benzylpenicillin, cephalothin, cefazolin, cefotaxime, and Fast-Flow DEAE-Sepharose were purchased from Sigma-Aldrich. Nitrocefin was purchased from Calbiochem.

*Bacterial Strains and Plasmids*—*E. coli* XL1-Blue (*supE44, hsdR17, recA1, endA1, gyrA46, thi, relA1, lac F'* [*proAB<sup>+</sup>, lacI<sup>q</sup>, lacZΔM15, Tn10(tet<sup>r</sup>)*]) was used for the propagation and expression of all plasmids. Plasmid pQE32Chl in which the *bla<sub>TEM-1</sub>* gene of pQE32 (Qiagen, Mississauga, ON) was replaced by a chloramphenicol acetyltransferase gene was a generous gift from François-Xavier Campbell-Valois and Stephen W. Michnick (Département de Biochimie, Université de Montréal, QC) and was used for protein expression. It was maintained using 12.5  $\mu$ g/ml chloramphenicol (Chl).<sup>1</sup> Plasmid pBR322, which contains the wild-type *bla<sub>TEM-1</sub>* gene (without the V84I and A184V mutations) was

kindly provided by Luis A. Rokeach (Département de Biochimie, Université de Montréal, QC).

*Oligonucleotides and Saturation Mutagenesis*—Oligonucleotide primers used for mutagenesis were synthesized by Alpha DNA (Montréal, QC) and Integrated DNA Technologies (Coralville, IA). Oligonucleotide primers used for DNA sequencing were synthesized by Li-Cor Biotechnology (Lincoln, NB). The Y105X mutants of TEM-1 were constructed using the site overlap extension mutagenesis method (25). The 861-bp *bla*<sub>TEM-1</sub> gene was PCR-amplified from plasmid pBR322 using the terminal oligonucleotides BamHITEMF (5'-CACACAGGATCCACATGAGTATTCAACATTCCGT-3') and TEMHindIIIR (5'-ACACACAAGCTTTACCAATGCTTAATCAGTGA-3') containing the BamHI and HindIII restriction sites (underlined), respectively. The 19-amino acid possibilities at codon 105 were introduced by a set of three complementary pairs of degenerate oligonucleotides (only the coding strands are shown): TEM105NTSF (5'-ATGACTTGGTTGAGNTTCACCAGTCACAG-3'), TEM105NGSF (5'-ATGACTTGGTTGAGNGSTCACCAGTCACAG-3'), and VMS105F (5'-ATGACTTGGTTGAGVMSTCACCAGTCACAG-3'). The use of three separate degenerate oligonucleotides encoding the possibilities NTS, NGS, and VMS instead of a single NNS codon was justified by the elimination of the wild-type tyrosine residue as well as the three stop codons.

The recombinant TEM genes were digested with BamHI/HindIII and cloned into BamHI/HindIII-digested and calf intestinal alkaline phosphatase-treated pQE32Chl before electroporation into *E. coli* XL1-Blue cells. Colonies were individually picked after selection on a Luria-Bertani (LB) medium containing 12.5 µg/ml Chl, and the sequence of each mutant was confirmed by the dideoxy chain termination method with the Thermo Sequenase Cycle Sequencing kit (Upstate Biotechnology Corp., Cleveland, OH) using a dye-labeled primer and a Li-Cor automated sequencer (Lincoln, NB).

*Expression and Purification of Mutant  $\beta$ -Lactamases*—An overnight culture of each XL1-Blue/pQE32Chl-TEM(Y105X) clone was used to inoculate 50 ml of LB that was grown with agitation at 37 °C until  $A_{600\text{ nm}} = 0.6$ . After the addition of 1 mM isopropyl 1-thio- $\beta$ -D-galactopyranoside, the cultures were propagated for an additional 3 h. After induction, the cells were pelleted by centrifugation (30 min, 3000  $\times g$ , 4 °C), resuspended in 10 ml of 10 mM Tris-Cl buffer, pH 7.0, and separated in 1-ml aliquots. A gentle lysis of the outer membrane of *E. coli* was performed by 3–4 1.5-min freeze-thaw cycles using a dry ice/ethanol and a 37 °C water bath followed by a centrifugation (15 min, 20,000  $\times g$ , 4 °C) to collect the supernatant.

Purification of TEM(Y105X) mutants of interest was performed according to the following single-step anion-exchange chromatography procedure. All steps were undertaken at 4 °C with a flow rate of 1 ml/min on a System Gold high performance liquid chromatography apparatus (Beckman Coulter Canada, Inc., Mississauga, ON). Supernatant (10 ml) was applied to a DEAE-Sepharose column (2  $\times$  25 cm) followed by a wash of 2.5 column volumes with 10 mM Tris-Cl, pH 7.0, buffer. Mutant enzymes were eluted with a linear gradient of 10–150 mM Tris-Cl, pH 7.0, buffer (1.5 column volume), and a subsequent wash with the same buffer was finally performed (2.5 column volumes). Fractions containing  $\beta$ -lactamase activity were identified by a qualitative nitrocefin hydrolysis test and pooled for subsequent analysis. Aliquots of each clone were analyzed by SDS-PAGE gel, and the purity was estimated in all cases to be between 80 and 90% using the public domain image analysis software Scion Image (National Institutes of Health, rsb.info.nih.gov/nih-image). The column was regenerated by applying 5 volumes of 8 M urea followed by 5 volumes of 10 mM Tris-Cl, pH 7.0, buffer between each purification. No significant  $\beta$ -lactamase activity carryover was detected by nitrocefin assay upon running a mock purification (cells expressing no TEM-1  $\beta$ -lactamase) following a purification of the native TEM-1.

*Antibiotic Susceptibility*—Minimum inhibitory concentrations (MICs) were determined by broth microdilutions according to Cantu *et al.* (26). The ranges of antibiotic concentrations tested were as follows (by stepwise 2-fold increases): 125–4000 µg/ml for benzylpenicillin and ampicillin, 4–500 µg/ml for cephalothin, 1–125 µg/ml for cefazolin, and 4–500 ng/ml for cefotaxime. Each MIC determination was performed at least in triplicate in independent experiments.

*Enzyme Kinetics*—The kinetic constants  $K_m$  and  $k_{\text{cat}}$  for benzylpenicillin and cephalothin were determined at room temperature in 50 mM sodium phosphate buffer, pH 7.0, for the mutants presented in Table 2.3. The following extinction coefficients (27) and concentration ranges were used:  $\Delta\varepsilon_{232 \text{ nm}} = 1100 \text{ M}^{-1} \text{ cm}^{-1}$  for benzylpenicillin (50–200 µM) and  $\Delta\varepsilon_{262 \text{ nm}} = 7960 \text{ M}^{-1} \text{ cm}^{-1}$  for cephalothin (30–300 µM). Substrate hydrolysis was monitored according to initial steady-state velocities for a minimum of six substrate concentrations generally flanking the  $K_m$  values (when the molar extinction coefficients and the  $K_m$  value allowed it) using a Cary 100 Bio UV-visible spectrophotometer (Varian Canada, Inc., Montréal, QC). For each assay the concentration of enzyme was kept at least 500 times lower than substrate for benzylpenicillin (BZ) and was generally 50 times lower for cephalothin (CF). The kinetic parameters were determined from the rates of hydrolysis calculated from the initial linear portion of the curve and fitted to a Lineweaver-Burk ( $1/[S]$  versus  $1/[V]$ ) and a Hanes ( $[S]$  versus  $[S]/V$ ) plot. In most cases initial rates were also analyzed with the software Graphpad Prism (Graphpad Software, San Diego, CA) by a non-linear regression curve corresponding to the Michaelis-Menten equation. The  $k_{\text{cat}}$  parameter was determined using the equation  $k_{\text{cat}} = V_{\text{max}}/[E]$ , where the concentration of enzyme was determined by a Bio-Rad protein assay kit (Bio-Rad) taking into account its purity, estimated as described above.

*Computer Modeling*—All computations were performed with the InsightII package, version 2000 (Accelrys, San Diego, CA). The BIOPOLYMER module was used to modify molecular structures, and all energy minimizations and molecular dynamics calculations

were performed with the DISCOVER module using the consistent valence force field. The dynamic trajectories were analyzed using the DECIPHER module. We performed the simulations with the coordinates of an acyl-enzyme intermediate of TEM-1 complexed with benzylpenicillin (BZ), and we created an acyl-enzyme model of TEM-1 complexed with CF to compare the behavior of this substrate with that observed for BZ over the course of a 200-ps dynamics. We also conducted molecular dynamics studies using the coordinates of an apoenzyme structure of TEM-1 with residue 105 mutated, to assess conformation before substrate binding. Comparison of these systems (BZ acyl-enzyme, CF acyl-enzyme, and apoenzyme) allowed for the evaluation of the conformation of residue 105 before and after substrate recognition.

The 1.8-Å crystallographic structure of the *E. coli* TEM-1 β-lactamase (Protein Data Bank, Brookhaven National Laboratory, code 1BTL) (28) was used for the starting coordinates for apoenzyme calculations, and the 1.7-Å crystallographic structure of a E166N deacylation-defective mutant of the same enzyme (PDB code 1FQG) (8) was used for the starting coordinates for calculations involving benzylpenicillin-bound enzyme. The crystallographic water molecules of both enzymes were conserved. The active site SO<sub>4</sub><sup>2-</sup> molecule was deleted from 1BTL, and the E166N mutation of 1FQG was reverted to wild type. Hydrogen atoms were added at the normal ionization state of the amino acids at pH 7.0. For 1FQG, the atomic potentials of the BZ substrate were fixed according to the consistent valence force field atom types recommended by the manufacturer. These coordinates served as the starting points for all the subsequent calculations in presence (1FQG) or absence (1BTL) of BZ.

The Y105G, Y105L, Y105N, Y105Q, Y105R, and Y105W mutations were introduced. Before minimization, the tryptophan side chain was repositioned according to the crystal structure of the structurally homologous Class A PER-1 β-lactamase (PDB code 1E25) (9). Residues contained in a simulation area within 15 Å from any atom of BZ (1FQG) or residue 105 (1BTL) were allowed to move as well as the loop encompassing

residues 96–116, with the remainder of the protein being fixed. A layer of 5 Å of explicit water was added to the surface of this assembly, and a nonbonded cutoff of 20 Å was fixed to reduce the time of calculation. Each structure was energy-minimized by applying 100 steps of steepest descents followed by a conjugate gradient minimization until convergence of 0.001 kcal mol<sup>-1</sup> Å<sup>-1</sup>. A short molecular dynamics simulation was performed starting from the energy-minimized structures. Accordingly, the molecular system was allowed to equilibrate at 310 K for 100 fs followed by the actual simulation to explore conformational space for 200 ps at the same temperature (time step = 1 fs). Snapshots were taken each picosecond, generating 201 different conformers. At this point the trajectories obtained for each mutant were analyzed.

To create the acyl-enzyme intermediate models of TEM-1 with cephalothin (TEM-CF and Y105G-CF), the atomic coordinates of CF were taken from the crystal structure of an acyl-enzyme intermediate of TOHO-1 β-lactamase (PDB code 1IYP) (10) and fitted to the 1.8-Å crystallographic structure of the *E. coli* TEM-1 β-lactamase (PDB code 1BTL). The active site SO<sub>4</sub><sup>2-</sup> molecule was deleted from 1BTL, and the CF substrate was positioned according to BZ in 1FQG by applying torsions to the Cβ-Oγ bond of Ser-70. Hydrogen atoms were adjusted to pH 7, and the atomic potentials of CF were adjusted as described herein. An energy minimization was performed on this structure by applying 100 steps of steepest descents followed by a conjugate gradient minimization until convergence of 0.001 kcal mol<sup>-1</sup> Å<sup>-1</sup>. This structure served as the starting coordinate for all subsequent steps of minimization and dynamics studies, which were performed as described above.

## RESULTS

*Antibiotic Susceptibility*—We mutated position 105 (Tyr) of TEM-1 β-lactamase to the 19 other possibilities and confirmed through DNA sequencing of the entire gene that no

secondary mutations had occurred. To assess the effect of the Y105X replacements on the capacity of TEM-1 to hydrolyze penicillin-type and cephalosporin antibiotics, MICs were calculated for *E. coli* XL1-Blue cells alone or expressing TEM-1 mutants. The antibiotics used are presented in Fig. 2.1. Table 2.1 presents MIC values determined for all mutants toward two classical penicillin-type substrates, BZ and ampicillin (AMP) as well as two typical first-generation cephalosporins, cephalothin (CF) and cefazolin (CZ). Thus, *in vivo* cell survival at higher antibiotic concentrations reflects a higher rate of hydrolysis by the enzyme. Because they are performed *in vivo*, MIC values serve as points of comparison rather than precise values and do not directly correlate with the  $K_m$  or  $k_{cat}$  parameters of each mutant enzyme. They nevertheless offer a rapid, qualitative assessment of the efficiency of mutants and allow for the identification of mutants deemed to be the most interesting with respect to detailed kinetic analysis.

As seen in Table 2.1, the range of resistance is higher for the penicillin substrates (500–4000 µg/ml for BZ and 500–7500 µg/ml for AMP) than for the cephalosporin substrates (16–125 µg/ml for CF and 4–250 µg/ml for CZ). This result was expected since Class A β-lactamases hydrolyze penicillins much more efficiently than cephalosporins, the latter having been historically developed to counteract the appearance of natural resistance to penicillins (29, 30). Nonetheless, the 20 mutants allow for a comparable breadth of resistance with respect to these four substrates. Thus, the ratio between the least and the most active mutants for BZ hydrolysis is approximately one order of magnitude (500 µg/ml relative to 4000 µg/ml), similar to that observed for CF hydrolysis (16 µg/ml relative to 125 µg/ml). AMP and CZ allow for slightly broader ranges but remain in the same range of resistance as BZ and CF, respectively.

This breadth of resistance illustrates that position 105 replacements can alter enzyme efficiency up to a factor of 10-fold. Nonetheless, this relatively weak effect confirms previous observations suggesting that position 105 cannot be considered essential for enzyme catalysis in Class A β-lactamases (15, 31). To understand the source of the

effect, we examined the following hypotheses; (a) disparity in enzyme solubility conferred by the Y105X replacements, (b) changes in periplasmic localization efficiency of some Y105X mutants, (c) an active site cavity disruption modifying substrate recognition or catalytic turnover. We verified that the mutations at position 105 have little effect on solubility and on periplasmic localization by quantifying the soluble expression levels for each Y105X mutant after outer-membrane lysis. The soluble, periplasmic  $\beta$ -lactamase concentration observed by SDS-PAGE for all Y105X mutants was within a factor of 2 relative to the wild-type enzyme. The small variations observed did not correlate with the MIC results and are most likely slight clonal variations (data not shown). This result indicates that the mutations at position 105 do not significantly affect solubility or periplasmic localization, suggesting little impact on enzyme structure. This observation is consistent with previous results of circular dichroism studies on the Y105F mutant of the Class A  $\beta$ -lactamase of *B. licheniformis* (15). Thus, these results imply that the Y105X replacements have an effect on substrate recognition and/or turnover in the active site of TEM-1.

A considerable number of mutants confer antibiotic resistance in the same range (or higher) as the wild-type enzyme for all of the substrates tested. This provides confirmation that position 105 does not need to be strictly conserved for enzyme activity and suggests that the observed differences in activity may result from a structural disturbance within the active site cleft that alters substrate recognition. It is striking to note that only aromatic replacements as well as Asn and the small residues Ala and Gly in some cases allow for survival rates in the same antibiotic concentration range as the wild-type enzyme for the four substrates tested. Notwithstanding a general similarity in the effects of the mutations toward penicillin-type and cephalosporin substrates, important differences were observed. Thus, Table 2.1 shows that all Y105X mutants confer at least a minimal resistance to BZ and AMP, which is not the case for CF and CZ. For instance, the lowest MIC recorded for BZ (Y105D) still confers a resistance to this antibiotic at least four times higher than the *E. coli* cells alone. On the contrary the majority of Y105X mutants was unable to confer any

survival over background in the presence of CF or conferred at most a 2-fold higher MIC than background toward CZ. These results demonstrate that the Y105X replacements are more deleterious toward turnover of the cephalosporin substrates than they are for the penicillin counterparts.

All except one of the highly active Y105X mutations (Ala) are found at the corresponding position in other natural Class A  $\beta$ -lactamases, which have a strong preference for aromatic residues, although Asn and Gly have also been identified to date (Table 2.2). Accordingly, the Y105X mutants show a high *in vivo* antibiotic resistance bias for aromatic residues as well as Asn at position 105 for all the substrates tested. The occurrence of Asn and two small, non-polar residues (Ala and Gly) among the most highly BZ- and AMP-resistant mutants confirms that aromatic residues are not essential for hydrolysis of penicillins. This relation is not so clear in the case of cephalosporin resistance, where the Ala and Gly mutants are in the lower portion of the resistance spectrum for CF and CZ, suggesting that the identity of the residue at position 105 may participate in ligand selectivity.

For BZ and AMP recognition, no charged mutant (Lys, Arg, Asp, and Glu) allowed for cell growth at concentrations greater than half that displayed by the native enzyme, whereas for CF and CZ, these mutants conferred a resistance to concentrations 4 and 8 times lower than the parental enzyme, respectively. These results suggest that aromatic residues as well as Asn at position 105 participate in substrate recognition or turnover, perhaps by providing favourable interactions with the substrate, whereas in the case of other residues at position 105 the interactions would be detrimental or simply absent.

To characterize the impact of Y105X mutations toward recognition of higher generation cephalosporins, MIC values were also determined for cefotaxime, a third generation cephalosporin substrate that is not efficiently recognized by wild-type TEM-1

(2). No cell survival above background for *E. coli* XL1-Blue cells was observed for the parental enzyme or for any Y105X mutant (results not shown).

*Enzyme Kinetics*—The MIC values for various antibiotics allowed us to identify specific Y105X mutants of interest for further enzymatic characterization, notably the Trp, Asn, Gly, Arg, and Asp mutants. Trp was chosen because of its aromatic similarity with the native Tyr, its high *in vivo* activity, and also because of its frequent occurrence in other Class A  $\beta$ -lactamases (Table 2.2). Asn was chosen because its side chain is non-aromatic and much smaller while still being a highly active mutant also occasionally represented in other Class A  $\beta$ -lactamases. To our knowledge Gly has been identified in one Class A  $\beta$ -lactamase (Table 2.2) and was selected because, like Ala, its *in vivo* behavior is different toward penicillins and cephalosporins. Finally, Asp and Arg are two charged residues that were chosen because of their low *in vivo* activity. Neither of the latter residues has been identified at position 105 in Class A  $\beta$ -lactamases. We performed the *in vitro* assays using BZ and CF as representatives of the penicillin and first generation cephalosporin substrate classes, respectively.

The steady-state kinetic parameters for native TEM-1 and the five selected mutants were calculated for BZ and CF (Table 2.3). The greater catalytic efficiency ( $k_{\text{cat}}/K_m$ ) of the wild-type TEM-1 for BZ is attributed to a 4-fold decrease in  $K_m$  and a 12-fold increase in  $k_{\text{cat}}$  toward BZ hydrolysis relative to CF. The most active mutant tested (Y105W) has a catalytic efficiency in the same range as the native enzyme, whereas the least active one (Y105D) displays a reduction of 2 orders of magnitude in its catalytic efficiency with respect to both substrates. Although both Y105G and Y105N have catalytic efficiencies 3–5 times lower than the wild-type enzyme for BZ, their kinetic properties with respect to CF hydrolysis are not alike. Indeed, although Y105N is 3-fold less efficient than the wild-type enzyme, the efficiency of Y105G drops to a value that is 20-fold lower for CF hydrolysis as a result of a significant  $K_m$  increase. The different effect of the Y105G mutation on  $K_m$  values for the two antibiotics indicates that the Y105G mutant behaves in a different manner

with respect to penicillin and cephalosporin recognition, confirming the trend that was observed in the MIC determinations.

In general, the deleterious effects of many of the Y105X mutations on catalytic efficiency is the result of a greater disruption of  $K_m$  than  $k_{cat}$ , although this trend is more pronounced for CF hydrolysis than for BZ. The greatest  $k_{cat}$  decreases observed were for BZ hydrolysis for the Y105R and Y105D mutants, which display a turnover number ( $k_{cat}$ ) ~2.5 and 5 times lower than the parental enzyme, respectively. However, Y105G, Y105N, and Y105W hydrolyze the penicillin at maximal rates ±30% relative to the native enzyme. With respect to  $K_m$ , the most active mutant (Y105W) shows a 2-fold decrease in  $K_m$  compared with the parental enzyme. Other mutants show important  $K_m$  increases that range from 3.5-fold (Y105G and Y105R) to 8.6-fold differences (Y105D). These combined effects on  $k_{cat}$  and  $K_m$  result in catalytic efficiencies for BZ hydrolysis that range between 20 and 130% of wild-type TEM-1 for mutants Y105G, Y105N, and Y105W, which showed native-like BZ MICs, whereas Y105R (12%) and Y105D (2%) are also less efficient *in vivo* (Table 2.1). These results indicate that position 105 mutants displaying a catalytic efficiency approximately one-fifth or higher than that of the wild-type enzyme (Y105G, Y105N, Y105W) confer *in vivo* survival rates in the same range as the wild-type parent for BZ hydrolysis, whereas those with lower efficiency (Y105R, Y105D) result in poor *in vivo* performance. Thus, the  $K_m$  of Y105R may define a threshold below which there is enough productive binding *in vivo* to guarantee drug resistance.

Although the five characterized mutants hydrolyze CF with a  $k_{cat}$  that remains within 50–100% of the wild-type enzyme,  $K_m$  is modified much more importantly. As with BZ, the most active mutant (Y105W) shows a 2-fold decrease in  $K_m$  compared with the parental enzyme for CF hydrolysis. However, the other mutants show  $K_m$  increases ranging from 1.7 (Y105N)- to 16.2 (Y105D)-fold higher than the wild-type enzyme.  $K_m$  differences are, thus, the greatest contributor to the differences seen in the catalytic efficiency of every mutant

tested for CF hydrolysis, confirming the implication of Tyr-105 in CF recognition by TEM-1  $\beta$ -lactamase.

Moreover, the comparison of  $k_{\text{cat}}$  and  $K_m$  of the best and the worst mutants toward CF and BZ hydrolysis demonstrates the importance of residue 105 with respect to affinity as opposed to catalysis. In fact, although  $k_{\text{cat}}$  differs by 4.9-fold for BZ and 2.3-fold for CF when comparing the best and the worst mutants with respect to  $k_{\text{cat}}$  (wild-type/Y105D for BZ, wild-type/Y105G for CF), the comparison of  $K_m$  values yields differences of 16-fold for BZ and 39-fold for CF (Y105D/Y105W for BZ and CF). These observations lend further support to previously published results describing the Y105F mutant of the *B. licheniformis*  $\beta$ -lactamase, which suggested that the main effect on activity was on substrate binding as a result of a 3–4-fold increase in  $K_m$  (15). Although  $K_m$  for BZ hydrolysis does not vary as much as for CF hydrolysis,  $k_{\text{cat}}$  is affected to a somewhat greater extent for less active mutants. These differences suggest that residue 105 may be a weak substrate determinant in TEM-1, participating in substrate stabilization and providing an element of selectivity in the recognition of penicillins and cephalosporins. To further investigate the *in vivo* and *in vitro* results obtained with BZ and CF as representatives of the penicillin and cephalosporin substrate classes, molecular dynamics studies were undertaken with selected TEM-1  $\beta$ -lactamase mutants in the presence and in the absence of these substrates.

*Computational Models*—Tyrosine 105 is a solvent-exposed active site residue with a side-chain conformation that is structurally conserved among almost all Class A  $\beta$ -lactamases of known structure. Fig. 2.2 shows the superimposition of residues 104–107 of the crystal structures of five Class A  $\beta$ -lactamases found in natural isolates harboring different residues at position 105 (Tyr, Trp, His, Asn, and Gly). Of these five structures only TEM-1 is complexed with a substrate molecule (BZ). In all cases, this 104–107-residue area defines one of the walls in contact with the substrate and constitutes the turn within a relatively rigid loop-helix motif encompassing residues 96–116. Although the side chain of residue 104 is quite flexible, residues 106 and 107 have a structurally conserved

conformation, as does position 105, unless it is an Asn. In all cases the side chain of residue 106 points toward the interior of the 96–116 loop-motif as a result of the sequence-conserved Pro107 (Table 2.2) creating a characteristic distorted Type-I  $\beta$ -turn in the structure (23, 24, 28). When the residue at position 105 is aromatic, it always lines up in an edge-to-face manner against Pro-107 (Fig. 2.2). However, Asn-105 of the *Mycobacterium fortuitum* enzyme points away from the motif directly toward the active site cavity. Despite the absence of a side chain in the *Streptomyces albus G* enzyme (which harbors Gly at position 105), it is interesting to note that the turn is conserved and that the shape of the 104–107 element is unaltered. This suggests that the identity of the residue at position 105 does not determine or greatly influence this helix-loop conformational bend. The structural homology in these natural  $\beta$ -lactamases with varying residues at position 105 is consistent with our observation that Y105X mutations did not have drastic effects on TEM-1 structure, as evidenced both by conservation of the protein solubility and by retention of at least a fraction of substrate recognition and catalytic capacity. Consequently, we performed molecular dynamics simulations of the Y105X mutations in TEM-1, assuming that no gross structural changes had occurred.

The Trp, Asn, Gly, Arg, Gln, and Leu mutants of TEM-1 in the presence of BZ were studied for the following reasons; Trp, as a positive control for highly active, aromatic residues; Asn, because of its native-like activity despite its small, non-aromatic side chain; Gly (with BZ and CF), because of its different kinetic behavior toward those substrates despite the lack of a side chain; Arg, as a weakly active mutant with a bulky and charged side chain; Gln, as a weakly active mutant structurally similar to the highly active Asn; and finally Leu, as a weakly active mutant with a neutral and branched side chain. In all models the backbone of the entire 96–116 loop-motif displayed little motion during the 200-ps dynamics simulation (root mean square deviation <0.86 Å). Throughout the dynamics, Tyr-105 is rigidly positioned in the center of an ~8-Å-wide cavity between Pro-107 and the substrate molecule in a manner that is quite similar to the crystallographically determined

conformation of other position 105 aromatic residues in Class A  $\beta$ -lactamases (Fig. 2.2). The BZ substrate also shows little motion relative to the crystal structure (root mean square deviation  $\leq 1 \text{ \AA}$ ). Previous studies suggest that this precise positioning of the aromatic moiety of Tyr-105 allows it to stack between Pro-107 and the thiazolidine ring of the substrate, although the nature of the proposed interaction has not been described in detail (21, 22). Our modeling results show that the distances maintained between the phenol ring of Tyr-105 and the thiazolidine ring on one side and Pro-107 on the other ( $\sim 3.5 \text{ \AA}$  on both sides) and the nature of the proximal atoms are consistent with van der Waals interactions. Furthermore, no significant difference was observed in the free-form model of TEM-1 regarding rigidity or conformation of Tyr-105 (not shown).

Thus, the aromatic side chain of Tyr-105 forms a “wall” preventing the thiazolidine ring of BZ from moving into the small cavity facing Pro107 (Fig. 2.3A). The Trp mutation (Fig. 2.3A) behaves in the same manner as the wild-type enzyme, which is consistent with the native-like *in vivo* and *in vitro* activities observed for the Y105W mutant and is also consistent with high productive binding reflected by low  $K_m$  values (2-fold decrease for CF and BZ). Although the side chain of Asn is considerably smaller than the aromatic residues, the Y105N mutation appears to behave in a very homologous manner, positioning the planar, structurally constrained  $\gamma$ -amide group parallel to the conformation adopted by the modeled aromatic side-chains Tyr and Trp (Fig. 2.3A). This again forms a wall in front of Pro-107, preventing the substrate from moving from its original position toward Pro-107, consistent with the high survival rates observed in the MIC determinations for the Y105N mutant.

In contrast with those mutations, the Y105G replacement leaves the active site cavity considerably more open (Fig. 2.4). Over the course of the 200-ps trajectory, the thiazolidine ring of BZ fills the cavity facing Pro-107, where it remains relatively rigid once placed in this alternate position. Accordingly,  $k_{\text{cat}}$  is unaffected, whereas  $K_m$  increases by a factor of 3.5-fold. Nevertheless, these modifications have virtually no impact on the

survival rate of this mutant with respect to BZ hydrolysis. On the other hand, CF recognition is more strongly affected by the mutation to glycine, as can be seen by the 9.2-fold increase in  $K_m$  coupled to a 2-fold drop in  $k_{cat}$ , which correlates with the low survival rates conferred by the Y105G mutant with respect to CF hydrolysis. To better characterize the *in vivo* and *in vitro* differences observed for BZ and CF with the Y105G mutant, we performed molecular dynamics studies with a TEM-1 model complexed with CF for the wild-type enzyme (Tyr-105) and for Y105G (not shown). Although we observe subtle differences in the positioning of CF relative to BZ, our models do not offer a clear explanation for the high substrate discrimination conferred by the Y105G mutant with respect to BZ and CF.

Most other residue replacements at position 105 had a detrimental effect on TEM-1 activity toward both penicillins and cephalosporins. After a 200-ps dynamics simulation performed with BZ for Arg or Gln at position 105, we observed large differences relative to position 105 mutants Trp, Asn, and Gly. The Arg-105 side chain rapidly shifts toward the entrance of the active site cavity, placing the charged group in direct contact with the solvent (results not shown). Consequently, the Arg side chain does not create the previously described physical barrier between BZ and Pro-107 in the same manner as the higher activity enzymes (Tyr, Trp, Asn). The resulting shift in the substrate is constrained by the presence of the long aliphatic side chain of Arg, which results in important steric interactions with the substrate molecule. Thus, a greater lateral movement of the BZ substrate is observed throughout the simulation, which may account for the 2.5-fold decrease observed in  $k_{cat}$ . In fact, the sulfur atom of the BZ thiazolidine ring in the Y105R mutant moves 2.65 Å from its original position during the 200-ps simulation relative to 0.36 Å for the wild-type complex. It should be noted that the Arg-105 side chain also shifts toward the entrance of the active site cavity in the absence of BZ, suggesting that solvation of the guanidinium group (rather than steric hindrance of the bound substrate) promotes this shift.

In the case of the Y105L mutant (Fig. 2.3B), the side chain of Leu is very flexible throughout the 200-ps trajectory (root mean square deviation = 1.35 Å as opposed to root mean square deviation values <0.8 Å for all other modeled mutants), possibly disrupting the efficient binding and stabilization of the substrate in the active site cavity. Similarly, we observed that the amide side chain of Gln is unable to adopt the parallel conformation shown for the aromatic and Asn mutants as a result of its greater length and flexibility (not shown). It is worth noting that both of these mutations (Leu and Gln) have a greater effect on the MIC values of cephalosporins than penicillins, suggesting that the bulkier dihydrothiazine ring of cephalosporin substrates does not support as much flexibility at position 105 than the thiazolidine ring of penicillin substrates. Taken with the poor MIC results of all other non-aromatic, branched mutations (with the exception of Asn), this suggests that a greater side-chain flexibility and size conferred by branched residues at position 105 have a detrimental effect on substrate binding. By conserving the planar conformation lined up against Pro-107, small or aromatic residues would prevent steric interactions with the substrate by forming a stabilizing wall that restricts the active site cavity size and, thus, substrate movement.

Finally, by monitoring the dynamics trajectory of the Y105X mutants in the presence and absence of BZ, we determined that the whole-residue distance between residues 105 and 107 for aromatics (Tyr, Trp) is ~1 Å wider in the absence than in the presence of substrate. This difference is less pronounced (~0.5 Å) for the Asn mutant but is not discernible for three other mutants tested (Gly, Arg, Gln). The difference in distance ( $\pm$ substrate) appears to be correlated to *in vivo* and *in vitro* activity, further suggesting a role for residue 105 in substrate stabilization at the active site.

## DISCUSSION

The results we have obtained indicate that the nature of the residue at position 105 in TEM-1  $\beta$ -lactamase has an important effect on substrate recognition and stabilization at the active site. Stabilizing effects have been previously proposed for Tyr-105 with respect to substrates and inhibitors. Notably, Mobashery and co-workers (32, 33) suggest the existence of a hydrophobic pocket created by the side chains of Tyr-105 and Val-216 in TEM-1, whereas other studies on Class A enzymes pointed out that the hydroxyphenyl group of Tyr-105 was within van der Waals distance of the thiazolidine ring of penicillin substrates or inhibitors (9, 18, 34, 35). Consequently, these crystal structure observations have led to the suggestion that Tyr-105 “stacks” with the thiazolidine ring of BZ or inhibitors (21, 22). Our studies suggest that the strong bias for aromatic residues at position 105 is not a functional prerequisite of hydrophobicity so much as a structural necessity to prevent unfavorable substrate displacement within the active site. This hypothesis is strengthened by the polar Asn side chain of the Y105N mutant, whose activity is in the same range as the wild-type enzyme for all substrates tested. Thus, polarity can be tolerated at position 105 as long as the residue causes no perturbation to substrate positioning. Moreover, as evidenced by comparing the relatively high penicillin hydrolysis of the Y105G, Y105N, Y105S mutants with the more hydrophobic Y105C mutant, hydrophobicity cannot be considered as a variable defining the stabilizing interaction conferred by Tyr-105 in TEM-1 and other Class A  $\beta$ -lactamases.

Aromatic residues and Asn would, thus, be favored at position 105 because of the intrinsic planarity of their side chains, which enables them to adopt a structurally “non-destructive” conformation where they fill the small cavity between the thiol ring of the substrate on one side and Pro-107 on the other, preventing extensive motion of the substrate within the active site cavity. This wall, formed by Tyr-105, has previously been suggested as an important determinant in clavulanate susceptibility for several Class A enzymes (23),

although this assertion needs more thorough investigation with respect to the susceptibility of Class A  $\beta$ -lactamases that do not harbor an aromatic residue at position 105. Because the Asp mutant would also be able to adopt the same planar conformation as that of Asn, it is reasonable to assume that the low *in vivo* and *in vitro* activities observed for Y105D with all the substrates tested is related to its negative charge. The presence of the wild-type glutamate residue at position 104 coupled to the Y105D mutation would generate a strong negative potential, which may account for the altered kinetic parameters. Finally, the side chains of other residues appear to be disfavored at position 105 as a result of their bulkier size, charge, and/or their inability to retain the particular non-destructive planar conformation described herein, which prevents unfavorable steric clashes of residue 105 with the substrate. Hence, small residues create a gap in this barrier, allowing for greater substrate displacement within the active site cavity, whereas larger and non-planar residues (except Asn) are too bulky and/or possess too many degrees of freedom to adopt this barrier conformation, interfering with productive substrate positioning. In the evolutionary context of this particular residue, our results are in accordance with the non-planar and bulky amino acids naturally excluded from this position, as their physical characteristics constitute a clear disadvantage with respect to catalytic efficiency, as opposed to the strongly conserved, structurally non-destructive residues (aromatics, Gly, Asn) found at position 105 in all Class A  $\beta$ -lactamases (Table 2.2). As noted above, we were unable to select a Y105X mutation of TEM-1 that allowed recognition of a higher generation cephalosporin. That the conformation of residue 105 is not in the immediate vicinity of the bulky C7 side chain of third-generation cephalosporins (Fig. 2.1) suggests this residue may not be a primary target for future adaptive mutations found in natural isolates of TEM variants.

Although the planar characteristic conferred by aromatic residues and Asn at position 105 appears to be essential for efficient cephalosporin hydrolysis, it is not a definitive requirement of high activity for penicillin substrates since high survival rates are additionally observed for mutants with small amino acid side chains at position 105 (Y105G and Y105A). This observation suggests that cephalosporin stabilization in the

active site of TEM-1 is more precarious and requires a greater structural integrity of the active site than penicillin substrates. This difference in recognition and stabilization may be attributed to the greater size of the 6-membered dihydrothiazine ring of cephalosporins coupled to the fact that these substrates always harbor a bulkier C3 substituent compared with the smaller, less substituted 5-membered thiazolidine ring of penicillins. Aromaticity, although not essential, may still contribute to affinity since the elimination of the aromatic moiety at position 105 results in  $K_m$  increases that could be explained by the loss of weak stabilizing forces conferred by aromatic residues. Accordingly, the lower  $K_m$  values observed toward BZ and CF for the Y105W mutant may result from the higher electron density of the Trp indole side chain compared with the hydroxyphenyl moiety of Tyr, resulting in stronger van der Waals contacts of the indole side chain with the substrate.

In the wild-type enzyme, ion-pairing interactions (36) and hydrogen bonding (37) of the C3 (C4) carboxylate group of substrates to the guanidinium group of Arg-244 have been suggested to play a role in stabilizing the substrate in the ground and transition states, although these assumptions have been the subject of debate (2, 4). Although our model of the acyl-enzyme intermediate cannot account for ground or transition states, the wild-type acyl-enzyme with BZ or CF supports this hypothesis by confirming the maintenance of appropriate distances between Arg-244 and the C3 (C4) carboxylic acid groups of both substrates throughout the 200-ps dynamics (shown in Fig. 2.4A for BZ). However, the large shift of the thiol rings of both BZ and CF observed for the Y105G mutant prevents any direct hydrogen bonding or ion-paring interaction of the C3 (C4) carboxylate moieties of substrates with Arg-244 as a result of increased distances (Fig. 2.4B). Should the increased distance also exist at the ground or transition states, this suggests either that interaction with Arg-244 is not essential for activity or that a bridging water molecule (as proposed by various authors (Ref. 4 and references therein)) would be displaced concurrently with the substrate, since the Y105G mutant is highly active for BZ hydrolysis.

We observed that the amide of Asn is positioned differently in the modeled, ligand-bound Y105N mutant and in the free-form crystal of the *M. fortuitum* enzyme. This suggests that the position of residue 105 is different in the free and ligand-bound enzymes, possibly as a result of substrate binding. Our monitoring of the distance between residues 105 and 107 during the 200-ps dynamics trajectory of the Y105X mutants modeled in the presence and absence of BZ supports this hypothesis. The correlation between the difference in distance ( $\pm$ substrate) and *in vivo* and *in vitro* activity suggests that aromatic residues at position 105 (and Asn to a certain extent) adopt two distinct conformations in the presence and absence of substrate and could, thus, be a determinant of recognition for substrate stabilization. This conformational change is in agreement with backbone NMR relaxation studies of TEM-1 showing that residue 105 harbors a higher-than-average flexibility in solution.<sup>2</sup> Moreover, previously published crystal structures of inhibitor-bound Class A  $\beta$ -lactamases showed Tyr-105 as a potentially flexible residue harboring distinct positions in the free and inhibitor-bound enzymes (17–21). Recently, a 1-ns molecular dynamics simulation of TEM-1 with BZ showed that the side chain of Tyr-105 can flip in the same plane to make favorable contacts with the phenyl moiety of this substrate (12). Although the side chain of Tyr-105 does not display this important conformational shift in our shorter modeling studies of TEM-1, our results nevertheless suggest that Tyr-105 as well as highly active Y105X mutations adopt slightly differing conformations in the presence and in absence of substrate.

In conclusion, our systematic investigation of the *in vivo* and *in vitro* kinetic effects of Y105X mutants of TEM-1  $\beta$ -lactamase coupled to molecular dynamics simulations identify this residue as being involved in  $\beta$ -lactam substrate selectivity and stabilization at the active site. We propose that the residue at position 105 is most propitious to substrate binding when it can stably adopt a planar conformation between the substrate and the conserved Pro-107, whereas more flexible residues create unfavorable steric hindrance with the substrate. Polarity (but not charge) is tolerated, whereas reduction of bulk at this

position results in discrimination between penicillin and first-generation cephalosporin substrates. We obtain good agreement between *in vivo*, *in vitro*, and *in silico* results, which also correlate well with the natural diversity observed at this position among Class A  $\beta$ -lactamases, thus suggesting a basis for the evolutionary selection of residues adopting a non-destructive conformation at position 105 in Class A  $\beta$ -lactamases.

## FOOTNOTES

\* This work was supported by grants from the Natural Sciences and Engineering Research Council of Canada and the Fond Québécois de la Recherche sur la Nature et les Technologies. The costs of publication of this article were defrayed in part by the payment of page charges. This article must therefore be hereby marked "advertisement" in accordance with 18 U.S.C. Section 1734 solely to indicate this fact.

¶ To whom correspondence should be addressed. Tel.: 514-343-2124; Fax: 514-343-7586; E-mail: joelle.pelletier@umontreal.ca.

<sup>1</sup> The abbreviations used are: Chl, chloramphenicol; AMP, ampicillin; BZ, benzylpenicillin; CF, cephalothin; CZ, cefazolin; MIC, minimum inhibitory concentration.

<sup>2</sup> P.-Y. Savard and S. M. Gagné, Université Laval, Québec, QC, personal communication.

## ACKNOWLEDGMENTS

We are grateful to Prof. Natalie C. J. Strynadka (University of British Columbia, Vancouver, BC) and Pierre-Yves Savard and Prof. Stéphane M. Gagné (Université Laval, Québec, QC) for helpful discussions. We also thank Peter D. Pawelek (McGill University,

Montréal, QC) and Roberto A. Chica and Prof. Jeffrey W. Keillor (Université de Montréal, Montréal, QC) for careful reading of the manuscript.

## REFERENCES

1. Orenicia, M. C., Yoon, J. S., Ness, J. E., Stemmer, W. P., and Stevens, R. C. (2001) *Nat. Struct. Biol.* **8**, 238-242
2. Matagne, A., and Frère, J. M. (1995) *Biochim. Biophys. Acta* **1246**, 109-127
3. Matagne, A., Lamotte-Brasseur, J., and Frère, J. M. (1998) *Biochem. J.* **330**, 581-598
4. Knox, J. R. (1995) *Antimicrob. Agents Chemother.* **39**, 2593-2601
5. Yang, Y., Rasmussen, B. A., and Shlaes, D. M. (1999) *Pharmacol. Ther.* **83**, 141-151
6. Minasov, G., Wang, X., and Shoichet, B. K. (2002) *J. Am. Chem. Soc.* **124**, 5333-5340
7. Chen, C. C., and Herzberg, O. (2001) *Biochemistry* **40**, 2351-2358
8. Strynadka, N. C. J., Adachi, H., Jensen, S. E., Johns, K., Sielecki, A., Betzel, C., Sutoh, K., and James, M. N. G. (1992) *Nature* **359**, 700-705
9. Tranier, S., Bouthors, A. T., Maveyraud, L., Guillet, V., Sougakoff, W., and Samama, J. P. (2000) *J. Biol. Chem.* **275**, 28075-28082
10. Shimamura, T., Ibuka, A., Fushinobu, S., Wakagi, T., Ishiguro, M., Ishii, Y., and Matsuzawa, H. (2002) *J. Biol. Chem.* **277**, 46601-46608

11. Meroueh, S. O., Roblin, P., Golemi, D., Maveyraud, L., Vakulenko, S. B., Zhang, Y., Samama, J. P., and Mobashery, S. (2002) *J. Am. Chem. Soc.* **124**, 9422-9430
12. Díaz, N., Sordo, T. L., Merz, K. M., Jr., and Suárez, D. (2003) *J. Am. Chem. Soc.* **125**, 672-684
13. Castillo, R., Silla, E., and Tuñón, I. (2002) *J. Am. Chem. Soc.* **124**, 1809-1816
14. Abraham, E. P., and Chain, E. (1940) *Nature* **146**, 837
15. Escobar, W. A., Miller, J., and Fink, A. L. (1994) *Biochem. J.* **303**, 555-558
16. Di Gleria, K., Halliwell, C. M., Jacob, C., and Hill, H. A. (1997) *FEBS Lett.* **400**, 155-157
17. Chen, C. C., Rahil, J., Pratt, R. F., and Herzberg, O. (1993) *J. Mol. Biol.* **234**, 165-178
18. Guo, F., Huynh, J., Dmitrienko, G. I., Viswanatha, T., and Clarke, A. J. (1999) *Biochim. Biophys. Acta* **1431**, 132-147
19. Wang, X., Minasov, G., Blázquez, J., Caselli, E., Prati, F., and Shoichet, B. K. (2003) *Biochemistry* **42**, 8434-8444
20. Maveyraud, L., Mourey, L., Kotra, L. P., Pedelacq, J. D., Guillet, V., Mobashery, S., and Samama, J. P. (1998) *J. Am. Chem. Soc.* **120**, 9748-9752
21. Strynadka, N. C. J., Martin, R., Jensen, S. E., Gold, M., and Jones, J. B. (1996) *Nat. Struct. Biol.* **3**, 688-695
22. Strynadka, N. C. J., Jensen, S. E., Alzari, P. M., and James, M. N. G. (1996) *Nat. Struct. Biol.* **3**, 290-297

23. Page, M. G. F. (2000) *Drug Resist. Updat.* **3**, 109-125
24. Huang, W. Z., Petrosino, J., Hirsch, M., Shenkin, P. S., and Palzkill, T. (1996) *J. Mol. Biol.* **258**, 688-703
25. Ho, S. N., Hunt, H. D., Horton, R. M., Pullen, J. K., and Pease, L. R. (1989) *Gene (Amst.)* **77**, 51-59
26. Cantu, C., III, Huang, W., and Palzkill, T. (1996) *J. Biol. Chem.* **271**, 22538-22545
27. Bouthors, A. T., Dagoneau-Blanchard, N., Naas, T., Nordmann, P., Jarlier, V., and Sougakoff, W. (1998) *Biochem. J.* **330**, 1443-1449
28. Jelsch, C., Mourey, L., Masson, J. M., and Samama, J. P. (1993) *Proteins* **16**, 364-383
29. Bush, K., and Mobashery, S. (1998) *Adv. Exp. Med. Biol.* **456**, 71-98
30. Page, M. I. (1987) *Adv. Phys. Org. Chem.* **23**, 165-270
31. Wolozin, B. L., Myerowitz, R., and Pratt, R. F. (1982) *Biochim. Biophys. Acta* **701**, 153-163
32. Taibi-Tronche, P., Massova, I., Vakulenko, S. B., Lerner, S. A., and Mobashery, S. (1996) *J. Am. Chem. Soc.* **118**, 7441-7448
33. Bulychev, A., Obrien, M. E., Massova, I., Teng, M., Gibson, T. A., Miller, M. J., and Mobashery, S. (1995) *J. Am. Chem. Soc.* **117**, 5938-5943
34. Maveyraud, L., Massova, I., Birck, C., Miyashita, K., Samama, J. P., and Mobashery, S. (1996) *J. Am. Chem. Soc.* **118**, 7435-7440

35. Ness, S., Martin, R., Kindler, A. M., Paetzel, M., Gold, M., Jensen, S. E., Jones, J. B., and Strynadka, N. C. (2000) *Biochemistry* **39**, 5312-5321
36. Moews, P. C., Knox, J. R., Dideberg, O., Charlier, P., and Frère, J. M. (1990) *Proteins* **7**, 156-171
37. Zafaralla, G., Manavathu, E. K., Lerner, S. A., and Mobashery, S. (1992) *Biochemistry* **31**, 3847-3852
38. Dideberg, O., Charlier, P., Wery, J. P., Dehottay, P., Dusart, J., Erpicum, T., Frère, J. M., and Ghysen, J. M. (1987) *Biochem. J.* **245**, 911-913
39. Swarén, P., Maveyraud, L., Raquet, X., Cabantous, S., Duez, C., Pedelacq, J. D., Mariotte-Boyer, S., Mourey, L., Labia, R., Nicolas-Chanoine, M. H., Nordmann, P., Frère, J. M., and Samama, J. P. (1998) *J. Biol. Chem.* **273**, 26714-26721
40. Ambler, R. P., Coulson, A. F., Frère, J. M., Ghysen, J. M., Joris, B., Forsman, M., Levesque, R. C., Tiraby, G., and Waley, S. G. (1991) *Biochem. J.* **276**, 269-270

## TABLES

**Table 2.1.** MICs of *E. coli* XL1-Blue cells expressing TEM-1  $\beta$ -lactamase with Tyr-105 replacements.

MIC ( $\mu\text{g/ml}$ )	Benzylpenicillin (BZ) Amino Acid 105 <sup>a</sup>	Ampicillin (AMP) Amino Acid 105
7500		
4000	<u>A</u> , <b>F</b> , <u>G</u> , <b>H</b> , <u>N</u> , <b>W</b> , <b>Y</b>	<b>F</b> , <u>N</u> , <b>W</b> , <b>Y</b>
2000	<u>C</u> , <b>K</b> , M, P, <u>Q</u> , S	<u>C</u> , <b>D</b> , <u>G</u> , <b>H</b> , <b>K</b> , L, P, Q, S, T, V
1000	<b>E</b> , I, L, <b>R</b> , T, V	<b>E</b> , I, M
500	<b>D</b>	<b>R</b>
125	None <sup>b</sup>	None
MIC ( $\mu\text{g/ml}$ )	Cephalothin (CF) Amino Acid 105	Cefazolin (CZ) Amino Acid 105
250		<b>W</b>
125	<b>W</b> , <b>Y</b>	
63	<b>F</b> , <b>H</b> , <u>N</u>	<b>H</b> , <b>Y</b>
32	<b>D</b> , M, P	<b>F</b> , <u>N</u>
16	<u>A</u> , C, <b>E</b> , <u>G</u> , I, <b>K</b> , L, <u>Q</u> , <b>R</b> , S, T, V, None	<u>G</u> , P
8		<u>A</u> , C, <b>E</b> , I, <b>K</b> , M, <u>Q</u> , <b>R</b> , S, T, V
4		<b>D</b> , L, None

<sup>a</sup> Aromatic residues are boxed in bold, and charged residues are boxed in white. Residues Asn and Gln are in italics, and Ala and Gly are underlined.

<sup>b</sup> *E. coli* XL1-Blue

**Table 2.2.** Sequence alignment of residues 103–107 for major representatives of Class-A  $\beta$ -lactamase. Data were compiled from previously published reports (9, 40).

Enzyme	Residue number <sup>a</sup>				
	103	104	<b>105</b>	106	107
TEM-1	V	E	<b>Y</b>	S	P
SHV-1	V	D	<b>Y</b>	S	P
TOHO-1	V	N	<b>Y</b>	N	P
PC-1	V	A	<b>Y</b>	S	P
PSE-4	V	T	<b>Y</b>	S	P
<i>P. aeruginosa</i>	V	T	<b>Y</b>	S	P
<i>S. aureus</i>	V	A	<b>Y</b>	S	P
<i>B. licheniformis</i>	V	N	<b>Y</b>	N	P
<i>B. cereus</i> III	S	N	<b>Y</b>	N	P
PER-1 <sup>b</sup>	L	T	<b>W</b>	A	P
VEB-1 <sup>b</sup>	L	T	<b>W</b>	S	P
<i>K. oxytoca</i>	V	V	<b>W</b>	S	P
CME-1 <sup>b</sup>	L	T	<b>W</b>	S	P
NMC-A	E	F	<b>H</b>	S	P
IMI-1	E	F	<b>H</b>	S	P
SME-1	E	Y	<b>H</b>	S	P
<i>M. fortuitum</i>	V	P	<b>N</b>	S	P
<i>S. cacaoi blaU</i>	V	D	<b>N</b>	S	P
<i>S. albus</i> G	E	D	<b>G</b>	A	P
<i>S. laventulae</i>	-	-	<b>F</b>	G	P

<sup>a</sup> Residue numbering according to Ambler *et al.* (40)

<sup>b</sup> These  $\beta$ -lactamases harbor a three-residue insertion between positions 103 and 104

**Table 2.3.** Kinetic parameters for wild-type TEM-1  $\beta$ -lactamase and Y105X mutant derivatives.

Substrate	TEM-1 variant	$k_{cat}$ ( $s^{-1}$ )	$k_{cat}$ <i>relative</i>	$K_m$ ( $\mu M$ )	$K_m$ <i>relative</i>	$k_{cat}/K_m$ ( $M^{-1}s^{-1}$ )	$k_{cat}/K_m$ <i>relative</i>
		<i>to WT</i>		<i>to WT</i>		<i>to WT</i>	
Benzylpenicillin (BZ)	Wild-type	1240 ± 125	1.00	43 ± 9	1.00	2.9 x 10 <sup>7</sup>	1.00
	Y105D	255 ± 20	0.21	369 ± 23	8.58	6.9 x 10 <sup>5</sup>	0.02
	Y105G	1203 ± 350	0.97	152 ± 61	3.53	7.9 x 10 <sup>6</sup>	0.27
	Y105N	1616 ± 339	1.30	276 ± 84	6.42	5.9 x 10 <sup>6</sup>	0.20
	Y105R	525 ± 70	0.42	156 ± 38	3.62	3.4 x 10 <sup>6</sup>	0.12
	Y105W	900 ± 78	0.73	23 ± 9	0.53	3.9 x 10 <sup>7</sup>	1.34
Cephalothin (CF)	Wild-type	105 ± 11	1.00	177 ± 27	1.00	5.9 x 10 <sup>5</sup>	1.00
	Y105D	51 ± 11	0.49	2860 ± 540	16.2	1.8 x 10 <sup>4</sup>	0.03
	Y105G	45 ± 18	0.43	1630 ± 750	9.21	2.8 x 10 <sup>4</sup>	0.05
	Y105N	61 ± 17	0.58	303 ± 97	1.71	2.0 x 10 <sup>5</sup>	0.34
	Y105R	90 ± 28	0.86	546 ± 34	3.08	1.6 x 10 <sup>5</sup>	0.27
	Y105W	65 ± 8	0.62	74 ± 22	0.42	8.8 x 10 <sup>5</sup>	1.49

## FIGURES

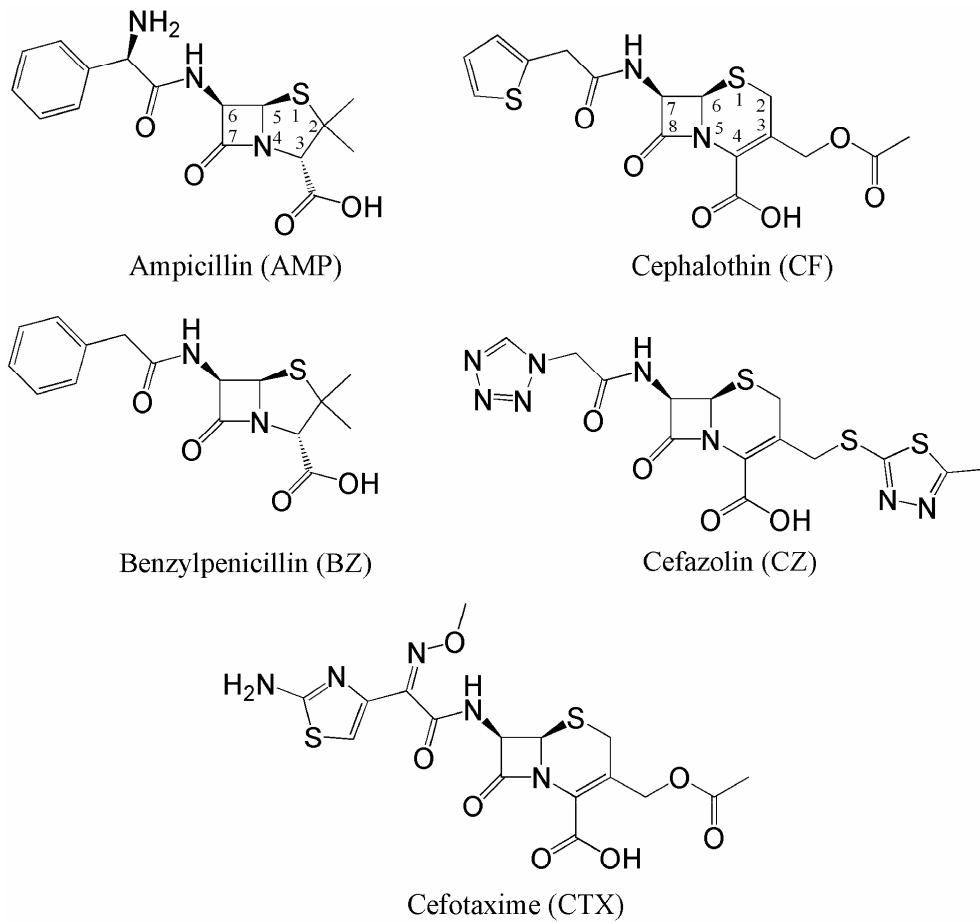


**Figure 2.1.** Structures of  $\beta$ -lactam antibiotics used in this study. Ampicillin and benzylpenicillin are classical penicillins, whereas cephalothin and cefazolin are first-generation cephalosporins. Cefotaxime is a third-generation cephalosporin.

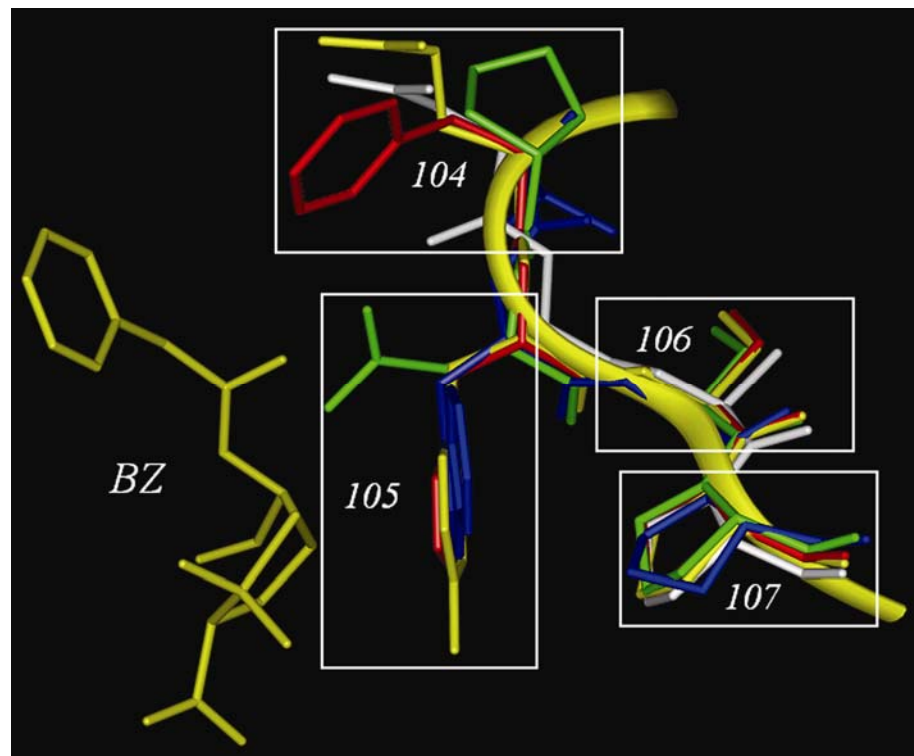


**Figure 2.2.** Superimposition of residues 104–107 of 5 Class A  $\beta$ -lactamases crystal structures. The following enzymes were used with the corresponding PDB entries; blue, *Pseudomonas aeruginosa* PER-1 apoenzyme (1E25) (9); green, *M. fortuitum* apoenzyme (1MFO); white, *S. albus* G apoenzyme (1BSG) (38); red, *Enterobacter cloacae* NMC-A apoenzyme (1BUE) (39); yellow, *E. coli* TEM-1 complexed with BZ (1FQG) (8). The structural alignment was undertaken using the backbone atoms of residues 104–107 with InsightII. Main chain atoms between residues 103–108 of TEM-1 are represented as a yellow ribbon.

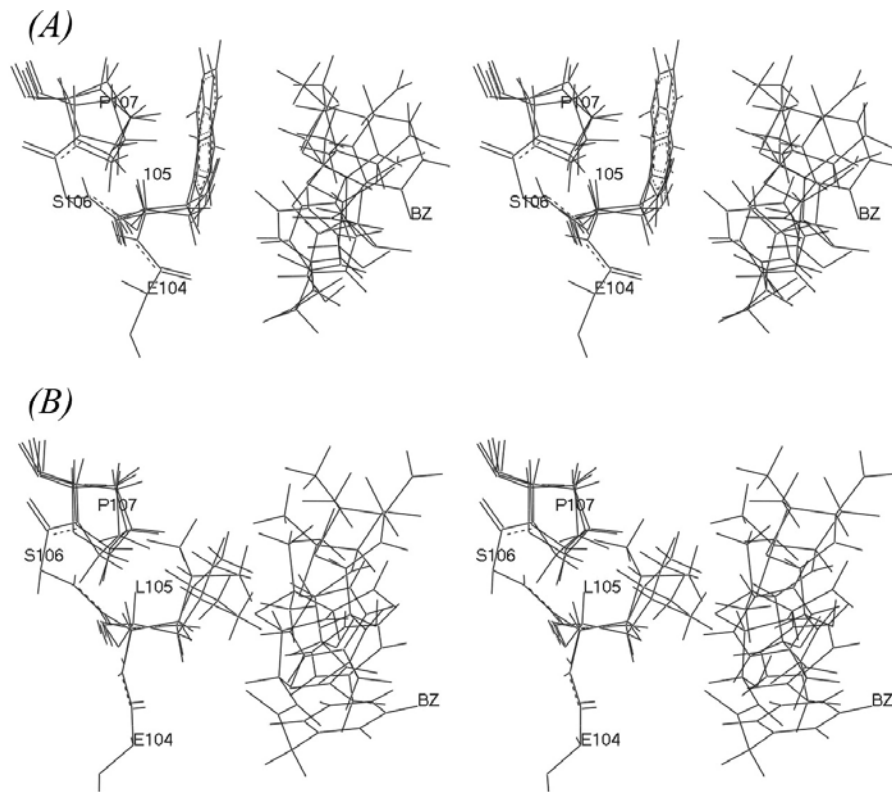


**Figure 2.3.** Superimpositions of snapshots from a 200-ps molecular dynamics simulation of various Y105X mutants of TEM-1, shown in stereo. *A*, superimposition of residues 105 and 107 for the 200-ps snapshot of wild-type TEM-1 and mutants Y105W and Y105N. Although only the 200-ps snapshot is shown for each of the three mutants, the side chains of residues Tyr, Trp, and Asn are all in the same plane, rigidly positioned in the center of an ~8-Å-wide cavity between Pro-107 and the substrate molecule (BZ) throughout the entire 200-ps dynamics simulations. *B*, superimposition of residues 105 and 107 for the 80-, 120-, and 160-ps snapshots of mutant Y105L. The increased flexibility of the branched side chain of Leu-105 prevents adoption of the physical barrier shown in *panel A*, resulting in substrate destabilization at the active site. For both *A* and *B* representations, only residues 104–107 and the BZ substrate are shown. For clarity, the side chains of residues 104 and 106 are omitted.

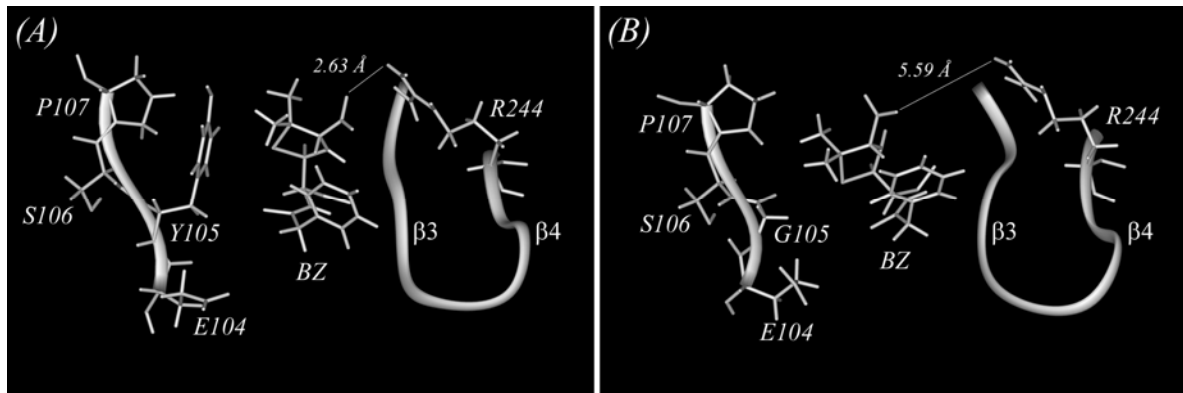


**Figure 2.4.** Conformation of benzylpenicillin in the active site of wild-type TEM-1 (A) and mutant Y105G (B) at the end of a 200-ps dynamics trajectory. The shortest distance between the C3-carboxylate moiety of the thiazolidine ring of BZ to the guanidinium moiety of Arg-244 is represented. The Y105G mutation results in removal of the wall created by Tyr-105, shifting the thiazolidine ring of the substrate in the direction of Pro-107. This resulting conformation of BZ prevents direct contact of the C3-carboxylate with Arg-244 in the Y105G mutant. Backbone direction between residues 104–107 and 235–245 is represented by a *ribbon* and is shown in the same orientation as in Fig. 2.3. Residues from β-strands 3 and 4 (except Arg-244) are omitted for clarity. Similar results were observed with CF.

## Préface au chapitre 3

Certaines structures cristallines de TEM-1 en présence d'inhibiteurs montrent l'adoption d'un conformère de Tyr105 différent de celui observé dans les structures cristallines de l'enzyme libre ou en présence de substrats. Puisque notre étude de dynamique moléculaire entreprise sur une courte échelle de temps (200 ps) suggère que l'effet des mutations en position 105 est en lien avec la dynamique de ce résidu (chapitre 2), nous avons entrepris une étude de recuit simulé sur TEM-1 dans le but d'explorer l'espace conformationnel pouvant être adopté par Tyr105 sur une échelle de temps plus longue que celle précédemment testée par dynamique moléculaire. Suite à une validation structurelle des conformères de recuit simulé obtenus en absence de ligand, nos résultats suggèrent que la chaîne latérale de Tyr105 adopte deux conformations alternatives stables au site actif de TEM-1, correspondant aux deux conformères de Tyr105 observés chez les diverses structures cristallines de l'enzyme en présence de ligands (rotamères **t**80° et **m**-30°/**m**-85°). Nos observations suggèrent ainsi que Tyr105 alterne d'un rotamère à l'autre sur une échelle de temps ps-ns et que l'un et l'autre des rotamères participent respectivement soit à la stabilisation du noyau thiazolidine/dihydrothiazine des ligands ou encore à celle du substituant benzyle en position R<sub>1</sub>, avec un échange sur une échelle de temps supérieure à 200 ps.

Les résultats de cette étude sont présentés au chapitre 3 sous la forme d'un article scientifique actuellement sous presse dans la revue *Proteins: Structure, Function and Bioinformatics* (avril 2007). Les conclusions de ce travail servent à compléter la dynamique moléculaire présentée au chapitre 2 et permettent d'étendre notre compréhension des mouvements adoptés par Tyr105 au site actif de TEM-1 sur une échelle de temps plus longue. En effectuant la corrélation avec certaines données extraites d'études précédentes, nos résultats fournissent également une explication partielle quant à la différence d'affinité observée entre les substrats pénicillines et céphalosporines.

Tout comme pour le chapitre précédent, il est à noter que le terme « apoenzyme », qui signifie spécifiquement la partie protéique et enzymatiquement inactive d'un complexe

holoenzyme [100], est utilisé tout au long de ce chapitre pour désigner l'enzyme *active* et *sans substrat* (sous forme libre). Bien que régulièrement utilisée dans la littérature, cette définition n'en demeure pas moins erronée puisque les  $\beta$ -lactamases n'utilisent pas de cofacteur et ne forment pas de complexe holoenzyme. Par souci de précision, le lecteur substituera volontiers ce terme par «*free form*» ou encore «*unbound form*» lors de la lecture de ce chapitre publié.

## CHAPITRE 3

### **Exploration par recuit simulé d'une tyrosine au site actif de la β-lactamase TEM-1 : Existence potentielle de conformères alternatifs**

**3.1 Article 2.** *Simulated annealing exploration of an active-site tyrosine in TEM-1 β-lactamase suggests the existence of alternate conformations*

“Reprinted with permission from: Nicolas Doucet and Joelle N. Pelletier. “Simulated annealing exploration of an active-site tyrosine in TEM-1 β-lactamase suggests the existence of alternate conformations.” *Proteins: Structure, Function and Bioinformatics* (2007), *In Press*. ©2007, Wiley-Liss, Inc. Reprinted with permission from Wiley-Liss, Inc.”

**Simulated annealing exploration of an active-site tyrosine  
in TEM-1  $\beta$ -lactamase suggests the existence of alternate  
conformations**

Nicolas Doucet<sup>1</sup> & Joelle N. Pelletier<sup>1,2</sup>

<sup>1</sup>*Département de biochimie and* <sup>2</sup>*Département de chimie*

*Université de Montréal*

*C.P. 6128, Succursale Centre-ville*

*Montréal (Québec)*

*H3C 3J7 CANADA*

*Proteins, In Press*

## ABSTRACT

TEM-1 is among the best-studied members of class A  $\beta$ -lactamases, a family of enzymes responsible for the primary defensive measure used by bacteria to hydrolyse the clinically-relevant  $\beta$ -lactam antibiotics. Several crystal structures of TEM-1 complexed with inhibitors display the active-site residue Tyr105 in an alternate orientation relative to that assigned in the free form or in the substrate-bound enzyme. This observation leads to the hypothesis that the alternate conformation is not favoured in the apoenzyme but may be adopted only in the presence of inhibitor. As the residue at position 105 is a determinant of specificity in substrate binding, we sought a better understanding of the relation between its conformation and its function in ligand binding. Here, we performed a molecular dynamics simulated annealing protocol on the apo form of TEM-1 to identify stable orientations adopted by Tyr105 in the active-site cavity of the free enzyme. In contrast to classical molecular dynamics, simulated annealing protocols use temperature cycles that allow for a greater sampling of conformational space, thus affording accelerated energy barrier crossing that can approximate molecular motions observed on a longer time scale. Our results demonstrate that, in absence of substrate, structurally validated conformers of Tyr105 predominantly adopt either of the two rotameric orientations observed in the TEM-1 crystal structures. This suggests that adoption of either conformation in the free enzyme is energetically favoured and is not strictly promoted by ligand binding. Our observations lead us to propose that free TEM-1 alternates between these two conformations of Tyr105 and that a dynamically heterogeneous population of both rotamers exists in solution. The flip from one conformation to the other results in significant reshaping of the active-site cavity, and thus in the potential for forming specific ligand contacts. Our results add to the body of evidence suggesting that Tyr105 displays a dynamical behaviour resulting in alternate ligand binding modes and are consistent with the lower affinity of TEM-1 for cephalosporins relative to penicillins.

## INTRODUCTION

Penicillin antibiotics were introduced in clinical settings for the treatment of various illnesses caused by bacteria in the 1940s. Since then, an important number of strains have become resistant to these drugs as a result of their exaggerated or inappropriate use by the clinical community<sup>1</sup>. While the vast majority of  $\beta$ -lactam drugs remain efficient in inhibiting their natural enzymatic targets (the penicillin binding proteins – PBPs), the primary defensive measure used by bacteria to destroy these clinically relevant antibiotics is the acquisition of  $\beta$ -lactamases<sup>2</sup>. These enzymes efficiently hydrolyse the  $\beta$ -lactam ring of almost all known natural and semi-synthetic  $\beta$ -lactam antibiotics, rendering these molecules biologically inactive. Discovered more than 40 years ago<sup>3</sup>, TEM-1  $\beta$ -lactamase (E.C. 3.5.2.6) is the prevalent member of this class of enzymes and has become a well-established case study of molecular evolution pathways subjected to selective antibiotic pressure. Using TEM-1  $\beta$ -lactamase as a model, a number of *in vivo* and *in vitro* studies have worked toward a detailed characterization of the enzymatic mechanism of drug resistance acquisition so as to develop new antibiotics that are less susceptible to this problem<sup>4,5</sup>. In addition to clarifying the substrate recognition pattern of  $\beta$ -lactamases, these studies pave the way to a better understanding of the underlying catalytic mechanism of class A  $\beta$ -lactamases, which remains controversial to this day.

Owing to its clinical importance toward antibiotic resistance and its relatively good behaviour in solution, a vast amount of structural information about TEM-1 has been acquired, mainly through protein crystallography. An impressive number of crystal structures of this enzyme have been resolved to this day, among which the wild type enzyme<sup>6-8</sup>, several mutants<sup>5,6,8-12</sup>, and structures that are either substrate<sup>13</sup>- or inhibitor<sup>12,14-20</sup>-bound, including one in ultrahigh resolution<sup>21</sup>. Interestingly, in these crystal structures, residues surrounding the active-site cavity of TEM-1 generally retain identical conformations whether in presence or absence of ligand, except where a mutation disrupts

the local environment. In addition to this observation, important catalytic residues (Ser70, Lys73, Ser130, Glu166, Lys234) have all been shown to display temperature factors below average values<sup>7</sup> and the active-site environment of TEM-1 was revealed to be dynamically more quiet than the rest of the enzyme<sup>21</sup>. Nevertheless, conformational differences in the active-site cavity are observed in many structures of TEM-1, notably in a number of surface residues that generally display high B factors (*e.g.* Glu104 and Glu240).

In addition to these small structural changes, one of the most important side-chain reorientations observed in various crystal structures of TEM-1 is the hydroxyphenyl moiety of Tyr105, an active-site residue that we have previously investigated by saturation mutagenesis, enzyme kinetics and *in silico* molecular dynamics simulations<sup>22</sup>. The side-chain of Tyr105 is proximal to the bound ligand (Figure 3.1a) and is located on a surface loop bordering the active-site cavity. Mutations at this position mainly affected  $K_m$  values and determination of kinetic parameters in hydrolysis of various substrates indicated that this residue is involved in substrate discrimination and stabilization<sup>22</sup>. Consequently, Tyr105 has been suggested to play the role of a gate-keeper in the active site of TEM-1. Molecular dynamics simulations conducted on a short time scale (200 ps) demonstrated that Tyr105 and other aromatic replacements at this position stabilize substrate molecules through presumed van der Waals contacts. As a result, the aromatic ring forms a rigid wall that restricts the active-site cavity size, and therefore substrate movement. Most non-aromatic residue replacements at position 105 were found to possess too many degrees of freedom for appropriate substrate stabilization, thus providing an explanation for the strong aromatic bias observed in class A  $\beta$ -lactamases at this active-site position. Interestingly, Y105G, Y105N and Y105A were moderately active in hydrolysis of penicillin substrates, despite the fact that they are not aromatic, apparently as a result of the few degrees of freedom these small side chains possess. Increasing side chain length (and flexibility) generally resulted in important decreases in activity and charged side chains (except the aromatic His) were also poorly compatible with reactivity<sup>22</sup>.

Most crystal structures of TEM-1 reveal that Tyr105 adopts a conformation where the hydroxyphenyl moiety points towards Val216, stacking between Pro107 on one side and the thiazolidine/dihydrothiazine moiety of ligand molecules on the other. However, a number of crystal structures<sup>12,15,16,23,24</sup> display Tyr105 with a  $\chi_1$  angle rotated by more than 90°-110°, thus pointing the hydroxyphenyl side chain in the opposite direction towards Glu104 (Figure 3.1a), facing the R<sub>1</sub> substituent of ligands. According to the ‘penultimate rotamer library’ defined by Richardson and coworkers<sup>25</sup>, these two conformations adopted by Tyr105 correspond to the **t** (*trans*, t80°) and **m** (*minus*, m-85°/m-30°) rotamer orientations allowed for tyrosine residues, which are respectively observed in 30% and 54% of random coil regions of proteins. Interestingly, the **t** conformation has been assigned in both the apoenzyme<sup>6-8,21</sup> and the substrate-bound TEM-1<sup>13</sup>, while only crystal structures complexed either with mechanism-based boronate inhibitors<sup>12,16,23</sup> or the natural protein inhibitors BLIP I<sup>24</sup> and BLIP II<sup>15</sup> have been shown to stabilize the **m** conformation of Tyr105. To date, **m** rotamers of Tyr105 have not been assigned in any free or substrate-bound crystal structure of this enzyme. This leads to the hypothesis that **m** rotamers are not favoured at this position in the apo form of TEM-1 and that they may occur only when stabilized by favourable interactions in presence of the aforementioned inhibitor molecules. However, we have noted that free WT TEM-1 crystal structures 1BTL<sup>7</sup> and 1XPB<sup>6</sup> display significant electron density in the area of the **m** conformer of Tyr105 (Figure 3.2), consistent with partial residency of Tyr105 at this second position. In addition, Tyr105 belongs to a short surface loop that displays higher-than-average temperature factors in many of TEM-1 crystal structures (B factor > 30), whether in presence or absence of ligand. Finally, a lower-than-average  $S^2$  value of the Tyr105 backbone NH vector has been observed by NMR spectroscopy of the apoenzyme, suggesting high flexibility of this side chain in solution<sup>26</sup>. These experimental results all suggest that the side chain of Tyr105 may adopt alternate conformations in TEM-1, even in absence of ligands. In our previous molecular dynamics simulations of TEM-1<sup>22</sup>, these extensive motions of Tyr105 were not observed as a result of the short 200-ps time scale investigated, where the surrounding

rotameric space could not be appropriately sampled. Within those experimental constraints, only the starting  $t$  rotamer was populated. Thus, the full conformational characterization of this residue necessitates further investigation.

Here, we present the investigation of stable side chain orientations adopted by Tyr105 in TEM-1  $\beta$ -lactamase. Using a simulated annealing approach to molecular modelling, we studied the free form of TEM-1 in accordance with the various data suggesting that Tyr105 may adopt alternate conformations. In contrast to classical molecular dynamics simulations, simulated annealing experiments involve adding energy to a system and gradually removing it in a process analogous to heating the system to a very high temperature and gradually cooling it down over the course of the molecular dynamics simulation<sup>27,28</sup>. This procedure allows the system to surmount energy barriers and climb out of local minima in order to explore conformational space before settling into a new local energy minimum, therefore allowing a wider sampling of conformational space than classical molecular dynamics simulations. The energy input allowed broad sampling of conformational space by the side-chains, which were unconstrained. Upon cooling and energy minimization, Tyr105 conformations were found to be restricted to a limited set. Conformational validation allowed us to propose plausible rotamers adopted by this hydroxyphenyl side chain in the active-site cavity of TEM-1, which further clarifies its role as a gate-keeper in this enzyme.

## METHODS

*Molecular Modelling*—The ‘Simulated Annealing’ method was applied to the conformational exploration of Tyr105 in TEM-1  $\beta$ -lactamase. This technique is a widely accepted molecular modelling methodology that allows a broad sampling of conformational space by accelerated barrier crossing and is computationally easy to implement<sup>28</sup>. While the

‘Replica Exchange’ approach holds promise for this type of application and may prove more computationally efficient, it is not yet well implemented for molecules of this complexity<sup>28</sup>. Other approaches, such as the ‘Normal Mode Analysis’ (NMA) technique for determination of low-frequency vibrational motions, are well-adapted to complex systems. While we did not apply NMA, its application should provide information that is complementary to that obtained here.

*Computer Tools*—All molecular models were prepared with the InsightII package, version 2000.1 (Accelrys, San Diego, CA) implemented on a Fuel Silicon Graphics Workstation running Irix 6.5. The BIOPOLYMER module was used to modify molecular structures and the ANALYSIS and DECIPHER modules were used to analyse all molecular dynamics simulated annealing trajectories. All energy minimizations and simulated annealing calculations were performed with the DISCOVER module using the constant valence force field (CVFF) and all calculations were executed on an Origin 2000 Silicon Graphics Server running Irix 6.5.

*Molecular Structure Preparation*—The 1.8-Å crystallographic structure of the *E. coli* TEM-1 β-lactamase (PDB coordinates 1BTL<sup>7</sup>) was used as starting coordinates for all calculations performed on wild-type TEM-1 and mutant Y105N. The crystallographic water molecules and the active site SO<sub>4</sub><sup>2-</sup> molecule were deleted and hydrogen atoms were added at the normal ionization state of the amino acids at pH 7.0. Atomic potentials were fixed according to the CVFF atom types recommended by the manufacturer. To eliminate potential steric clashes, the initial structure was energy-minimized by applying 100 steps of steepest descents followed by a conjugate gradient minimization until convergence of 0.001 kcal mol<sup>-1</sup> Å<sup>-1</sup>. Minimization protocols attempt to identify conformations approximating local minima on the potential energy surface. The convergence criteria continuously monitor the variation in energy gradient with respect to the coordinates of each successive minimization step. The end point chosen here (0.001 kcal mol<sup>-1</sup> Å<sup>-1</sup>) provides sufficient minimization for the given application without undue computational demand. Preparation

of the Y105N mutant was performed in a similar fashion but the Asn105 mutation was introduced prior to energy minimization. These minimized structures served as the starting coordinates for all subsequent steps of modelling.

*Simulated Annealing*—To explore plausible conformations adopted by the hydroxyphenyl side chain of Tyr105 in the free form of TEM-1  $\beta$ -lactamase, we conducted a molecular dynamics simulated annealing protocol according to the following iterative procedure. The initial minimized structure was heated to 1000 K over 5 ps, equilibrated at 1000 K for 3 ps, and then cooled down to 300 K in 5 ps using an exponential rate constant (defining the relaxation time) of 0.7 ps for both heating and cooling steps. The time step of the molecular dynamics simulations was set to 1 fs and a distance-dependent dielectric constant of 1 was applied to the system. This dielectric constant is an empirical, dimensionless scaling factor used to reflect the polarizability of implicit solvent and its numeric value is not proportional to the chemical dielectric constant experimentally calculated for solvents<sup>29</sup>. During the protocol, backbone atoms of the whole protein were tethered to their initial position by applying a force constant of 800 kcal mol<sup>-1</sup> Å<sup>-2</sup>. This force constant sufficiently restricts secondary structure to prevent local unfolding while permitting subtle backbone movements that allow for broader side chain conformational exploration than by fixing the backbone to its crystallographic position. Finally, each cooled conformation was submitted to unrestrained energy minimization by applying 500 iterations of steepest descents followed by a conjugate gradient minimization until convergence of 0.001 kcal mol<sup>-1</sup> Å<sup>-1</sup>. This cycle was repeated 9 times and was performed in duplicate for a total simulation time of 260 ps yielding 20 minimized conformations. The protocol was also performed with the Y105N mutant of TEM-1 to yield a total of 10 minimized conformations.

*Model Analysis*—Each minimized conformation was subjected to a validation procedure in which Tyr105 (or Asn105) was analyzed for proper atom contacts and geometry. Backbone *cis-trans* isomerization was estimated using the Vega ZZ software,

version 2.0.6<sup>30,31</sup> while C $\alpha$  geometry, side chain rotamers, Ramachandran angles, atomic clashes and C $\beta$  deviation were evaluated using the MolProbity software developed by the Richardson group<sup>32</sup>.  $\chi_1$  (N-C $\alpha$ -C $\beta$ -C $\gamma$ ) and  $\chi_2$  (C $\alpha$ -C $\beta$ -C $\gamma$ -C $\delta$ ) torsion angles for validated conformers were calculated using the DECIPHER module of InsightII (Accelrys, San Diego, CA). All rotamer angles are expressed on the basis of a 0° to 360° nomenclature in contrast to the ±180° nomenclature adopted by Lovell *et al.*<sup>25</sup>. For the validated conformers, residues in the local environment of Tyr105 (among which Glu104, Met129 and Asn132) were analyzed using the same procedure to verify the validity of favourable interactions (Table S3.1, Supplementary Material, *Annexe 4*). Structural alignments between validated conformers were either generated with the BIOPOLYMER module of InsightII or performed with the Multiple Alignment Interface<sup>33</sup> implemented in the VMD molecular graphics software, version 1.8.4 (<http://www.ks.uiuc.edu/Research/vmd/>)<sup>34</sup>. Active-site cavity volumes were estimated by calculating spherical harmonic molecular surfaces<sup>35</sup> using the MSSH program kindly provided by Bernard Maigret. For these calculations, the cavity volume was estimated for conformers 053 ( $\chi_1 = 294^\circ$ ,  $\chi_2 = 82^\circ$ ), 118 ( $\chi_1 = 173^\circ$ ,  $\chi_2 = 232^\circ$ ) and 131 ( $\chi_1 = 186^\circ$ ,  $\chi_2 = 263^\circ$ ) using a 1.4-Å radius probe sphere centered about the position of the crystallized SO<sub>4</sub><sup>2-</sup> molecule originally present in the apoenzyme crystal structure of TEM-1 (PDB coordinates 1BTL<sup>7</sup>). An 8-Å cut-off radius was applied to all axes and the generated cavity volumes were analyzed using the Surface1.0 plug-in implemented in the VMD molecular graphics software, version 1.8.4. To verify if the repositioning of other active-site residues could account for significant decreases in cavity volume and to validate that Tyr105 was responsible for the calculated active-site volume reduction observed in conformer 053, volumes were also calculated for Y105G mutants of conformers 053 and 118 using the same procedure. For this validation, the Y105G mutant was generated and analyzed without further energy minimization to conserve the same active-site topology.

## RESULTS AND DISCUSSION

In order to verify if the hydroxyphenyl moiety of Tyr105 can adopt various stable orientations in the free form of TEM-1  $\beta$ -lactamase, we sampled a large number of conformations of this residue using a molecular dynamics simulated annealing protocol where the protein was subjected to cyclical heating/cooling cycles. This procedure allowed a wider sampling of conformational space than classical molecular dynamics simulations. Loosely based on similar protocols<sup>36-38</sup>, we developed a method in which the backbone atoms of a minimized structure of TEM-1 (PDB coordinates 1BTL<sup>7</sup>) were tethered with a force of 800 kcal mol<sup>-1</sup> Å<sup>-2</sup>. The entire enzyme was heated to 1000 K, equilibrated at this temperature, cooled down to 300 K and energy-minimized without constraints. Continuing with this new structure, the protocol was iterated 9 times, and the process was duplicated to yield 20 minimized conformations. Each conformation displayed a backbone RMSD of  $\leq$ 1.24 Å relative to the starting crystal structure (1BTL). As Tyr105 is an active-site surface residue that is only partially buried, the hydroxyphenyl side chain moved extensively over the course of each heating cycle, during which it was always extracted from its previously stable and minimized position to be completely solvent exposed. This procedure allowed the exploration of a vast conformational population and prevented any positional bias of the side chain resulting from each previous minimized conformation (Figure 3.3).

The wide sampling of conformational space tested by simulated annealing protocols often represents extreme scenarios in terms of allowed flexibility for a given side chain, even upon energy minimization. For quality control, the 20 minimized conformations were subjected to a validation protocol using the MolProbity software<sup>32</sup>. This structural validation allowed for the elimination of Tyr105 conformers displaying either atomic clashes, erroneous  $\phi$  and  $\psi$  angle values, disfavoured rotamers or geometrical abnormalities around C $\alpha$  (C $\beta$  deviation)<sup>32</sup> (Table S3.1, Supplementary Material, *Annexe 4*). Based on these validation criteria, 60 % (12/20) of the minimized conformations were removed from

our analysis, mostly due to C $\beta$  deviations 0.01 to 0.23 Å higher than the accepted 0.25 Å threshold value, suggesting undesired geometrical distortions in the local environment of Ca. The remaining eight conformations of Tyr105 displayed adequate  $\phi$  and  $\psi$  values, rotameric side chains, no atomic clashes and ideal covalent geometries, thus confirming that Tyr105 was adequately modelled<sup>32</sup>.

All eight validated conformations obtained in the simulated annealing protocol displayed the side chain of Tyr105 positioned in either the **t** (**t**80°) or **m** (**m**-85°/**m**-30°) rotamer orientations (Figure 3.3), consistent with conformations of Tyr105 observed in crystallographic structures of TEM-1 (Figure 3.1b-c). While **t**80° rotamers of tyrosine residues are structurally conserved and display few  $\chi_2$  variations, when  $\chi_1$  is in **m**,  $\chi_2$  angles allow greater spatial coverage of the tyrosine side chain<sup>25</sup>, a result that is confirmed by our minimized conformers (Figure 3.1c). The fact that our results display both **t** and **m** rotamers very similar to various crystal structures of TEM-1 (Figure 3.1a) confirms the validity of the modelling procedure. Only the **t** rotamer has been assigned in structures of free TEM-1 (PDB coordinates 1BTL<sup>7</sup> and 1XPB<sup>6</sup>). Our observation of both the **t** and **m** rotamers by modelling of free TEM-1 suggests that there is a potential for stabilization of both rotamers in the local environment of the active site in absence of ligand. We thus provide evidence that adoption of the **m** conformation by Tyr105 is not strictly promoted by ligand binding. Our observations lead us to propose that free TEM-1 alternates between the **t** and **m** conformations of Tyr105 and that a dynamically heterogeneous population of both rotamers exists in solution. This observation is also supported by significant electron density in the area of the **m** conformer of Tyr105 in two crystal structures of the free enzyme (1BTL<sup>7</sup> and 1XPB<sup>6</sup>) (Figure 3.2).

Unlike its highly exposed neighbour Glu104, our results show that Tyr105 does not remain completely solvent-exposed and randomly oriented following minimization but shows a strong tendency to come back to either of the two favoured, well-packed conformations described above (Figure 3.1b-c). Thus, the high B factor<sup>7</sup> and low  $S^2$  values

of Tyr105<sup>26</sup> would not result from high structural variability but rather from dynamic exchange between a restricted subset of favoured rotamers. The minimized simulated annealing conformations display hydrogen-bonding patterns that are consistent with stabilization of both the **t** and **m** side chain rotamers of Tyr105 in absence of ligand. In fact, in addition to the highly-conserved hydrogen bond observed between the backbone carbonyl oxygen of Tyr105 and the backbone nitrogen of Asn132 ( $\text{HN}_{132}\text{-O}_{105}$ ) in both the **t** and **m** conformers, the **t** rotamer side chain of Tyr105 was anchored in many of the validated conformers by a second hydrogen bond between the hydroxyl moiety and the backbone carbonyl oxygen of Met129 ( $\text{HO}_{\eta_{105}}\text{-O}_{129}$ ). Both hydrogen bonds were also inferred from the ultrahigh resolution crystal structure of wild-type TEM-1<sup>21</sup> with optimal orientation and distance (2.0 Å and 1.9 Å, respectively). In the 066B **m** rotamer ( $\chi_1 = 295^\circ$ ,  $\chi_2 = 103^\circ$ ; Figure 3.3), the side chain hydroxyl group of Tyr105 was appropriately positioned to hydrogen bond with  $\text{O}_{\varepsilon 1}$  of Glu104 ( $\text{HO}_{\eta_{105}}\text{-O}_{\varepsilon 104}$ ), suggesting that this hydrogen bond may help stabilize **m** conformations of Tyr105.

Since Tyr105 is located in a short surface loop with residues displaying high B factor values, our results suggest that high backbone flexibility in this area could hamper substrate entry or release. For instance, the hydroxyphenyl side chain of Tyr105 of conformer 053 ( $\chi_1 = 294^\circ$ ,  $\chi_2 = 82^\circ$ ) juts towards the active site cavity as a result of local  $\text{C}\alpha\text{-C}\beta$  reorientation (Figure 3.1d). Consequently, its orientation significantly reduced the active-site cavity volume and blocked access to the catalytic Ser70. In fact, as a result of this side chain reorientation, the solvent-accessible cavity volume was reduced to  $\sim 210 \text{ \AA}^3$  in this conformer, relative to the calculated  $>300 \text{ \AA}^3$  for the other validated rotamers. Although the simulated annealing procedure showed that Tyr105 can adopt both **t** and **m** orientations in absence of substrate, this observation nevertheless suggests that, to prevent obstruction of the active-site cavity and to allow productive binding of ligands, not all **m** rotameric orientations that can be structurally validated for Tyr105 are compatible with function.

Tyrosine residues have been shown to adopt **p**90° rotamer orientations in 12% of random coil regions of proteins<sup>25</sup>, which could be expected for Tyr105 as it is located on a surface loop. We did not observe **p**90° rotamers in any of our simulated annealing conformers (Figure 3.3). This result, and molecular visualization of the active-site environment, suggests that adoption of this rotamer orientation by Tyr105 would create important steric clashes between the hydroxyphenyl moiety and the amide side chain of Asn132, severely perturbing substrate stabilization. Moreover, the **p**90° conformer of Tyr105 would also considerably decrease active-site cavity volume and prevent substrate access to catalytic residues.

Our previous molecular dynamics studies on Y105X mutants in the presence of benzylpenicillin (BZ) suggested a rationalization for the strong aromatic bias observed at this active-site position in class A  $\beta$ -lactamases<sup>22</sup>. It was found that most bulky and non-aromatic residue replacements at position 105 possess too many degrees of freedom for appropriate substrate stabilization since their side chain would severely clash with substrate molecules. Interestingly, mutant Y105N was shown to retain high activity as a result of its side chain preserving a structurally-constrained conformation in the same plane as that adopted by aromatic residues in presence of substrates, on a picosecond time scale. In contrast to bulkier residues and however flexible Asn105 may be, it appears that this side chain is sufficiently small to prevent severe steric clashes with substrate molecules in the active site cavity, thus offering an explanation for its high *in vivo* and *in vitro* activities<sup>22</sup>. Using the aforementioned simulated annealing procedure, we tested whether mutant Y105N adopted alternate orientations in free TEM-1. Our results yielded two validated conformers of Asn105 corresponding to rotamers **t**30° and **m**-80° permitted for asparagine residues<sup>25</sup> (results not shown). These orientations are similar to the **t** and **m** rotamers observed for tyrosine residues, suggesting that Asn105 adopts orientations similar to those observed for Tyr105 in the free enzyme. Also, the theoretically allowed **p**-10° and **p**30° rotamers of Asn105 would be disfavored since the side chain of Asn105 would potentially

create disruptive steric clashes with Asn132 and thus severely disrupt substrate stabilization, analogous to the **p** rotamers of Tyr105.

While the current molecular modelling study was performed exclusively on free TEM-1, our observations lend support to previous molecular dynamics simulations performed by Díaz *et al.* on a one nanosecond time scale using TEM-1/substrate complexes (BZ and CF)<sup>39,40</sup>. Visual analysis of their reported results shows that Tyr105 reorients from the **t**80° rotamer of 1BTL used as starting coordinates ( $\chi_1 = 194^\circ$ ,  $\chi_2 = 70^\circ$ ) to adopt a conformation similar to the **m** rotamers observed in our simulated annealing protocol. Because of the magnitude of this reorientation, the initial contacts formed between the **t** rotamer and the thiazolidine/dihydrothiazine ring of ligands are disrupted and new contacts are formed between the adopted **m** rotamers and the R<sub>1</sub> substituent of ligands. In the first of their studies (performed with a TEM-1/BZ complex<sup>39</sup>), Díaz *et al.* demonstrated that adoption of the **m** rotamer was accompanied by establishment of  $\pi$ - $\pi$  contact with the benzyl moiety of the R<sub>1</sub> substituent in BZ. In fact, the authors observed a small-amplitude correlated motion between Tyr105 and the R<sub>1</sub> substituent as a result of this new contact. Their second study (performed with a TEM-1/CF complex<sup>40</sup>), again resulted in adoption of the **m** rotamer, although no  $\pi$ - $\pi$  contacts nor correlated motions between Tyr105 and the R<sub>1</sub> substituent of CF were observed. This suggests that the adopted **m** rotamer of Tyr105 does not stabilize CF as efficiently as BZ<sup>40</sup>. However, our previous 200-ps molecular dynamics study<sup>22</sup> suggested that the initial **t** rotamer of Tyr105 forms efficient contacts with the thiazolidine/dihydrothiazine ring of both BZ and CF. If we postulate that both **t** and **m** interactions contribute to optimal ligand stabilization in the active site of TEM-1, failure to adopt either of these rotameric orientations by Tyr105 should result in reduced affinity. The observed failure of the **m** conformers of Tyr105 to stabilize CF in the same manner as BZ may thus provide a partial explanation for the lower affinity of TEM-1 for cephalosporins relative to penicillins<sup>22</sup>. This further evidence of implication of Tyr105 in ligand discrimination confirms its importance as a gate-keeper in TEM-1.

The reorientation of the Tyr105 side chain exhibited in the work of Díaz *et al.* for substrate-bound TEM-1<sup>39,40</sup> and in the simulated annealing of free TEM-1 performed in the present study suggest that Tyr105 can sample two stable and functionally-relevant conformations in both free and ligand-bound enzyme. In the ligand-bound form, Tyr105 would play two distinct roles in the stabilization of  $\beta$ -lactam molecules during turnover: 1) through van der Waals and hydrophobic contacts with the thiazolidine/dihydrothiazine ring of ligands when positioned in the **t** orientation<sup>22</sup>, and 2) through possible  $\pi$ - $\pi$  contacts with the aromatic R<sub>1</sub> substituent of a restricted set of ligands when positioned in the **m** orientation<sup>39</sup>. In the absence of ligand, the present study demonstrates that sampling of both **t** and **m** conformers is possible, and suggests the existence of a heterogeneous population of both Tyr105 rotamers in solution. This conclusion is also supported by the electronic density of crystal structures of free TEM-1 (Figure 3.2), thus ruling out the possibility that ligand binding is the sole factor contributing to conformational flipping of Tyr105 in TEM-1  $\beta$ -lactamase.

## CONCLUSION

The present simulated annealing protocol performed on free TEM-1 allowed the observation of both **t** and **m** rotamers of Tyr105 similar to those observed in crystal structures of free and ligand-bound TEM-1 and suggests that a dynamically heterogeneous population of both conformations exists in the free enzyme. Thus, adoption of the **m** conformer is not strictly promoted by ligand binding. By alternating between **t** and **m** orientations over a functionally-relevant time scale, we propose that the side chain of Tyr105 could not only form a stabilizing wall to the active site of TEM-1 in its **t** conformation<sup>22</sup> but could also create favourable interactions with the R<sub>1</sub> aromatic substituent of ligands in its **m** conformation (as observed by Díaz *et al.*<sup>39</sup>). Moreover, the present study suggests that the **p**90° conformer of Tyr105 is not energetically favoured

because it would considerably decrease active-site cavity volume and prevent substrate access to catalytic residues. The current study further supports the relevance of the functional importance of alternate conformations adopted by active-site residues. Only in TEM-1, 64% of residues have been shown to occupy more than one low-energy conformation<sup>21</sup>, suggesting caution when drawing functional conclusions based on low resolution crystal structures. If only a small fraction of these low-energy conformations are relevant to folding mechanisms, structural integrity or enzymatic activity, motional and conformational characterization of such rotamers may yield important information regarding enzymatic function.

## ACKNOWLEDGEMENTS

The authors thank Alexandre Beautrait and Bernard Maigret (CNRS/Université Henri-Poincaré, Vandoeuvre-lès-Nancy, France) for providing the MSSH program as well as Dominic Pilon and Miguel St-Jean (Université de Montréal, Montréal, QC) for advice and helpful discussions. We also thank Albert M. Berghuis (McGill University, Montréal, QC) for his helpful comments. This work was supported by grants from the Natural Sciences and Engineering Research Council of Canada (NSERC) and the Canada Foundation for Innovation (CFI).

## REFERENCES

1. Medeiros AA. Evolution and dissemination of beta-lactamases accelerated by generations of beta-lactam antibiotics. *Clin Infect Dis* 1997;24 Suppl 1:S19-S45.
2. Davies J. Inactivation of antibiotics and the dissemination of resistance genes. *Science* 1994;264(5157):375-382.

3. Datta N, Kontomichalou P. Penicillinase synthesis controlled by infectious R factors in Enterobacteriaceae. *Nature* 1965;208(7):239-241.
4. Hall BG. Predicting the evolution of antibiotic resistance genes. *Nat Rev Microbiol* 2004;2(5):430-435.
5. Orencia MC, Yoon JS, Ness JE, Stemmer WP, Stevens RC. Predicting the emergence of antibiotic resistance by directed evolution and structural analysis. *Nat Struct Biol* 2001;8(3):238-242.
6. Fonzé E, Charlier P, To'th Y, Vermeire M, Raquet X, Dubus A, Frère JM. TEM-1 beta-lactamase structure solved by molecular replacement and refined structure of the S235A mutant. *Acta Crystallogr D Biol Crystallogr* 1995;51(5):682-694.
7. Jelsch C, Mourey L, Masson JM, Samama JP. Crystal structure of *Escherichia coli* TEM-1 beta-lactamase at 1.8 Å resolution. *Proteins* 1993;16(4):364-383.
8. Stec B, Holtz KM, Wojciechowski CL, Kantrowitz ER. Structure of the wild-type TEM-1 beta-lactamase at 1.55 Å and the mutant enzyme Ser70Ala at 2.1 Å suggest the mode of noncovalent catalysis for the mutant enzyme. *Acta Crystallogr D Biol Crystallogr* 2005;61(8):1072-1079.
9. Swarén P, Golemi D, Cabantous S, Bulychev A, Maveyraud L, Mobashery S, Samama JP. X-ray structure of the Asn276Asp variant of the *Escherichia coli* TEM-1 beta-lactamase: Direct observation of electrostatic modulation in resistance to inactivation by clavulanic acid. *Biochemistry* 1999;38(30):9570-9576.
10. Thomas VL, Golemi-Kotra D, Kim C, Vakulenko SB, Mobashery S, Shoichet BK. Structural consequences of the inhibitor-resistant Ser130Gly substitution in TEM beta-lactamase. *Biochemistry* 2005;44(26):9330-9338.

11. Wang X, Minasov G, Shoichet BK. The structural bases of antibiotic resistance in the clinically derived mutant beta-lactamases TEM-30, TEM-32, and TEM-34. *J Biol Chem* 2002;277(35):32149-32156.
12. Wang X, Minasov G, Shoichet BK. Evolution of an antibiotic resistance enzyme constrained by stability and activity trade-offs. *J Mol Biol* 2002;320(1):85-95.
13. Strynadka NC, Adachi H, Jensen SE, Johns K, Sielecki A, Betzel C, Sutoh K, James MN. Molecular structure of the acyl-enzyme intermediate in beta-lactam hydrolysis at 1.7 Å resolution. *Nature* 1992;359(6397):700-705.
14. Horn JR, Shoichet BK. Allosteric inhibition through core disruption. *J Mol Biol* 2004;336(5):1283-1291.
15. Lim D, Park HU, De Castro L, Kang SG, Lee HS, Jensen S, Lee KJ, Strynadka NC. Crystal structure and kinetic analysis of beta-lactamase inhibitor protein-II in complex with TEM-1 beta-lactamase. *Nat Struct Biol* 2001;8(10):848-852.
16. Maveyraud L, Mourey L, Kotra LP, Pedelacq JD, Guillet V, Mobashery S, Samama JP. Structural basis for clinical longevity of carbapenem antibiotics in the face of challenge by the common class A beta-lactamases from the antibiotic-resistant bacteria. *J Am Chem Soc* 1998;120(38):9748-9752.
17. Ness S, Martin R, Kindler AM, Paetzl M, Gold M, Jensen SE, Jones JB, Strynadka NC. Structure-based design guides the improved efficacy of deacylation transition state analogue inhibitors of TEM-1 beta-lactamase. *Biochemistry* 2000;39(18):5312-5321.
18. Wang X, Minasov G, Blázquez J, Caselli E, Prati F, Shoichet BK. Recognition and resistance in TEM beta-lactamase. *Biochemistry* 2003;42(28):8434-8444.

19. Wang X, Minasov G, Shoichet BK. Noncovalent interaction energies in covalent complexes: TEM-1 beta-lactamase and beta-lactams. *Proteins* 2002;47(1):86-96.
20. Maveyraud L, Pratt RF, Samama JP. Crystal structure of an acylation transition-state analog of the TEM-1 beta-lactamase. Mechanistic implications for class A beta-lactamases. *Biochemistry* 1998;37(8):2622-2628.
21. Minasov G, Wang XJ, Shoichet BK. An ultrahigh resolution structure of TEM-1 beta-lactamase suggests a role for Glu166 as the general base in acylation. *J Am Chem Soc* 2002;124(19):5333-5340.
22. Doucet N, De Wals PY, Pelletier JN. Site-saturation mutagenesis of Tyr-105 reveals its importance in substrate stabilization and discrimination in TEM-1 beta-lactamase. *J Biol Chem* 2004;279(44):46295-46303.
23. Strynadka NCJ, Martin R, Jensen SE, Gold M, Jones JB. Structure-based design of a potent transition state analogue for TEM-1 beta-lactamase. *Nat Struct Biol* 1996;3(8):688-695.
24. Strynadka NC, Jensen SE, Alzari PM, James MN. A potent new mode of beta-lactamase inhibition revealed by the 1.7 Å X-ray crystallographic structure of the TEM-1-BLIP complex. *Nat Struct Biol* 1996;3(3):290-297.
25. Lovell SC, Word JM, Richardson JS, Richardson DC. The penultimate rotamer library. *Proteins* 2000;40(3):389-408.
26. Savard PY, Gagné SM. Backbone dynamics of TEM-1 determined by NMR: Evidence for a highly ordered protein. *Biochemistry* 2006;45(38):11414-11424.

27. Kozack RE, Loechler EL. Molecular modeling of the conformational complexity of (+)-anti-B[a]PDE-adducted DNA using simulated annealing. *Carcinogenesis* 1997;18(8):1585-1593.
28. Tai K. Conformational sampling for the impatient. *Biophys Chem* 2004;107(3):213-220.
29. Harvey SC. Treatment of electrostatic effects in macromolecular modeling. *Proteins* 1989;5(1):78-92.
30. Pedretti A, Villa L, Vistoli G. VEGA: A versatile program to convert, handle and visualize molecular structure on Windows-based PCs. *J Mol Graph Model* 2002;21(1):47-49.
31. Pedretti A, Villa L, Vistoli G. VEGA. An open platform to develop chemo-bio-informatics applications, using plug-in architecture and script programming. *J Comput Aided Mol Des* 2004;18(3):167-173.
32. Lovell SC, Davis IW, Arendall WB, 3rd, de Bakker PI, Word JM, Prisant MG, Richardson JS, Richardson DC. Structure validation by Calpha geometry: phi,psi and Cbeta deviation. *Proteins* 2003;50(3):437-450.
33. Eargle J, Wright D, Luthey-Schulten Z. Multiple Alignment of protein structures and sequences for VMD. *Bioinformatics* 2006;22(4):504-506.
34. Humphrey W, Dalke A, Schulten K. VMD: Visual molecular dynamics. *J Mol Graph Model* 1996;14(1):33-38.
35. Cai W, Shao X, Maigret B. Protein-ligand recognition using spherical harmonic molecular surfaces: Towards a fast and efficient filter for large virtual throughput screening. *J Mol Graph Model* 2002;20(4):313-328.

36. Constantine KL. Evaluation of site-directed spin labeling for characterizing protein-ligand complexes using simulated restraints. *Biophys J* 2001;81(3):1275-1284.
37. Kurutz JW, Lee KY. NMR structure of lung surfactant peptide SP-B(11-25). *Biochemistry* 2002;41(30):9627-9636.
38. Patargias G, Zitzmann N, Dwek R, Fischer WB. Protein-protein interactions: Modeling the hepatitis C virus ion channel p7. *J Med Chem* 2006;49(2):648-655.
39. Díaz N, Sordo TL, Merz KM, Suárez D. Insights into the acylation mechanism of class A beta-lactamases from molecular dynamics simulations of the TEM-1 enzyme complexed with benzylpenicillin. *J Am Chem Soc* 2003;125(3):672-684.
40. Díaz N, Suárez D, Merz KM, Sordo TL. Molecular dynamics simulations of the TEM-1 beta-lactamase complexed with cephalothin. *J Med Chem* 2005;48(3):780-791.
41. Schrauber H, Eisenhaber F, Argos P. Rotamers: To be or not to be? An analysis of amino acid side-chain conformations in globular proteins. *J Mol Biol* 1993;230(2):592-612.

## FIGURES

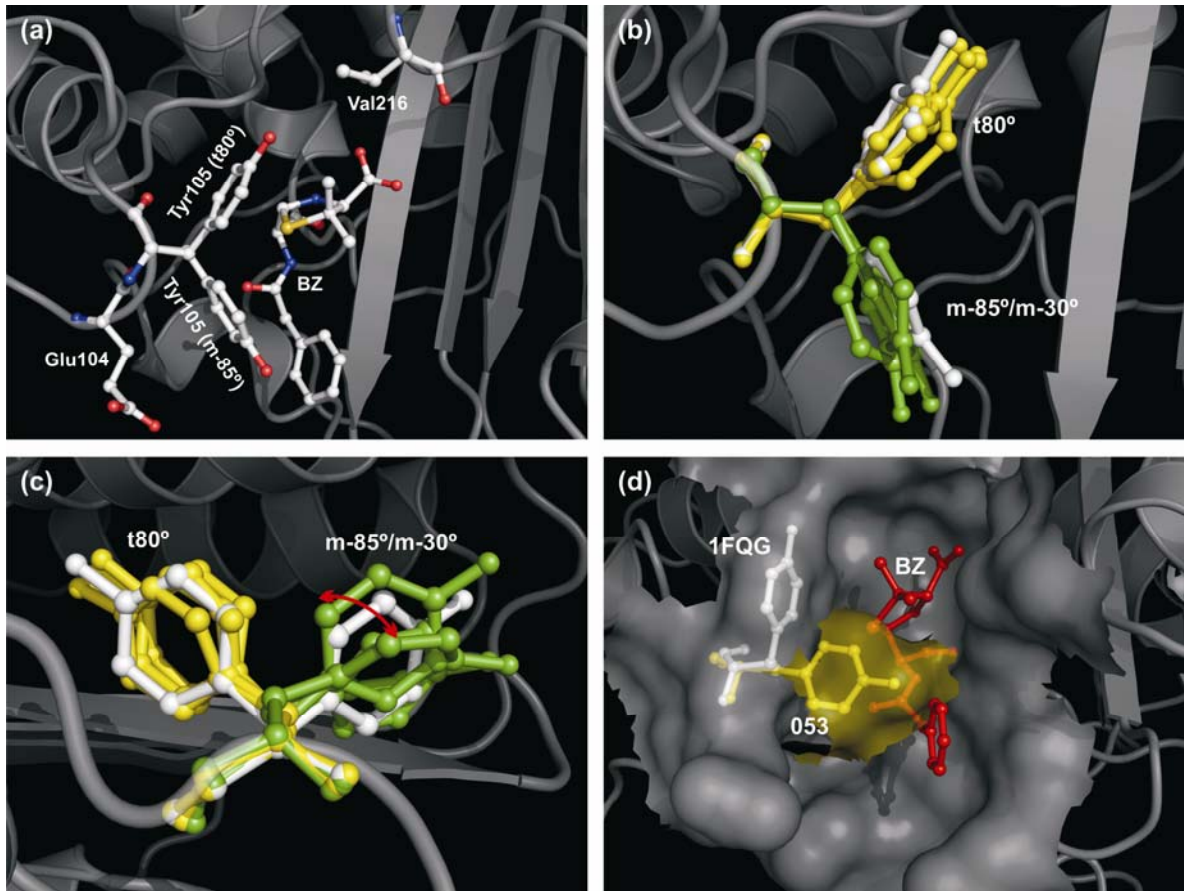


**Figure 3.1.** Representation of Tyr105 rotamers in TEM-1  $\beta$ -lactamase. a) Tyr105 backbone superimposition for 1FQG<sup>13</sup> and 1BT5<sup>16</sup> showing two crystallized rotamers of Tyr105 (**t**80° in 1FQG and **m**-85° in 1BT5). Glu104, Tyr105, Val216 and benzylpenicillin (BZ) are shown in ball-and-stick representation. b) Tyr105 backbone superimposition for validated simulated annealing conformers, with the exception of conformer 053 ( $\chi_1 = 294^\circ$ ,  $\chi_2 = 82^\circ$ ). **t**80° rotamers are coloured yellow and **m**-85°/**m**-30° rotamers are coloured green. Both 1FQG and 1BT5 crystal structures are displayed as in panel A and are coloured white. c) Alternate view of panel B showing that  $\chi_1/\chi_2$  distribution is populated throughout  $\chi_2$  when

$\chi_1$  is in **m**<sup>25,41</sup>. The  $\chi_2$  torsion angle is represented by a red arrow. d) Backbone superimposition of 1FQG<sup>13</sup> and conformer 053 ( $\chi_1 = 294^\circ$ ,  $\chi_2 = 82^\circ$ ). When  $\chi_1$  is in **m**, validated  $\chi_2$  may restrict cavity volume in TEM-1 by blocking access to the active site. In validated conformer 053 where  $\chi_2 < 90^\circ$ , the space occupied by benzylpenicillin (BZ) crosses through that occupied by Tyr105. BZ is coloured red while Tyr105 is coloured white in 1FQG and yellow in conformer 053. Connolly surfaces were generated using a 1.3-Å radius probe and are represented for active-site residues in 1FQG (grey surface) and for Tyr105 in conformer 053 (yellow surface).

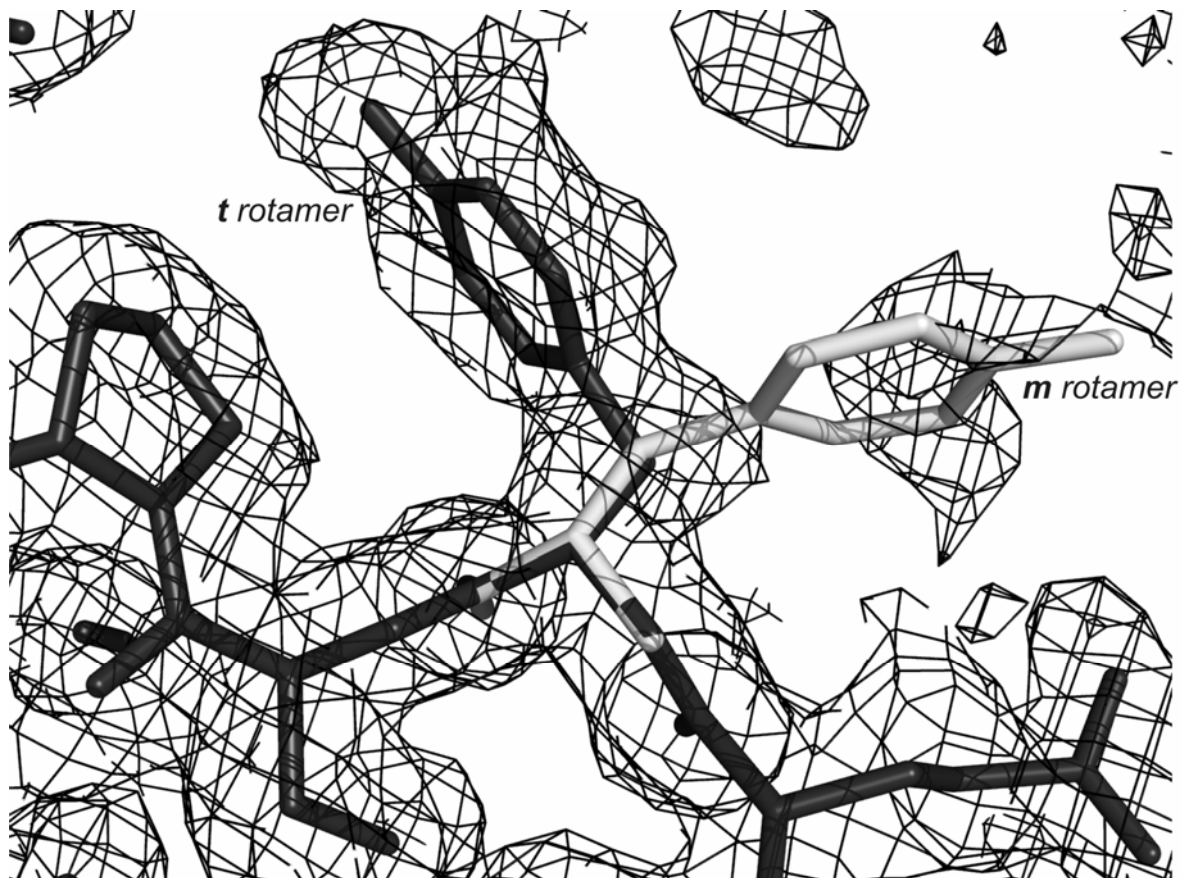


**Figure 3.2.** Electron density surrounding residue Tyr105 in the apoenzyme structure of TEM-1  $\beta$ -lactamase (PDB coordinates 1BTL<sup>7</sup>). Backbone atoms of Tyr105 in the validated simulated annealing conformer 027B ( $\chi_1 = 324^\circ$ ,  $\chi_2 = 302^\circ$ ) (**m** rotamer, in white) are superimposed on backbone atoms of the assigned Tyr105 in 1BTL (**t** rotamer, in dark grey). While the electron density clearly supports assignment of the Tyr105 **t** rotamer in 1BTL, significant electron density in the **m** rotamer area suggests that Tyr105 may also adopt this orientation in free TEM-1. A similar observation was made with another crystal structure of free TEM-1 (PDB coordinates 1XPB<sup>6</sup>).

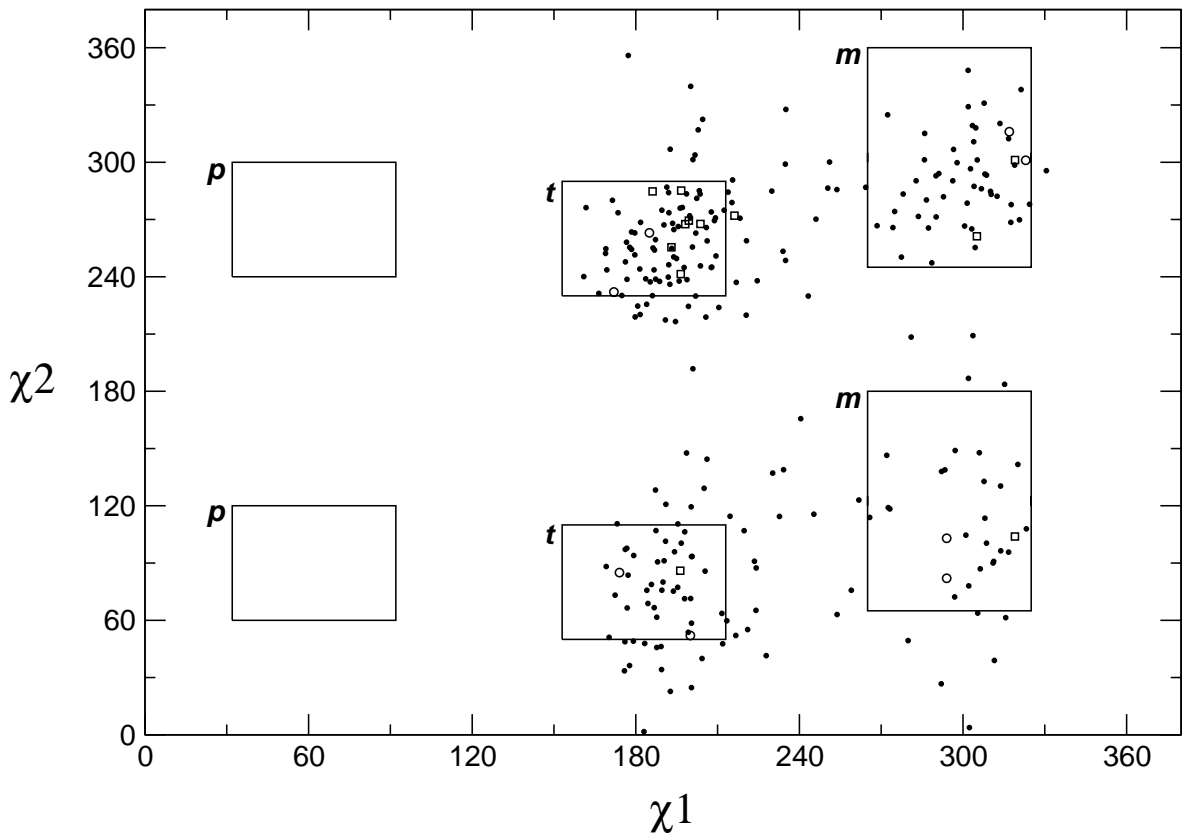


**Figure 3.3.**  $\chi_1/\chi_2$  distribution of Tyr105 for the 260 1-ps simulated annealing snapshots generated in this study. Each conformer is represented by a black circle ( $\bullet$ ), except for the 20 minimized structures, which are represented as follows: the eight MolProbity-validated conformers are shown as open circles ( $\circ$ ) and the 12 non-validated minimized conformers are displayed as open squares ( $\square$ ) (Table S3.1, Supplementary Material, *Annexe 4*). Black boxes delineate  $\chi_1$  and  $\chi_2$  angles allowed for each rotamer of tyrosine and correspond to the following common angles ( $\pm 30^\circ$ )<sup>25</sup>: **p**  $90^\circ$  rotamer ( $\chi_1 = 62^\circ$ ,  $\chi_2 = 90^\circ$  or  $270^\circ$ ) and **t**  $80^\circ$  rotamer ( $\chi_1 = 183^\circ$ ,  $\chi_2 = 80^\circ$  or  $260^\circ$ ). For **m**, the neighbouring **m**- $30^\circ$  ( $\chi_1 = 295^\circ$ ,  $\chi_2 = 150^\circ$  or  $330^\circ$ ) and **m**- $85^\circ$  ( $\chi_1 = 295^\circ$ ,  $\chi_2 = 95^\circ$  or  $275^\circ$ ) rotamers are grouped into a single box defined by the outer angle values of each rotamer. The local environment of Tyr105 in TEM-1  $\beta$ -lactamase prevents adoption of the **p** rotamer as a result of steric hindrance. The

broad  $\chi_1/\chi_2$  distribution, within allowed as well as disallowed regions, illustrates the wide conformational sampling provided by the simulated annealing protocol. The eight validated conformers were observed in both **t** and **m** rotamer regions.

## Préface au chapitre 4

Dans le but de tester les hypothèses dynamiques présentées aux deux chapitres précédents, nous avons entrepris une analyse expérimentale par résonance magnétique nucléaire sur TEM-1 natif et sur les mutants d'intérêt Y105D, Y105G, Y105N et Y105W. Les résultats de déplacements chimiques démontrent que l'effet électronique du remplacement de ce résidu chez TEM-1 ne se limite pas à son environnement immédiat et affecte notamment certains résidus de l'enzyme situés à des distances importantes du site de mutation. Par ailleurs, une analyse de relaxation RMN entreprise sur le mutant Y105D démontre la modification d'événements dynamiques variés sur deux échelles de temps (ps-ns et μs-ms) qui sont observés chez certains résidus essentiels à la reconnaissance et à la stabilisation des substrats chez TEM-1. Globalement, nos résultats nous ont permis d'identifier des effets dynamiques à courte et à longue portée qui suggèrent l'existence d'un réseau complexe de motions moléculaires liées à la fonction parmi les résidus du site actif de cette enzyme.

Ces travaux ont été entrepris en collaboration avec le groupe RMN de Stéphane M. Gagné (Université Laval, Québec) et les résultats de ce chapitre sont présentés sous la forme d'un article scientifique actuellement sous presse dans la revue *The Journal of Biological Chemistry*. En plus d'avoir construit tous les mutants dont il est question dans cette étude, j'ai également été impliqué au niveau des travaux de RMN sous la supervision et l'aide de Pierre-Yves Savard. Ainsi, en plus d'avoir effectué les expériences d'expression et de purification des protéines marquées en commun avec ce dernier, je fus personnellement responsable de l'attribution des spectres de tous les mutants Y105X, de l'analyse de relaxation du mutant Y105D et de la rédaction d'une bonne partie du manuscrit. En plus de fournir une aide RMN précieuse et d'effectuer l'acquisition des spectres, Pierre-Yves Savard fut impliqué au niveau de l'analyse complète de l'enzyme native (attribution, relaxation, « Model-free ») et participa également de manière importante à la rédaction de l'article.

À titre d'introduction aux techniques RMN employées dans ce présent chapitre, le lecteur est encouragé à lire le document présenté en Annexe 3, qui effectue un bref survol de la RMN multidimensionnelle en plus de fournir une brève présentation de la relaxation de l'azote-15 ( $^{15}\text{N}$ ) et des analyses « Model-free » dont il est question au chapitre 4. De plus, il est à noter que le matériel supplémentaire de ce chapitre est présenté en Annexe 4.

## CHAPITRE 4

### Analyse RMN de mutants Y105X de la $\beta$ -lactamase TEM-1 : Corrélation entre dynamique et fonction

#### 4.1 Article 3. *NMR investigation of Tyr-105 mutants in TEM-1 $\beta$ -lactamase: Dynamics are correlated with function*

“Reprinted with permission from: Nicolas Doucet, Pierre-Yves Savard, Joelle N. Pelletier and Stéphane M. Gagné. “NMR investigation of Tyr-105 mutants in TEM-1  $\beta$ -lactamase: Dynamics are correlated with function.” *The Journal of Biological Chemistry* (2007), *In Press*. ©2007, *The American Society for Biochemistry and Molecular Biology, Inc.* Reprinted with permission from *The American Society for Biochemistry and Molecular Biology, Inc.*”

# **NMR investigation of Tyr-105 mutants in TEM-1 β-lactamase: Dynamics are correlated with function**

Nicolas Doucet<sup>1\*</sup>, Pierre-Yves Savard<sup>2\*</sup>, Joelle N. Pelletier<sup>1,3</sup> &  
Stéphane M. Gagné<sup>2</sup>

<sup>1</sup>*Département de chimie and* <sup>3</sup>*Département de biochimie, Université de  
Montréal, C.P. 6128, Succursale Centre-ville, Montréal (Québec), H3C 3J7  
CANADA*

<sup>2</sup>*Département de biochimie et de microbiologie et CREFSIP, Université Laval,  
Québec (Québec), G1K 7P4  
CANADA*

*J. Biol. Chem.*, In Press

(published online ahead of print April 10, 2007;  
doi:10.1074/jbc.M609777200)

\* = These authors made an equal contribution to this work

## ABSTRACT

The existence of coupled residue motions on various timescales in enzymes is now well accepted and their detailed characterization has become an essential element in understanding the role of dynamics in catalysis. To this day, a handful of enzyme systems have been shown to rely on essential residue motions for catalysis but the generality of such phenomena remains to be elucidated. Using NMR spectroscopy, we investigated the electronic and dynamical effects of several mutations at position 105 in TEM-1  $\beta$ -lactamase, an enzyme responsible for antibiotic resistance. Even in absence of substrate, our results show that the number and magnitude of short- and long-range effects on  $^1\text{H}$ - $^{15}\text{N}$  chemical shifts are correlated with the catalytic efficiencies of the various Y105X mutants investigated. In addition,  $^{15}\text{N}$  relaxation experiments on mutant Y105D show that several active-site residues of TEM-1 display significantly altered motions on both ps-ns and  $\mu\text{s}$ -ms timescales despite many being far away from the site of mutation. The altered motions among various active-site residues in mutant Y105D may account for the observed decrease in catalytic efficiency, therefore suggesting that short- and long-range residue motions could play an important catalytic role in TEM-1  $\beta$ -lactamase. These results support previous observations suggesting that internal motions play a role in promoting protein function.

## INTRODUCTION

Enzymes are extremely efficient catalysts that can accelerate biochemical reactions up to a factor of  $10^{18}$  when compared to the same uncatalyzed reaction (1). Although considerable progress has been made in understanding enzyme catalysis over the past few years (2, 3), the detailed explanation of this large rate enhancement remains a significant challenge. Historically regarded as relatively static entities, increasing evidence now

suggests that enzymes behave as dynamical machines and that motions on various timescales play important roles in promoting enzyme catalysis (4). To this day, only a small number of enzymes have been shown to rely on essential proximal and/or distal coupled-residue motions for catalysis, among which dihydrofolate reductase (5-8), cyclophilin A (9, 10), liver alcohol dehydrogenase (11-14), triosephosphate isomerase (15-19) and ribonuclease A (20-22) remain some of the best characterized systems (for recent reviews see (23, 24)). Analogous behaviour among other enzymes remains to be elucidated, although the confirmation of such phenomena in structurally and functionally unrelated protein families and folds suggests that this may be a widespread process (24). A general view of such correlation between structure, function and dynamics in enzymes would greatly improve our current understanding of these powerful catalysts. In the present work, we provide experimental evidence supporting the importance of active-site residue motions in the enzyme TEM-1  $\beta$ -lactamase through the characterization of various Y105X mutants by NMR spectroscopy.

We have previously investigated the role of the active-site residue Tyr105 in TEM-1  $\beta$ -lactamase using saturation mutagenesis, enzyme kinetics and *in silico* molecular dynamics studies (25). Our results show that this residue is mainly involved in substrate discrimination and stabilization at the active site of TEM-1. Aromatic residues at position 105 were shown to play an important role in substrate stabilization by preventing steric hindrance with substrate molecules through the formation of a rigid, stabilizing wall that restricts the active-site cavity size, and therefore substrate movement. Most non-aromatic residue replacements at position 105 were found to possess too many degrees of freedom for appropriate substrate stabilization, thus explaining the strong aromatic bias observed in other class A  $\beta$ -lactamases at this active-site position. Interestingly, Y105G, Y105N and Y105A were moderately active in hydrolysis of penicillin substrates, despite the fact that they are not aromatic. Increasing side chain length (and flexibility) generally resulted in important decreases in activity. Charged side chains (except the aromatic His) were also

poorly compatible with reactivity. These kinetic observations correlated with the extent of Y105X side chain motion upon molecular modeling in the presence of a penicillin substrate: only the aromatic and the small residues provided a stable, well-organized binding environment over the short timescale tested (picosecond; ps). In order to further explore dynamics of these TEM-1  $\beta$ -lactamase active-site mutants, we turned to nuclear magnetic resonance.

NMR relaxation experiments are powerful techniques that can provide valuable information on the dynamical effects of mutations in the active site cavity of enzymes during catalysis (10). In addition to providing information on fast dynamics (ps-ns) of protein backbones (26), the timescale of NMR dynamics ranges up to the catalytically-relevant  $\mu$ s-ms (27). The recent and complete  $^1\text{H}$ ,  $^{15}\text{N}$ ,  $^{13}\text{C}$  backbone resonance assignments of TEM-1 (E28G)  $\beta$ -lactamase by NMR (28) as well as  $^{15}\text{N}$  relaxation backbone dynamics studies on the same enzyme (29) now pave the way to the motional characterization of important active site residues with respect to their effect on catalysis in this enzyme family. In order to improve the interpretation of our previous molecular modeling and kinetics observations at the molecular level and to verify the proposed motion of residue 105 in TEM-1, the present study describes the backbone resonance assignments of TEM-1 mutants Y105D, Y105G, Y105N and Y105W as well as  $^{15}\text{N}$  backbone relaxation dynamics of wild-type TEM-1 and mutant Y105D. To our surprise, the localized dynamical effects we had originally observed by molecular modeling in the area of position 105 extend to a far broader environment, affecting catalytically-relevant motional timescales of important catalytic residues in the active site cavity of TEM-1. The dynamical investigation of the Y105D mutant and the effects of the Y105X mutations on the surrounding environment provide evidence for the importance of active-site residue motions in TEM-1  $\beta$ -lactamase as well as their possible role in substrate stabilization and catalysis. In addition to long-range effects observed for residues distal to the active site as well as evidence offered by previous molecular dynamics investigation performed on a TEM-1 mutant (30), these

experimental observations suggest that class A  $\beta$ -lactamases may rely on long-range residue motions in substrate recognition as well as for catalysis.

## EXPERIMENTAL PROCEDURES

*Reagents*—Unless otherwise indicated, all chemicals were purchased from Sigma-Aldrich Canada (Oakville, ON). Bis-tris propane was purchased from GE Healthcare (Mississauga, ON) and nitrocefin was purchased from Oxoid (Nepean, ON). Restriction and DNA-modifying enzymes were purchased from MBI Fermentas (Burlington, ON) and New England Biolabs, Ltd. (Mississauga, ON).  $^{15}\text{NH}_4\text{Cl}$ ,  $^{13}\text{C}$ -glucose, 2,2-dimethylsilapentane-5-sulfonic acid (DSS) and  $^2\text{H}_2\text{O}$  were purchased from Cambridge Isotope Laboratories (Andover, MA).

*Bacterial strains and plasmids*—*E. coli* XL1-Blue (*supE44, hsdR17, recA1, endA1, gyrA46, thi, relA1, lac F'* [*proAB<sup>+</sup>, lacI<sup>q</sup>, lacZΔM15, Tn10(tet<sup>r</sup>)*]) was used for cloning and plasmid propagation while *E. coli* BL21(DE3) (*hsdS gal [λcIts857 ind1 Sam7 nin5 lacUV5-T7 gene 1]*) was used for protein expression. Plasmid pET-TEM-1 (31), in which the wild-type *bla<sub>TEM-1</sub>* gene was fused to the leader sequence of *ompA* was a generous gift from Marvin D. Makinen (University of Chicago, IL). It was maintained using 30 µg/ml kanamycin (Kan) and was used for extracellular protein expression under the control of the T7 promoter in *E. coli* BL21(DE3). The construction of plasmids pQE32Chl-TEM(Y105X) containing the Y105X mutations of TEM-1 was described elsewhere (25).

*Oligonucleotides and mutagenesis*—Oligonucleotide primers used for mutagenesis were synthesized by Integrated DNA Technologies (Coralville, IA) and by the Laboratoire de Synthèse et d'Analyse d'Acides Nucléiques (Université Laval, QC). Oligonucleotide primers used for DNA sequencing were synthesized by Li-Cor Biotechnology (Lincoln, NB). The E28G mutation originally present in the pET-TEM-1 construction was reverted

back to WT using the QuickChange Site-directed mutagenesis kit from Stratagene (La Jolla, CA) with mutagenic primers TEM-G28E-UPPER (5'-CAGGCCACCCAGAAACGCTGGTGAAAGTA-3') and TEM-G28E-LOWER (5'-TACTTCACCAGCGTTCTGGGTGGGCCTG-3'). The Y105D, Y105G, Y105N and Y105W mutants of TEM-1 (25) were PCR-amplified from vectors pQE32Chl-TEM(Y105X) using the two following terminal primers: TEMhinDIIIR (5'-ACACACAAGCTTTACCAATGCTTAATCAGTGA-3') and NdeIompATEMF (5'-CACACACACATATGAAAAAGACAGCTATCGCGATTGCAGTGGCACTGGCTG GTTCGCTACCGTAGCGCAGGCCACCCAGAAACGCTGGTGAAA-3'), a 95-bp forward primer containing both the *NdeI* restriction site and the *ompA* leader sequence. The resulting recombinant *ompA*-TEM(Y105X) genes were sequentially digested with *NdeI* and *PstI* and cloned into *NdeI/PstI*-digested and shrimp alkaline phosphatase-treated pET-TEM-1 before electroporation into *E. coli* XL1-Blue cells. Colonies were individually picked after selection on Luria-Bertani (LB) medium containing 30 µg/ml Kan, and the sequence of each mutant was confirmed by the dideoxy chain termination method with the Thermo Sequenase Cycle Sequencing kit from Upstate Biotechnology Corp. (Cleveland, OH) using dye-labeled primers and a Li-Cor automated sequencer (Lincoln, NB). For protein expression purposes, DNA constructs were transformed into *E. coli* BL21(DE3) cells and sequenced again.

*Expression and purification of <sup>15</sup>N-<sup>13</sup>C-labeled WT and TEM-1(Y105X) mutants*—Uniformly <sup>15</sup>N-<sup>13</sup>C labeled TEM-1 samples were prepared using <sup>15</sup>NH<sub>4</sub>Cl and <sup>13</sup>C-glucose as the sole nitrogen and carbon sources according to the following protocol. A 2-ml overnight culture of each BL21(DE3)/pET-TEM-1(Y105X) clone was used to inoculate 500 ml of M9 minimal medium containing 0.04 M Na<sub>2</sub>HPO<sub>4</sub>, 0.02 M KH<sub>2</sub>PO<sub>4</sub>, 0.02 M <sup>15</sup>NH<sub>4</sub>Cl, 0.01 M NaCl, 0.3 % <sup>13</sup>C-glucose, 2 mM MgSO<sub>4</sub>, 2 µM FeCl<sub>3</sub>, 0.1 mM CaCl<sub>2</sub>, 50 µM ZnSO<sub>4</sub>, 0.5 % thiamine, 2.5 mM betain and 30 µg/ml kanamycin. The proteins were expressed by propagating the host cells at 37°C (250 rpm) to an A<sub>600 nm</sub> = 0.8

followed by induction with 0.4 mM isopropyl 1-thio- $\beta$ -D-galactopyranoside (IPTG) and addition of 15  $\mu$ g/ml kanamycin for 16-18 hours at 25°C (250 rpm). After induction, cells were pelleted by centrifugation (30 min, 10 000 g, 4 °C) and the supernatant was filtered using a 0.45  $\mu$ m membrane filter prior to a fivefold concentration using a 8400 Stirred-Cell apparatus from Millipore (Nepean, ON) with an Ultracel Amicon YM-10 membrane (molecular weight cutoff 10 000 Da).

After overnight dialysis at 4°C against a 10 mM Bis-tris Propane buffer (pH 6.6), purification of WT and TEM(Y105X) mutants was performed on an ÄKTAexplorer chromatography system from GE Healthcare (Mississauga, ON) as previously reported (29). In all cases, purity was estimated to be higher than 95 % by SDS-PAGE and LC/MS/ESI and yields were typically ~50 mg/L of pure protein for all TEM-1(Y105X) mutants.

*NMR samples*—For the acquisition of NMR spectra, WT and mutants Y105D, Y105G, Y105N and Y105W were lyophilized after extensive dialysis against H<sub>2</sub>O. The enzymes were subsequently dissolved to a concentration of 0.8 mM in a 90 % H<sub>2</sub>O:10 % <sup>2</sup>H<sub>2</sub>O solution containing 4 mM imidazole and 0.1 mM DSS for internal pH and chemical shift referencing, respectively. All experiments were performed at pH 6.6.

*NMR spectroscopy*—All NMR experiments were performed at 30°C on a Varian INOVA 600 spectrometer operating at a proton frequency of 599.739 MHz equipped with a z-axis gradient and a triple resonance cryoprobe. 2D <sup>1</sup>H-<sup>15</sup>N HSQC, 3D-HNCO, 3D-HN(CO)CA and 3D-CBCA(CO)NH spectra (Biopack, Varian Inc., Palo Alto, CA) together with assignments obtained for TEM-1 E28G (28) were used to determine sequence-specific assignments for the polypeptide backbone of WT and mutant Y105W. Other mutants (Y105D, Y105G and Y105N) were assigned by comparison using a combination of 2D <sup>1</sup>H-<sup>15</sup>N HSQC and 3D-HNCO spectra.

<sup>15</sup>N relaxation experiments were performed on WT and on the Y105D mutant using <sup>15</sup>N-<sup>13</sup>C double-labeled samples for all experiments. <sup>15</sup>N-T<sub>1</sub> experiments were performed using sensitivity-enhanced inversion-recovery pulse sequence with pulsed field gradients developed by Kay and coworkers (32). <sup>15</sup>N-T<sub>2</sub> experiments were performed using the BioPack pulse sequence from Varian, Inc. (Palo Alto, CA) (33). A RF field strength of 6.579 kHz was used for the <sup>15</sup>N 180 degree pulses in the CPMG sequence with an inter-pulse delay of 587 μs. Delay times were 10.9, 21.7, 43.5, 87.0, 173.9, 347.8, 695.7, 1391.3 and 1989.1 ms for T<sub>1</sub> and 10, 30, 50, 70, 90, 110, 130, 150 and 190 ms for T<sub>2</sub>. {<sup>1</sup>H}-<sup>15</sup>N steady state NOEs were obtained by acquiring spectra with and without <sup>1</sup>H saturation applied before the start of the experiments using a pulse sequence obtained from the Kay group (32). A saturation time of four seconds was used for {<sup>1</sup>H}-<sup>15</sup>N NOE experiments. In order to eliminate the potential effect of sample or field homogeneity degradation over time on measured exponential decays, relaxation delays were acquired in an interleaved manner. For example, the acquisition order for the <sup>15</sup>N-T<sub>2</sub> relaxation experiments was: 10, 50, 90, 130, 30, 70, 110, 150 and 190 ms (34, 35).

*Data analysis*—All NMR data were processed with NMRPipe/NMRDraw (36) and analyzed with NMRView (37). For relaxation experiments, <sup>1</sup>H-<sup>15</sup>N spectra were processed using either a 90° or a 60° shifted sine apodization function in F2 (<sup>1</sup>H) and either a 90° or a 60° shifted sine-squared function in F1 (<sup>15</sup>N). The 90° processing was used for the great majority of residues, and the 60° processing allowed the separation of a few peaks exhibiting slight overlapping. Linear prediction was performed in F1 to extend the time domain by a factor of 1.5 and both dimensions were zero-filled to the next power of 2. For each <sup>15</sup>N-T<sub>1</sub> and <sup>15</sup>N-T<sub>2</sub> experiment, the spectrum with the shortest relaxation delay (highest intensities) was peak-picked with NMRView and each ellipse was manually adjusted to fit the peak. The same procedure was used for {<sup>1</sup>H}-<sup>15</sup>N NOE spectra.

The <sup>15</sup>N R<sub>1</sub> and R<sub>2</sub> relaxation rates were determined by fitting T<sub>1</sub> and T<sub>2</sub> curves to a two-parameter exponential decay of the form:

$$V(t) = V_0 e^{(-Rt)} \quad (1)$$

where  $V(t)$  is the volume after a delay time  $t$ ,  $V_0$  is the volume at time  $t = 0$  and  $R$  is either  $R_1 = 1/T_1$  or  $R_2 = 1/T_2$ . Fitting was accomplished using the program CURVEFIT (AG Palmer, Columbia University, New York, NY).  $R_1$  and  $R_2$  uncertainties were calculated using Jackknife simulations and for each dataset the minimum error used for further calculation was set to the mean error.  $\{^1\text{H}\}-^{15}\text{N}$  NOE values were obtained from the ratio of the volumes of experiments recorded with and without proton saturation. The uncertainties on the  $\{^1\text{H}\}-^{15}\text{N}$  NOE values were obtained using the method described by Nicholson *et al.* (38).

*Model-free*—The internal motion parameters were optimized for the relaxation data according to the model-free formalism pioneered by Lipari and Szabo (39, 40) and extended by Clore *et al.* (41, 42) using the program ModelFree 4.16 (AG Palmer, Columbia University, New York, NY) and the statistical approach of Mandel *et al.* (43). An axially symmetric diffusion model was used in our analysis. Initial estimates of the global tumbling parameters were obtained using the program QUADRIC (AG Palmer, Columbia University, New York, NY). Residues with  $\{^1\text{H}\}-^{15}\text{N}$  NOE  $< 0.65$  were not considered, neither were residues with high  $R_2$  ( $R_2 \geq \langle R_2 \rangle + \sigma_{R2}$ ), unless their corresponding  $R_1$  values were low ( $R_1 \leq \langle R_1 \rangle - \sigma_{R1}$ ) (44). The value used for  $^{15}\text{N}$  chemical shift anisotropy was -172 ppm and the N-H bond length was set to 1.02 Å. For each simulation, 500 randomly distributed data sets were generated and discrimination between models was performed using F-statistics analysis.

The five models used to describe the spin-relaxation data were:

Model 1:  $S^2$

Model 2:  $S^2, \tau_e$

Model 3:  $S^2$ ,  $R_{ex}$

Model 4:  $S^2$ ,  $\tau_e$ ,  $R_{ex}$

Model 5:  $S^2$ ,  $\tau_e$ ,  $S^2_f$

in which  $S^2$  is the order parameter used to characterize the amplitude of the internal motions on the ps-ns timescale.  $S^2$  is a measure of the degree of spatial restriction of the  $^1\text{H}$ - $^{15}\text{N}$  bond vector, and has values ranging from zero, indicating unrestricted motions, to one, for completely restricted motions.  $S^2_f$  is the order parameter for fast motions,  $\tau_e$  is the effective correlation time for internal motions, and  $R_{ex}$  is an exchange term to account for contributions to  $R_2$  from  $\mu\text{s-ms}$  timescale motions.

*Estimation of the Tyr105 ring current effects and prediction of chemical shifts changes induced by the mutation*—Ring current effects of the Tyr105 aromatic group on the chemical shifts of other residues were estimated using the program SHIFTS (version 4.1.1) (45) for TEM-1 with Tyr105 positioned in two alternate conformations (positions A and B). Position A places Tyr105 as observed in the free-enzyme conformation of TEM-1 (Protein Data Bank, Brookhaven National Laboratory, coordinates 1BTL) (46) while position B places Tyr105 as observed in the imipenem-bound flipped conformation (PDB coordinates 1BT5) (47). Minimized PDB files were created using the InsightII package, version 2000.1 (Accelrys, San Diego, CA) according to the following protocol. For position A, the 1.8-Å crystallographic structure of the *E. coli* TEM-1  $\beta$ -lactamase (PDB coordinates 1BTL) was used as starting coordinates. The crystallographic water molecules and the active site  $\text{SO}_4^{2-}$  molecule were deleted and hydrogen atoms were added at the normal ionization state of the amino acids at pH 7.0. The structure was energy-minimized by applying 1000 steps of steepest descent followed by a conjugate gradient minimization until convergence of 0.001 kcal mol $^{-1}$  Å $^{-1}$ . For position B, backbone atoms of 1BTL and 1BT5 were superimposed and the Tyr105 side chain of 1BTL was repositioned according to

Tyr105 in 1BT5 by applying  $\chi_1$  and  $\chi_2$  angle torsions. The structure was then minimized using the same protocol as for position A. The contribution of Tyr105 to ring current shifts was estimated with all aromatic residues mutated to Ala, except for Tyr105. SHIFTS was also used in order to predict the effect of the mutation on chemical shifts of other residues of the protein. Observed chemical shift changes were considered meaningful when they were significantly greater than the predicted ones.

*Sequence numbering*—Because of technical requirements in NMR analysis, sequence numbering used for TEM-1 and mutants Y105X is different from the classical nomenclature proposed by Ambler *et al.* (48). Although sequence numbering starts at 26 to give the active-site serine residue the number 70, residues 239 and 253 are not skipped and the numbering is sequential from 26 to 288. In order to avoid any confusion in catalytic and structural interpretation, both nomenclatures are appropriately labeled.

## RESULTS

$^{15}\text{N}$ - $^{13}\text{C}$ -labeled proteins corresponding to mutants Y105D, Y105G, Y105N and Y105W of TEM-1  $\beta$ -lactamase were expressed and purified to homogeneity. These mutants were chosen based on the following structural and functional considerations: Trp because of its aromatic similarity with the native Tyr, the native-like activity of mutant Y105W toward penicillins and cephalosporins, and also because of its frequent occurrence in other class A  $\beta$ -lactamases; Asn because its side-chain is much smaller than the native, aromatic Tyr while still being a highly active mutant also occasionally represented in other class A  $\beta$ -lactamases; Gly because, like Ala, it exhibits discrimination with respect to penicillins (high catalytic efficiency) and cephalosporins (low catalytic efficiency); and Asp as a representative of a low-activity mutant despite its structural similarity with the highly-active Asn mutant (25).

*Chemical shift differences*— Although our previous NMR studies of TEM-1 were carried on the E28G mutant (28, 29), the present study was performed without this mutation and assignments of WT TEM-1 were used (Biological Magnetic Resonance Data Bank accession number 6357). A combination of 2D  $^1\text{H}$ - $^{15}\text{N}$  HSQC, 3D-HNCO, 3D-HN(CO)CA and 3D-CBCA(CO)NH spectra (Biopack, Varian Inc., Palo Alto, CA) were used to sequentially assign nearly all the backbone  $^1\text{H}$ ,  $^{15}\text{N}$  and  $^{13}\text{C}$  atoms (BMRB numbers for Y105W, Y105G, Y105N and Y105D are 7236, 7237, 7238, and 7239, respectively). More than 99 % of backbone  $^1\text{H}$ ,  $^{15}\text{N}$  and  $^{13}\text{C}$  assignments were obtained for non-proline residues of each enzyme tested. For WT and mutants Y105D, Y105G and Y105N, the missing assignments are  $^1\text{H}/^{15}\text{N}$ -Ser70,  $^1\text{H}/^{15}\text{N}$ -Ala237 whereas for mutant Y105W, the missing assignments are  $^1\text{H}/^{15}\text{N}$ -Ser70,  $^1\text{H}/^{15}\text{N}$ -Asn132 and  $^1\text{H}/^{15}\text{N}$ -Ala237. As previously observed for the E28G assignments (28), the missing chemical shifts are attributed to peaks overlapping or missing resonances caused by line broadening. Regardless of the functional differences resulting from the Y105X mutations, the 2D and 3D NMR spectra of all mutants are quite similar to those of the WT enzyme (Figure in supplementary material). However, depending on the mutation at position 105, important chemical shift differences were observed at specific residues relative to WT. Figure 4.1 presents the structural mapping of backbone amide chemical shift differences ( $\Delta\delta_{\text{HN}}$ ) observed between WT and mutants Y105X while Figure 4.2 presents the magnitude of these  $\Delta\delta_{\text{HN}}$  displayed on the primary sequence of the enzyme. For all mutants, the most important effects observed on  $\Delta\delta_{\text{HN}}$  occur in three major areas of the enzyme corresponding to residues 100-115, 120-140 and 213-218 (Figure 4.2). To a lesser extent, all mutants also display higher-than-background effects on  $\Delta\delta_{\text{HN}}$  in regions encompassing residues 68-80, 163-170 and 235-246. Finally, with the exception of residue 215,  $\Delta\delta_{\text{HN}}$  is generally smaller for mutant Y105W than for the three other Y105X mutants investigated.

Residues in contact with substrate molecules or directly implicated in catalysis in TEM-1  $\beta$ -lactamase are all located within active-site walls encompassing residues Met69-

Lys73, Val103-Ser106, Met129-Asn132, Glu166-Asn170, Val214-Gly218, Lys234-Glu239 (Ambler Lys234-Glu240), Arg243 (Ambler Arg244), Met270 (Ambler Met272) and Asn274 (Ambler Asn276) (Figure 4.3 and grayed regions in Figures 4.2 and 4.5). Since these residues are generally located in the immediate vicinity of the substrate molecule and, in some cases, are very close to the mutated residue, some  $\Delta\delta_{HN}$  may be the result of a direct short-range interaction with residues in close proximity to the Tyr105 mutation. For instance, the shortest distance between Tyr105 and Asn132 ( $O_{105}-N_{132}$ ) is only 3.0 Å in the crystal structure of the free enzyme (PDB coordinates 1BTL), therefore providing an explanation for the magnitude of  $\Delta\delta_{HN}$  observed at position Asn132 in all Y105X mutants. In contrast, although they form the substrate cavity in TEM-1, some of these active-site walls are constituted by residues separated by large distances (*e.g.* the shortest distance between Tyr105 and Glu166,  $O_{105}-O\varepsilon_{166} = 7.6$  Å). Interestingly, the active-site walls are generally more affected by the Y105X mutation than any other portion in the enzyme and most segments of each wall contain at least one residue displaying higher-than-average  $\Delta\delta_{HN}$  (Figure 4.2). Moreover, while being generally concentrated near the active site cavity, significant effects on  $\Delta\delta_{HN}$  are nevertheless observed throughout the enzyme for all mutants, sometimes more than 20 Å from the site of mutation (Figure 4.1). This result illustrates that the effect of mutations at position 105 is not restricted to a local environment. In fact, while 57 residues of mutant Y105W display backbone  $\Delta\delta_{HN}$  greater than 11 Hz when compared with WT (22 % of the total enzyme), this number jumps to 78 residues (30 %) in Y105G, 91 residues (35 %) in Y105N and 104 residues (40 %) in Y105D (Table 4.1), thus clearly extending beyond the immediate environment of position 105. In fact, the Y105X mutation is too far away from several residues displaying significant  $\Delta\delta_{HN}$  to result in any direct contribution to chemical shift changes (*e.g.* backbone  $^{15}N_{105}-^{15}N_x$  distances = 12.7 Å for Gly238, 12.9 Å for Leu169, 19.0 Å for Leu76), therefore suggesting the existence of coupled long-range effects caused by the mutation at position 105.

The  $\pi$ -system of aromatic residues such as tyrosine can generate a local magnetic field known as ring current which opposes the externally applied field and may significantly affect the chemical shift of surrounding nuclei. To verify whether short- and long-range chemical shift differences observed in the Y105X mutants could simply be attributed to the disappearance of the aromatic hydroxyphenyl side-chain of Tyr105, we used the program SHIFTS (45) to predict ring current effects originating from Tyr105. Ring current shifts were calculated for both previously observed conformations of the Tyr105 side-chain in crystal structures of TEM-1 (46, 47). Significant ring current shifts for Tyr105 were predicted in the immediate vicinity of position 105 (90 Hz predicted for backbone  $^1\text{H}_\text{N}$  of residue 106, 72 Hz for 108, less than 36 Hz for residues 109, 110, 130-132), but no other significant effect ( $>15$  Hz) was predicted for either of the two side-chain conformations of residue 105 (results not shown). This indicates that significant long-range chemical shift differences observed in all Y105X mutants are not attributed to direct electronic perturbation caused by the elimination of the hydroxyphenyl side-chain of Tyr105, and therefore must rely on a combination of concerted effects that have consequences throughout the enzyme.

It is also interesting to note that the number and magnitude of the effects on  $\Delta\delta_{\text{HN}}$  generally correlate with the previously reported catalytic efficiencies of the same mutants for the classical substrate benzylpenicillin (Table 4.1) (25), suggesting that electronic perturbations and/or dynamical effects observed by NMR may adequately reflect catalytic effects caused by this mutation in TEM-1. Thus, mutant Y105W displays fewer affected residues (22 %), consistent with its high catalytic efficiency, while 40 % of the residues of the weakly-active Y105D mutant show significant  $^1\text{H}$ - $^{15}\text{N}$  chemical shift perturbation. This mutant also displays chemical shift perturbation for a greater number of catalytic residues than the other Y105X mutants, consistent with its low catalytic efficiency (Y105D- $k_{cat} = 255 \text{ s}^{-1}$ , Y105D- $K_M = 369 \mu\text{M}$ , Y105D- $k_{cat}/K_M = 6.9 \times 10^5 \text{ M}^{-1} \text{ s}^{-1}$  versus WT- $k_{cat} = 1240 \text{ s}^{-1}$ ,

WT- $K_M = 43 \mu\text{M}$ , WT- $k_{cat}/K_M = 2.9 \times 10^7 \text{ M}^{-1} \text{ s}^{-1}$ ) (Table 4.2) (25). In addition, these  $\Delta\delta_{\text{HN}}$  are generally of greater magnitude as catalytic efficiency decreases.

*<sup>15</sup>N backbone relaxation dynamics*— Previous experimental observations made by X-ray crystallography on TEM-1 have shown that Tyr105 can adopt two alternate conformations in presence of substrates or inhibitors (47). While the Tyr105 hydroxyphenyl side-chain points toward Val216 in the free enzyme, a  $\chi_1$ -angle rotation of more than 110° has been observed in presence of the inhibitor imipenem (47), making this the largest conformational change observed in the enzyme. High flexibility of Tyr105 is suggested by high B-factor values of Tyr105 in several crystal structures of TEM-1 (46, 49) and confirmed by a lower-than-average order parameter of this amide in solution as evaluated by NMR (29). However, our previous dynamical modelling studies of this residue showed a low propensity of Tyr105 for conformational change on the ps timescale relative to more flexible Y105X replacements, suggesting that positioning and restricted dynamical motions of the Tyr105 side-chain could be a determinant of recognition for substrate stabilization in TEM-1  $\beta$ -lactamase (25).

TEM-1 Y105D displayed the most important effects on  $\Delta\delta_{\text{HN}}$  relative to WT as well as a reduction of two orders of magnitude in its catalytic efficiency for benzylpenicillin (25). We therefore conducted <sup>15</sup>N backbone relaxation dynamics studies in order to evaluate the importance of local and global dynamical effects caused by the Y105D mutation. To obtain dynamical information on timescales of picoseconds-nanoseconds (ps-ns) and microseconds-milliseconds ( $\mu\text{s-ms}$ ), both longitudinal ( $R_1$ ) and transverse ( $R_2$ ) <sup>15</sup>N relaxation rates as well as {<sup>1</sup>H}-<sup>15</sup>N NOE values were measured and are presented in Figure 4.4 for both WT and mutant Y105D (raw data presented in supplementary material). We observed a significant variation of relaxation data and global-tumbling times as a function of protein concentration. For example, the global correlation time for TEM-1 varied from 12.8 ns at 0.4 mM to 13.8 ns at 0.8 mM. This increase in correlation time is most likely due to an increase in viscosity at high protein concentration. It was therefore crucial for our

analysis that both proteins be at exactly the same concentration. From the  $^1\text{H}$ - $^{15}\text{N}$  HSQC spectra recorded for the relaxation experiments, it was possible to obtain reliable data for 206 and 230 out of 250 potentially observable amides for WT and mutant Y105D, respectively. Table 4.3 presents average values for relaxation data and parameters obtained for TEM-1 and mutant Y105D.

The general comparison of  $R_1$ ,  $R_2$  and  $\{^1\text{H}\}$ - $^{15}\text{N}$  NOE values for TEM-1 and mutant Y105D shows that both enzymes behave in a very similar manner, displaying comparable values throughout the sequence (Table 4.3, Figure 4.4 A-C). The general constant pattern observed in the relaxation data from one extremity of the enzyme to the other is uncommon relative to the pattern generally observed in other proteins, where an important decrease in both N- and C-terminal regions as well as in unstructured regions is frequently observed. This feature reflects the high rigidity of both enzymes in solution, a property that we have also previously observed in TEM-1 (E28G) (29). However, there are significant local differences between the relaxation data for both enzymes, especially concentrated in regions showing important chemical shift differences (*e.g.* residues 70-80, 124-135 and most importantly 211-221) (Figure 4.4 A-C). Figure 4.5 shows the Y105D/WT ratios for all relaxation parameters, highlighting the residues displaying the most important differences between both enzymes. Changes in  $R_1$  and  $\{^1\text{H}\}$ - $^{15}\text{N}$  NOE values reflect differences in the ps-ns dynamics of proteins while changes in  $R_2$  values may also reflect changes in  $\mu\text{s}$ -ms motions. Interestingly, 88 residues are significantly affected in either  $R_1$  and  $\{^1\text{H}\}$ - $^{15}\text{N}$  NOE relaxation parameters, suggesting significant dynamical differences on the ps-ns timescale for these residues (supplementary material, Table S4.3). Among these, fourteen belong to the active-site walls of TEM-1 and may be implicated in substrate stabilisation (Table 4.4). Since it has been proposed that motions on the ps-ns timescale may influence the thermodynamics of binding as well as the kinetics of enzyme-catalyzed reactions (50-52), disruption of ps-ns motions among these active-site residues may reduce substrate stabilization and/or catalysis in mutant Y105D. Similarly, among the 30 residues significantly affected in  $R_2$  (Table S4.3), eleven belong to the active-site walls (Table 4.4),

suggesting that differences in  $\mu$ s-ms motions of these residues between WT and mutant Y105D may also affect substrate stabilization and/or catalysis. Residues 211-221 correspond to the region where the  $R_2$  values are the most affected by the Y105D mutations, both in terms of magnitude and number of residues affected. In addition, since  $\mu$ s-ms dynamics are directly related to the timescale of catalysis, these modified motions may also affect turnover in mutant Y105D. Residue Lys234 is also a particularly good candidate for this, as it has been shown to be an essential member of the catalytically-important hydrogen-bonding sub-network of class A  $\beta$ -lactamases through the formation of a hydrogen bond with Ser130 (an equally-important member of the SDN loop implicated in catalysis (53)).

*Model-free analysis*— In order to correlate our relaxation data with the internal dynamics of the protein, further dynamical analyses were conducted using the model-free formalism pioneered by Lipari and Szabo (39, 40). Such analyses allow for the direct investigation of local and global dynamical effects observed in the protein of interest, namely through the extraction of the order parameter ( $S^2$ ), the conformational exchange parameter ( $R_{ex}$ ) and the overall correlation time of the molecule ( $\tau_m$ ) (Tables 4.3 and 4.4, Figure 4.4 D-E).

Average values of model-free parameters for WT and mutant Y105D confirm that both enzymes behave very similarly with respect to their global dynamical properties (Table 4.3). Following the model selection, there was only a slight divergence between both proteins: for WT and mutant Y105D respectively, 82 % and 81 % of the residues fitted well for model 1, 7 % and 9 % for model 2, and 10 % and 8 % for model 3. No residue was fitted to model 4 nor model 5 in either protein. Both WT and Y105D display a small prolate axial anisotropy with  $D_{||}/D_{\perp}$  values of 1.16 and 1.18 and similar global correlation times ( $\tau_m$ ) of 13.8 and 13.7 ns, respectively (Table 4.3). Considering that the two enzymes differ only by a single mutation, this result was expected. In addition, the average order parameter values ( $S^2$ ) obtained for TEM-1 and mutant Y105D are exceptionally high (> 0.9 for both

enzymes), confirming previous observations reported for TEM-1 (E28G) (29). Since the order parameter measures the amplitude of ps-ns motions and varies from 0 for unrestricted internal motions to 1 for completely restricted motions (43), values  $> 0.9$  are indicative of highly-ordered proteins in solution.

Six residues display distinct behaviour patterns in their order parameters ( $S^2$ ) (Table S4.3), two of which are located in the active-site walls (Ser106 and Glu239) (Table 4.4). These residues display a significant decrease in their order parameters indicating an increase in ps-ns motion amplitude in the mutant compared to WT. Furthermore, five residues display distinct  $\mu$ s-ms motions when compared to WT (Table S4.3), four of which belong to active-site walls (Lys215, Val216, Gly218 and Lys234) (Table 4.4). The model-free analysis for these residues required an  $R_{ex}$  term, which is related to local conformational exchange and refers to motions observed on the  $\mu$ s-ms timescale (43). As the  $^{15}\text{N}$ -HSQC signal of residue Lys215 was significantly weaker for the WT than for Y105D, it was impossible to obtain relaxation data for this residue in the WT. We therefore conclude that  $R_2$  value was significantly higher for the WT, reflecting significantly higher  $R_{ex}$  for Lys215 in the WT. The important decrease of  $R_2$  and  $R_{ex}$  for residues 215, 216, 218 and 234 in mutant Y105D (Figure 4.4 E) suggests a slowdown in motions of these residues on the catalytically-relevant  $\mu$ s-ms timescale. These residues delineate two active-site walls of TEM-1 and Lys215, Val216 and Gly218 are located in the most dynamically-affected region observed between WT and mutant Y105D (Figure 4.4). It is interesting that for this region (211-221), only two residues exhibit small but significant chemical shift differences (Lys215 and Val216), although changes in motional parameters occur for a greater number of residues and are more important, as reflected in the fact that this region displays the most significant changes in  $R_2$  and  $R_{ex}$  values. Assuming exchange in a two-state model, this could suggest that for these residues the rate of exchange between the two states is significantly affected by the mutation, but that the population of each state is roughly the

same in the wt and in mutant Y105D. Therefore, only the rate of exchange would be significantly affected by the mutation.

Despite the fact that the model-free approach is not the most comprehensive evaluation of  $\mu$ s-ms timescale motions, dynamics on this timescale can be inferred from  $R_2$ . Crude  $R_2$  values do not necessarily provide an adequate portrayal of  $\mu$ s-ms dynamics for an enzyme but differences in  $R_2$  for WT and mutant Y105D suggest  $\mu$ s-ms motion differences resulting from this mutation. In addition to the important  $R_{ex}$  differences noted for positions 215, 216, 218 and 234, 13 additional active-site wall or invariant residues may have different  $\mu$ s-ms motions between WT and Y105D, based on significant variation in  $R_2$  (Table 4.4). Motions of Val216 and Lys234 on a catalytically-relevant timescale could affect catalysis by perturbing the hydrogen bonding network observed in WT (Figure 4.6), therefore partly explaining the differences in  $k_{cat}$  previously observed with mutant Y105D (25).

## DISCUSSION

The investigation of the correlations between enzyme dynamics and function is required in order to gain a detailed understanding of the mechanisms underlying the catalytic activity of these important molecules. Implication of ps-ns and  $\mu$ s-ms motions in enzyme activities and catalytic rates is now well accepted and NMR spectroscopy is a valuable tool to probe these time windows (21). In an attempt to explain the differences in the catalytic efficiency of several Y105X mutants of TEM-1, we previously conducted a short 200-ps molecular dynamics simulation that allowed for the partial explanation of differences in affinity through the formation of a stabilizing wall created by residues exhibiting few degrees of freedom at position 105, therefore restricting substrate motion in the active site (25). However, this molecular dynamics simulation model was relatively

limited in that it only allowed for the investigation of small motions explored on a short timescale and exclusively concentrated in the local environment of position 105. In order to better characterize these motions, we investigated the role of the conserved active-site residue Tyr105 by comparing its structural and dynamical features with respect to the Y105W, Y105G, Y105N and Y105D mutants using NMR spectroscopy. The chemical shift differences observed between TEM-1 and these various mutants allowed us to focus our dynamical characterization on the Y105D mutant.

Overall, although the Y105D mutation considerably affects the electronic and dynamic environment of several residues throughout the enzyme, the backbone dynamics of residue 105 is not significantly affected relative to WT, suggesting that local dynamics at position 105 is not the sole element contributing to the differences observed in catalysis. Indeed, despite the important steric and ionic alterations offered by the Y105D replacement, R<sub>1</sub>, R<sub>2</sub>, and {<sup>1</sup>H}-<sup>15</sup>N NOE values of mutant Y105D remain similar to WT. On the other hand, our present analyses revealed significant short- and long-range changes in motion throughout the enzyme, providing further clarification of the effect of this mutation in substrate stabilization and catalysis. We show significant alterations in the ps-ns and  $\mu$ s-ms dynamics of important residues, often either in or near the active-site walls of TEM-1, as a result of this mutation at position 105. For instance, Ser106 and Glu239 show significant increase in ps-ns motions with respect to WT. Such a decrease of the order parameter for residues located in the active site could result in a higher conformational entropy cost associated with substrate binding, hence contributing to the catalytically impaired active-site observed in the Y105D mutant. In addition, Arg164 is a highly-conserved residue in class A  $\beta$ -lactamases that is considered to be important in anchoring the base of the  $\Omega$ -loop through a salt bridge with Asp179 (54). Although more than 17 Å away from the mutation at position 105, a significant change in the R<sub>1</sub> is observed. This change in ps-ns dynamics through a possible network of active-site motions could affect the stability of the  $\Omega$ -loop and thus reduce appropriate substrate stabilization and catalysis.

Moreover, our results show a significant decrease in the  $\mu$ s-ms motions for residues Glu212, Lys215, Val216, Gly218, and Lys234. It is interesting to note that among these residues, Val216 and Lys234 were shown to be intolerant to any amino acid substitutions with respect to benzylpenicillin hydrolysis in TEM-1 (55). These results suggest that this activity requirement may partly be governed by  $\mu$ s-ms dynamics in the vicinity of these residues. Lys 215, Val216 and Lys234 are positioned in the immediate vicinity of the substrate molecule and their ground-state dynamical behaviour may have a direct impact on substrate recognition and stabilization, therefore partly explaining the decreased affinity observed for mutant Y105D (25). In fact, while Lys234 is implicated in the initial recognition of the substrate molecule as an electrostatic anchor for the carboxylate moiety of substrates (56), its implication in proton shuttling during catalysis is still the subject of debate (57). On the other hand, with help from the guanidinium group of Arg244, the backbone carbonyl group of Val216 has been shown to anchor a conserved water molecule that interacts with the C3 carboxylate group of the substrate for appropriate stabilization (58) (Figure 4.6). Thus, this residue has been suggested to influence substrate binding and catalysis in both TEM-1 (55) and PSE-4 (59). Since the  $\mu$ s-ms motions surrounding Glu212, Lys215, Val216 and Lys234 are decreased in mutant Y105D, these changes on the catalytically-relevant timescale of their local environment may reduce substrate stabilization in the active-site of Y105D, consistent with the large increase in  $K_m$  previously observed with this mutant (25). In addition to affecting the correct stabilization of the substrate through a conserved water molecule by Val216 (Figure 4.6), the attenuation of  $\mu$ s-ms motions in the Y105D mutant could reflect a reduction of the possible conformations that the enzyme can adopt on this timescale. These ‘productive’ conformations could be responsible for the appropriate positioning of the substrate in the active site and their loss upon mutation could account for the decline of the enzymatic activity. It should be noted that the present study confirmed the presence as well as the importance of previously observed  $\mu$ s-ms motions in the active site and in the  $\Omega$ -loop of TEM-1 (29). Although it was observed that  $\mu$ s-ms motions were present in the vicinity of the active site (29), it was

impossible to determine whether these motions were catalytically relevant. The changes in  $\mu$ s-ms timescale motions we observe upon a mutation that affects kinetic properties of TEM-1 indicates a correlation between motion timescales and the kinetic properties, consistent with causality, although causality has not been demonstrated. To date, the numerous X-ray studies of TEM-1 have provided no indication of catalytically-related motions. As a result of the current NMR studies, we propose that the combination of these subtle but significant effects within the active-site cavity are directly related to the two-orders of magnitude reduction in catalytic efficiency observed for the Y105D mutant of TEM-1 (25). It is important to note that the available data does not allow us to differentiate whether the  $\mu$ s-ms motions observed for the amides of Glu212, Lys215, Val216, Gly218, and Lys234 are resulting from their own motions or from motions of other surrounding residues. However, it is now clear that these  $\mu$ s-ms motions are correlated with the fine-tuning of catalytic properties of TEM-1, and possibly of other  $\beta$ -lactamases.

*Long-range dynamical effects*—Although important residues displaying modified ps-ns and  $\mu$ s-ms dynamics in mutant Y105D are elements of the active-site walls and therefore generally considered in close proximity to the substrate molecule, it is important to keep in mind that motions characterized in the present study are exclusively focused on the backbone relaxation of  $^{15}\text{N}$  atoms. To that extent, it is important to estimate relevant distances separating residues of interest and therefore to clarify what is considered short-range ( $< 5 \text{ \AA}$ ) or long-range ( $> 5 \text{ \AA}$ ) interactions. For instance, the shortest distance between Tyr105 and Val216 ( $\text{OH}_{105}-\text{C}\gamma_{216} = 4.2 \text{ \AA}$ ) may be considered short-range whereas the distance between both their  $^{15}\text{N}$  atoms would be considered long-range ( $14.7 \text{ \AA}$ ). This important difference in atom distances is observed for several residues located in the active-site walls of TEM-1. Nonetheless, most of the calculated distances among dynamically-affected residues should be considered long-range because they do not permit any direct contact with residue 105. For instance, Lys234 displays a shortest residue distance of  $7.8 \text{ \AA}$  with Tyr105 ( $\text{C}\epsilon_{2105}-\text{N}\zeta_{234}$ ) and a  $^{15}\text{N}_{105}-^{15}\text{N}_{234}$  distance of  $18.7 \text{ \AA}$  (both long-range).

This observation raises two important points regarding dynamical results characterized in the present study. The first point is the fact that, except for dynamically-affected residues located in the immediate vicinity of the mutation (*e.g.* Ser106, Asn132 and to a certain extent Val216), both shortest inter-residue or NMR observable (backbone  $^{15}\text{N}$  atoms) distances between position 105 and any other dynamically-affected residue are too important to account for any direct interaction (*e.g.* Lys234, Leu76, Gly218, etc.). This observation raises the second important point: the long-range dynamical effects observed as a consequence of the Y105D mutation is consistent with the existence of a network of motions among residues of TEM-1  $\beta$ -lactamase. This hypothesis is strengthened by a previous molecular dynamics study performed on the inhibitor-resistant M69L mutant of TEM-1, suggesting that only differences in dynamics of this mutant account for the resistance to clavulanate (30). This type of dynamical network explaining long-range dynamical effects has been previously characterized in detail for other enzymes and has often been shown to play a crucial role in catalysis (reviewed in (23, 24)). It has also been observed in allosteric (60) and other non-catalytic proteins (61) with long-range motions characterized as contiguous (displaying a traceable pathway) or disperse (non-contiguous with an untraceable pathway). The evidence presented here not only suggests dynamical ‘cross talk’ between residues constituting opposite walls of the active-site cavity of TEM-1 (often separated by large distances) but also suggests that residues distal to the active-site cavity may disrupt catalysis in TEM-1 through their altered motional behaviour. For instance, it is interesting to note that several residues displaying significant ps-ns and/or  $\mu$ s-ms motional differences have been shown to be intolerant to any amino acid substitution in TEM-1 (Table 4.4), among which several are conserved in all class A  $\beta$ -lactamases (55). Although some residues of the active-site walls are expected to be intolerant to any mutation because of their direct importance in catalysis (*e.g.* Lys234 and Val216), others are distal to the active-site cavity and display significant dynamical alterations between TEM-1 and mutant Y105D. For example, two dynamically-affected residues (Tyr46 and Leu76, both  $> 20 \text{ \AA}$  from the mutation) are completely buried in TEM-1 and their motional

disruption through a possible long-range network of coupled motions may affect the appropriate packing of the hydrophobic core of the enzyme and/or catalysis.

The fact that our NMR studies on WT and mutant Y105X were performed in absence of any substrate or inhibitor is of considerable interest because it supports previous investigations showing that catalytically-relevant motions are often observed in the free enzyme (10, 20). The conservation of motions in absence of substrate may be an essential component of enzyme evolution and may contribute to explain the exceptionally high acceleration rates observed in enzyme catalysis. In addition, as previously pointed out (23), this finding may have interesting implications for the understanding of the secondary and tertiary elements conserved in several protein folds. Assuming that the conserved fold observed for all class A  $\beta$ -lactamases is partly governed by an evolutionary constraint preserving elements that define dynamical motions essential to their catalytic function, the characterization of such elements would greatly advance our understanding of class A  $\beta$ -lactamase catalysis as well as their importance in antibiotic resistance. A common structural organization of functionally relevant regions that undergo similar concerted movements was recently revealed in the protease enzymatic superfamily (62). Whether the presence of such a network of motions is relevant to the class A  $\beta$ -lactamase fold and similar catalytic mechanism is beyond the scope of this study. Nevertheless, considering the long-range dynamical effects characterized here, it is reasonable to assume that dynamical differences between TEM-1 and various mutants are involved in the observed differences in activity.

## FOOTNOTES

\*This work was supported by grants from the Natural Sciences and Engineering Research Council of Canada (J.N.P. and S.M.G.), the Fond Québécois de la Recherche sur

la Nature et les Technologies (J.N.P) and the Fonds de la Recherche en Santé du Québec (P.Y.S.). Equipment was purchased with grants from the Canada Foundation for Innovation (S.M.G.).

## REFERENCES

1. Neet, K. E. (1998) *J. Biol. Chem.* **273**(40), 25527-25528
2. Garcia-Viloca, M., Gao, J., Karplus, M., and Truhlar, D. G. (2004) *Science* **303**(5655), 186-195
3. Benkovic, S. J., and Hammes-Schiffer, S. (2003) *Science* **301**(5637), 1196-1202
4. Hammes-Schiffer, S. (2002) *Biochemistry* **41**(45), 13335-13343
5. Epstein, D. M., Benkovic, S. J., and Wright, P. E. (1995) *Biochemistry* **34**(35), 11037-11048
6. Osborne, M. J., Schnell, J., Benkovic, S. J., Dyson, H. J., and Wright, P. E. (2001) *Biochemistry* **40**(33), 9846-9859
7. Agarwal, P. K., Billeter, S. R., Rajagopalan, P. T., Benkovic, S. J., and Hammes-Schiffer, S. (2002) *Proc. Natl. Acad. Sci. USA* **99**(5), 2794-2799
8. Radkiewicz, J. L., and Brooks, C. L. (2000) *J. Am. Chem. Soc.* **122**(2), 225-231
9. Agarwal, P. K., Geist, A., and Gorin, A. (2004) *Biochemistry* **43**(33), 10605-10618
10. Eisenmesser, E. Z., Millet, O., Labeikovsky, W., Korzhnev, D. M., Wolf-Watz, M., Bosco, D. A., Skalicky, J. J., Kay, L. E., and Kern, D. (2005) *Nature* **438**(7064), 117-121

11. Agarwal, P. K., Webb, S. P., and Hammes-Schiffer, S. (2000) *J. Am. Chem. Soc.* **122**(19), 4803-4812
12. Bahnsen, B. J., Colby, T. D., Chin, J. K., Goldstein, B. M., and Klinman, J. P. (1997) *Proc. Natl. Acad. Sci. USA* **94**(24), 12797-12802
13. Billeter, S. R., Webb, S. P., Agarwal, P. K., Iordanov, T., and Hammes-Schiffer, S. (2001) *J. Am. Chem. Soc.* **123**(45), 11262-11272
14. Colby, T. D., Bahnsen, B. J., Chin, J. K., Klinman, J. P., and Goldstein, B. M. (1998) *Biochemistry* **37**(26), 9295-9304
15. Derreumaux, P., and Schlick, T. (1998) *Biophys. J.* **74**(1), 72-81
16. Desamero, R., Rozovsky, S., Zhadin, N., McDermott, A., and Callender, R. (2003) *Biochemistry* **42**(10), 2941-2951
17. Guallar, V., Jacobson, M., McDermott, A., and Friesner, R. A. (2004) *J. Mol. Biol.* **337**(1), 227-239
18. Rozovsky, S., Jogl, G., Tong, L., and McDermott, A. E. (2001) *J. Mol. Biol.* **310**(1), 271-280
19. Rozovsky, S., and McDermott, A. E. (2001) *J. Mol. Biol.* **310**(1), 259-270
20. Beach, H., Cole, R., Gill, M. L., and Loria, J. P. (2005) *J. Am. Chem. Soc.* **127**(25), 9167-9176
21. Kovrigin, E. L., and Loria, J. P. (2006) *Biochemistry* **45**(8), 2636-2647
22. Kovrigin, E. L., and Loria, J. P. (2006) *J. Am. Chem. Soc.* **128**(24), 7724-7725
23. Agarwal, P. K. (2006) *Microb. Cell. Fact.* **5**(1), 2

24. Tousignant, A., and Pelletier, J. N. (2004) *Chem. Biol.* **11**(8), 1037-1042
25. Doucet, N., De Wals, P. Y., and Pelletier, J. N. (2004) *J. Biol. Chem.* **279**(44), 46295-46303
26. Jarymowycz, V. A., and Stone, M. J. (2006) *Chem. Rev.* **106**(5), 1624-1671
27. Akke, M. (2002) *Curr. Opin. Struct. Biol.* **12**(5), 642-647
28. Savard, P. Y., Sosa-Peinado, A., Levesque, R. C., Makinen, M. W., and Gagné, S. M. (2004) *J. Biomol. NMR* **29**(3), 433-434
29. Savard, P. Y., and Gagné, S. M. (2006) *Biochemistry* **45**(38), 11414-11424
30. Meroueh, S. O., Roblin, P., Golemi, D., Maveyraud, L., Vakulenko, S. B., Zhang, Y., Samama, J. P., and Mobashery, S. (2002) *J. Am. Chem. Soc.* **124**(32), 9422-9430
31. Sosa-Peinado, A., Mustafi, D., and Makinen, M. W. (2000) *Protein Expr. Purif.* **19**(2), 235-245
32. Farrow, N. A., Muhandiram, R., Singer, A. U., Pascal, S. M., Kay, C. M., Gish, G., Shoelson, S. E., Pawson, T., Forman-Kay, J. D., and Kay, L. E. (1994) *Biochemistry* **33**(19), 5984-6003
33. Zhu, G., Xia, Y. L., Nicholson, L. K., and Sze, K. H. (2000) *J. Magn. Reson.* **143**(2), 423-426
34. Gagné, S. M., Tsuda, S., Spyracopoulos, L., Kay, L. E., and Sykes, B. D. (1998) *J. Mol. Biol.* **278**(3), 667-686
35. Tjandra, N., Wingfield, P., Stahl, S., and Bax, A. (1996) *J. Biomol. NMR* **8**(3), 273-284

36. Delaglio, F., Grzesiek, S., Vuister, G. W., Zhu, G., Pfeifer, J., and Bax, A. (1995) *J. Biomol. NMR* **6**(3), 277-293
37. Johnson, B. A., and Blevins, R. A. (1994) *J. Biomol. NMR* **4**, 603-614
38. Nicholson, L. K., Kay, L. E., Baldissari, D. M., Arango, J., Young, P. E., Bax, A., and Torchia, D. A. (1992) *Biochemistry* **31**(23), 5253-5263
39. Lipari, G., and Szabo, A. (1982) *J. Am. Chem. Soc.* **104**, 4559-4570
40. Lipari, G., and Szabo, A. (1982) *J. Am. Chem. Soc.* **104**, 4546-4559
41. Clore, G. M., Driscoll, P. C., Wingfield, P. T., and Gronenborn, A. M. (1990) *Biochemistry* **29**(32), 7387-7401
42. Clore, G. M., Szabo, A., Bax, A., Kay, L. E., Driscoll, P. C., and Gronenborn, A. M. (1990) *J. Am. Chem. Soc.* **112**, 4989-4991
43. Mandel, A. M., Akke, M., and Palmer, A. G., 3rd. (1995) *J. Mol. Biol.* **246**(1), 144-163
44. Pawley, N. H., Wang, C., Koide, S., and Nicholson, L. K. (2001) *J. Biomol. NMR* **20**(2), 149-165
45. Xu, X. P., and Case, D. A. (2001) *J. Biomol. NMR* **21**(4), 321-333
46. Jelsch, C., Mourey, L., Masson, J. M., and Samama, J. P. (1993) *Proteins* **16**(4), 364-383
47. Maveyraud, L., Mourey, L., Kotra, L. P., Pedelacq, J. D., Guillet, V., Mobashery, S., and Samama, J. P. (1998) *J. Am. Chem. Soc.* **120**(38), 9748-9752

48. Ambler, R. P., Coulson, A. F., Frère, J. M., Ghuysen, J. M., Joris, B., Forsman, M., Levesque, R. C., Tiraby, G., and Waley, S. G. (1991) *Biochem. J.* **276** (1), 269-270
49. Strynadka, N. C., Adachi, H., Jensen, S. E., Johns, K., Sielecki, A., Betzel, C., Sutoh, K., and James, M. N. (1992) *Nature* **359**(6397), 700-705
50. Kern, D., and Zuiderweg, E. R. (2003) *Curr. Opin. Struct. Biol.* **13**(6), 748-757
51. Wand, A. J. (2001) *Nat. Struct. Biol.* **8**(11), 926-931
52. Wand, A. J. (2001) *Science* **293**(5534), 1395
53. Matagne, A., Lamotte-Brasseur, J., and Frère, J. M. (1998) *Biochem. J.* **330**(2), 581-598
54. Vakulenko, S. B., Taibi-Tronche, P., Toth, M., Massova, I., Lerner, S. A., and Mobashery, S. (1999) *J. Biol. Chem.* **274**(33), 23052-23060
55. Huang, W. Z., Petrosino, J., Hirsch, M., Shenkin, P. S., and Palzkill, T. (1996) *J. Mol. Biol.* **258**(4), 688-703
56. Lenfant, F., Labia, R., and Masson, J. M. (1991) *J. Biol. Chem.* **266**(26), 17187-17194
57. Meroueh, S. O., Fisher, J. F., Schlegel, H. B., and Mobashery, S. (2005) *J. Am. Chem. Soc.* **127**(44), 15397-15407
58. Wang, X., Minasov, G., and Shoichet, B. K. (2002) *J. Biol. Chem.* **277**(35), 32149-32156
59. Sabbagh, Y., Thériault, E., Sanschagrin, F., Voyer, N., Palzkill, T., and Levesque, R. C. (1998) *Antimicrob. Agents Chemother.* **42**(9), 2319-2325

60. Suel, G. M., Lockless, S. W., Wall, M. A., and Ranganathan, R. (2003) *Nat. Struct. Biol.* **10**(1), 59-69
61. Clarkson, M. W., Gilmore, S. A., Edgell, M. H., and Lee, A. L. (2006) *Biochemistry* **45**(25), 7693-7699
62. Carnevale, V., Raugei, S., Micheletti, C., and Carloni, P. (2006) *J. Am. Chem. Soc.* **128**(30), 9766-9772

## TABLES

**Table 4.1.** Distribution of  $^1\text{H}$ - $^{15}\text{N}$  backbone chemical shift differences ( $\Delta\delta_{\text{HN}}$ ) for residues affected by the Y105X mutation.

$\Delta\delta_{\text{HN}}$ (Hz) <sup>a</sup>	Y105W	Y105G	Y105N	Y105D
10-20	35	54	59	66
20-30	8	5	11	12
30-40	3	4	4	11
40-50	2	3	4	2
50-60	2	1	2	2
60-70	2	2	2	0
70-80	3	1	2	2
80-90	0	1	0	1
90-100	0	1	0	0
100-125	1	1	3	3
125-150	0	1	1	2
150-200	1	1	1	2
> 200	0	3	2	1
Total number of affected residues	<b>57</b> <b>(22 %)</b>	<b>78</b> <b>(30 %)</b>	<b>91</b> <b>(35 %)</b>	<b>104</b> <b>(40 %)</b>
$k_{\text{cat}}$ relative to WT <sup>b</sup>	0.73	0.97	1.30	0.21
$K_M$ relative to WT <sup>b</sup>	0.53	3.53	6.42	8.58
$k_{\text{cat}}/K_M$ relative to WT <sup>b</sup>	<b>1.34</b>	<b>0.27</b>	<b>0.20</b>	<b>0.02</b>

<sup>a</sup> Experimental error = 5.5 Hz. Only values greater than twice the experimental error were considered as significant.

<sup>b</sup> Values for benzylpenicillin, taken from ref (25). WT TEM-1 values:  $k_{cat} = 1240 \text{ s}^{-1}$ ;  $K_M = 43 \mu\text{M}$ ;  $k_{cat}/K_M = 2.9 \times 10^7 \text{ M}^{-1}\text{s}^{-1}$ .

**Table 4.2.** Backbone  $^1\text{H}$ - $^{15}\text{N}$  chemical shift differences ( $\Delta\delta_{\text{HN}}$ ) between Y105X mutants and wild-type TEM-1 for selected active-site residues.

Mutant	$\Delta\delta_{\text{HN}}$ (Hz)						$k_{\text{cat}}/K_M$ relative to wild type <sup>a</sup>
	<i>Lys73</i> (15.5 Å) <sup>b</sup>	<i>Ser130</i> (10.2 Å)	<i>Asn132</i> (6.1 Å)	<i>Glu166</i> (11.0 Å)	<i>Lys234</i> (18.7 Å)	<i>Arg244</i> (17.3 Å)	
Y105W	<i>NS</i> <sup>c</sup>	<b>27.4</b> <sup>d</sup>	<i>NA</i> <sup>e</sup>	<b>20.2</b>	<i>NS</i>	<i>NS</i>	1.34
Y105G	5.7	<b>81.0</b>	<b>131.5</b>	6.8	7.2	5.6	0.27
Y105N	10.6	<b>107.4</b>	<b>55.2</b>	<b>31.3</b>	9.7	5.7	0.20
Y105D	<b>23.4</b>	<b>123.2</b>	<b>140.4</b>	<b>30.8</b>	<i>NS</i>	<i>NS</i>	0.02

<sup>a</sup>Values for benzylpenicillin, taken from ref (25).

<sup>b</sup>Distance between backbone  $^{15}\text{N}_{105}$ - $^{15}\text{N}_x$  atoms (PDB coordinates 1BTL).

<sup>c</sup>Not significant.

<sup>d</sup> $\Delta\delta_{\text{HN}} > 20$  Hz are in bold character.

<sup>e</sup>Not available.

**Table 4.3.** Average backbone relaxation and model-free parameters for wild-type TEM-1 and mutant Y105D.

	TEM-1	Y105D
R <sub>1</sub>	0.98 ± 0.01	0.97 ± 0.02
R <sub>2</sub>	19.5 ± 0.6	18.8 ± 0.7
NOE	0.82 ± 0.04	0.81 ± 0.04
S <sup>2</sup>	0.93 ± 0.02	0.92 ± 0.02
D <sub>  </sub> /D <sub>⊥</sub>	1.16 ± 0.01	1.18 ± 0.01
τ <sub>m</sub> (ns)	13.8 ± 0.01	13.7 ± 0.01

**Table 4.4.** Active-site wall and invariant residues displaying significant<sup>a</sup> relaxation parameter variation between wild-type TEM-1 and mutant Y105D.

Relaxation parameter	Residues <sup>b</sup>
R <sub>1</sub>	<u>Y46</u> , <u>L76</u> , <b>E104</b> , <u>S106</u> , <u>N132</u> , <u>R164</u> , <u>V216</u> , <b>G218</b> , <u>L220</u> , <u>A232</u> , <b>E239</b> , <u>G250</u> , <b>M270</b> , <u>W288</u>
R <sub>2</sub>	<u>Y46</u> , <b>T71</b> , <u>F72</u> , <u>L76</u> , <u>V103</u> , <b>E104</b> , <u>S106</u> , <b>K215<sup>c</sup></b> , <u>V216</u> , <b>G218</b> , <u>L220</u> , <b>K234</b> , <b>E239</b> , <u>G244</u> , <b>M270</b> , <u>I280</u> , <u>W288</u>
{ <sup>1</sup> H}-{ <sup>15</sup> N} NOE	<b>T71</b> , <u>F72</u> , <u>V103</u> , <b>E104</b> , <u>S106</u> , <b>M129</b> , <u>E168</u> , <u>N170</u> , <u>T181</u> , <b>G218</b> , <b>R243</b> , <u>L249</u> , <b>M270</b> , <u>I280</u>
S <sup>2</sup>	<b>S106</b> , <b>E239</b>
R <sub>ex</sub>	<b>K215</b> , <u>V216</u> , <b>G218</b> , <b>K234</b>

<sup>a</sup> Variations in R<sub>1</sub>, R<sub>2</sub> and NOE were considered significant if the Y105D/WT ratio was larger than the average ratio  $\pm 1\sigma$ . Variations in S<sup>2</sup> were considered significant if the difference was larger than the sum of the errors + 0.01. Variations in R<sub>ex</sub> were considered significant if the difference was larger than the sum of the errors + 1.0 s<sup>-1</sup>.

<sup>b</sup> Residues defining active-site walls are in bold character and residues intolerant to any amino acid substitution in TEM-1 (55) are underlined. Sequential numbering is used.

<sup>c</sup> As the <sup>15</sup>N-HSQC signal of residue Lys215 was significantly weaker for the WT than for Y105D, it was impossible to obtain relaxation data for the WT. We therefore conclude that R<sub>2</sub> value was significantly higher for the WT, reflecting significantly higher R<sub>ex</sub>.

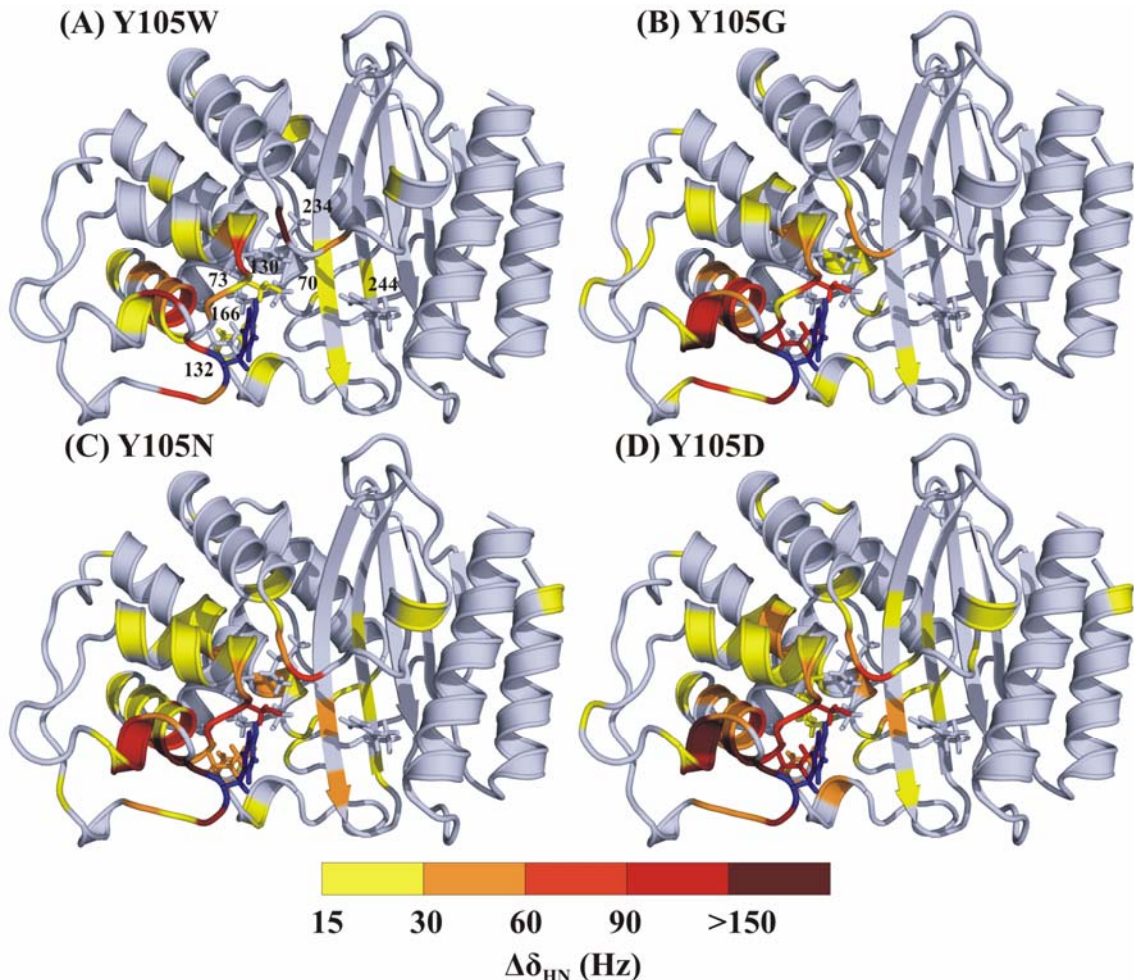


**Figure 4.1.** Structural mapping of  $^1\text{H}$ - $^{15}\text{N}$  backbone chemical shift differences ( $\Delta\delta_{HN}$ ) (Hz) calculated between wild-type TEM-1 and mutants a) Y105W, b) Y105G, c) Y105N and d) Y105D. Values were obtained from 2D  $^1\text{H}$ - $^{15}\text{N}$  HSQC spectra by calculating the differences in peak positions for all assigned residues of the enzyme ( $\Delta\delta_{HN} = \sqrt{\Delta\delta_H^2 + \Delta\delta_N^2}$ ). The yellow to dark-red gradient displays  $\Delta\delta_{HN}$  from 15 Hz to  $>150$  Hz while unassigned residues and  $\Delta\delta_{HN} < 15$  Hz (not significant) are colored grey. Catalytic residues Ser70, Lys73, Ser130, Asn132, Glu166, Lys234 and Arg244 are labeled and displayed as stick representation. Tyr105 is colored blue and displayed as stick representation. 1 ppm ( $^1\text{H}$ ) = 599.739 Hz and 1 ppm ( $^{15}\text{N}$ ) = 60.778 Hz.

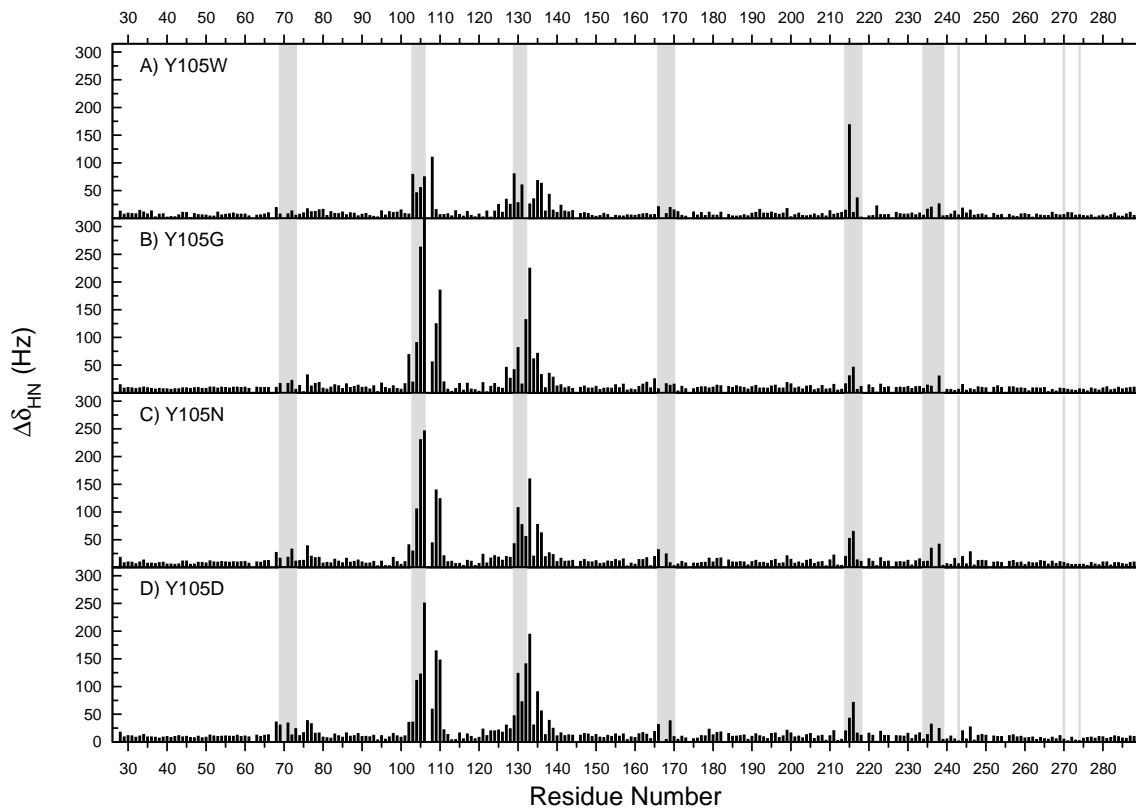


**Figure 4.2.** Sequence mapping of  $^1\text{H}$ - $^{15}\text{N}$  backbone chemical shift differences ( $\Delta\delta_{\text{HN}}$ ) (Hz) calculated between wild-type TEM-1 and mutants Y105W, Y105G, Y105N and Y105D. Residues that define active-site walls of TEM-1 are highlighted in grey (see Figure 4.3).

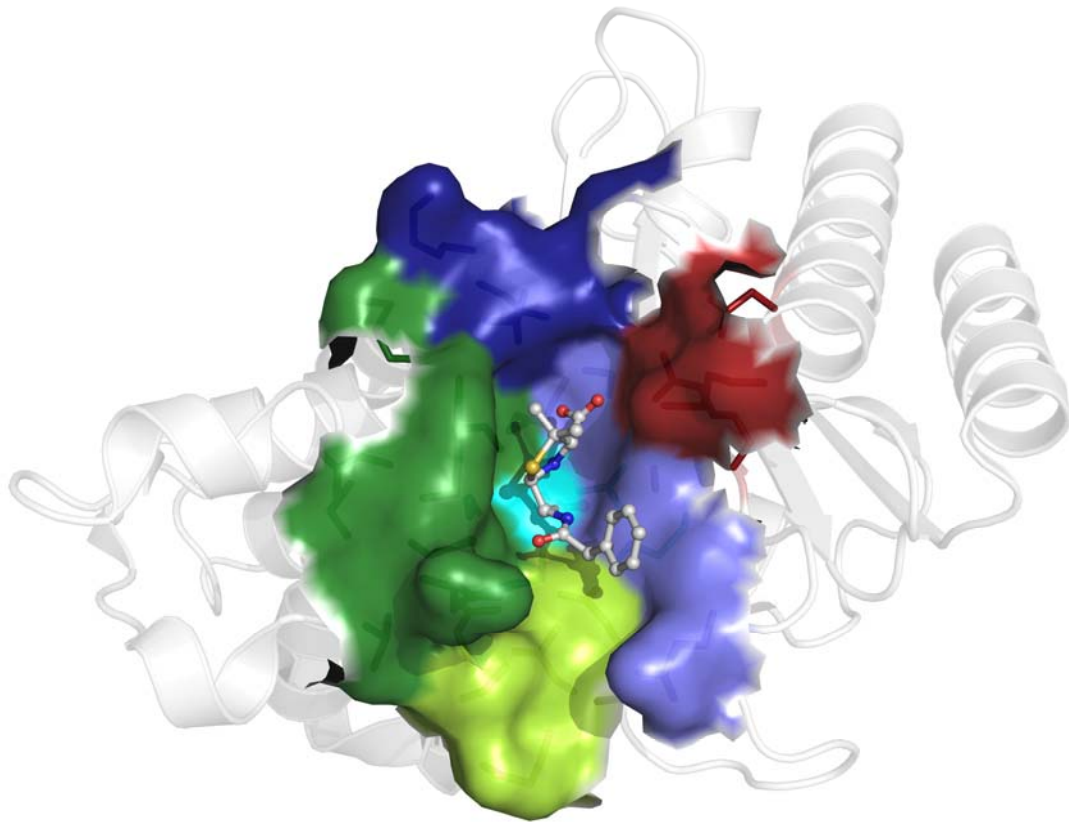


**Figure 4.3.** Solvent-accessible surface representation of the active-site walls in TEM-1  $\beta$ -lactamase. Residues forming the active-site cavity and either implicated in substrate recognition or catalysis are grouped as follows: Met69-Lys73 (cyan), Val103-Ser106 + Met129-Asn132 (SDN loop) (dark green), Glu166-Asn170 ( $\Omega$ -loop) (light green), Val214-Gly218 (dark blue), Lys234-Glu239 (Ambler Lys234-Glu240) (light blue), Arg243 (Ambler Arg244) + Met270 (Ambler Met272) + Asn274 (Ambler Asn276) (dark red). The acylated benzylpenicillin substrate is displayed as balls and sticks (PDB coordinates 1FQG). Residue numbering according to Ambler *et al.* (48).

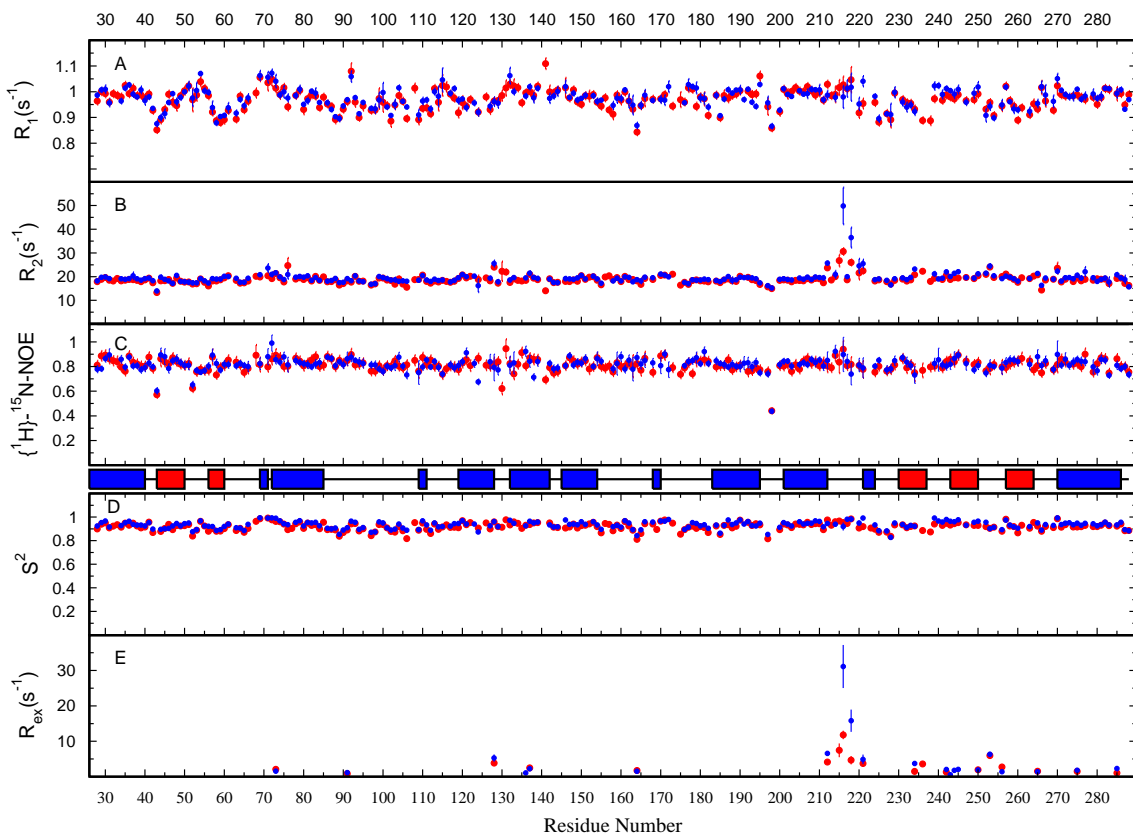


**Figure 4.4.**  $R_1$ ,  $R_2$  and  $\{{}^1\text{H}\}-{}^{15}\text{N}$  NOE relaxation parameters and the model-free-calculated order ( $S^2$ ) and  $R_{\text{ex}}$  parameters plotted on the sequence of TEM-1  $\beta$ -lactamase. Values for WT are colored blue while values for mutant Y105D are colored red. Secondary structure elements are plotted on the sequence as blue rectangles for  $\alpha$ -helices and red rectangles for  $\beta$ -strands.

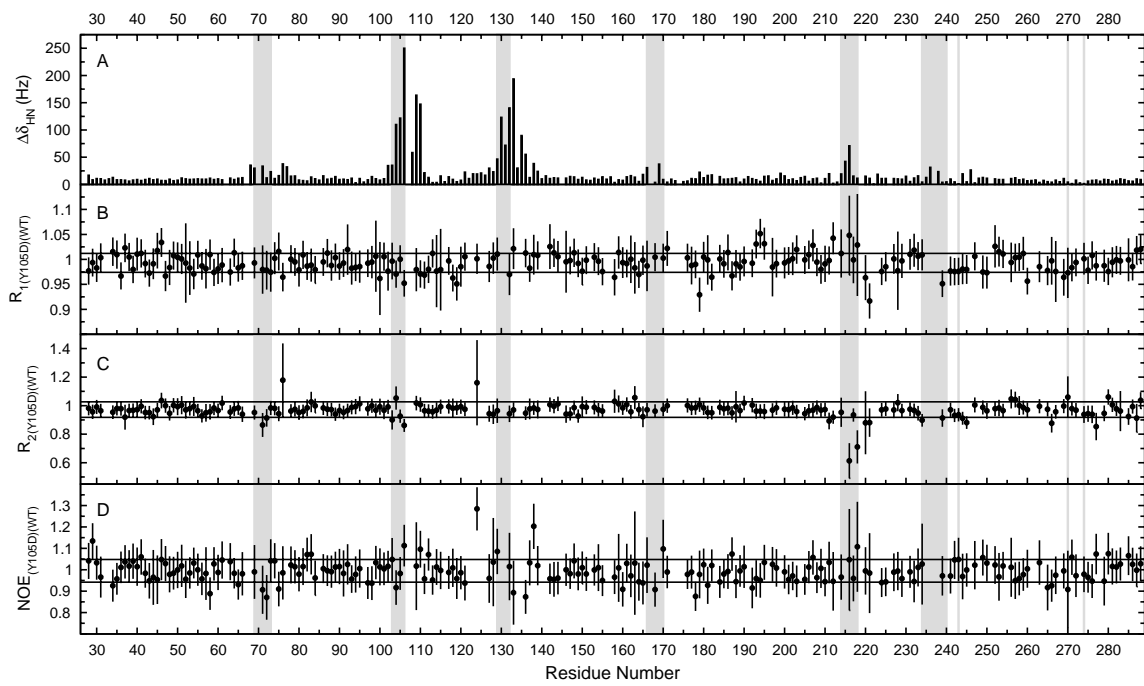


**Figure 4.5.** Y105D/WT ratios for the relaxation parameters ( $R_1$ ,  $R_2$ , and  $\{{}^1\text{H}\}-{}^{15}\text{N}$  NOE). Standard deviation on the mean value are represented as a rectangle for each ratio. Values outside of the standard deviation areas were considered as significant. Panel A displays  $\Delta\delta_{\text{HN}}$  (Hz) calculated for mutant Y105D.

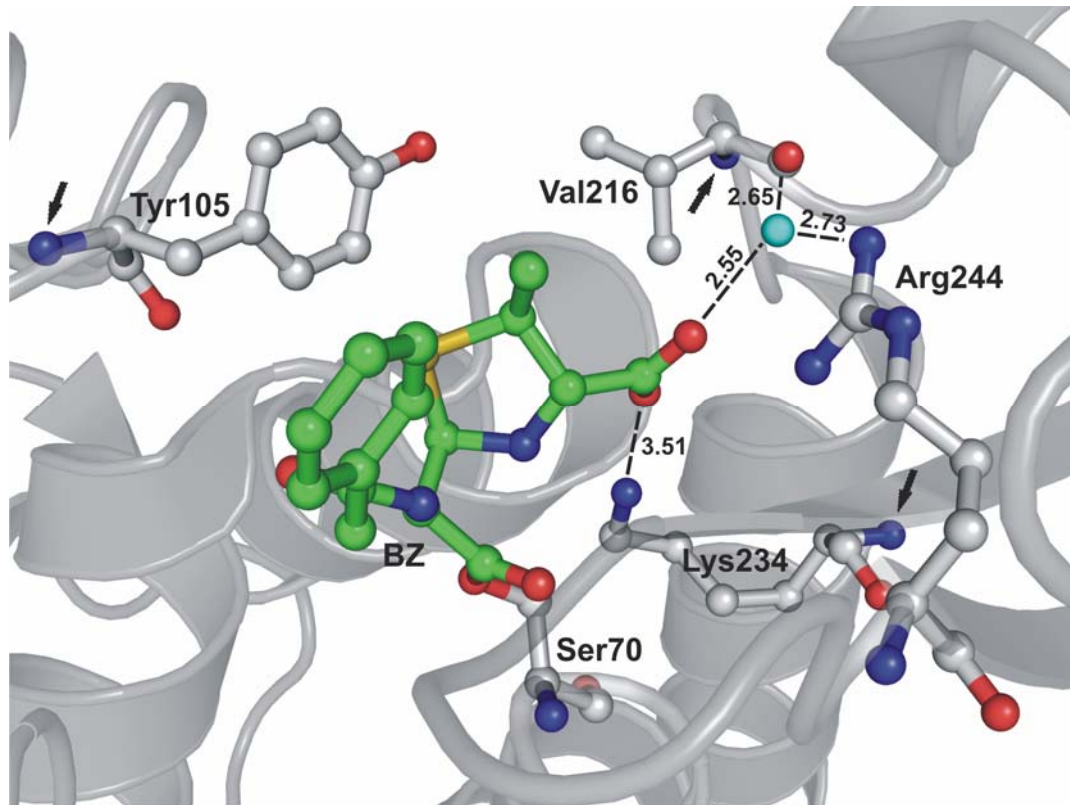


**Figure 4.6.** Substrate anchoring at the active site of TEM-1  $\beta$ -lactamase (PDB coordinates 1FQG). Conserved water molecule 294 (Wat294, represented as a cyan ball) is anchored by the guanidinium moiety of Arg244 and the backbone carbonyl of Val216 (adapted from (58)). Lys234 and Wat294 contribute to ligand binding by stabilizing the C3 carboxylate group of the substrate. Backbone  $^{15}\text{N}$  atoms of residues Tyr105, Val216 and Lys234 are identified by arrows (distances in 1BTL:  $^{15}\text{N}_{105}\text{-}^{15}\text{N}_{234} = 18.7 \text{ \AA}$  and  $^{15}\text{N}_{105}\text{-}^{15}\text{N}_{216} = 14.7 \text{ \AA}$ ). Residues Ser70, Tyr105, Val216, Lys234, Arg244 and the acylated benzylpenicillin substrate are displayed as balls and sticks. Ambler numbering (48) is used and all distances are expressed in  $\text{\AA}$ .

## Préface au chapitre 5

À titre de complément à l'analyse structure-fonction du résidu Tyr105 chez TEM-1 présentée aux chapitres précédents, la seconde partie de cette thèse se consacre à l'analyse du site actif de cette enzyme à l'aide d'une technique de mutagenèse combinatoire semi-aléatoire. Puisqu'il s'agit d'une méthodologie moins commune que la modification enzymatique par design rationnel ou par évolution dirigée, le présent chapitre entreprend une revue de la littérature de cette technique en faisant ressortir ses avantages, qui combinent à la fois les points positifs du design rationnel à ceux de l'évolution dirigée strictement aléatoire. Ainsi, sur la base d'études structurelle et fonctionnelle précédentes, la mutagenèse semi-aléatoire permet notamment la création de librairies « intelligentes » qui améliorent les chances d'obtenir des enzymes mutantes possédant une caractéristique fonctionnelle désirée. Puisque les avantages de cette technique ne sont pas présentés en détail au chapitre suivant, le lecteur est encouragé à lire le présent chapitre à titre d'introduction à la méthodologie de mutagenèse semi-aléatoire présentée au chapitre 6 et appliquée à certains résidus du site actif de TEM-1. Le lecteur pourra toutefois concentrer sa lecture sur les sections expérimentales du présent chapitre (« *Modifying enzyme activity using experimental semi-rational approaches* ») puisque la méthodologie semi-aléatoire présentée au chapitre 6 n'applique pas la méthode de design computationnel présentée dans la section « *Semi-rational and combinatorial design using computational approaches* » du présent chapitre.

Ce chapitre est présenté sous la forme d'un article de revue publié dans *Current Opinion in Biotechnology* au mois d'août 2005 et qui fut écrit en collaboration égale avec mon collègue Roberto Chica. Bien que l'analyse générale des différents concepts et conclusions ait été effectuée en commun, ce dernier fut responsable de la rédaction de l'introduction et de la section touchant à l'analyse computationnelle. Ma contribution personnelle se situe au niveau de la revue et de l'écriture des sections centrales de l'article,

qui analysent les diverses méthodes expérimentales de mutagenèse semi-aléatoire employées dans la littérature et qui s'appliquent directement à l'étude sur TEM-1 présentée au chapitre suivant.

## CHAPITRE 5

### Ingénierie enzymatique par mutagenèse semi-aléatoire : Combiner les avantages de l'évolution dirigée à ceux du design rationnel

#### 5.1 Article 4. *Semi-rational approaches to engineering enzyme activity: Combining the benefits of directed evolution and rational design*

“Reprinted with permission from: Roberto A. Chica, Nicolas Doucet and Joelle N. Pelletier. “Semi-rational approaches to engineering enzyme activity: Combining the benefits of directed evolution and rational design.” *Curr. Opin. Biotechnol.*, 16 (4), 378-384 (2005). ©2005, Elsevier. Reprinted with permission from Elsevier.”

# **Semi-rational approaches to engineering enzyme activity: Combining the benefits of directed evolution and rational design**

Roberto A. Chica<sup>1\*</sup>, Nicolas Doucet<sup>2\*</sup> & Joelle N. Pelletier<sup>1,2</sup>

<sup>1</sup>*Département de chimie and* <sup>2</sup>*Département de biochimie*

*Université de Montréal*

*C.P. 6128, Succursale Centre-ville*

*Montréal (Québec)*

*H3C 3J7 CANADA*

*Curr. Opin. Biotechnol.*, 2005, 16 (4), 378-384

\* = These authors made an equal contribution to this work

## ABSTRACT

Many research groups successfully rely on whole-gene random mutagenesis and recombination approaches for the directed evolution of enzymes. Recent advances in enzyme engineering have used a combination of these random methods of directed evolution with elements of rational enzyme modification to successfully by-pass certain limitations of both directed evolution and rational design. Semi-rational approaches that target multiple, specific residues to mutate on the basis of prior structural or functional knowledge create ‘smart’ libraries that are more likely to yield positive results. Efficient sampling of mutations likely to affect enzyme function has been conducted both experimentally and, on a much greater scale, computationally, with remarkable improvements in substrate selectivity and specificity and in the *de novo* design of enzyme activities within scaffolds of known structure.

## INTRODUCTION

Enzymes are powerful catalysts that are able to increase reaction rates by up to 17 orders of magnitude [1 and 2]. Certain enzymes display perfect control over stereochemistry and regioselectivity, while others display a breadth of specificity; either feature may be attractive for industrial and synthetic applications [3]. However, few enzymes naturally catalyze the reactions that chemists need under conditions that are industrially convenient and economically advantageous. Many efforts are currently devoted to the modification of enzyme activities to meet the needs of today's chemists.

Multiple approaches have been developed to allow the identification of mutant enzymes possessing desirable qualities such as increased activity, modified specificity, selectivity or cofactor binding [4]. The earliest approach was rational design, which was

used to modify the specificity of enzymes [5, 6, 7, 8 and 9]. This approach requires an in-depth knowledge of the structural features of the enzyme active site and their contribution to function. The complexity of the structure/function relationship in enzymes has proven to be the factor limiting the general application of rational design. More recently, directed evolution has proven to be a powerful tool for the modification of enzyme activities and has become the most widely used approach. Briefly, directed evolution consists of the low frequency introduction of randomly distributed mutations in a gene of interest, followed by selection of the mutated proteins possessing the desired properties. Recent advances in this area include the application of the immune system ‘hypermutation’ process, which is conducted entirely in live cells [10]. Directed evolution can enable the relatively rapid engineering of enzymes without requiring an in-depth understanding of structure/function relationships, unlike rational design. The numerous methodologies and successes of directed evolution will not be detailed here as recent reviews have been devoted to the topic [11, 12, 13, 14 and 15] (also see the article by AA Henry and FE Romesberg in this issue). Because large numbers of mutants must generally be screened to obtain a significant, desired effect on enzyme activity, the main limitation of directed evolution is the necessity of developing a high-throughput screening methodology that allows identification of the desired property under relevant conditions. Not all enzyme activities are readily amenable to developing a high-throughput screening method, nor are all screening methodologies easy to implement at the required scale.

A further limitation of directed evolution relates to the random nature of the mutations introduced: in the case where functional information (from point mutations, random mutagenesis or deduction by sequence alignment) or structural information exists, it would be advantageous to exploit this by concentrating mutations where they might be the most effective [16]. Analysis of enzyme modification results indicates that the majority of mutations that beneficially affect certain enzyme properties (enantioselectivity, substrate specificity and new catalytic activities) are located in or near the active site, and more specifically near residues that are implicated in binding or catalysis [15, 17, 18• and 19].

Other properties (stability and activity) can be improved by mutations either near or far from the active site, although there are many more mutations far from the active site to test out [19]. Consequently, saturation mutagenesis (where all 20 natural amino acids are tested at residues in or near the active site) can be coupled to recombination of these mutations in order to increase the likelihood of beneficially modifying the catalytic activity relative to random mutagenesis approaches. This ‘semi-rational’ approach could be particularly advantageous in instances where no high-throughput screening method is available, based on the argument that a ‘smarter’ library can be built with the same number of mutants than with a random whole-gene mutagenesis approach [15] (Table 5.1; Figure 5.1).

This review provides an overview of recent articles where the semi-rational design of enzyme activities has been successfully demonstrated through the use of combinatorial mutagenesis biased toward the active site, based both on experimental and computational approaches.

## **MODIFYING ENZYME ACTIVITY USING EXPERIMENTAL SEMI-RATIONAL APPROACHES**

The experimental combination of rational and random protein engineering approaches has been successfully applied toward the modification of enzyme activities. The following examples have been grouped according to the specific experimental approaches applied, which are guided by the amount and nature of structural and functional information available at the outset of the study.

## TARGETED RANDOMIZATION OF DEFINED RESIDUES BASED ON STRUCTURAL KNOWLEDGE

Structural information, when available, can allow one to target specific residues in direct contact with the substrate or near the active-site cavity for mutagenesis, alone or in combination. Although the choice of the positions to mutate remains rational in most cases, the choice of amino acids to be encoded can be broad; furthermore, the simultaneous randomization at targeted positions may result in synergistic effects [20] that could not have been predicted by mutating positions individually.

Santoro and Schultz [21] have used targeted randomization to modify the substrate specificity of a Cre DNA recombinase from bacteriophage P1 that recognizes DNA sequences known as *loxP* sites. The researchers used structural information of the Cre–DNA complex to target two regions of the Cre recombinase in contact with *loxP* base pairs suspected to be important for recombination activity. By creating two distinct libraries (C1 and C2; see Figure 5.2a) of five and six simultaneously randomized residues in contact with variants of *loxP* sites (library size  $\sim 10^8$ ) and by subjecting the *E. coli*-transformed libraries to a powerful recombination assay of fluorescent reporter proteins sorted by FACS (fluorescence-activated cell sorting), they isolated a mutant that efficiently recombined a new *loxP* site not recognized by the wild-type enzyme. Moreover, this Cre mutant retained the ability to recognize the native *loxP* site. The authors favored this targeted library approach because they anticipated that a higher likelihood of success would be observed, while requiring fewer rounds of selective amplification and mutagenesis compared with random mutagenesis of the whole gene.

Similarly, in a successful attempt to investigate the detoxification role of epoxide hydrolases, Rui *et al.* [22] used a combination of rational design and saturation mutagenesis at targeted active-site positions to expand the substrate range of an epoxide hydrolase from *Agrobacterium radiobacter* AD1 (EchA) to include chlorinated epoxides. On the basis of a

careful investigation of the active site by structural comparison to related enzymes, residues F108, C248, I219 and I111 (in single-letter amino acid code), in the vicinity of the catalytic triad, were separately randomized by saturation mutagenesis. As mutant C248I showed a slight increase in rate of *cis*-1,2-dichloroethylene (*cis*-DCE) mineralization (2.7-fold increase with respect to the wild type), it was used as a template for successive rounds of saturation mutagenesis targeting residues F108 and I219. The approach generated the triple active-site area mutant F108L-I219L-C248L, which displayed a 10-fold enhancement in *cis*-DCE mineralization relative to wild-type EchA.

Several other groups [23, 24, 25 and 26] have also successfully conducted simultaneous or successive targeted randomization of multiple active-site positions based on structural knowledge, as an efficient means to circumvent limitations inherent either to site-directed mutagenesis or to whole-gene random mutagenesis. Recently, Schultz and colleagues [27] combinatorially randomized two active-site residues of an aminoacyl-tRNA synthetase as a step in the generation of an orthogonal synthetase/tRNA pair that efficiently and selectively incorporates an unnatural amino acid into proteins.

In some cases, the structural information available is not sufficient to rationally select residues to be randomized. Thus, molecular modelling studies have been successfully used to identify residues most likely to be in contact with substrate molecules. Our group used this approach to perform combinatorial targeted mutagenesis of all 16 principal active-site residues of type II R67 dihydrofolate reductase, allowing the selection of new, highly modified active-site environments with activity at least as great as the native enzyme [28]. Similarly, the substrate specificity of *Bacillus stearothermophilus* SD1 D-hydantoinase was modified by a semi-rational mutagenesis approach targeting residues chosen on the basis of previous modelling studies [29].

## SIMULTANEOUS RANDOM MUTAGENESIS AND SITE-SATURATION OF DEFINED RESIDUES

Based on evolutionary protein-fold similarity between two related enzyme families, Peimbert and Segovia [30] introduced a  $\beta$ -lactamase activity into PBP2X DD-transpeptidase from *Streptococcus pneumonia* through a combination of error-prone polymerase chain reaction (epPCR) and saturation mutagenesis at targeted positions. This approach was used to increase the odds of obtaining beneficial mutations at unpredictable locations in combination with mutations at carefully chosen residues. This approach should increase the return using the same number of mutants as a random whole-gene mutagenesis scheme. Thus, two active-site residues (F450 and W374) were targeted for saturation mutagenesis in combination with simultaneous amino acid replacements at eight positions near the active-site cavity (see Figure 5.2b). After the oligonucleotide-based mutagenesis, the gene was further amplified with a 0.8% random mutagenesis rate. This library was selected for cefotaxime resistance and mutants with 10-fold increased resistance relative to wild-type PBP2X were obtained. The random mutagenesis resulted in additional mutations at positions 312, 452 and 554, both proximal to and distal from the active site. To assess the impact of certain randomly inserted mutations, saturation mutagenesis was undertaken at positions 312, 336, 450 and 452. Although no further increase in cefotaxime resistance was observed compared with the original mutants, one new mutant showed  $\beta$ -lactamase activity without compromising the original DD-peptidase activity of PBP2X, thus generating a mutant with dual substrate specificity.

## RANDOM MUTAGENESIS FOLLOWED BY SITE-SATURATION OF DEFINED RESIDUES

The structural or functional information necessary to make rational choices for the residues to mutate is not always available. To circumvent this limitation, several research groups have efficiently undertaken rounds of whole-gene randomization to provide ‘leads’ (*i.e.* residues identified as potentially advantageous when mutated) in conjunction with fine-tuning of the ‘lead mutants’ through site-saturation mutagenesis of the identified residues.

Using such a cyclical random/targeted approach, Reetz and collaborators greatly improved the enantioselectivity ( $E$ ) of *Pseudomonas aeruginosa* lipases toward a *p*-nitrophenyl ester in favour of the (2S) enantiomer (reviewed in [31<sup>”</sup>]). Initial improvement from  $E = 1.1$  (wild-type enzyme) to  $E = 11.3$  was achieved after four rounds of epPCR. Using the mutational knowledge obtained by epPCR, they conducted saturation mutagenesis at given mutational ‘hot spots’ of the lipase, obtaining  $E = 20$ . Subsequent rounds of epPCR increased  $E$  to 25. In addition, they developed a modified version of Stemmer’s combinatorial multiple-cassette mutagenesis method [32] to mutate a defined region of the lipase (residues 160–163) as well as several ‘hot spots’ (residues 155 and 162). This semi-rational method yielded their most highly enantioselective lipase variant to date ( $E = 51$ ). Other groups have recently demonstrated the power of similar semi-rational approaches toward the evolution of enantioselective enzymes. As a result of the multiple random mutagenesis steps, this approach has also generated many mutations far from the active-site cavity in addition to mutations designed within the active-site cavity [33, 34 and 35].

Geddie and Matsumura [36] have modified the substrate specificity of *Escherichia coli*  $\beta$ -glucuronidase through combinatorial site-saturation mutagenesis of several ‘hot spots’, using knowledge previously obtained from DNA shuffling studies. The resulting

mutants displayed up to a 70-fold increase in xylosidase activity and were further improved by several steps of whole-gene random mutagenesis using DNA shuffling, epPCR and Staggered Extension Process (StEP) to generate mutants displaying 100-fold improvement in xylosidase activity compared with their ancestor. Similar studies were undertaken to modify the enzymatic specificity and activity toward 7-aminodesacetoxycephalosporanic acid (7-ADCA) of a glutaryl acylase of *Pseudomonas* SY-77 [37] and to modify and improve fluorescent proteins from *Discosoma* sp. [38']. In all of these studies, whole-gene randomization was generally undertaken in a first round of mutagenesis, followed by ‘fine-tuning’ of the most interesting mutants through single or combinatorial site-saturation mutagenesis at targeted positions. Afterwards, mutants obtained were further improved using subsequent rounds of random mutagenesis.

In the absence of structural or functional information, the ‘Evolutionary Trace’ method [39] can pinpoint residues to mutate. This method entails correlating evolutionary variations within a gene of interest with divergences in the phylogenetic tree of that sequence family. This has been shown to reveal the relative functional importance of residues and to identify functional sites [40]. A recent review by Minshull *et al.* [41] provides a highly comprehensive overview of this and other approaches for identifying residues that may be functionally relevant.

These recent examples demonstrate the power of structure-based semi-rational approaches targeting active-site residues in enzyme engineering by enhancing our capacity for rational design, while exploiting the advantageous aspects of random mutagenesis. We can thus cycle between light sampling of randomly distributed mutations and saturation mutagenesis at a limited number of positions likely to affect the property under study, increasing the likelihood of identifying beneficial, cooperative effects with respect to enzyme catalysis.

## SEMI-RATIONAL AND COMBINATORIAL DESIGN USING COMPUTATIONAL APPROACHES

Although semi-rational, combinatorial mutagenesis directed at active-site residues limits the number of variants generated relative to available sequence space and theoretically focuses on an area of sequence space where improvements have a greater likelihood of occurring, it can nonetheless generate greater numbers of mutants than can be screened. Indeed, combinatorial randomization of only five residues generates a library of  $20^5$  possibilities ( $3.2 \times 10^6$  mutants), too large a number for manual screening. Thus, to increase the power of semi-rational and combinatorial modification of enzyme activities, computational methods have been developed based on protein design algorithms. These methods can either perform a virtual screening of a vast library or can be applied to the design of enzyme active sites.

The first method is the computational screening of mutant sequences of a virtual library. Computational screening can screen libraries of  $10^{80}$  variants [42], allowing for a first layer of virtual screening to eliminate mutations inconsistent with the protein fold. This is an emerging area in protein design and has seldom yet been applied specifically to enzyme design. However, its resounding success and great promise merit discussion herein. Hayes *et al.* [43] developed a strategy for the computational screening of large libraries called Protein Design Automation (PDA), for prediction of the optimal sequence that can adopt a desired fold. PDA was used for prescreening large, virtual libraries of mutants ( $10^{23}$ ), thus decreasing the sequence space of interest by many orders of magnitude. PDA allows all, or a rationally defined set of residues, to change. The optimal sequence is chosen based on its lowest conformational energy and is used to identify other near-optimal sequences through Monte Carlo simulated annealing. The mutations that occur most frequently define the library to be experimentally screened. Using PDA, Hayes and colleagues pinpointed 19 residues of interest in TEM-1  $\beta$ -lactamase (see Figure 5.2c),

generated *in silico*  $7 \times 10^{23}$  combinatorial mutants of these residues, and chose cut-offs to define the library of roughly 200 000 lowest-energy mutants that were then generated experimentally by mutagenesis and recombination. By selection against the antibiotic cefotaxime, the authors identified a mutant harbouring six mutations in the vicinity of the active site, with a 1280-fold increase in resistance to cefotaxime that was attributed to an increase in relative substrate specificity toward cefotaxime versus ampicillin.

The advantage of PDA is that it samples a vast sequence diversity and allows for multiple mutations to be identified simultaneously, which is particularly beneficial when the effect of multiple mutations is synergistic (non-additive) [20 and 44]. Furthermore, PDA generates mutations at the level of the amino acid sequence rather than at the level of the nucleotide sequence. Thus, there is no bias against mutations requiring two or three nucleotide modifications, contrary to the important bias that exists in standard random mutagenesis methods. This approach vastly increases explorable sequence space, but has not been specifically designed for improvement of enzyme activity.

The second computational method for semi-rational and combinatorial design, which has been specifically applied to the design of enzyme active sites, was developed by Hellinga and co-workers [45<sup>\*\*</sup>]. This ground-breaking work, involving the prediction of mutations that are necessary for the introduction of catalytically active sites in non-catalytic protein scaffolds, allowed the authors to achieve the most dramatic success in computational enzyme design to date. In their report, Dwyer *et al.* [45<sup>\*\*</sup>] converted a non-catalytic ribose-binding protein (RBP) into an analog of triose phosphate isomerase (TIM). Their protein design algorithm first predicted mutations at the ribose-binding area to allow binding of the TIM substrate, dihydroxyacetone phosphate (DHAP) [46]. The algorithm then positioned a set of TIM catalytic residues in the new DHAP-binding pocket. Finally, 14 virtual constructs were experimentally generated and tested for TIM activity. Seven of the mutants possessed TIM activity greater than the background reaction. One of the seven designs was particularly active and through further improvements by computational design

and random mutagenesis, allowed the generation of TIM analogs from a non-catalytic protein. The computational design allowed for the definition of 13 to 21 mutations, depending on the TIM analog, that introduce the necessary catalytic residues as well as residues forming a stereochemically complementary substrate-binding cavity. The most active TIM analogs displayed a  $10^5$ – $10^6$ -fold increase in reaction rate over background, which is the largest increase in reaction rate for a rationally designed enzyme to date [47, 48 and 49], and was sufficiently active to support growth of TIM-deficient *E. coli*. An important contributing factor to the success of this work results from their superior treatment of electrostatic interactions in a heterogeneous protein environment [50]. Although this formidable achievement required prior knowledge of the precise chemical and steric requirements of the target activity, it opens the door to the broader creation of desirable catalytic activities within stable and well-behaved frameworks.

## CONCLUSIONS

Targeted, combinatorial semi-rational mutagenesis is proving highly effective for improving enzyme activities, as it readily allows the creation of neighbouring mutations, of multiple simultaneous mutations and of mutations requiring multiple nucleotide substitutions. This could be particularly advantageous in the modification of enzyme activities, as active-site mutations are frequently coupled and have synergistic effects [20 and 44]. Important developments in computational methodologies promise to vastly increase the searchable sequence space. Taken with a judicious choice of experimental input, semi-rational mutagenesis permits the experimenter to focus mutations in areas more likely to yield ‘lead’ results. These methodologies pave the way to exciting areas of enzyme research including efficient modification of existing activities, the development of new activities within existing frameworks, as well as the evolution of ‘promiscuous’ catalytic activities allowing their efficient exploitation [51 and 52].

## REFERENCES AND RECOMMENDED READING

Papers of particular interest, published within the annual period of review, have been highlighted as:

- of special interest
- of outstanding interest

## ACKNOWLEDGEMENTS

The authors thank Romas J Kazlauskas for his careful reading of the manuscript and his helpful comments.

## REFERENCES

1. A. Radzicka and R. Wolfenden, A proficient enzyme, *Science* **267** (1995), pp. 90–93.
2. S.J. Benkovic and S. Hammes-Schiffer, A perspective on enzyme catalysis, *Science* **301** (2003), pp. 1196–1202.
3. O. Kirk, T.V. Borchert and C.C. Fuglsang, Industrial enzyme applications, *Curr Opin Biotechnol* **13** (2002), pp. 345–351.
4. U.T. Bornscheuer and M. Pohl, Improved biocatalysts by directed evolution and rational protein design, *Curr Opin Chem Biol* **5** (2001), pp. 137–143.

5. N.S. Scrutton, A. Berry and R.N. Perham, Redesign of the coenzyme specificity of a dehydrogenase by protein engineering, *Nature* **343** (1990), pp. 38–43.
6. C.S. Craik, C. Largman, T. Fletcher, S. Rocznak, P.J. Barr, R. Fletterick and W.J. Rutter, Redesigning trypsin: alteration of substrate specificity, *Science* **228** (1985), pp. 291–297.
7. P. Carter, B. Nilsson, J.P. Burnier, D. Burdick and J.A. Wells, Engineering subtilisin BPN' for site-specific proteolysis, *Proteins* **6** (1989), pp. 240–248.
8. J.A. Wells, D.B. Powers, R.R. Bott, T.P. Graycar and D.A. Estell, Designing substrate specificity by protein engineering of electrostatic interactions, *Proc Natl Acad Sci USA* **84** (1987), pp. 1219–1223.
9. F. Cedrone, A. Ménez and E. Quéméneur, Tailoring new enzyme functions by rational redesign, *Curr Opin Struct Biol* **10** (2000), pp. 405–410.
10. L. Wang, W.C. Jackson, P.A. Steinbach and R.Y. Tsien, Evolution of new nonantibody proteins via iterative somatic hypermutation, *Proc Natl Acad Sci USA* **101** (2004), pp. 16745–16749.
11. K.E. Jaeger and T. Eggert, Enantioselective biocatalysis optimized by directed evolution, *Curr Opin Biotechnol* **15** (2004), pp. 305–313.
12. J.L. Jestin and P.A. Kaminski, Directed enzyme evolution and selections for catalysis based on product formation, *J Biotechnol* **113** (2004), pp. 85–103.
13. H. Tao and V.W. Cornish, Milestones in directed enzyme evolution, *Curr Opin Chem Biol* **6** (2002), pp. 858–864.
14. G.J. Williams, A.S. Nelson and A. Berry, Directed evolution of enzymes for biocatalysis and the life sciences, *Cell Mol Life Sci* **61** (2004), pp. 3034–3046.

15. P.A. Dalby, Optimising enzyme function by directed evolution, *Curr Opin Struct Biol* **13** (2003), pp. 500–505.
16. K. Chockalingam, Z. Chen, J.A. Katzenellenbogen and H. Zhao, Directed evolution of specific receptor–ligand pairs for use in the creation of gene switches, *Proc Natl Acad Sci USA* **102** (2005), pp. 5691–5696.
17. S. Park, K.L. Morley, G.P. Horsman, M. Holmquist, K. Hult and R.J. Kazlauskas, Focusing mutations into the *P. fluorescens* esterase binding site increases enantioselectivity more effectively than distant mutations, *Chem Biol* **12** (2005), pp. 45–54.
- 18•. S.L. Strausberg, B. Ruan, K.E. Fisher, P.A. Alexander and P.N. Bryan, Directed coevolution of stability and catalytic activity in calcium-free subtilisin, *Biochemistry* **44** (2005), pp. 3272–3279.

A great example of semi-rational design of enzymatic activity and stability based on structural and functional data previously obtained with subtilisin. Jointly rational and semi-rational, the approach is based on a stepwise increase in the activity of mutants obtained by a randomization of targeted residues near the active-site cavity.

19. K.L. Morley and R.J. Kazlauskas, Improving enzyme properties: when are closer mutations better?, *Trends Biotechnol* **23** (2005), pp. 231–237.
20. A.S. Mildvan, Inverse thinking about double mutants of enzymes, *Biochemistry* **43** (2004), pp. 14517–14520.
- 21•. S.W. Santoro and P.G. Schultz, Directed evolution of the site specificity of Cre recombinase, *Proc Natl Acad Sci USA* **99** (2002), pp. 4185–4190.

Using structural knowledge, residues of Cre recombinase from bacteriophage P1 that are in direct contact with variants of the *loxP* DNA substrate were subjected to

a semi-rational saturation mutagenesis approach to successfully switch the substrate specificity of the Cre enzyme. A powerful screening method using FACS is also described.

22. L. Rui, L. Cao, W. Chen, K.F. Reardon and T.K. Wood, Active site engineering of the epoxide hydrolase from *Agrobacterium radiobacter* AD1 to enhance aerobic mineralization of *cis*-1,2-dichloroethylene in cells expressing an evolved toluene ortho-monooxygenase, *J Biol Chem* **279** (2004), pp. 46810–46817.
23. C.M. Hill, W.S. Li, J.B. Thoden, H.M. Holden and F.M. Raushel, Enhanced degradation of chemical warfare agents through molecular engineering of the phosphotriesterase active site, *J Am Chem Soc* **125** (2003), pp. 8990–8991.
24. M. Wilming, A. Iffland, P. Tafelmeyer, C. Arrivoli, C. Saudan and K. Johnsson, Examining reactivity and specificity of cytochrome *c* peroxidase by using combinatorial mutagenesis, *ChemBioChem* **3** (2002), pp. 1097–1104.
25. N.M. Antikainen, P.J. Hergenrother, M.M. Harris, W. Corbett and S.F. Martin, Altering substrate specificity of phosphatidylcholine-preferring phospholipase C of *Bacillus cereus* by random mutagenesis of the headgroup binding site, *Biochemistry* **42** (2003), pp. 1603–1610.
26. W.S. Yew, J. Akana, E.L. Wise, I. Rayment and J.A. Gerlt, Evolution of enzymatic activities in the orotidine 5'-monophosphate decarboxylase superfamily: enhancing the promiscuous D-arabino-hex-3-ulose 6-phosphate synthase reaction catalyzed by 3-keto-L-gulonate 6-phosphate decarboxylase, *Biochemistry* **44** (2005), pp. 1807–1815.
27. J.C. Anderson, N. Wu, S.W. Santoro, V. Lakshman, D.S. King and P.G. Schultz, An expanded genetic code with a functional quadruplet codon, *Proc Natl Acad Sci USA* **101** (2004), pp. 7566–7571.

28. A.R. Schmitzer, F. Lépine and J.N. Pelletier, Combinatorial exploration of the catalytic site of a drug-resistant dihydrofolate reductase: creating alternative functional configurations, *Protein Eng Des Sel* **17** (2004), pp. 809–819.
29. Y.H. Cheon, H.S. Park, J.H. Kim, Y. Kim and H.S. Kim, Manipulation of the active site loops of D-hydantoinase, a  $(\beta/\alpha)_8$ -barrel protein, for modulation of the substrate specificity, *Biochemistry* **43** (2004), pp. 7413–7420.
30. M. Peimbert and L. Segovia, Evolutionary engineering of a  $\beta$ -lactamase activity on a D-Ala D-Ala transpeptidase fold, *Protein Eng* **16** (2003), pp. 27–35.
- 31•. M.T. Reetz, Controlling the enantioselectivity of enzymes by directed evolution: practical and theoretical ramifications, *Proc Natl Acad Sci USA* **101** (2004), pp. 5716–5722.

An impressive example of enzyme evolution using a combination of semi-rational and random mutagenesis approaches to overcome the respective limitations of each method. The author consolidates the progression in modification of enantioselectivity in *P. aeruginosa* lipases from  $E = 1.1$  (wild type) to  $E = 51$ , clearly describing improvements obtained with each mutational step.

32. M.T. Reetz, S. Wilensek, D.X. Zha and K.E. Jaeger, Directed evolution of an enantioselective enzyme through combinatorial multiple-cassette mutagenesis, *Angew Chem Int Ed Engl* **40** (2001), pp. 3589–3591.
33. Y. Koga, K. Kato, H. Nakano and T. Yamane, Inverting enantioselectivity of *Burkholderia cepacia* KWI-56 lipase by combinatorial mutation and high-throughput screening using single-molecule PCR and *in vitro* expression, *J Mol Biol* **331** (2003), pp. 585–592.
34. G.P. Horsman, A.M.F. Liu, E. Henke, U.T. Bornscheuer and R.J. Kazlauskas, Mutations in distant residues moderately increase the enantioselectivity of *Pseudomonas*

*fluorescens* esterase towards methyl 3-bromo-2-methylpropanoate and ethyl 3-phenylbutyrate, *Chemistry* **9** (2003), pp. 1933–1939.

35. B. Lingen, J. Grotzinger, D. Kolter, M.R. Kula and M. Pohl, Improving the carboligase activity of benzoylformate decarboxylase from *Pseudomonas putida* by a combination of directed evolution and site-directed mutagenesis, *Protein Eng* **15** (2002), pp. 585–593.
36. M.L. Geddie and I. Matsumura, Rapid evolution of  $\beta$ -glucuronidase specificity by saturation mutagenesis of an active site loop, *J Biol Chem* **279** (2004), pp. 26462–26468.
37. C.F. Sio, A.M. Riemens, J.M. van der Laan, R.M. Verhaert and W.J. Quax, Directed evolution of a glutaryl acylase into an adipyl acylase, *Eur J Biochem* **269** (2002), pp. 4495–4504.
- 38•. N.C. Shaner, R.E. Campbell, P.A. Steinbach, B.N. Giepmans, A.E. Palmer and R.Y. Tsien, Improved monomeric red, orange and yellow fluorescent proteins derived from *Discosoma* sp. red fluorescent protein, *Nat Biotechnol* **22** (2004), pp. 1567–1572.

Simultaneous saturation mutagenesis at many targeted positions coupled to epPCR allowed the authors to generate an impressive array of multiple fluorescent and stable monomer variants of *Discosoma* sp. fluorescent protein (DsRed) based solely on sequence comparison of mutants of interest. These stable monomers are now applicable to discrimination of cell types, transcriptional activities and/or fusion proteins. Although not oriented toward catalysis, this example nevertheless demonstrates the power of semi-rational approaches.

39. O. Lichtarge, H.R. Bourne and F.E. Cohen, An evolutionary trace method defines binding surfaces common to protein families, *J Mol Biol* **257** (1996), pp. 342–358.

40. O. Lichtarge, H. Yao, D.M. Kristensen, S. Madabushi and I. Mihalek, Accurate and scalable identification of functional sites by evolutionary tracing, *J Struct Funct Genomics* **4** (2003), pp. 159–166.
41. J. Minshull, J.E. Ness, C. Gustafsson and S. Govindarajan, Predicting enzyme function from protein sequence, *Curr Opin Chem Biol* **9** (2005), pp. 202–209.
42. B.I. Dahiyat, *In silico* design for protein stabilization, *Curr Opin Biotechnol* **10** (1999), pp. 387–390.
- 43•. R.J. Hayes, J. Bentzien, M.L. Ary, M.Y. Hwang, J.M. Jacinto, J. Vielmetter, A. Kundu and B.I. Dahiyat, Combining computational and experimental screening for rapid optimization of protein properties, *Proc Natl Acad Sci USA* **99** (2002), pp. 15926–15931.  
An innovative approach to the use of computational tools in protein engineering. The prescreen described here could be invaluable for the application of a semi-rational approach to enzyme improvement.
44. C.A. Voigt, S. Kauffman and Z.G. Wang, Rational evolutionary design: the theory of *in vitro* protein evolution, *Adv Protein Chem* **55** (2000), pp. 79–160.
- 45•. M.A. Dwyer, L.L. Looger and H.W. Hellinga, Computational design of a biologically active enzyme, *Science* **304** (2004), pp. 1967–1971.  
Computational design of an enzymatic activity in a protein scaffold of known structure. Ground-breaking in that it demonstrates the feasibility of creating new enzymatic activities where there was none by introducing mutations at or near the substrate-binding site.
46. L.L. Looger, M.A. Dwyer, J.J. Smith and H.W. Hellinga, Computational design of receptor and sensor proteins with novel functions, *Nature* **423** (2003), pp. 185–190.

47. D. Hilvert, Critical analysis of antibody catalysis, *Annu Rev Biochem* **69** (2000), pp. 751–793.
48. D.N. Bolon and S.L. Mayo, Enzyme-like proteins by computational design, *Proc Natl Acad Sci USA* **98** (2001), pp. 14274–14279.
49. D.N. Bolon, C.A. Voigt and S.L. Mayo, *De novo* design of biocatalysts, *Curr Opin Chem Biol* **6** (2002), pp. 125–129.
50. M.S. Wisz and H.W. Hellinga, An empirical model for electrostatic interactions in proteins incorporating multiple geometry-dependent dielectric constants, *Proteins* **51** (2003), pp. 360–377.
51. R.J. Kazlauskas, Enhancing catalytic promiscuity for biocatalysis, *Curr Opin Chem Biol* **9** (2005), pp. 195–201.
52. A. Aharoni, L. Gaidukov, O. Khersonsky, Q.G.S. Mc, C. Roodveldt and D.S. Tawfik, The ‘evolvability’ of promiscuous protein functions, *Nat Genet* **37** (2005), pp. 73–76.

## TABLES

**Table 5.1.** Comparison of approaches for engineering enzyme activity.

	Rational Design	Random Mutagenesis	Semi-rational Design
High-throughput screening or selection method	Not essential	Essential	Advantageous but not essential
Structural and/or functional information	Both essential	Neither essential	Either is sufficient
Sequence space exploration	Low	Moderate, random	Experimental : moderate, targeted; Computational: vast, targeted
Probability of obtaining synergistic mutations	Moderate	Low	High

## FIGURES

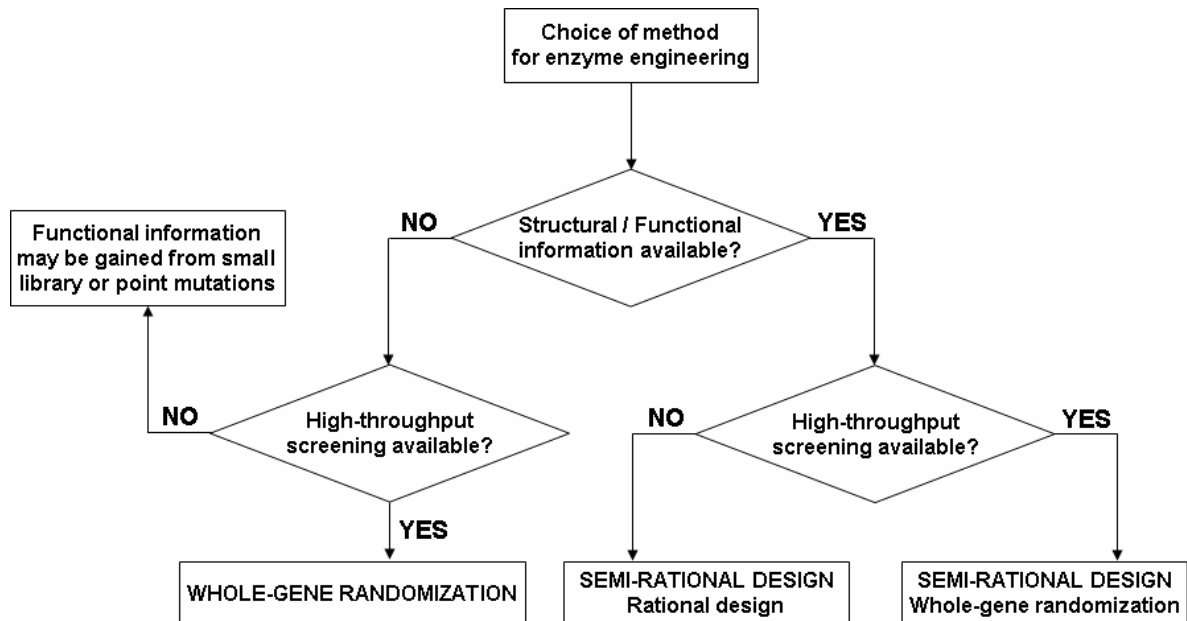


**Figure 5.1.** Selection of the preferred experimental approach for enzyme engineering based on the availability of experimental tools and prior knowledge of structure and function. Rational design, semi-rational design or whole-gene randomization each refer to multiple methodologies, as outlined in the text. The enzyme engineering approach that may have the greatest potential for success is in upper case letters, while alternative approaches are in lower case letters.

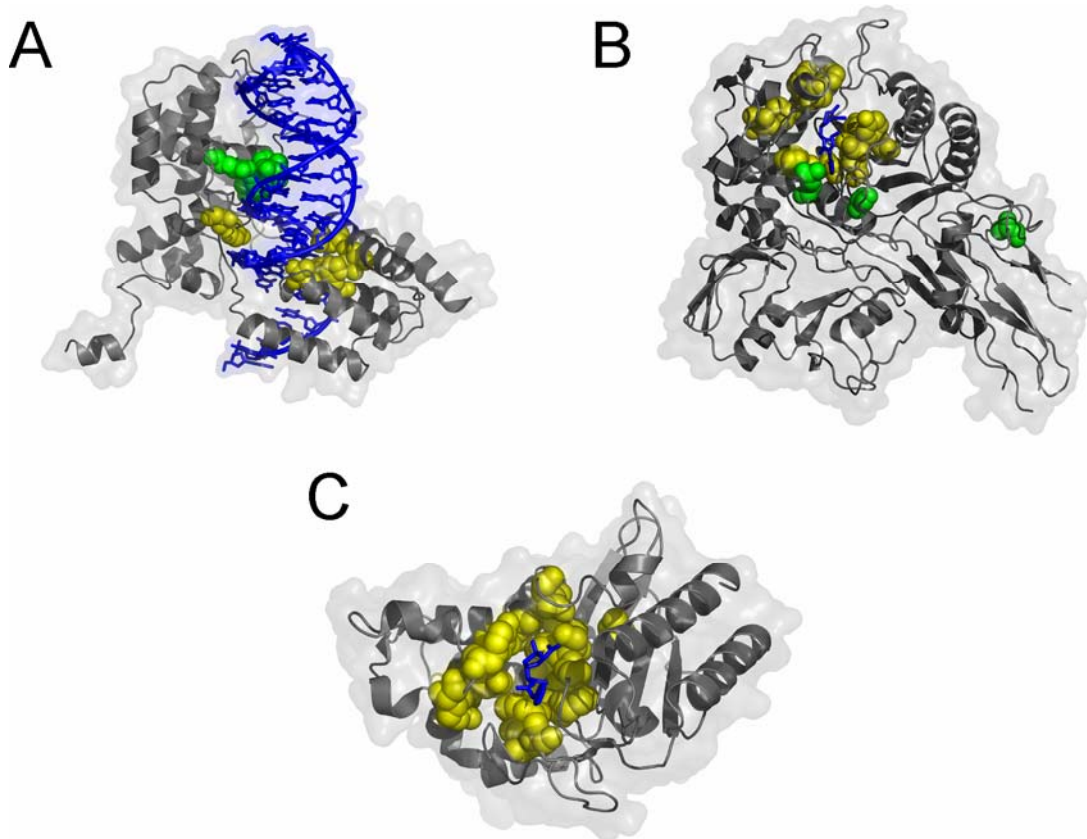


**Figure 5.2.** Residues in or near the enzyme active site that were targeted for semi-rational combinatorial mutagenesis. The enzymes are shown as grey ribbon diagrams with space-filling in semi-transparent gray. (a) Cre DNA recombinase from bacteriophage P1 [21] (PDB accession number 1CRX). Residues from libraries C1 (six residues) and C2 (five residues) and the DNA substrate are colored yellow, green and blue, respectively. (b) PBP2X DD-transpeptidase from *S. pneumoniae* [30] (PDB accession number 1QMF). The ten residues targeted for combinatorial site-directed mutagenesis are colored yellow and the three subsequent unforeseen beneficial mutations obtained by epPCR are colored green. Cefuroxime is acylated at the active-site residue Ser337 and is colored blue. (c) TEM-1  $\beta$ -lactamase from *E. coli* [43] (PDB accession number 1FQG). The 19 active-site residues targeted for *in silico* mutagenesis using PDA are colored yellow. The benzylpenicillin antibiotic is acylated at the active-site residue Ser70 and is colored blue. Figure generated with Pymol Release 0.98 (<http://www.pymol.org>).

## Préface au chapitre 6

Le chapitre 6 présente une étude combinatoire de cinq positions au site actif de TEM-1 mutées simultanément par saturation (Glu104, Tyr105, Gly238, Glu240 et Arg244). Ce chapitre s'avère être une application directe de la méthodologie semi-aléatoire présentée dans l'introduction et dans les sections expérimentales du chapitre précédent, particulièrement dans la sous-section « *Targeted randomization of defined residues based on structural knowledge* ». En plus d'offrir un complément à nos études précédentes chez la position 105 de TEM-1, nous avons entrepris ces travaux dans le but d'étudier l'effet coopératif du remplacement de ces résidus sur l'activité et la spécificité de reconnaissance des substrats, dont plusieurs furent individuellement démontrés comme étant essentiels à l'apparition des phénotypes ESBL ou IRT chez diverses  $\beta$ -lactamases de classe A. Suite à la sélection de nouvelles combinaisons de mutants résistants à l'oxyiminocéphalosporine céfotaxime, nos résultats démontrent que les deux parois du site actif de TEM-1 formées par ces cinq résidus agissent généralement de manière indépendante. De plus, nous observons que l'effet combiné du remplacement de ces résidus peut être additif ou synergique en plus de conférer une certaine plasticité au site actif de l'enzyme. En effet, bien que les mutants sélectionnés sur CTX démontrent une importante diminution de l'hydrolyse des pénicillines, ils conservent une activité similaire pour les substrats céphalosporine classiques.

Ce chapitre est présenté sous la forme d'un manuscrit scientifique actuellement en préparation et dont la forme est pratiquement finale. En plus d'avoir aidé à la création de certaines librairies individuelles initiales, ma contribution à ces travaux se situe au niveau du design expérimental global de cette étude et dans le choix des positions à muter. Par ailleurs, je fus impliqué dans l'analyse des résultats et dans l'écriture d'une partie de la discussion avec Pierre-Yves De Wals. En revanche, ma contribution expérimentale à ces travaux demeure mineure par rapport à la sienne puisqu'il fut responsable de tous les aspects expérimentaux en plus de l'écriture de la majeure partie du manuscrit.

## CHAPITRE 6

### Analyse de la coopérativité au site actif de la $\beta$ -lactamase TEM-1 par mutagenèse combinatoire semi-aléatoire

#### 6.1 Article 5. *Combinatorial active-site mutations in TEM-1 $\beta$ -lactamase provide more generalized drug recognition*

“Reprinted with permission from: Pierre-Yves De Wals, Nicolas Doucet and Joelle N. Pelletier. “Combinatorial active-site mutations in TEM-1  $\beta$ -lactamase provide more generalized drug recognition” *Manuscript in preparation* (2007). ©2007, Pierre-Yves De Wals, Nicolas Doucet and Joelle N. Pelletier.”

# **Combinatorial active-site mutations in TEM-1 β-lactamase provide more generalized drug recognition**

Pierre-Yves De Wals<sup>1</sup>, Nicolas Doucet<sup>1</sup> & Joelle N. Pelletier<sup>1,2</sup>

<sup>1</sup>*Département de biochimie and* <sup>2</sup>*Département de chimie*

*Université de Montréal*

*C.P. 6128, Succursale Centre-ville*

*Montréal (Québec)*

*H3C 3J7 CANADA*

*Manuscript in preparation*

*April 2007*

## ABSTRACT

The diversity in substrate recognition spectra exhibited by various  $\beta$ -lactamases can result from one or a few mutations in the active-site area. Using *Escherichia coli* TEM-1  $\beta$ -lactamase as a template that efficiently hydrolyses penicillins, we performed site-saturation mutagenesis simultaneously on two opposite faces of the active-site cavity. Residues 104 and 105 as well as 238, 240 and 244 were targeted to verify their combinatorial effects on substrate specificity and enzyme activity and to probe for cooperativity between these residues. Selection for hydrolysis of a third-generation cephalosporin, cefotaxime (CTX), led to the identification of a variety of novel mutational combinations at the targeted positions, five of which were characterized in greater detail. *In vivo* survival assays demonstrated a general tendency toward increased CTX and decreased penicillin resistance, while susceptibility to first-generation cephalosporins was relatively unchanged. The five variants characterized had catalytic efficiencies toward CTX improved by two to three orders of magnitude relative to wild-type TEM-1. Productive binding was improved for all substrates tested, even for benzylpenicillin, for which  $k_{\text{cat}}$  was importantly reduced. This indicates broadened substrate specificity, resulting in less specialized (or more generalized) variants. Present in most of the selected variants, the previously-characterized mutation G238S largely accounted for the observed properties. The additional mutations acted in an additive fashion to enhance these properties. The most efficient variant in CTX hydrolysis did not harbour the mutation G238S but combined two neighbouring mutations that resulted in a similar catalytic generalization. We observed no evidence of synergy between the two faces of the cavity. This work confirms that the active site of TEM-1  $\beta$ -lactamase tolerates multiple simultaneous amino acid substitutions and that its plastic character allows for substrate spectrum diversification.

## INTRODUCTION

The rapid evolution of the hydrolase specificity in  $\beta$ -lactamases is an important contributor to antibiotic resistance world-wide.  $\beta$ -Lactamases active sites exhibit increasing sequence diversity, with decades of penicillin and cephalosporin antibiotic use providing the required selective pressure. The appearance and combination of point mutations have resulted in varied recognition spectra for drugs of earlier generations and, increasingly, for more recently developed cephalosporins.

Extended-spectrum  $\beta$ -lactamases (ESBLs)<sup>1</sup> are variants that have become efficient at hydrolysing a variety of  $\beta$ -lactam antibiotics that are not normally recognized by native  $\beta$ -lactamases. Generally, the amino acids responsible for ESBL activity are positioned near the substrate-binding site and do not directly contribute to catalysis (1). Residues at positions 104, 238 and 240 (numbering according to Ambler *et al.* (2)) are frequently associated with ESBL resistance and have been previously characterized by mutagenesis in several class A  $\beta$ -lactamases (3-5). A lysine for glutamate substitution at position 104 (E104K) is associated with ESBL activity through the potential formation of an electrostatic bond between the side chain of Lys-104 and the bulky R<sub>1</sub> substituent of a third-generation cephalosporin substrate (4-6) (Figure 6.1). Mutation G238S (7) is perhaps the best documented example of conversion of a class A  $\beta$ -lactamase into an ESBL, apparently acting by expanding the active-site cavity to accommodate bulkier substrates such as the third-generation cephalosporin cefotaxime (CTX) (8-11). Also, in a similar fashion to position 104, residue 240 has been suggested to form an electrostatic bond with the oxime carboxylate of the third-generation cephalosporin ceftazidime (CAZ) (10) or a hydrogen bond with the oxime substituent of CTX, which lacks the carboxylic acid group of CAZ (5). The E240K substitution is particularly advantageous for CAZ hydrolysis, as exemplified by the fact that random mutants of TEM-1  $\beta$ -lactamase selected in presence of CAZ exhibit either the positively-charged, long-chain residues Lys or Arg (12).

TEM-1  $\beta$ -lactamase belongs to the serine hydrolase class A and is the most prevalent member found among Gram-negative bacteria (13). Many drug-resistant mutants of TEM-1, both clinically-identified and laboratory-generated, have been characterized (1, 7, 12, 14). Importantly, acquisition of resistance toward bulky third-generation cephalosporins (which are not conventional substrates of native TEM-1) has been shown to occur, in several instances, concomitant with the loss of resistance toward classical substrates such as penicillins and first-generation cephalosporins (5, 15-17). Switching of substrate profile was often the result of subtle alterations in the active-site topology (17, 18). Synergy has been previously observed for both double mutants G238S:E240K (11) and E104M:G238S (19) toward CAZ and CTX hydrolysis, respectively. In these cases, the combination of two mutations yielded multiplicative effects of each point mutation as opposed to a simple additive effect on enzyme activity (20). The E104M:G238S variant has the particularity that the two mutations belong to opposite faces of the active-site cavity (Figure 6.2). Residue 104 belongs to the 96-116 loop in the  $\alpha$  domain while residue 238 belongs to the  $\beta$ 3 strand in the  $\alpha/\beta$  domain; these two residues are in contact with distinct atoms of the substrate.

Here, we further explore the cooperative effects of multiple active-site mutations on binding and turnover of  $\beta$ -lactam antibiotics in TEM-1  $\beta$ -lactamase variants. By mutating opposite faces of the active site simultaneously, we probe the extent to which mutations that contact different functional groups of the substrate work in concert to modify substrate recognition. Specifically, we simultaneously randomized five amino acids: Glu-104, Tyr-105, Gly-238, Glu-240 and Arg-244, that are in close proximity to the substrate and belong to two opposite faces of the active-site cavity (Figure 6.2). In addition to the well-characterized mutations at position 104, we examined its neighbour Tyr-105, which is moderately conserved in class A  $\beta$ -lactamases, showing a strong bias for aromatic and, occasionally, small amino acids. We have previously shown that this residue contributes to the structural integrity of the active site, preventing hindrance between more flexible side

chains and the substrates (21). On the opposite face of the active site, we mutated the well-characterized positions 238 and 240, as well as Arg-244, which is partially conserved in class A  $\beta$ -lactamases (2) and is thought to be involved in the formation of a hydrogen bond with the carboxylate moiety of substrates (22). Using a semi-random approach (23, 24), we performed saturation mutagenesis at these five positions in a combinatorial fashion to probe for increased spectrum activity. Selection yielded a variety of combinatorial mutants that exhibit increased third-generation cephalosporin resistance and decreased penicillin resistance. Although mutants displayed increased affinity toward all substrates, turnover was only enhanced for CTX and considerably reduced for penicillins. Overall, our results show that the active site of TEM-1  $\beta$ -lactamase tolerates multiple simultaneous amino acid substitutions, indicating a certain degree of plasticity that allows for substrate spectrum diversification.

## MATERIALS AND METHODS

*Reagents* – All enzymes were purchased from MBI Fermentas (Burlington, ON) or New England Biolabs Ltd. (Mississauga, ON). Nitrocefin was purchased from Calbiochem (Mississauga, ON), chloramphenicol (Chl) from A&C American Chemicals Ltd. (Saint-Laurent, QC), ampicillin (AMP) from Bioshop Canada Inc. (Burlington, ON), while benzylpenicillin (BZ), cephalothin (CF), cefazolin (CZ), cefotaxime (CTX) and Fast-Flow DEAE-Sepharose were obtained from Sigma-Aldrich (Oakville, ON).

*Bacterial strains and Plasmids* – *Escherichia coli* strain SS320 (F<sup>-</sup> lacI22 lacZ pro-48 met-90 trpA trpR his-85 rpsL azi-9 gyrA λ<sup>-</sup> P1<sup>S</sup>) was used for site-directed mutagenesis and *E. coli* strain XL1-Blue (*supE44*, *hsdR17*, *recA1*, *endA1*, *gyrA46*, *thi*, *relA1* lac<sup>-</sup> F<sup>+</sup> [*proAB*<sup>+</sup> *lacI*<sup>q</sup> lacZΔM15 Tn10(*tet*<sup>r</sup>)]) was used for the propagation and expression of

plasmid DNA. Plasmid pQE32Chl (21) was used for protein expression and maintained using 12.5 µg/mL Chl.

*Oligonucleotides and Library Creation* – Oligonucleotide primers used for mutagenesis were synthesized by Alpha DNA (Montréal, QC) or Integrated DNA Technologies (Coralville, IA). PCR reactions were performed with a PTC-200 DNA Engine Thermal Cycler (MJ Research Inc., Waltham, MA).

The five positions selected for mutagenesis were initially split into two libraries: library 104-105 and library 238-240-244. Library 104-105 was constructed using the Site-Overlap Extension (SOE) method (25), while library 238-240-244 was constructed using the Megaprimer technique (26). The 861-bp *bla<sub>TEM-1</sub>* gene was PCR-amplified from pBR322 (which does not contain the V84I and A184V mutations) using the previously described terminal primers BamHITEMF and TEMHindIIIR, containing the *Bam*HI and *Hind*III restriction sites respectively (21). Library 104-105 used degenerate primer Lib104-105NNSR (5'-GATGCTTTCTGTGACTGGTGASNNNSNNAACCAAGTCATTCTGAGAATAGT-3') and primer Lib104-105F (5'-TCACCAGTCACAGAAAAGCATC-3') while library 238-240-244 used degenerate primer Lib238,240,244NNSF (5'-GATAAATCTGGAGCCNNNSNNSCGTGGGTCTNNNSGGTATCATTGCAGCA-3'). It should be noted that there is no residue 239 in TEM-1 according to the Ambler numbering scheme (2). Digestion of the full-length amplicons with *Bam*HI/*Hind*III was followed by subcloning into *Bam*HI/*Hind*III-digested and shrimp alkaline phosphatase-treated pQE32Chl. The library DNA was electroporated into *E. coli* SS320. Libraries 104-105 and 238-240-244 were constructed individually and later combined via the TEM-1 internal *Pst*I restriction site and transformed into *E. coli* XL1-Blue to generate the combinatorial library 104-105-238-240-244. The resulting library contains  $\sim 3.4 \times 10^7$  DNA variants (32<sup>5</sup>) encoding for  $3.2 \times 10^6$  unique protein variants (20<sup>5</sup>). Prior to selection, library quality was assessed by DNA sequencing. Plasmid DNA was prepared as previously described (27).

Sequencing of 36 clones was performed by the dideoxy chain termination method using the Thermo Sequenase Cycle Sequencing Kit (USB Corporation, Cleveland, OH) with a dye-labeled primer (Li-Cor Biotechnology, Lincoln, NB) and a Long ReadIR 4200 Li-Cor automated DNA sequencer.

*Selection of Cefotaxime-resistant Variants* – The 104-105-238-240-244 combinatorial library in *E. coli* XL1-Blue was plated on solid Luria-Bertani (LB) medium containing 250 ng/mL CTX, thus inhibiting wild-type growth. After selection, colonies were individually picked for identification of mutations by DNA sequencing.

*β-lactamase Expression and Purification* – A 10-ml overnight culture of each selected mutant of interest was used to inoculate 1 L of LB without antibiotics. Cells were propagated at 37 °C with agitation until  $A_{600\text{ nm}} = 0.6\text{-}0.8$ . Protein expression was induced with 1 mM isopropyl 1-thio-β-D-galactopyranoside (IPTG) at 37 °C for an additional 3 hrs until the culture reached late log phase. Cells were pelleted by centrifugation (20 min, 6000 g, 4 °C), resuspended in 10-15 mL of 10 mM Tris-Cl buffer pH 7.0 and separated into 1 mL aliquots. A gentle lysis of the outer membrane of *E. coli* was performed by four 2-min freeze-thaw cycles using a dry ice/ethanol bath and a 37 °C water bath followed by centrifugation (15 min, 20 000 g, 4 °C) to collect the supernatant.

Purification of mutants was performed according to the following single-step anion-exchange chromatography procedure. All steps were undertaken at room temperature on a Pharmacia LKB high performance liquid chromatography apparatus (Pharmacia LKB Technology, Uppsala, Sweden). Pooled supernatant (~15 mL) was applied to a DEAE-Sepharose column (1.6 cm × 30 cm) at a flow rate of 1 mL/min followed by a wash with 4.5 column volumes (CV) of 10 mM Tris-Cl buffer pH 7.0 at a flow rate of 3 mL/min. Mutant enzymes were eluted with a linear gradient of 10-150 mM Tris-Cl buffer pH 7.0 (6.5 CV) and a subsequent wash was performed with 150 mM Tris-Cl pH 7.0 (3 CV). The

column matrix was regenerated by applying  $\geq 6$  CV of 1 M Tris-Cl pH 7.0 between each purification.

Fractions containing  $\beta$ -lactamase were identified by a qualitative nitrocefin hydrolysis assay and SDS-polyacrylamide gel electrophoresis with Coomassie Brilliant Blue staining. Analysis of gel patterns with Scion Image (National Institute of Health, <http://rsb.info.nih.gov/nih-image>) revealed that wild-type TEM-1 and mutants VNSTR and VNSLR were purified to 80-90% homogeneity while the purity of mutants SWSSR, PHSER and EYNHR was estimated to be 30-50%. The approximate yield was 2 mg/L except for mutant SWSSR that gave a low yield upon purification (1.2 mg/L), likely as a result of poor solubility and/or expression. The purified enzymes were stored at 4 °C. To ensure that no  $\beta$ -lactamase activity was carried over following each mutant purification, a mock purification was run by injecting 10 mM Tris-Cl buffer as a sample, followed by a nitrocefin assay.

The low purity of mutants SWSSR, PHSER and EYNHR was attributed to a predominant contaminating band that ran at a molecular weight of  $\sim 3$  kDa above the mutants on SDS-PAGE and which may correspond to the immature form of the enzyme. This contaminant could be resolved using a Ni-NTA agarose affinity column according to the procedure recommended by the manufacturer (Qiagen, Mississauga, ON). Following a 3-hour dialysis at 4 °C against 50 mM sodium phosphate buffer (pH 7.0), a spectrophotometric assay with nitrocefin ( $\Delta\epsilon_{482 \text{ nm}} = 17\ 400 \text{ M}^{-1}\text{cm}^{-1}$ ; (22)) on eluted fractions demonstrated that only the band corresponding to the TEM-1 mutant was responsible for the hydrolysis of nitrocefin, confirming that the contaminant does not contribute to  $\beta$ -lactam hydrolysis. Despite the greater purity of these samples, the overall purification yield was too low to perform the required kinetic experiments. Thus, all kinetics were performed using the DEAE-purified samples.

*Antibiotic Susceptibility* – Minimum inhibitory concentrations (MICs) were determined by broth microdilutions according to Cantu III *et al.* (28). Briefly,  $1 \times 10^4$  *E. coli* XL1-Blue CFUs were inoculated into microtiter plates containing 100 µL of LB media and 2-fold dilutions of the antibiotic being tested. The ranges tested were as follows: 250-10,000 µg/mL BZ, 64-10,000 µg/mL AMP, 32-125 µg/mL CF, 8-64 µg/mL CZ and 0.125-2 µg/mL CTX. Each MIC determination was performed in triplicate. The plates were examined visually and the lowest antibiotic concentration at which bacterial growth was inhibited was recorded as the MIC.

*Enzyme Kinetics* –  $K_M$  and  $k_{cat}$  for BZ, CF, CZ and CTX were determined at room temperature in 50 mM sodium phosphate buffer pH 7.0. The following extinction coefficients and concentration ranges were used:  $\Delta\epsilon_{232\text{ nm}} = 1100\text{ M}^{-1}\text{cm}^{-1}$  for BZ (50-300 µM) (29),  $\Delta\epsilon_{262\text{ nm}} = 7960\text{ M}^{-1}\text{cm}^{-1}$  for CF (20-250 µM) (29),  $\Delta\epsilon_{260\text{ nm}} = 7900\text{ M}^{-1}\text{cm}^{-1}$  for CZ (20-250 µM) (30) and  $\Delta\epsilon_{264\text{ nm}} = 7250\text{ M}^{-1}\text{cm}^{-1}$  for CTX (25-250 µM) (3). Substrate hydrolysis was monitored according to initial steady-state velocities for six substrate concentrations generally flanking the  $K_M$  values (where allowed by the extinction coefficients and the  $K_M$  values) using a Cary 100 Bio UV-visible spectrophotometer (Varian Canada Inc., Montréal, QC). The kinetic parameters were determined from the rates of hydrolysis calculated from the initial linear portion of the curve and fitted to a Lineweaver-Burk ( $1/V$  vs.  $1/[S]$ ) plot. In most cases, initial rates were also analyzed with the software GraphPad Prism (GraphPad Software, San Diego, CA) by a non-linear regression curve corresponding to the Michaelis-Menten equation. The  $k_{cat}$  parameter was determined using the equation  $k_{cat} = V_{max}/[E]$ , where the concentration of enzyme was determined using a Bio-Rad protein assay kit (Bio-Rad) taking into account its purity, estimated as described above.

## RESULTS

*Selection of Resistant Mutants from the Combinatorial Library* – In order to gain a better understanding of the role of specific residues giving rise to ESBLs, of their implication in  $\beta$ -lactam drug hydrolysis and on the potential cooperativity between specific areas of the active site, codons 104, 105, 238, 240 and 244 were combinatorially replaced using a semi-random saturation mutagenesis approach (23). These residues belong to two opposite active-site faces of TEM-1  $\beta$ -lactamase (Figure 6.2).

Prior to selection, DNA sequencing of 36 clones from the library revealed no secondary mutations. The randomized nucleotides diverged quantitatively from the expected distribution although all expected nucleotides were encoded at a frequency ensuring adequate randomization of the five target residues. Selection of the combinatorial library yielded 34 resistant clones, several of which were redundant (Table 6.1). The double mutant EYSKR<sup>2</sup> was the most prevalent variant selected, representing over one-third of the sequenced population, while other variants were all found in a small number of copies. In total, 4 double-, 3 triple- and 4 quadruple-mutant combinations were identified. Among the variants, nine novel mutational combinations were identified while two mutational combinations have been previously characterized (EYSKR and EYSRR) (10, 28).

The opposite active-site walls 104-105 and 238-240-244 exhibited different mutational patterns in the selected variants. For instance, roughly two-thirds of all variants displayed wild-type amino acids at positions 104 and 105 while position 238 was mutated in all cases. Similarly, position 240 was replaced in most cases, with the exception of variants PHSER, QWSER and RWSER (Table 6.1). Interestingly, all selected mutants carried the wild-type arginine at position 244, suggesting that this residue is intolerant to mutation in this particular combinatorial context. Moreover, with the sole exception of variant EYNHR, all selected mutants encoded the G238S mutation, which is sufficient to confer extended-spectrum antibiotic resistance on its own (7). Based on the widest

chemical diversity observed at these five mutated positions, the novel variants VNSLR, SWSSR, PHSER and EYNHR were chosen for further characterization by *in vivo* antibiotic resistance and enzyme kinetics. Mutant VNSTR was also characterized in order to compare it to VNSLR, as they differ only by one amino acid at codon 240 (Leu or Thr). Variant VNSLR combines three mutations: E104V, which has only been observed in the CTX-hydrolysing class A D488  $\beta$ -lactamase from *Kebsiella oxytoca* (31); the highly-active Y105N mutation described in TEM-1 (21); and the novel E240L replacement that has never been characterized. The E240T substitution of the similar variant VNSTR has been observed in other class A  $\beta$ -lactamases, such as in the PC1  $\beta$ -lactamase from *Staphylococcus aureus* (2, 32), but has not been characterized in detail.

*In vivo Antibiotic Susceptibility* – In order to assess the effects of the multiple mutations on *in vivo* antibiotic resistance, we determined the MICs for *E. coli* XL1-Blue cells expressing the TEM-1 mutants VNSTR, VNSLR, SWSSR, PHSER and EYNHR (Table 6.2). Wild-type TEM-1 and *E. coli* XL1-Blue lacking TEM-1 expression both served as positive and negative controls, respectively. MIC values were calculated for two classical penicillins (BZ and AMP), two first-generation cephalosporins (CF and CZ), and the third-generation cephalosporin cefotaxime (CTX) that was used for the selection step. The range of concentrations inhibiting bacterial growth is higher for penicillins (64-10,000  $\mu$ g/mL) than for cephalosporins (0.125-125  $\mu$ g/mL). This result was not unexpected since cephalosporins have been developed in order to counteract the resistance phenotypes experienced with standard penicillins (33, 34). This difference is yet more pronounced for CTX since this extended-spectrum antibiotic belongs to a subsequent generation of cephalosporin substrates that are not efficiently hydrolysed by the native enzyme (35). As a consequence, the wild-type MIC value for CTX is no higher than for the negative control (*E. coli* XL1-Blue) (Table 6.2).

Because the library selection was undertaken on CTX-containing media, increased CTX MIC values were expected from the five selected variants investigated. Indeed, CTX

resistance was significantly improved for all five mutants, as demonstrated by their increase in MIC values up to one order of magnitude (Table 6.2). The susceptibility of all mutants toward first-generation cephalosporins (CF and CZ) remained in the same range as the wild-type enzyme. Thus, a maximum two-fold decrease for CF was observed relative to the wild-type enzyme. The conservation of high resistance toward first-generation cephalosporins demonstrates a certain mutational tolerance in the active site of the enzyme. This result suggests that mutants preserved an active-site topology and structural interactions appropriate for the recognition of all cephalosporin substrates tested. Interestingly, these CTX-resistant variants exhibit an important reduction in resistance toward penicillin substrates. For both AMP and BZ, MIC values dropped by a minimum of one order of magnitude relative to wild-type TEM-1. With the exception of CTX, no significant *in vivo* survival enhancements were observed for the other substrates tested. Even mutant VNSTR, that exhibited the highest MIC for CTX (2 µg/mL), with an approximate 3-fold increase relative to the second best CTX-resistant mutant (SWSSR, 0.75 µg/mL), showed no increase in resistance toward any other substrate tested. Moreover, it should be noted that despite their different mutations, the MICs calculated for the five selected variants were similar, with only two- to four-fold differences amongst each other. This suggests that TEM-1 can withstand various combinations of multiple mutations in the vicinity of the active site while maintaining a certain level of resistance, albeit lower than wild-type TEM-1 in the case of penicillins.

*Enzyme Kinetics* – Steady-state kinetic parameters ( $k_{cat}$  and  $K_M$ ) were determined for the five selected mutants as well as for wild-type TEM-1, toward BZ, CF, CZ and CTX (Table 6.3). The kinetic parameters of the point mutant G238S determined under similar conditions for these substrates (3, 17) are provided as a basis for assessment of the role of the additional mutations on catalysis. The low molar absorptivity coefficient of AMP and the resulting high background precluded rigorous quantification of its hydrolysis and is not presented.

In agreement with previous reports (3, 36), wild-type TEM-1  $\beta$ -lactamase exhibited relatively low CTX turnover ( $k_{\text{cat}}$ ) and poor productive CTX binding ( $K_M$ ), resulting in a weak catalytic efficiency ( $k_{\text{cat}}/K_M$ ) toward CTX hydrolysis (Table 6.3). Overall, the greatest improvement in CTX hydrolysis relative to the wild-type was the ~80-fold enhancement in  $k_{\text{cat}}$  for variant PHSER. This variant also exhibited the greatest reduction of BZ hydrolysis ( $k_{\text{cat}} = 1\%$  of wild-type, as for variant VNSTR).

While the native amino acid at position 240 (Glu) is negatively charged, the mutation to a neutral polar residue (E240T) in variant VNSTR relative to the hydrophobic mutation (E240L) in VNSLR resulted in variants with similar kinetic parameters ( $k_{\text{cat}}$ ,  $K_M$ ) relative to all substrates tested, differing 3-fold at most. VNSTR and VNSLR exhibited 10- to 30-fold improvements in their  $k_{\text{cat}}$  (increased) and  $K_M$  (decreased) parameters for CTX relative to wild-type (Table 6.3). Decreased  $K_M$  was also observed for the two first-generation cephalosporins tested as well as for benzylpenicillin. In contrast, their turnover number for first-generation cephalosporin hydrolysis decreased 2- to 8-fold. Their reduction in  $k_{\text{cat}}$  was even more pronounced for the penicillin BZ, reaching 1% of wild-type activity. Overall, mutant VNSLR exhibited one of the highest affinities and catalytic efficiencies for most substrates tested. Importantly, the greatest differences lie in comparing all variants to the wild-type enzyme; differences among the mutants are much less important for any given parameter, consistent with the results of *in vivo* resistance experiments (Table 6.2). Interestingly, all mutants displayed similar  $K_M$  ratios relative to wild-type toward CTX (third-generation cephalosporin) and CF (first-generation cephalosporin) but not CZ (also a first-generation cephalosporin). However, higher  $k_{\text{cat}}$  ratios relative to wild-type for CTX than for CF yield greater relative improvements in catalytic efficiency toward CTX (Table 6.3).

Point mutant G238S is known to enhance extended-spectrum hydrolysis (3, 7). In order to discern the effects of the additional mutations relative to the single G238S substitution, kinetic parameters of the selected variants were compared to that mutant

(Table 6.3). For almost all variants and for the four substrates tested, the catalytic efficiencies ( $k_{\text{cat}}/K_M$ ) show improvements relative to the G238S mutant. These enhancements in  $k_{\text{cat}}/K_M$  can be attributed to the additional mutations at positions 104, 105 and 240. Comparison of kinetic parameters of the selected variants with the wild-type or with the G238S mutant generally shows that improvements in either  $k_{\text{cat}}$  or  $K_M$  did not exceed one order of magnitude for CF and CZ hydrolysis. Changes were more important for BZ and CTX because native TEM-1 is not efficient in CTX recognition or hydrolysis but has the highest activity toward BZ. On the other hand, poor BZ hydrolysis and good activity toward CTX is observed for mutant G238S (Table 6.3). Thus, comparison of mutant kinetic efficiencies with the wild-type enzyme yielded high values for CTX and low values for BZ.

## DISCUSSION

In this work, we systematically investigated the potential cooperative effects of amino acid substitutions at five positions belonging to two opposite active-site walls of TEM-1  $\beta$ -lactamase. We performed saturation mutagenesis at residues 104, 105, 238, 240 and 244 in a combinatorial fashion to probe for increased ESBL activity and cooperativity between mutated residues. Selection against CTX allowed identification of several active TEM-1 mutants displaying a variety of substitutions at four of the five targeted positions. Among all randomized positions, only Arg-244 remained invariable.

Arg-244 – The conservation of this residue was not entirely unexpected since Arg-244 mutations in TEM-1 are not associated with ESBL activity, but rather with inhibitor resistance (7, 12). We nonetheless randomized this residue to evaluate if changes in its environment resulting from neighbouring, concomitant mutations would allow its contribution to the ESBL phenotype. Its strict conservation is consistent with its proposed role in substrate stabilization (22) and suggests that the role of Arg-244 in CTX recognition

cannot be compensated by any other mutation (or combination of mutations) at positions 104, 105, 238 or 240.

Glu-240 – Position 240 displays a fair diversity in amino acid substitutions, both among the CTX-resistant combinatorial variants we selected (Glu, Arg, Lys, Thr, Ser, His and Leu) and also among class A  $\beta$ -lactamases (2, 37). While TEM ESBLs either harbour Arg, Lys or Val at this position (<http://lahey.org/studies/temtable.asp>), the most frequent mutation identified in natural isolates (E240K) was identified in only one combination among the CTX-resistant variants selected here, albeit in the most frequently selected sequence (EYSKR, Table 6.1). This diversity suggests that other residues than lysine at position 240 may confer similarly advantageous properties toward CTX hydrolysis when combined with simultaneous mutations at positions 104, 105 and 238. On the basis of its electrostatic potential, the E240K mutation has been suggested to assist in the binding of third-generation cephalosporins, enhancing the kinetic properties of the enzyme (5, 10). The effect of this mutation relies on chemical complementarity with the substrate, with which it may form electrostatic or hydrogen bonding interactions. Among the selected variants, all but Leu have hydrogen-bonding capacity, suggesting that this feature may be exploited in most of the mutants. However, the Leu mutation suggests that it is not an essential feature. The consistently low  $K_M$  of mutant VNSLR for all substrates tested illustrates that mutation E240L is not detrimental for substrate recognition in the context of the additional mutations at positions 104, 105 and 238 (Table 6.3). Moreover this replacement confirms the moderate natural variability observed at position 240 in class A  $\beta$ -lactamases.

Gly-238 – CAZ-selected mutants of TEM-1 harbouring either a serine or an asparagine at position 238 have previously been observed (28). Natural TEM ESBL isolates frequently harbour the same G238S mutation (approximately 20% of isolates) but not the asparagine mutation (see <http://lahey.org/studies/temtable.asp>). This is likely due to the requirement for two nucleotide changes necessary to modify the glycine codon to

asparagine rather than the evolutionarily more achievable single nucleotide change required for the serine substitution. While the G238N mutation only provides for modest ESBL activity and is approximately one order of magnitude less efficient in third-generation cephalosporin hydrolysis than G238S (3), this single substitution still provides a catalytic efficiency one order of magnitude greater than wild-type toward hydrolysis of CTX and CAZ (3). Consistent with a previous report that identified Ser and Asn as the only productive replacements of Gly-238 conferring high *in vivo* CAZ activities (28), all the CTX-resistant mutants identified in the present study display the G238S mutation with the sole exception of the double mutant EYNHR (displaying G238N).

While it was initially proposed that the Ser-238 hydroxyl was implicated in hydrogen bonding with the R<sub>1</sub> substituent of CTX (38, 39), CTX hydrolysis has also been observed with the hydrogen bonding-deficient G238A mutant (15), illustrating that this interaction is not essential for CTX hydrolysis. Moreover, crystal structures and molecular modelling studies have shown that Ser-238 is not appropriately positioned to hydrogen bond with CTX (9, 36). Consequently, several authors have suggested that substitution of the native Gly-238 displaces the bottom edge of the β3 strand (9, 10), expanding the active-site cavity to accommodate bulkier substrates (*i.e.* extended-spectrum β-lactams). Alternatively, steric hindrance observed between the Ser-238 hydroxyl and the main-chain of Asn-170 has been proposed to be relieved through a shift of the Ω-loop, also resulting in the widening of the active-site cavity (3, 36, 40, 41). While both of these structural hypotheses have been supported by elements of kinetic evidence (3, 10, 11, 36), analysis of the crystal structures of ESBL mutants TEM-52 (9) and SHV-2 (8) have substantiated the β3 strand displacement hypothesis.

The observation of the G238S and G238N mutations in all our CTX-resistant variants suggests that the structural effect of these replacements on CTX hydrolysis is unmatched by any other mutation at this position. Moreover, considering that the catalytic improvements resulting from additional mutations at positions 104, 105 and 240 only

moderately increase CTX hydrolysis relative to mutant G238S (Table 6.3), it is likely that displacement of the  $\beta$ 3 strand is an independent and compulsory structural requirement of CTX hydrolysis in TEM-1 that is expected to be present in most, if not all of the mutants selected in the present study.

**Tyr-105** – With few exceptions, aromatic and small amino acids are conserved at position 105 in class A  $\beta$ -lactamases, a structural and functional requirement that has previously been rationalized by the necessity to form a stable wall to the active-site cavity in TEM-1 (21). The mutations observed at position 105 in the combinatorial context of the variants selected in the present study (Tyr, Trp, His, Asn and Ser) form a sub-group of those amino acids and support the necessity for this residue to be small or planar to prevent steric clashes with the substrate. The neighbouring mutations at positions 104, 238 and 240 did not broaden the variety of functional residues at position 105, demonstrating that the previously observed negative effects of its replacement on binding and catalysis (21) cannot be compensated by mutations at positions 104, 238 and 240. Interestingly, while the selected mutants contained the wild-type tyrosine at position 105 in combination with a variety of mutations at positions 238 and 240 (Table 6.1), it was combined with no other residue than the wild-type glutamate at position 104 (and *vice versa*). This suggests that the wild-type E104:Y105 sequence is a highly favoured pair in which Glu-104 and Tyr-105 act in an interdependent fashion. Mutation of either one may allow mutation of the second to form new, favoured pairs. Similar results had been obtained in a previous combinatorial study of TEM-1 residues 103-105 (14).

**Glu-104** – In class A  $\beta$ -lactamases, position 104 displays a modest variety of side chains, either hydrophobic (Val or Pro), polar (Ser) or charged (Glu) (2, 14, 37). In addition, the E104K mutation is the only substitution observed among natural ESBL TEM isolates, being present in >25% of cases (<http://lahey.org/studies/temtable.asp>). While this mutation increases hydrolysis of third-generation cephalosporins, the E104K mutation alone is not sufficient to confer *in vivo* resistance unless combined with G238S, yielding

the clinically-significant double mutant E104K:G238S (TEM-15) (15, 42). In TEM-1, the wild-type Glu-104 is involved in correct positioning of the catalytically-significant SDN loop, encompassing residues 130-132 (4). In SHV-1  $\beta$ -lactamase, certain Asp-104 substitutions have been suggested to modify the topology of loop 101-111, thereby potentially affecting enzyme function and substrate spectrum (6). The E104K mutation has been suggested to hydrogen-bond with the oxime substituent of CTX and to form an electrostatic contact with the oxime carboxylate moiety of CAZ (5). Similar to the results observed at position 240, our selected mutational combinations displayed a relatively wide variety of mutations at position 104. However, although we sequenced it among the non-selected clones, the E104K mutation found in many ESBL enzymes was not observed in any of our combinatorial CTX-selected mutants, suggesting that other E104 replacements offer similar or greater catalytic advantages in this combinatorial context.

The fair diversity observed at positions 104 and 240 did not result in large variation in kinetic parameters among the selected mutants. This may result from both positions being solvent-exposed and relatively unconstrained (6, 21). For instance, the conformation adopted by Ser-104 in BlaC  $\beta$ -lactamase from *Mycobacterium tuberculosis* is oriented away from the substrate-binding site, expanding the active site and partly accounting for its broad-spectrum substrate profile (43). Variations in the positioning of residue 104 can also affect the SDN loop (4), or loop 101-111 as observed in SHV-1  $\beta$ -lactamase (6). Thus, repositioning of residues 104 and 240 in the selected variants could contribute to active-site expansion, leading to binding of bulkier substrates in the cavity. The chemical diversity of side chains allowed at position 240 in the CTX-resistant mutants (charged, polar or hydrophobic) (Table 6.1) demonstrates that the previously suggested electrostatic interaction of residue 240 with the oxime substituent of third generation cephalosporins (10) is not strictly essential to confer increased CTX activity in the combinatorial context presented here. Moreover, this observation is supported by the previous selection of the CTX-resistant mutant E240G (44), which also displays a higher catalytic efficiency than

wild-type toward CTX (45). We therefore propose that replacements at both positions 104 and 240 are mainly structural requirements that support productive binding of CTX rather than to favour direct molecular interactions with the substrate. Our experimental results are consistent both with the active-site expansion through displacement of the  $\beta$ 3-strand caused by the G238S and G238N mutations and flexibility of residues 104 and 240, that could open the lower region of the active site and allow expansion.

#### Catalytic Properties of the Combinatorial Mutants

**EYNHR** – Upon simultaneous mutation, residues may behave either in an independent or in an interdependent fashion toward protein function (20). In TEM-1, synergy has previously been observed for both double mutants G238S:E240K (11) and E104M:G238S (19) toward CAZ and CTX hydrolysis, respectively (while in other cases additivity has been reported). Comparing our selected mutants to G238S demonstrates that the major contribution in CTX catalytic efficiency comes from this substitution (Table 6.3). However, the double mutant EYNHR (G238N:E240H) confers an important  $10^3$ -fold catalytic efficiency improvement relative to wild-type TEM-1, a result that cannot be attributed to the G238N mutation alone. G238N has been shown to account only for a 10-fold increase in catalytic efficiency toward the third-generation cephalosporins CTX and CAZ, as well as mild improvements in  $K_M$  toward penicillins and first- and second-generation cephalosporins (CF and cephaloridine) (3). Unless mutation E240H provides a 900-fold improvement in catalytic efficiency on its own (which is unlikely considering the negative effects in CTX catalytic efficiencies conferred by various mutations at this position in several class A enzymes (29, 46)), the G238N:E240H combination would therefore behave in a synergistic manner in promoting CTX hydrolysis. This observation may partly explain the fact that EYNHR, which does not carry the G238S mutation, nevertheless boasts the greatest increase in efficiency of CTX hydrolysis.

Comparing EYNHR with the G238N point mutant (3) also reveals that the combination of the two mutations is responsible for the decrease in penicillin resistance (5- to 10-fold). EYNHR showed a 10-fold  $K_M$  increase for BZ (106 vs. 9  $\mu\text{M}$ ), a 10-fold  $K_M$  decrease for CF (11 vs. 100  $\mu\text{M}$ ) and a modest 4-fold  $K_M$  decrease for CTX (61 vs. 244  $\mu\text{M}$ ) relative to G238N (3). Therefore, mutation E240H raised the  $K_M$  of BZ while reducing the  $K_M$  of cephalosporins, thus switching the substrate profile of mutant EYNHR to improve discrimination between penicillins *vs.* cephalosporins in favour of cephalosporin binding and hydrolysis. Thus, the association of G238N:E240H was sufficient for acquisition of the extended substrate spectrum, survival and kinetic enhancements, with no mutation at the opposite face of the active site (104 and/or 105).

**SWSSR** – Mutant SWSSR, which harbours the four mutations E104S:Y105W:G238S:E240S, encodes E104S, a point mutation responsible for increased catalytic efficiency toward penicillins and cephalosporins (4) as well as a Trp at position 105, which was the only point mutation that increased catalytic efficiency toward BZ and CF in TEM-1 (21). E104S and Y105W, which are individually responsible for modest increases in  $k_{\text{cat}}/K_M$  relative to WT, appear to display cooperativity with G238S and the uncharacterized E240S to provide SWSSR with increased catalytic efficiencies toward cephalosporins. Interestingly, this TEM-1 quadruple mutant showed a modest six-fold increase in CTX MIC relative to wild-type TEM-1, while the SHV-1  $\beta$ -lactamase double mutant D104S:G238S boasted a 130-fold increase in CTX MIC relative to wild-type SHV-1 (albeit only an eight-fold increase for the other third-generation cephalosporin CAZ) (6). Although the combinatorial contexts are not identical and both enzymes may behave differently as a result of other differences at their active sites, mutations Y105W and/or E240S in the TEM-1 mutant SWSSR may have a damping effect on CTX resistance.

**PHSER** – In addition to G238S, the triple mutant PHSER (E104P:Y105H:G238S) also combines two previously characterized beneficial point mutations, which likely account for its high catalytic efficiency for all substrates tested. In TEM-1, mutation E104P

is advantageous toward the affinity and hydrolysis of various substrates (including CTX) (4) while mutation Y105H displays native-like levels of resistance toward penicillins and first-generation cephalosporins (21). In SHV-1, MICs of mutant D104P:G238S have revealed that its cephalosporin resistance is one to two orders of magnitude above WT and practically unchanged for AMP (6). Although differentiated by the Y105H substitution, PHSER remains similar to the SHV-1 double mutant D104P:G238S, showing no significant variation for first-generation cephalosporin substrates. However, PHSER showed a great decrease in AMP resistance (Table 6.2). The antagonistic effect toward AMP hydrolysis may result from mutation Y105H or from the combinatorial context in which these mutations arise.

VNSTR/VNSLR – The two quadruple mutants VNSTR and VNSLR (E104V:Y105N:G238S:E240T/L) differ only by their substitution at position 240. While both variants displayed important increases in CTX hydrolysis *in vivo* and *in vitro*, this latter mutation resulted in a greater MIC for CTX by mutant VNSTR while mutant VNSLR displayed a slightly better catalytic efficiency toward all substrates tested. It has been proposed that a hydrophilic residue at position 240 could interact with a cephalosporin substrate such as CTX by hydrogen-bonding to the oxygen or nitrogen atoms of the oxime substituent of the ligand (5). One would thus expect that mutant VNSTR, exhibiting a polar threonine at position 240, should manifest the best productive affinity (lowest  $K_M$ ) for the cephalosporin substrates. However, although both VNSTR and VNSLR featured similar  $K_M$  values for the three cephalosporins tested (Table 6.3), VNSLR always exhibited slightly better  $K_M$  values relative to VNSTR (~2.5-fold reduction). This observation demonstrates that productive binding is slightly better with a hydrophobic residue (Leu) at position 240 in the context of concomitant replacements at positions 104, 105 and 238 and demonstrates that a hydrophilic residue at this position is not strictly essential to confer the ESBL phenotype.

Promiscuity, Robustness and Plasticity in Substrate Binding

Our results illustrate that TEM-1 can incorporate several combinations of mutations in the vicinity of the active site with conservation or improvement of its hydrolytic function toward a variety of substrates. It has been previously noted that mutants at position 238, alone and in combination with substitutions at position 104, lose a great deal of activity toward the penicillins AMP and BZ while increasing their efficiency for third-generation cephalosporins hydrolysis (15, 17, 28). The overall behaviour of the mutants selected in the present study follows the same pattern since all variants selected against CTX exhibited increased activity toward CTX at the expense of that for BZ. In fact, the combined effects of  $k_{cat}$  and  $K_M$  resulted in a two- to three-order of magnitude improvement of catalytic efficiency toward CTX hydrolysis, a conservation or slight improvement in the hydrolysis of first-generation cephalosporins and a one- to two-order of magnitude decrease in BZ hydrolysis (Table 6.3). This property appears to be generalized also among naturally-occurring ESBLs but is not limited to this family of enzymes. Thus, despite selection having been directed exclusively toward CTX hydrolysis, the evolution of this promiscuous binding function (47) (CTX binding) remained compatible with recognition of first-generation cephalosporins. Being relatively innocuous toward enzyme function, the additional mutations at positions 104, 105 and 240 indicate a certain degree of robustness in TEM-1 (48), which tolerated multiple active-site mutations and still allowed recognition of related compounds. Such emergence of a new phenotypic trait (CTX resistance) by the introduction of a small number of mutations has been defined as enzyme plasticity (49).

When evolving an enzyme toward a new function, negative trade-offs often compromise the original activity. Two possible routes are envisaged for this evolution process to take place, depending on the selection method applied. Starting from the native, “specialized” enzyme, selection for a new specialized promiscuous activity may yield either strong or weak negative trade-offs. In most directed evolution experiments, the weak trade-off route is privileged and yields “generalized” enzymes, as intermediates between the two

specialized enzymes, whereas strong trade-offs often arise in the cases of dual selections (49). Our combinatorial mutants, selected only for CTX hydrolysis, appear to follow the weak trade-off route, apparently stopping at the generalized stage, as evidenced by a comparison of mutant kinetic efficiencies with the specialized wild-type enzyme. Nonetheless, although they have evolved in the direction of improved CTX hydrolysis, they remain less specialized than other engineered  $\beta$ -lactamase mutants (44, 50).

While the TEM-1 active-site cavity was considerably mutated relative to the wild-type enzyme, mutations apparently maintained the spatial integrity of functional groups important for binding and catalysis of cephalosporin substrates rather than selecting for one specific  $\beta$ -lactam compound (*e.g.* CTX). This “plasticity” character that allows enzymes to recognize a broad range of substrates on the basis of a restricted set of functional elements has been observed in many protein families (51) and confirms that the active sites of enzymes have been designed by evolution to work as cooperative entities that do not only rely on a restricted set of amino acids for catalysis (52).

The capacity of an active site to accommodate mutations is a function of the relation between the residues: by maintaining a degree of independence between key residues, introduction of a mutation will not necessarily be deleterious for enzymatic activity. Such weakly-linked residues can potentially lead to robust systems, which may serve as starting points for evolution of new enzymatic functions. According to Wagner (48), an enzyme that can perform its native function following multiple neutral amino acid substitutions should possess the necessary characteristics for emergence of a promiscuous activity. The reason for which the penicillin-hydrolysing activity of TEM-1  $\beta$ -lactamase has dropped significantly could be that both the native and promiscuous activities are mutually exclusive, due to structural requirements for the specific recognition and hydrolysis of one particular substrate over the other. In this work, mutant catalytic efficiency enhancements relative to mutant G238S were modest and appear to be the result of additive effects, as opposed to synergistic effects, of the additional mutations. If this is the case, then the

residues targeted for mutagenesis behave independently. However, mutant EYNHR appears to display mutational synergy, illustrating that complex effects can prevail depending on the identity of the residues. Globally, we observed no evidence of mutational linkage between the two active-site faces we modified, despite some previous evidence to this effect (mutant E104M:G238S (19)), suggesting that these two areas of the active site are not highly interdependent. This may be an evolutionary strategy to limit loss of activity that would occur upon mutation of highly linked residues. Nonetheless, we observed some evidence that mutation of the neighbour residues 104 and 105 may be linked, setting a restriction to the plasticity of the active site.

## CONCLUSION

All the novel TEM-1 variants described herein displayed improved affinities toward all antibiotics investigated, relative to the wild-type enzyme. In addition, most variants displayed improved CTX and CZ binding relative to the point mutant G238S. In light of these results, it is clear that the active site of TEM-1 can sustain multiple substitutions to broaden its substrate spectrum and thus allow a better fit of the aminothiazole moiety, as hypothesized by Bush and coworkers (5). Substrate discrimination was enhanced and hydrolysis of penicillins was reduced in all mutants. Hence, our results support the hypothesis that active-site cavities can tolerate a relatively large number of mutations that confer a certain level of “evolvability” toward a set of related substrates. This evolvability is an indication of enzyme plasticity.

In conclusion, our *in vivo* and *in vitro* experiments led us to identify cooperative effects from the combination of mutations that appear to be mostly additive and independent, although some linkages (104/105) are suggested and synergy possible (EYNHR). Mutants selected for increased CTX hydrolysis maintained or improved their activity toward first-generation cephalosporins, compatible with functional diversification

and adaptability by the enzyme. Mutation G238S accounts for most of the effects observed (especially regarding CTX) while the other substitutions contribute for modest enhancements.

## FOOTNOTES

<sup>1</sup> The abbreviations used are: ESBL, extended-spectrum  $\beta$ -lactamase; AMP, ampicillin; BZ, benzylpenicillin; CF, cephalothin; CZ, cefazolin; CTX, cefotaxime; CAZ, ceftazidime; MIC, minimum inhibitory concentration; Chl, chloramphenicol; CV, column volume.

<sup>2</sup> The five-letter nomenclature identifies mutants according to amino acids found at positions 104, 105, 238, 240 and 244, respectively.

## REFERENCES

1. Matagne, A., Lamotte-Brasseur, J., and Frère, J. M. (1998) *Biochem. J.* **330**(2), 581-598
2. Ambler, R. P., Coulson, A. F., Frère, J. M., Ghysen, J. M., Joris, B., Forsman, M., Levesque, R. C., Tiraby, G., and Waley, S. G. (1991) *Biochem. J.* **276** (1), 269-270
3. Cantu, C., 3rd, and Palzkill, T. (1998) *J. Biol. Chem.* **273**(41), 26603-26609
4. Petit, A., Maveyraud, L., Lenfant, F., Samama, J. P., Labia, R., and Masson, J. M. (1995) *Biochem. J.* **305** ( Pt 1), 33-40

5. Sowek, J. A., Singer, S. B., Ohringer, S., Malley, M. F., Dougherty, T. J., Gougoutas, J. Z., and Bush, K. (1991) *Biochemistry* **30**(13), 3179-3188
6. Bethel, C. R., Hujer, A. M., Hujer, K. M., Thomson, J. M., Ruszczycky, M. W., Anderson, V. E., Pusztai-Carey, M., Taracila, M., Helfand, M. S., and Bonomo, R. A. (2006) *Antimicrob. Agents Chemother.* **50**(12), 4124-4131
7. Fisher, J. F., Meroueh, S. O., and Mobashery, S. (2005) *Chem. Rev.* **105**(2), 395-424
8. Nukaga, M., Mayama, K., Hujer, A. M., Bonomo, R. A., and Knox, J. R. (2003) *J. Mol. Biol.* **328**(1), 289-301
9. Orencia, M. C., Yoon, J. S., Ness, J. E., Stemmer, W. P., and Stevens, R. C. (2001) *Nat. Struct. Biol.* **8**(3), 238-242
10. Huletsky, A., Knox, J. R., and Levesque, R. C. (1993) *J. Biol. Chem.* **268**(5), 3690-3697
11. Venkatachalam, K. V., Huang, W., LaRocco, M., and Palzkill, T. (1994) *J. Biol. Chem.* **269**(38), 23444-23450
12. Knox, J. R. (1995) *Antimicrob. Agents Chemother.* **39**(12), 2593-2601
13. Ambler, R. (1980) *Philos. Trans. R. Soc. Lond. B. Biol. Sci.* **289**(1036), 321-331
14. Huang, W. Z., Petrosino, J., Hirsch, M., Shenkin, P. S., and Palzkill, T. (1996) *J. Mol. Biol.* **258**(4), 688-703
15. Lenfant, F., Labia, R., and Masson, J. M. (1990) *Biochimie* **72**(6-7), 495-503
16. Bush, K., and Singer, S. B. (1989) *Infection* **17**(6), 429-433

17. Raquet, X., Lamotte-Brasseur, J., Fonze, E., Goussard, S., Courvalin, P., and Frère, J. M. (1994) *J. Mol. Biol.* **244**(5), 625-639
18. Imtiaz, U., Manavathu, E. K., Mobashery, S., and Lerner, S. A. (1994) *Antimicrob. Agents Chemother.* **38**(5), 1134-1139
19. Viadiu, H., Osuna, J., Fink, A. L., and Soberón, X. (1995) *J. Biol. Chem.* **270**(2), 781-787
20. Mildvan, A. S. (2004) *Biochemistry* **43**(46), 14517-14520
21. Doucet, N., De Wals, P.-Y., and Pelletier, J. N. (2004) *J. Biol. Chem.* **279**(44), 46295-46303
22. Zafaralla, G., Manavathu, E. K., Lerner, S. A., and Mobashery, S. (1992) *Biochemistry* **31**(15), 3847-3852
23. Chica, R. A., Doucet, N., and Pelletier, J. N. (2005) *Curr. Opin. Biotechnol.* **16**(4), 378-384
24. Reetz, M. T., Bocola, M., Carballeira, J. D., Zha, D., and Vogel, A. (2005) *Angew. Chem. Int. Ed. Engl.* **44**(27), 4192-4196
25. Ho, S. N., Hunt, H. D., Horton, R. M., Pullen, J. K., and Pease, L. R. (1989) *Gene* **77**(1), 51-59
26. Sarkar, G., and Sommer, S. S. (1990) *Biotechniques* **8**(4), 404-407
27. Sambrook, J., Fritsch, E. F., and Maniatis, T. (1989) *Molecular cloning: A laboratory manual*, 2nd Ed., Cold Spring Harbor Laboratory, Cold Spring Harbor, NY

28. Cantu, C., 3rd, Huang, W., and Palzkill, T. (1996) *J. Biol. Chem.* **271**(37), 22538-22545
29. Bouthors, A. T., Dagoneau-Blanchard, N., Naas, T., Nordmann, P., Jarlier, V., and Sougakoff, W. (1998) *Biochem. J.* **330** (Pt 3), 1443-1449
30. Tribuddharat, C., Moore, R. A., Baker, P., and Woods, D. E. (2003) *Antimicrob. Agents Chemother.* **47**(7), 2082-2087
31. Reynaud, A., Peduzzi, J., Barthelemy, M., and Labia, R. (1991) *FEMS Microbiol. Lett.* **65**(2), 185-192
32. Chan, P. T. (1986) *Nucleic Acids Res.* **14**(14), 5940
33. Bush, K., and Mobashery, S. (1998) *Adv. Exp. Med. Biol.* **456**, 71-98
34. Page, M. I. (1987) The mechanisms of reactions of  $\beta$ -lactam antibiotics. In. *Advances in physical organic chemistry*, Academic Press Inc., London
35. Medeiros, A. A. (1997) *Clin. Infect. Dis.* **24**(Suppl 1), S 19-S 45
36. Saves, I., Burlet-Schiltz, O., Maveyraud, L., Samama, J. P., Prome, J. C., and Masson, J. M. (1995) *Biochemistry* **34**(37), 11660-11667
37. Tranier, S., Bouthors, A. T., Maveyraud, L., Guillet, V., Sougakoff, W., and Samama, J. P. (2000) *J. Biol. Chem.* **275**(36), 28075-28082
38. Barthélémy, M., Péduzzi, J., Ben Yaghane, H., and Labia, R. (1988) *FEBS Lett.* **231**(1), 217-220
39. Labia, R., Morand, A., Tiwari, K., Sirot, J., Sirot, D., and Petit, A. (1988) *Rev. Infect. Dis.* **10**(4), 885-891

40. Jelsch, C., Mourey, L., Masson, J. M., and Samama, J. P. (1993) *Proteins* **16**(4), 364-383
41. Shimamura, T., Ibuka, A., Fushinobu, S., Wakagi, T., Ishiguro, M., Ishii, Y., and Matsuzawa, H. (2002) *J. Biol. Chem.* **277**(48), 46601-46608
42. Mabilat, C., and Courvalin, P. (1990) *Antimicrob. Agents Chemother.* **34**(11), 2210-2216
43. Wang, F., Cassidy, C., and Sacchettini, J. C. (2006) *Antimicrob. Agents Chemother.* **50**(8), 2762-2771
44. Zaccolo, M., and Gherardi, E. (1999) *J. Mol. Biol.* **285**(2), 775-783
45. Lenfant, F., Petit, A., Labia, R., Maveyraud, L., Samama, J. P., and Masson, J. M. (1993) *Eur. J. Biochem.* **217**(3), 939-946
46. Cantu, C., 3rd, Huang, W., and Palzkill, T. (1997) *J. Biol. Chem.* **272**(46), 29144-29150
47. Aharoni, A., Gaidukov, L., Khersonsky, O., Mc, Q. G. S., Roodveldt, C., and Tawfik, D. S. (2005) *Nat. Genet.* **37**(1), 73-76
48. Wagner, A. (2005) *FEBS Lett.* **579**(8), 1772-1778
49. Khersonsky, O., Roodveldt, C., and Tawfik, D. S. (2006) *Curr. Opin. Chem. Biol.* **10**(5), 498-508
50. Stemmer, W. P. (1994) *Nature* **370**(6488), 389-391
51. Todd, A. E., Orengo, C. A., and Thornton, J. M. (2002) *Trends Biochem. Sci.* **27**(8), 419-426

52. Peracchi, A. (2001) *Trends. Biochem. Sci.* **26**(8), 497-503

## TABLES

**Table 6.1.** Identification of TEM-1  $\beta$ -lactamase mutants selected on media containing 250 ng/mL CTX.

Mutated positions					Frequency of occurrence
104	105	238	240	244	
E	Y	G	E	R	0 (WT TEM-1)
E	Y	S	K	R	14
E	Y	S	R	R	4
Q	W	S	E	R	4
E	Y	S	T	R	3
V	N	S	T	R	2
R	S	S	T	R	2
E	Y	N	H	R	1
P	H	S	E	R	1
R	W	S	E	R	1
S	W	S	S	R	1
V	N	S	L	R	1

**Table 6.2.** Minimum inhibitory concentrations of *E. coli* XL1-Blue cells containing wild-type or mutant  $\beta$ -lactamases.

$\beta$ -lactamase variants	Substrates ( $\mu\text{g/mL}$ )				
	CTX	AMP	BZ	CF	CZ
None <sup>a</sup>	0.125	64	250	32	8
(WT TEM-1) <sup>b</sup>	0.125	10,000	10,000	125	64
E Y G E R					
V N S L R	0.5	250	500	64	64
P H S E R	0.5	250	500	125	32
E Y N H R	0.5	500	500	64	16
S W S S R	0.75	1,000	1,000	64	32
V N S T R	2	250	1,000	64	32

<sup>a</sup>*E. coli* XL1-Blue.

<sup>b</sup> The five-letter nomenclature identifies mutants according to amino acids found at positions 104, 105, 238, 240 and 244, respectively.

**Table 6.3.** Kinetic parameters for wild-type TEM-1  $\beta$ -lactamase and the combinatorial mutants.

Substrates	TEM-1 variants	$k_{\text{cat}}$ (s <sup>-1</sup> )	$k_{\text{cat}}$ relative to WT	$K_M$ ( $\mu\text{M}$ )	$K_M$ relative to WT	$k_{\text{cat}}/K_M$ (M <sup>-1</sup> s <sup>-1</sup> )	$k_{\text{cat}}/K_M$ relative to WT	$k_{\text{cat}}/K_M$ relative to G238S
<b>CTX<sup>c</sup></b>	TEM-1 WT (EYGER <sup>a</sup> )	0.74 ± 0.1 <sup>b</sup>	1	840 ± 160	1	8.8 × 10 <sup>2</sup>	1	6.3 × 10 <sup>-3</sup>
	VNSTR	23 ± 7	31	72 ± 13	0.09	3.2 × 10 <sup>5</sup>	360	2.3
	VNSLR	20 ± 2	27	28 ± 7	0.03	7.1 × 10 <sup>5</sup>	810	5.1
	SWSSR	20 ± 2	27	40 ± 7	0.05	5.0 × 10 <sup>5</sup>	570	3.6
	PHSER	61 ± 6	82	113 ± 9	0.13	5.4 × 10 <sup>5</sup>	614	3.9
	EYNHR	55 ± 10	74	61 ± 9	0.07	9.0 × 10 <sup>5</sup>	1020	6.4
<b>CF</b>	G238S <sup>d</sup> (EYSER)	16 ± 2	22	124 ± 47	0.15	1.4 × 10 <sup>5</sup>	160	1
	TEM-1 WT (EYGER)	77 ± 4	1	180 ± 28	1	4.3 × 10 <sup>5</sup>	1	1.1
	VNSTR	10 ± 0.3	0.13	16 ± 0.6	0.09	6.3 × 10 <sup>5</sup>	1.5	1.6
	VNSLR	16 ± 0.5	0.21	5 ± 1	0.03	3.2 × 10 <sup>6</sup>	7.4	8.2
	SWSSR	24 ± 3	0.31	10 ± 5	0.06	2.4 × 10 <sup>6</sup>	5.6	6.2
	PHSER	31 ± 6	0.40	7 ± 2	0.04	4.4 × 10 <sup>6</sup>	10.2	11.3
<b>CZ</b>	EYNHR	31 ± 5	0.40	11 ± 1	0.06	2.8 × 10 <sup>6</sup>	6.5	7.2
	G238S <sup>d</sup> (EYSER)	3 ± 1	0.04	8 ± 5	0.05	3.9 × 10 <sup>5</sup>	0.91	1
	TEM-1 WT (EYGER)	69 ± 13	1	130 ± 9	1	5.3 × 10 <sup>5</sup>	1	1.1
	VNSTR	38 ± 7	0.55	83 ± 7	0.67	4.6 × 10 <sup>5</sup>	0.87	0.94
	VNSLR	41 ± 1	0.59	28 ± 2	0.22	1.5 × 10 <sup>6</sup>	2.8	3.1
	SWSSR	50 ± 9	0.72	55 ± 14	0.44	9.1 × 10 <sup>5</sup>	1.7	1.9
<b>BZ</b>	PHSER	88 ± 4	1.3	61 ± 9	0.49	1.4 × 10 <sup>6</sup>	2.6	2.9
	EYNHR	82 ± 9	1.2	120 ± 23	0.98	6.8 × 10 <sup>5</sup>	1.3	1.4
	G238S <sup>e</sup> (EYSER)	170	2.5	347	2.8	4.9 × 10 <sup>5</sup>	0.93	1
	TEM-1 WT (EYGER)	1660 ± 230	1	62 ± 21	1	2.7 × 10 <sup>7</sup>	1	79
	VNSTR	19 ± 1	0.01	17 ± 7	0.27	1.1 × 10 <sup>6</sup>	0.04	3.2
	VNSLR	29 ± 2	0.02	15 ± 2	0.24	1.9 × 10 <sup>6</sup>	0.07	5.6
	SWSSR	ND <sup>f</sup>	ND	ND	ND	ND	ND	ND
	PHSER	20 ± 4	0.01	31 ± 6	0.50	6.5 × 10 <sup>5</sup>	0.02	1.9
	EYNHR	35 ± 4	0.02	106 ± 18	1.7	3.2 × 10 <sup>5</sup>	0.01	0.94
	G238S <sup>d</sup> (EYSER)	3.9 ± 0.4	0.002	12 ± 1	0.19	3.4 × 10 <sup>5</sup>	0.01	1

<sup>a</sup> The five-letter nomenclature identifies mutants according to amino acids found at positions 104, 105, 238, 240 and 244, respectively.

<sup>b</sup> Mean value  $\pm$  standard deviation error

<sup>c</sup> Values obtained from Cantu III *et al.* (28).

<sup>d</sup> Values obtained from Raquet *et al.* (17).

<sup>e</sup> ND, not determined.

## FIGURES

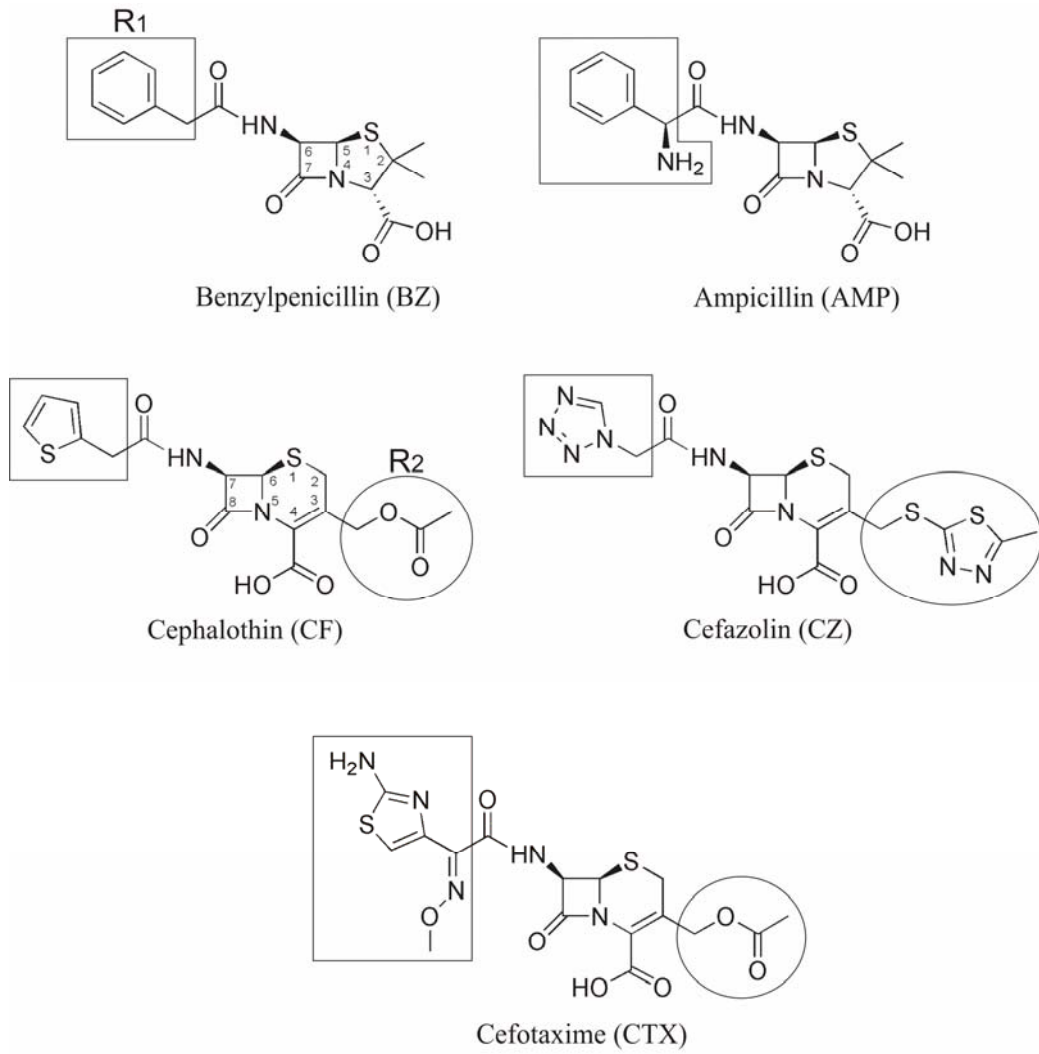


**Figure 6.1.** Structure of the  $\beta$ -lactam antibiotics used in this study. BZ and AMP are two classical penicillins. CF and CZ are first-generation cephalosporins, whereas CTX is a third-generation cephalosporin. R<sub>1</sub> substituents are framed and R<sub>2</sub> are circled to highlight the structural differences among the various substrates. Note the bulkiness of R<sub>1</sub> from CTX relative to CF and CZ.

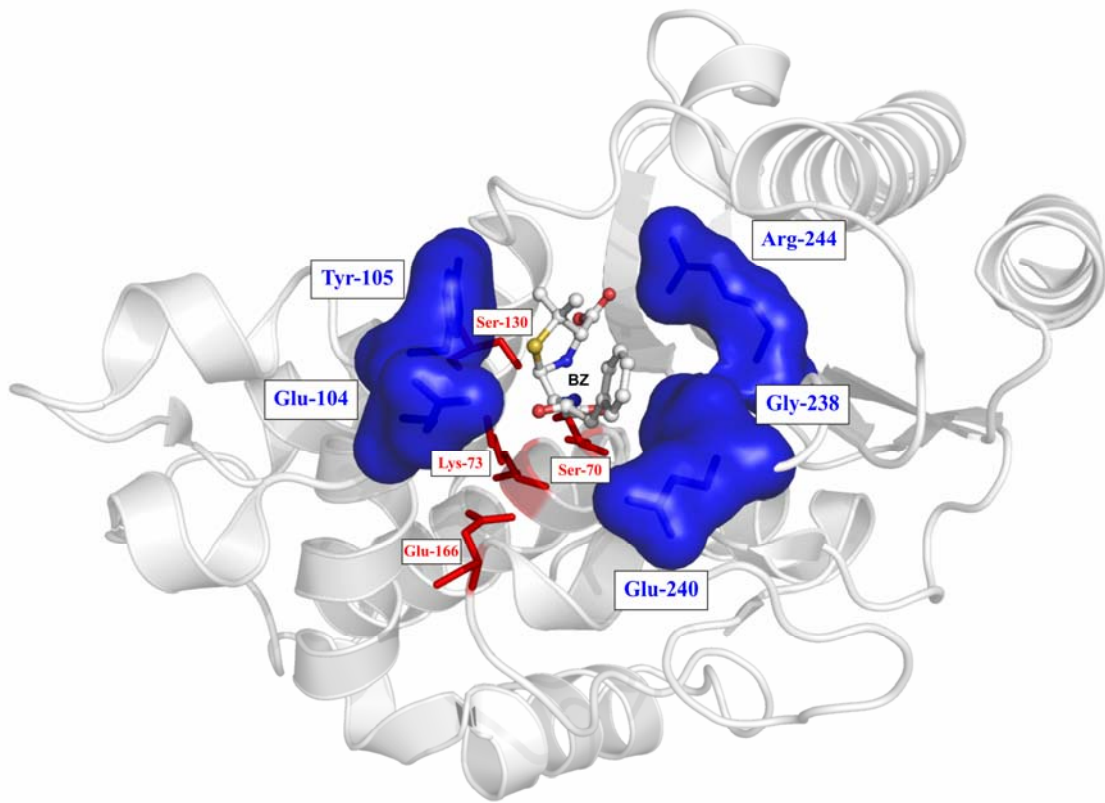


**Figure 6.2.** Schematic representation of the active site of TEM-1  $\beta$ -lactamase. Residues targeted for saturation mutagenesis (Glu-104, Tyr-105, Gly-238, Glu-240 and Arg-244) are represented in blue according to their Connolly surface, defined by a 1.6 Å solvent radius. These amino acids form 2 distinct “walls” of the active-site cavity. Residues known to be involved in the catalytic mechanism (Ser-70, Lys-73, Ser-130 and Glu-166) are coloured in red. The co-crystallized BZ is shown in ball-and-sticks representation and is displayed to show its proximity to the targeted active-site wall positions. PDB coordinates 1FQG.

## **CHAPITRE 7**

### **Conclusions et perspectives**

## 7.0 – Conclusions générales

La résistance enzymatique aux antibiotiques à noyau  $\beta$ -lactame est l'une des causes principales à la base de la lutte à finir entre l'être humain et les micro-organismes responsables de nombreuses infections affectant la santé humaine et animale. Ainsi, la compréhension détaillée de l'inactivation moléculaire de ces antibiotiques par les  $\beta$ -lactamases s'avère être un outil essentiel à la prédiction de mutations futures responsables de l'émergence de la résistance aux antibiotiques chez plusieurs organismes pathogènes. Centré sur cette problématique générale, le thème principal de cette thèse fut d'entreprendre une étude structure-fonction détaillée de certains résidus du site actif de la  $\beta$ -lactamase TEM-1 avec objectif d'améliorer la compréhension de leur rôle au niveau de la catalyse enzymatique ainsi que dans la discrimination et la stabilisation des différents antibiotiques à noyau  $\beta$ -lactame. À cet effet, la première partie de cette thèse (chapitres 2, 3 et 4) fut consacrée à l'étude spécifique d'un résidu (Tyr105) faisant partie d'une boucle dynamique au site actif de TEM-1 et dont le positionnement par rapport aux ligands s'avère être critique au niveau de leur reconnaissance et de leur stabilisation.

Au chapitre 2, nous avons démontré que le remplacement de Tyr105 par de gros résidus flexibles, chargés et/ou non-planaires affectait de manière significative la reconnaissance des substrats alors que le remplacement par des résidus aromatiques, planaires ou petits n'affectait que modérément l'activité des divers variants enzymatiques. En plus d'illustrer la faible discrimination de reconnaissance entre les pénicillines et les céphalosporines chez les mutants Gly et Ala, nos résultats démontrent que la formation d'une paroi stabilisatrice à cette position du site actif est favorable (mais pas strictement essentielle dans le cas des pénicillines) au positionnement approprié du cycle thiazolidine/dihydrothiazine des substrats sur une échelle de temps de 200 ps.

Au chapitre 3, sur la base de calculs de modélisation moléculaire effectués par recuit simulé, nous avons suggéré la possibilité que Tyr105 puisse alterner entre la conformation de deux rotamères stables au site actif de TEM-1 sur une échelle de temps plus longue que celle testée dans nos études de dynamique moléculaire précédentes ( $>200$  ps). Ces deux rotamères correspondent à  $t80^\circ$ , retrouvé dans les structures cristallines de l'enzyme libre ou en présence de substrat, et  $m-85^\circ/m-30^\circ$ , retrouvé chez certaines structures cristallines de TEM-1 en présence d'inhibiteurs. Nos résultats suggèrent que l'adoption de ce second conformère par Tyr105 n'est pas strictement promue par la liaison d'un ligand au site actif de l'enzyme et que l'alternance d'un rotamère à l'autre est également observée sur une échelle de temps ps-ns en absence de ligand. Ainsi, en fonction du conformère adopté par Tyr105, cette chaîne latérale pourrait être impliquée dans la stabilisation du noyau thiazolidine/dihydrothiazine des ligands ou encore dans celle de leur substituant  $R_1$ .

Finalement, les études RMN présentées au chapitre 4 ont démontré que les effets dynamiques locaux initialement observés par modélisation moléculaire suite à l'introduction d'une mutation à la position 105 ne sont pas exclusivement confinés à l'environnement immédiat de ce résidu. En plus d'identifier des effets à courte et à longue portée, nos résultats démontrent également l'existence d'une corrélation négative entre le nombre, l'étendue et la magnitude des déplacements chimiques induits par la mutation en position 105 et l'activité catalytique de chacun des mutants. Par ailleurs, une étude de relaxation RMN détaillée entreprise sur le variant Y105D nous a permis d'observer d'importantes variations dynamiques affectant des résidus impliqués dans la reconnaissance des substrats chez TEM-1 (notamment Val216 et Lys234) sur diverses échelles de temps. Les variations dynamiques observées entre TEM-1 et le mutant Y105D nous ont permis de soulever des hypothèses fonctionnelles quant à la corrélation possible existant entre la modification des motions moléculaires de ces résidus et l'importante diminution d'affinité observée chez ce variant de TEM-1.

À titre de complément à l'analyse mutationnelle du résidu 105 chez TEM-1, la seconde partie de cette thèse fut consacrée à l'analyse combinatoire du site actif de cette enzyme par mutagenèse semi-aléatoire. La revue de la littérature présentée au chapitre 5 nous a permis de faire ressortir les avantages de cette technique d'ingénierie enzymatique, qui combine à la fois les points positifs du design rationnel à ceux offerts par l'évolution dirigée strictement aléatoire. En appliquant les préceptes de cette méthodologie semi-aléatoire, nous avons remplacé divers résidus de la cavité du site actif de TEM-1 (Glu104, Tyr105, Gly238, Glu240 et Arg244) par mutagenèse combinatoire pour vérifier l'interdépendance de ces remplacements au niveau de la reconnaissance des substrats et dans le but de tester la tolérance mutationnelle du site actif de cette enzyme. Présentés au chapitre 6, les résultats de cette étude démontrent l'apparition du phénotype ESBL chez divers mutants doubles, triples et quadruples de TEM-1 sélectionnés sur un milieu contenant le substrat oxyiminocéphalosporine céfotaxime (CTX). Nos résultats illustrent que la résistance acquise par l'introduction de ces mutations s'effectue aux dépens de l'activité des substrats pénicillines, mais qu'elle n'a que peu d'effet sur l'activité des céphalosporines classiques. De manière générale, ces résultats démontrent l'existence d'une certaine plasticité au site actif de TEM-1.

## 7.1 – Perspectives

### 7.1.1 – Inhibition et études cristallographiques

En plus de clarifier l'importance du résidu Tyr105 chez la  $\beta$ -lactamase TEM-1, les informations structurelles et fonctionnelles présentées aux chapitres 2, 3 et 4 nous ont permis de soulever certaines hypothèses quant à son importance structurelle et fonctionnelle générale chez les  $\beta$ -lactamases de classe A. Bien que complémentaires, les études présentées dans ces quelques chapitres demeurent à certains égards fragmentaires et

gagneraient à être complétées par certaines expériences supplémentaires améliorant l'impact du présent travail. À cet effet, une étude d'inhibition enzymatique entreprise sur les mutants Y105X à l'aide de certains inhibiteurs de TEM-1 (*e.g.* clavulanate, sulbactame, tazobactame et BLIP) pourrait s'avérer intéressante sur la base des informations structurelles suggérant notamment l'importance de Tyr105 dans la reconnaissance des inhibiteurs protéiques BLIP I et BLIP II [46, 101]. De plus, puisque la molécule d'eau strictement conservée dont il est question au chapitre 4 s'avère être essentielle au mécanisme d'inactivation de TEM-1 par les inhibiteurs chimiques susmentionnés [102], une étude d'inhibition des mutants Y105X pourrait éventuellement donner des informations importantes quant à l'apparition du phénotype IRT causé par cette mutation.

Bien que nos études enzymatiques aient démontré d'importantes variations dans la reconnaissance des substrats pénicilline et céphalosporine chez les mutants Y105G et Y105A de TEM-1, les analyses *in silico* entreprises au chapitre 2 ne permirent pas d'expliquer avec certitude la nature des interactions moléculaires à la base de cette discrimination des substrats. À cet effet, suite à l'introduction d'une mutation supplémentaire ralentissant l'étape de désacylation du mécanisme catalytique et permettant l'obtention d'un intermédiaire acyl-enzyme suffisamment stable (*e.g.* E166N) [44], des études cristallographiques pourraient être entreprises sur ces deux mutants dans le but de résoudre leur structure cristalline en présence de substrats d'intérêt. Ainsi, une analyse structurelle de ces intermédiaires réactionnels pourrait éventuellement fournir des informations supplémentaires en ce qui a trait aux interactions moléculaires à la base de la discrimination des substrats observée chez ces deux mutants de TEM-1. De manière similaire, les mutants combinatoires démontrant le phénotype ESBL présentés au chapitre 6 bénéficieraient également d'une étude structurelle semblable. En effet, la visualisation moléculaire préliminaire entreprise dans cette étude nous a permis de soulever de nombreuses hypothèses structurelles et fonctionnelles mettant en jeu un nombre important d'interactions moléculaires qui gagneraient à être analysées de manière précise et scrupuleuse par des études structurelles plus approfondies.

### 7.1.2 – Analyse *in silico* en présence de ligands

À défaut d'obtenir les structures cristallines susmentionnées pour le mutant Y105G du chapitre 2, des études de dynamique moléculaire *in silico* plus élaborées auraient intérêt à être entreprises sur ce mutant en présence de BZ et de CF. Ainsi, il est probable que des interactions moléculaires spécifiques puissent être décelées à plus longue échelle ( $> 200$  ps) pour expliquer les différences d'affinité observées entre Y105G et les substrats BZ et CF. De plus, à partir de ces simulations de dynamique moléculaire, le calcul de l'énergie d'interaction entre les différents substrats d'intérêt et l'enzyme mutée donnerait assurément des informations pertinentes à cet effet. Alternativement, des études d'arrimage moléculaire (du « *docking* ») permettraient également d'extraire ces informations. En complément, des études similaires pourraient être entreprises sur divers mutants présentés au chapitre 6 dans le but d'élucider à la fois l'importance de la mutation en position 238 (G238S, G238N) et celle des mutations concomitantes aux positions 104, 105 et 240 par rapport à la reconnaissance du substrat oxyiminocéphalosporine céfotaxime (CTX). Ces études de modélisation moléculaire permettraient d'améliorer l'impact de l'étude présentée au chapitre 6 et fourniraient une analyse quantitative par rapport aux différences de généralisation et de spécialisation évolutives observées entre les mutants présentés dans ce chapitre.

Finalement, il apparaît clair que des dynamiques moléculaires à plus longue échelle entreprises sur TEM-1 sous forme libre et sur TEM-1 acylée avec divers substrats et/ou inhibiteurs permettraient de tester les hypothèses fonctionnelles soulevées dans l'étude de recuit simulé présentée au chapitre 3. Cette analyse de recuit simulé souffre des deux principaux inconvénients d'avoir été entreprise en absence de solvant explicite en ne tenant pas compte des effets structuraux causés par l'élimination du sulfate et des molécules d'eau conservées qui sont retrouvées au site actif de l'enzyme libre cristallisée. En revanche, il est

à noter que le RMSD entre les résidus formant les parois du site actif de la forme libre de TEM-1 (contenant la molécule de SO<sub>4</sub><sup>2-</sup> au site actif) (1BTL) et ceux de TEM-1 sous forme acylée avec BZ (1FQG) n'est que de 0,7 Å, laissant ainsi suggérer que la présence ou l'absence d'un ligand β-lactame n'a que peu d'effet sur la géométrie du site actif.

### 7.1.3 – Analyse RMN en présence de ligands

Quoique très informatives à l'égard des motions moléculaires globales causées par la mutation en position 105 chez TEM-1, les conclusions dynamiques des études RMN présentées au chapitre 4 souffrent néanmoins du désavantage d'avoir été exclusivement entreprises en absence de ligand. Malgré tout, les informations dynamiques obtenues s'avèrent d'une importance cruciale puisqu'elles démontrent la différence de motions moléculaires observées entre l'enzyme native et le mutant Y105D sur une échelle de temps similaire à celle de la catalyse (μs-ms). Ces observations nous permettent ainsi de suggérer un lien probable existant entre les différences de dynamique moléculaire observées chez certains résidus essentiels à la stabilisation des substrats au site actif de TEM-1 et la perte d'affinité calculée pour le mutant Y105D. En revanche, étant effectuées en absence de ligand, nos études RMN ne permettent pas d'affirmer hors de tout doute que les différences de motions moléculaires observées en absence de ligand sont conservées ou même identiques à celles que l'on observerait en présence d'un ligand au site actif. Conséquemment, ceci nous empêche d'effectuer une corrélation directe entre les motions moléculaires observées chez les résidus d'intérêt et leur effet sur l'événement catalytique en soi.

Pour pallier cette limite, l'étude RMN d'un intermédiaire acyl-enzyme stable entre un substrat ou un analogue de l'état de transition pourrait permettre l'acquisition d'informations plus précises par rapport aux motions moléculaires observées à l'état de

transition ou suite à l'acylation d'un ligand au site actif de TEM-1 (ou d'un mutant d'intérêt). En revanche, les trois limites expérimentales suivantes s'avèrent difficiles à contourner et réduisent la faisabilité de ce type d'étude : 1) Les délais nécessaires à l'acquisition des spectres RMN nécessitent la création d'un échantillon enzymatique homogène et stable sur une période de temps minimale de plusieurs semaines. Or, l'hydrolyse rapide par TEM-1 de tous les ligands connus empêche la production d'une solution homogène d'un complexe acyl-enzyme qui demeure stable sur cette longue période de temps. 2) Tel que discuté précédemment, la création d'un intermédiaire acyl-enzyme entre TEM-1 et un substrat  $\beta$ -lactame d'intérêt nécessiterait l'introduction d'une mutation supplémentaire au site actif de l'enzyme dans le but de réduire la vitesse de désacylation de l'événement catalytique (*e.g.* E166N) [44]. Étant introduite dans l'environnement d'intérêt et à proximité de la mutation 105, les effets dynamiques causés par cette mutation supplémentaire ne pourraient être ignorés et empêcheraient toute comparaison directe avec le mutant simple. 3) En plus de s'avérer rapidement hydrolysables par l'enzyme native, les inhibiteurs de TEM-1 qui pourraient être utilisés dans cette étude possèdent des mécanismes de décomposition différents de ceux des substrats, diminuant ainsi la portée des conclusions qui pourraient être tirées d'une telle étude.

#### 7.1.4 – Études dynamiques de $\beta$ -lactamases chimériques

En raison de la forte conservation d'un résidu aromatique à la position 105 chez les  $\beta$ -lactamases de classe A, les conclusions et les hypothèses soulevées dans cette thèse quant à l'importance structurelle et fonctionnelle de ce résidu chez TEM-1 demeurent généralement applicables à la plupart des enzymes de cette famille. Or, puisque la catalyse enzymatique et la spécificité de reconnaissance sont tributaires d'une panoplie d'interactions électrostatiques interdépendantes qui peuvent notamment être influencées par

des mutations distales [15], les comparaisons directes effectuées entre les divers membres de cette famille doivent toutefois être entreprises avec prudence. Cette affirmation est d'autant plus importante à la lumière de la caractérisation récente d'une  $\beta$ -lactamase de classe A retrouvée chez *Mycobacterium tuberculosis* (BlaC) et dont la séquence possède plusieurs mutations généralement considérées cruciales au maintien de la structure du site actif et/ou à la stabilisation des ligands (notamment Y105I, N132G, R164A, R244A et R278E) [103]. Bien que la structure tridimensionnelle de BlaC soit similaire à celle de nombreuses autres  $\beta$ -lactamases de classe A (RMSD des C $\alpha$  entre 0,95 et 3,66 Å), cette enzyme ne démontre que ~40 % d'identité de séquence avec les autres membres de cette famille et possède une cavité du site actif significativement plus étendue [103]. En raison de la variabilité de provenance des divers membres de la famille des  $\beta$ -lactamases de classe A, plusieurs de ces enzymes possèdent une structure et une spécificité de reconnaissance très semblables, mais une homologie de séquence plutôt faible. À cet effet, un exemple particulièrement probant est celui des  $\beta$ -lactamases TEM-1 de *Escherichia coli* et PSE-4 de *Pseudomonas aeruginosa*. À l'exception de la carbénicilline (substrat spécifiquement reconnu par PSE-4), ces deux enzymes possèdent un spectre de reconnaissance et des paramètres cinétiques comparables. Par analogie avec BlaC, leur similarité structurelle est également très grande (RMSD des C $\alpha$  = 1,3 Å) [104], mais leur identité de séquence n'est que de 40 %.

Ces diverses observations comparatives soulèvent de nombreuses interrogations quant au lien évolutif existant entre l'identité de séquence, l'activité catalytique et la structure conservée chez divers membres d'une même famille enzymatique. Par ailleurs, ajoutant à ces éléments de structure et de fonction, l'une des interrogations fondamentales de l'enzymologie moderne est de savoir si les événements dynamiques caractérisés chez de nombreuses enzymes [97, 105] sont des processus ordonnés et universellement conservés chez les protéines, ayant ainsi pu évoluer pour assister à l'événement catalytique chez les enzymes. À la lumière des effets dynamiques observés à courte et à longue portée dans nos

études RMN entreprises sur TEM-1 et sur divers mutants Y105X, nous nous intéressons actuellement à la comparaison dynamique entre TEM-1 et PSE-4 dans le but de répondre aux interrogations fondamentales suivantes concernant la dynamique interne de ces  $\beta$ -lactamases de classe A :

- Malgré la faible identité de séquence existant entre ces deux  $\beta$ -lactamases de classe A, existe-t-il des motions moléculaires similaires chez TEM-1 et PSE-4 pouvant être liées à leur similarité structurelle ?
- La dynamique moléculaire interne observée chez TEM-1 et PSE-4 est-elle liée d'une manière ou d'une autre à leur activité catalytique et peut-elle partiellement expliquer leur spécificité de reconnaissance respective ?

Dans le but de répondre à ces questions, des études de relaxation RMN sont actuellement en cours sur les deux parents enzymatiques TEM-1 et PSE-4 afin d'en comparer les paramètres dynamiques. De surcroît, à titre d'outil complémentaire permettant d'étudier la contribution dynamique provenant de chacun des parents, nous étudions également la dynamique interne de chimères actives de ces deux enzymes en plus d'un nombre restreint de chimères inactives bien exprimées et bien repliées. Ayant été obtenues par sélection antibiotique suite à la recombinaison aléatoire de fragments des deux gènes parentaux préalablement scindés en de multiples sections [106, 107] (Figure 7.1), ces chimères possèdent un nombre important de mutations par rapport à chacun des parents et sont par conséquent des homologues plus ou moins rapprochés de TEM-1 ou PSE-4. Effectuée en parallèle à l'étude entreprise sur les deux parents, la caractérisation de la dynamique interne de ces chimères enzymatiques fournira d'importantes informations complémentaires permettant notamment de répondre aux questions suivantes :

- La dynamique interne des chimères actives et inactives composées de fragments de TEM-1 et de PSE-4 est-elle similaire à celle des deux parents enzymatiques ?

- Existe-t-il une corrélation entre les motions moléculaires observées chez les chimères actives et celles des parents enzymatiques ?
- Les chimères inactives qui sont néanmoins bien exprimées et bien repliées possèdent-elles des variations dynamiques pouvant en partie expliquer leur perte d'activité ?

En plus de permettre la caractérisation des événements dynamiques retrouvés chez les  $\beta$ -lactamases de classe A, ces études permettront d'analyser l'importance des motions moléculaires liées à la catalyse chez divers membres de cette famille d'enzyme. De surcroît, ces études permettront peut-être de fournir une explication quant à la stricte conservation d'éléments structuraux retrouvés chez toutes les  $\beta$ -lactamases de classe A et fourniront également des indices supplémentaires quant à l'importance générale de la dynamique moléculaire chez divers représentants d'une même famille d'enzymes possédant une structure tridimensionnelle conservée.

## FIGURE



**Figure 7.1.** Représentation schématique de trois chimères de TEM-1 et PSE-4 actuellement à l'étude. Issues de la fragmentation et de la recombinaison aléatoire des segments parentaux TEM-1 et PSE-4, les chimères actives 16 et 18 permettent une survie cellulaire similaire à celle conférée par les deux parents enzymatiques (les valeurs de MIC pour AMP sont présentées en  $\mu\text{g/ml}$ ). Bien que la recombinaison des fragments et le niveau d'expression de la chimère 19 soient similaires à ceux de la chimère 18, celle-ci semble démontrer une activité catalytique considérablement affectée. Le paramètre « m » correspond au nombre minimal de mutations ponctuelles nécessaires pour convertir une chimère en son parent le plus proche (TEM-1 ou PSE-4) (voir référence [106]). Des chimères actives possédant les extrémités *N*- et *C*-terminales de TEM-1 ainsi que des sites de recombinaisons différents sont également à l'étude. Figure adaptée de [106].

## Bibliographie

- 1 Fleming, A. (1929) On the antibacterial action of cultures of a penicillium, with special reference to their use in the isolation of *B. influenzae* *Br. J. Exp. Pathol.* **10**, 226-236
- 2 Abraham, E. P. (1999) Some aspects of the development of the penicillins and cephalosporins. *J. Ind. Microbiol. Biot.* **22**, 275-287
- 3 Bentley, R. (2005) The development of penicillin: Genesis of a famous antibiotic. *Perspect. Biol. Med.* **48**, 444-452
- 4 Singh, S. B. & Barrett, J. F. (2006) Empirical antibacterial drug discovery. Foundation in natural products. *Biochem. Pharmacol.* **71**, 1006-1015
- 5 Finch, R. (2002) Bacterial resistance. The clinical challenge. *Clin. Microbiol. Infect.* **8**, 21-32
- 6 Pechère, J.-C. (2002) Chairman's discussion and conclusions. *Clin. Microbiol. Infect.* **8**, 33-35
- 7 Jones, R. N. (1996) Impact of changing pathogens and antimicrobial susceptibility patterns in the treatment of serious infections in hospitalized patients. *Am. J. Med.* **100**, 3S-12S
- 8 Kotra, L. P., Golemi, D., Vakulenko, S. & Mobashery, S. (2000) Bacteria fight back. *Chem. Ind.* **10**, 341-344
- 9 Abraham, E. P. & Chain, E. (1940) An enzyme from bacteria able to destroy penicillin. *Nature* **146**, 837
- 10 Fernandes, P. (2006) Antibacterial discovery and development. The failure of success? *Nat. Biotechnol.* **24**, 1497-1503

- 11 Normark, B. H. & Normark, S. (2002) Evolution and spread of antibiotic resistance. *J. Intern. Med.* **252**, 91-106
- 12 Lambert, P. A. (2005) Bacterial resistance to antibiotics: Modified target sites. *Adv. Drug Deliv. Rev.* **57**, 1471-1485
- 13 Kumar, A. & Schweizer, H. P. (2005) Bacterial resistance to antibiotics: Active efflux and reduced uptake. *Adv. Drug Deliv. Rev.* **57**, 1486-1513
- 14 Wright, G. D. (2005) Bacterial resistance to antibiotics: Enzymatic degradation and modification. *Adv. Drug Deliv. Rev.* **57**, 1451-1470
- 15 Fisher, J. F., Meroueh, S. O. & Mobashery, S. (2005) Bacterial resistance to  $\beta$ -lactam antibiotics: Compelling opportunism, compelling opportunity. *Chem. Rev.* **105**, 395-424
- 16 Matagne, A., Lamotte-Brasseur, J. & Frère, J. M. (1998) Catalytic properties of class A  $\beta$ -lactamases: Efficiency and diversity. *Biochem. J.* **330**, 581-598
- 17 Bradford, P. A. (2001) Extended-spectrum  $\beta$ -lactamases in the 21st century: Characterization, epidemiology, and detection of this important resistance threat. *Clin. Microbiol. Rev.* **14**, 933-951
- 18 Walsh, C. (2000) Molecular mechanisms that confer antibacterial drug resistance. *Nature* **406**, 775-781
- 19 Paterson, D. L. & Bonomo, R. A. (2005) Extended-spectrum  $\beta$ -lactamases: A clinical update. *Clin. Microbiol. Rev.* **18**, 657-686
- 20 Palumbi, S. R. (2001) Humans as the world's greatest evolutionary force. *Science* **293**, 1786-1790
- 21 Medeiros, A. A. (1997) Evolution and dissemination of  $\beta$ -lactamases accelerated by generations of  $\beta$ -lactam antibiotics. *Clin. Infect. Dis.* **24**, S19-S45

- 22 Page, M. I. (1987) The mechanisms of reactions of  $\beta$ -lactam antibiotics. *Adv. Phys. Org. Chem.* **23**, 165-270
- 23 Brown, A. G., Butterworth, D., Cole, M., Hanscomb, G., Hood, J. D., Reading, C. & Rolinson, G. N. (1976) Naturally-occurring beta-lactamase inhibitors with antibacterial activity. *J. Antibiot. (Tokyo)* **29**, 668-669
- 24 Knowles, J. R. (1985) Penicillin resistance: The chemistry of  $\beta$ -lactamase inhibition. *Acc. Chem. Res.* **18**, 97-104
- 25 Tipper, D. J. & Strominger, J. L. (1965) Mechanism of action of penicillins: A proposal based on their structural similarity to acyl-D-alanyl-D-alanine. *Proc. Natl. Acad. Sci. USA* **54**, 1133-1141
- 26 Davies, J. (1994) Inactivation of antibiotics and the dissemination of resistance genes. *Science* **264**, 375-382
- 27 Matagne, A., Dubus, A., Galleni, M. & Frère, J. M. (1999) The  $\beta$ -lactamase cycle: A tale of selective pressure and bacterial ingenuity. *Nat. Prod. Rep.* **16**, 1-19
- 28 Ambler, R. P. (1980) The structure of  $\beta$ -lactamases. *Philos. Trans. R. Soc. Lond. B. Biol. Sci.* **289**, 321-331
- 29 Wang, Z., Fast, W., Valentine, A. M. & Benkovic, S. J. (1999) Metallo- $\beta$ -lactamase: Structure and mechanism. *Curr. Opin. Chem. Biol.* **3**, 614-622
- 30 Walsh, T. R., Toleman, M. A., Poirel, L. & Nordmann, P. (2005) Metallo- $\beta$ -lactamases: The quiet before the storm? *Clin. Microbiol. Rev.* **18**, 306-325
- 31 Ambler, R. P. & Scott, G. K. (1978) Partial amino acid sequence of penicillinase coded by *Escherichia coli* plasmid R6K. *Proc. Natl. Acad. Sci. USA* **75**, 3732-3736
- 32 Sutcliffe, J. G. (1978) Nucleotide sequence of the ampicillin resistance gene of *Escherichia coli* plasmid pBR322. *Proc. Natl. Acad. Sci. USA* **75**, 3737-3741

- 33 Datta, N. & Kontomichalou, P. (1965) Penicillinase synthesis controlled by infectious R factors in *Enterobacteriaceae*. *Nature* **208**, 239-241
- 34 Medeiros, A. A. (1984)  $\beta$ -Lactamases. *Br. Med. Bull.* **40**, 18-27
- 35 Fonzé, E., Charlier, P., To'th, Y., Vermeire, M., Raquet, X., Dubus, A. & Frère, J. M. (1995) TEM-1  $\beta$ -lactamase structure solved by molecular replacement and refined structure of the S235A mutant. *Acta Crystallogr. D Biol. Crystallogr.* **51**, 682-694
- 36 Jelsch, C., Mourey, L., Masson, J. M. & Samama, J. P. (1993) Crystal structure of *Escherichia coli* TEM-1  $\beta$ -lactamase at 1.8 Å resolution. *Proteins* **16**, 364-383
- 37 Stec, B., Holtz, K. M., Wojciechowski, C. L. & Kantrowitz, E. R. (2005) Structure of the wild-type TEM-1  $\beta$ -lactamase at 1.55 Å and the mutant enzyme Ser70Ala at 2.1 Å suggest the mode of noncovalent catalysis for the mutant enzyme. *Acta Crystallogr. D Biol. Crystallogr.* **61**, 1072-1079
- 38 Minasov, G., Wang, X. J. & Shoichet, B. K. (2002) An ultrahigh resolution structure of TEM-1  $\beta$ -lactamase suggests a role for Glu166 as the general base in acylation. *J. Am. Chem. Soc.* **124**, 5333-5340
- 39 Orenica, M. C., Yoon, J. S., Ness, J. E., Stemmer, W. P. & Stevens, R. C. (2001) Predicting the emergence of antibiotic resistance by directed evolution and structural analysis. *Nat. Struct. Biol.* **8**, 238-242
- 40 Swarén, P., Golemi, D., Cabantous, S., Bulychev, A., Maveyraud, L., Mobashery, S. & Samama, J. P. (1999) X-ray structure of the Asn276Asp variant of the *Escherichia coli* TEM-1  $\beta$ -lactamase: Direct observation of electrostatic modulation in resistance to inactivation by clavulanic acid. *Biochemistry* **38**, 9570-9576
- 41 Thomas, V. L., Golemi-Kotra, D., Kim, C., Vakulenko, S. B., Mobashery, S. & Shoichet, B. K. (2005) Structural consequences of the inhibitor-resistant Ser130Gly substitution in TEM  $\beta$ -lactamase. *Biochemistry* **44**, 9330-9338

- 42 Wang, X., Minasov, G. & Shoichet, B. K. (2002) The structural bases of antibiotic resistance in the clinically derived mutant  $\beta$ -lactamases TEM-30, TEM-32, and TEM-34. *J. Biol. Chem.* **277**, 32149-32156
- 43 Wang, X., Minasov, G. & Shoichet, B. K. (2002) Evolution of an antibiotic resistance enzyme constrained by stability and activity trade-offs. *J. Mol. Biol.* **320**, 85-95
- 44 Strynadka, N. C., Adachi, H., Jensen, S. E., Johns, K., Sielecki, A., Betzel, C., Sutoh, K. & James, M. N. (1992) Molecular structure of the acyl-enzyme intermediate in  $\beta$ -lactam hydrolysis at 1.7 Å resolution. *Nature* **359**, 700-705
- 45 Horn, J. R. & Shoichet, B. K. (2004) Allosteric inhibition through core disruption. *J. Mol. Biol.* **336**, 1283-1291
- 46 Lim, D., Park, H. U., De Castro, L., Kang, S. G., Lee, H. S., Jensen, S., Lee, K. J. & Strynadka, N. C. (2001) Crystal structure and kinetic analysis of  $\beta$ -lactamase inhibitor protein-II in complex with TEM-1  $\beta$ -lactamase. *Nat. Struct. Biol.* **8**, 848-852
- 47 Maveyraud, L., Mourey, L., Kotra, L. P., Pedelacq, J. D., Guillet, V., Mobashery, S. & Samama, J. P. (1998) Structural basis for clinical longevity of carbapenem antibiotics in the face of challenge by the common class A  $\beta$ -lactamases from the antibiotic-resistant bacteria. *J. Am. Chem. Soc.* **120**, 9748-9752
- 48 Maveyraud, L., Pratt, R. F. & Samama, J. P. (1998) Crystal structure of an acylation transition-state analog of the TEM-1  $\beta$ -lactamase. Mechanistic implications for class A  $\beta$ -lactamases. *Biochemistry* **37**, 2622-2628
- 49 Ness, S., Martin, R., Kindler, A. M., Paetz, M., Gold, M., Jensen, S. E., Jones, J. B. & Strynadka, N. C. (2000) Structure-based design guides the improved efficacy of deacylation transition state analogue inhibitors of TEM-1  $\beta$ -lactamase. *Biochemistry* **39**, 5312-5321

- 50 Wang, X., Minasov, G., Blázquez, J., Caselli, E., Prati, F. & Shoichet, B. K. (2003) Recognition and resistance in TEM  $\beta$ -lactamase. *Biochemistry* **42**, 8434-8444
- 51 Wang, X., Minasov, G. & Shoichet, B. K. (2002) Noncovalent interaction energies in covalent complexes: TEM-1  $\beta$ -lactamase and  $\beta$ -lactams. *Proteins* **47**, 86-96
- 52 Ambler, R. P., Coulson, A. F., Frère, J. M., Ghysen, J. M., Joris, B., Forsman, M., Levesque, R. C., Tiraby, G. & Waley, S. G. (1991) A standard numbering scheme for the class A  $\beta$ -lactamases. *Biochem. J.* **276**, 269-270
- 53 Hedstrom, L. (2002) Serine protease mechanism and specificity. *Chem. Rev.* **102**, 4501-4524
- 54 Guillaume, G., Vanhove, M., Lamotte-Brasseur, J., Ledent, P., Jamin, M., Joris, B. & Frère, J. M. (1997) Site-directed mutagenesis of glutamate 166 in two  $\beta$ -lactamases. Kinetic and molecular modeling studies. *J. Biol. Chem.* **272**, 5438-5444
- 55 Oefner, C., D'Arcy, A., Daly, J. J., Gubernator, K., Charnas, R. L., Heinze, I., Hubschwerlen, C. & Winkler, F. K. (1990) Refined crystal structure of  $\beta$ -lactamase from *Citrobacter freundii* indicates a mechanism for  $\beta$ -lactam hydrolysis. *Nature* **343**, 284-288
- 56 Atanasov, B. P., Mustafi, D. & Makinen, M. W. (2000) Protonation of the  $\beta$ -lactam nitrogen is the trigger event in the catalytic action of class A  $\beta$ -lactamases. *Proc. Natl. Acad. Sci. USA* **97**, 3160-3165
- 57 Damblon, C., Raquet, X., Lian, L. Y., Lamotte-Brasseur, J., Fonzé, E., Charlier, P., Roberts, G. C. & Frère, J. M. (1996) The catalytic mechanism of  $\beta$ -lactamases: NMR titration of an active-site lysine residue of the TEM-1 enzyme. *Proc. Natl. Acad. Sci. USA* **93**, 1747-1752
- 58 Díaz, N., Sordo, T. L., Merz, K. M. & Suárez, D. (2003) Insights into the acylation mechanism of class A  $\beta$ -lactamases from molecular dynamics simulations of the TEM-1 enzyme complexed with benzylpenicillin. *J. Am. Chem. Soc.* **125**, 672-684

- 59 Hermann, J. C., Hensen, C., Ridder, L., Mulholland, A. J. & Höltje, H. D. (2005) Mechanisms of antibiotic resistance: QM/MM modeling of the acylation reaction of a class-A  $\beta$ -lactamase with benzylpenicillin. *J. Am. Chem. Soc.* **127**, 4454-4465
- 60 Lamotte-Brasseur, J., Dive, G., Dideberg, O., Charlier, P., Frère, J. M. & Ghysen, J. M. (1991) Mechanism of acyl transfer by the class-A serine  $\beta$ -lactamase of *Streptomyces albus* G. *Biochem. J.* **279**, 213-221
- 61 Vijayakumar, S., Ravishanker, G., Pratt, R. F. & Beveridge, D. L. (1995) Molecular dynamics simulation of a class a  $\beta$ -lactamase. Structural and mechanistic Implications. *J. Am. Chem. Soc.* **117**, 1722-1730
- 62 Ishiguro, M. & Imajo, S. (1996) Modeling study on a hydrolytic mechanism of class A  $\beta$ -bactamases. *J. Med. Chem.* **39**, 2207-2218
- 63 Knox, J. R., Moews, P. C., Escobar, W. A. & Fink, A. L. (1993) A catalytically-impaired class A  $\beta$ -lactamase: 2 Å crystal structure and kinetics of the *Bacillus licheniformis* E166A mutant. *Protein Eng.* **6**, 11-18
- 64 Lietz, E. J., Truher, H., Kahn, D., Hokenson, M. J. & Fink, A. L. (2000) Lysine-73 is involved in the acylation and deacylation of  $\beta$ -lactamase. *Biochemistry* **39**, 4971-4981
- 65 Swarén, P., Maveyraud, L., Guillet, V., Masson, J. M., Mourey, L. & Samama, J. P. (1995) Electrostatic analysis of TEM-1  $\beta$ -lactamase: Effect of substrate binding, steep potential gradients and consequences of site-directed mutations. *Structure* **3**, 603-613
- 66 Adachi, H., Ohta, T. & Matsuzawa, H. (1991) Site-directed mutants, at position 166, of RTEM-1  $\beta$ -lactamase that form a stable acyl-enzyme intermediate with penicillin. *J. Biol. Chem.* **266**, 3186-3191

- 67 Escobar, W. A., Tan, A. K. & Fink, A. L. (1991) Site-directed mutagenesis of  $\beta$ -lactamase leading to accumulation of a catalytic intermediate. *Biochemistry* **30**, 10783-10787
- 68 Gibson, R. M., Christensen, H. & Waley, S. G. (1990) Site-directed mutagenesis of  $\beta$ -lactamase I. Single and double mutants of Glu-166 and Lys-73. *Biochem. J.* **272**, 613-619
- 69 Golemi-Kotra, D., Meroueh, S. O., Kim, C., Vakulenko, S. B., Bulychev, A., Stemmler, A. J., Stemmler, T. L. & Mobashery, S. (2004) The importance of a critical protonation state and the fate of the catalytic steps in class A  $\beta$ -lactamases and penicillin-binding proteins. *J. Biol. Chem.* **279**, 34665-34673
- 70 Savard, P. Y., Sosa-Peinado, A., Levesque, R. C., Makinen, M. W. & Gagné, S. M. (2004)  $^1\text{H}$ ,  $^{13}\text{C}$  and  $^{15}\text{N}$  backbone resonance assignments for TEM-1, a 28.9 kDa  $\beta$ -lactamase from *E. coli*. *J. Biomol. NMR* **29**, 433-434
- 71 Lamotte-Brasseur, J., Lounnas, V., Raquet, X. & Wade, R. C. (1999)  $pK_a$  calculations for class A  $\beta$ -lactamases: Influence of substrate binding. *Protein Sci.* **8**, 404-409
- 72 Raquet, X., Lounnas, V., Lamotte-Brasseur, J., Frère, J. M. & Wade, R. C. (1997)  $pK_a$  calculations for class A  $\beta$ -lactamases: Methodological and mechanistic implications. *Biophys. J.* **73**, 2416-2426
- 73 Meroueh, S. O., Fisher, J. F., Schlegel, H. B. & Mobashery, S. (2005) *Ab initio* QM/MM study of class A  $\beta$ -lactamase acylation: Dual participation of Glu166 and Lys73 in a concerted base promotion of Ser70. *J. Am. Chem. Soc.* **127**, 15397-15407
- 74 Matagne, A. & Frère, J. M. (1995) Contribution of mutant analysis to the understanding of enzyme catalysis: The case of class A  $\beta$ -lactamases. *Biochim. Biophys. Acta* **1246**, 109-127

- 75 Jacob, F., Joris, B., Lepage, S., Dusart, J. & Frère, J. M. (1990) Role of the conserved amino acids of the 'SDN' loop (Ser130, Asp131 and Asn132) in a class A  $\beta$ -lactamase studied by site-directed mutagenesis. *Biochem. J.* **271**, 399-406
- 76 Lenfant, F., Labia, R. & Masson, J. M. (1991) Replacement of lysine 234 affects transition state stabilization in the active site of  $\beta$ -lactamase TEM1. *J. Biol. Chem.* **266**, 17187-17194
- 77 Dubus, A., Wilkin, J. M., Raquet, X., Normark, S. & Frère, J. M. (1994) Catalytic mechanism of active-site serine  $\beta$ -lactamases: Role of the conserved hydroxy group of the Lys-Thr(Ser)-Gly triad. *Biochem. J.* **301**, 485-494
- 78 Imtiaz, U., Manavathu, E. K., Lerner, S. A. & Mobashery, S. (1993) Critical hydrogen bonding by serine 235 for cephalosporinase activity of TEM-1  $\beta$ -lactamase. *Antimicrob. Agents Chemother.* **37**, 2438-2442
- 79 Knox, J. R. (1995) Extended-spectrum and inhibitor-resistant TEM-type  $\beta$ -lactamases. Mutations, specificity, and three-dimensional structure. *Antimicrob. Agents Chemother.* **39**, 2593-2601
- 80 Buynak, J. D. (2006) Understanding the longevity of the  $\beta$ -lactam antibiotics and of antibiotic/ $\beta$ -lactamase inhibitor combinations. *Biochem. Pharmacol.* **71**, 930-940
- 81 Meroueh, S. O., Roblin, P., Golemi, D., Maveyraud, L., Vakulenko, S. B., Zhang, Y., Samama, J. P. & Mobashery, S. (2002) Molecular dynamics at the root of expansion of function in the M69L inhibitor-resistant TEM-1  $\beta$ -lactamase from *Escherichia coli*. *J. Am. Chem. Soc.* **124**, 9422-9430
- 82 Hall, A. & Knowles, J. R. (1976) Directed selective pressure on a  $\beta$ -lactamase to analyse molecular changes involved in development of enzyme function. *Nature* **264**, 803-804
- 83 Stemmer, W. P. (1994) Rapid evolution of a protein in vitro by DNA shuffling. *Nature* **370**, 389-391

- 84 Hall, B. G. (2004) Predicting the evolution of antibiotic resistance genes. *Nat. Rev. Microbiol.* **2**, 430-435
- 85 Livermore, D. M. (1995)  $\beta$ -Lactamases in laboratory and clinical resistance. *Clin. Microbiol. Rev.* **8**, 557-584
- 86 Case, D. A. (2002) Molecular dynamics and NMR spin relaxation in proteins. *Acc. Chem. Res.* **35**, 325-331
- 87 Hansson, T., Oostenbrink, C. & van Gunsteren, W. (2002) Molecular dynamics simulations. *Curr. Opin. Struct. Biol.* **12**, 190-196
- 88 Karplus, M. & McCammon, J. A. (2002) Molecular dynamics simulations of biomolecules. *Nat. Struct. Biol.* **9**, 646-652
- 89 McCammon, J. A., Gelin, B. R. & Karplus, M. (1977) Dynamics of folded proteins. *Nature* **267**, 585-590
- 90 Lefèvre, J.-F. (1996) Analyse RMN de la dynamique des protéines. *École Supérieure de Biotechnologie de Strasbourg, Université Louis Pasteur, France*, Notes de cours
- 91 Mittermaier, A. & Kay, L. E. (2006) New tools provide new insights in NMR studies of protein dynamics. *Science* **312**, 224-228
- 92 Palmer, A. G., 3rd (2004) NMR characterization of the dynamics of biomacromolecules. *Chem. Rev.* **104**, 3623-3640
- 93 Davis, I. W., Arendall, W. B., 3rd, Richardson, D. C. & Richardson, J. S. (2006) The backrub motion: How protein backbone shrugs when a sidechain dances. *Structure* **14**, 265-274
- 94 Lee, A. L., Kinnear, S. A. & Wand, A. J. (2000) Redistribution and loss of side chain entropy upon formation of a calmodulin-peptide complex. *Nat. Struct. Biol.* **7**, 72-77

- 95 Mildvan, A. S. (2004) Inverse thinking about double mutants of enzymes. *Biochemistry* **43**, 14517-14520
- 96 Bush, K. & Mabashery, S. (1998) How  $\beta$ -lactamases have driven pharmaceutical drug discovery. From mechanistic knowledge to clinical circumvention. *Adv. Exp. Med. Biol.* **456**, 71-98
- 97 Agarwal, P. K. (2006) Enzymes: An integrated view of structure, dynamics and function. *Microb. Cell. Fact.* **5**, 2
- 98 Benkovic, S. J. & Hammes-Schiffer, S. (2003) A perspective on enzyme catalysis. *Science* **301**, 1196-1202
- 99 Hammes, G. G. (2002) Multiple conformational changes in enzyme catalysis. *Biochemistry* **41**, 8221-8228
- 100 Voet, D. & Voet, J. G. (1998) *Biochimie*. DeBoeck Université
- 101 Strynadka, N. C., Jensen, S. E., Alzari, P. M. & James, M. N. (1996) A potent new mode of  $\beta$ -lactamase inhibition revealed by the 1.7 Å X-ray crystallographic structure of the TEM-1-BLIP complex. *Nat. Struct. Biol.* **3**, 290-297
- 102 Imtiaz, U., Billings, E., Knox, J. R., Manavathu, E. K., Lerner, S. A. & Mabashery, S. (1993) Inactivation of class A  $\beta$ -lactamases by clavulanic acid: The role of arginine-244 in a proposed nonconcerted sequence of events. *J. Am. Chem. Soc.* **115**, 4435-4442
- 103 Wang, F., Cassidy, C. & Sacchettini, J. C. (2006) Crystal structure and activity studies of the *Mycobacterium tuberculosis*  $\beta$ -lactamase reveal its critical role in resistance to  $\beta$ -lactam antibiotics. *Antimicrob. Agents Chemother.* **50**, 2762-2771
- 104 Lim, D., Sanschagrin, F., Passmore, L., De Castro, L., Levesque, R. C. & Strynadka, N. C. (2001) Insights into the molecular basis for the carbenicillinase activity of PSE-4  $\beta$ -lactamase from crystallographic and kinetic studies. *Biochemistry* **40**, 395-402

- 105 Tousignant, A. & Pelletier, J. N. (2004) Protein motions promote catalysis. *Chem. Biol.* **11**, 1037-1042
- 106 Meyer, M. M., Silberg, J. J., Voigt, C. A., Endelman, J. B., Mayo, S. L., Wang, Z. G. & Arnold, F. H. (2003) Library analysis of SCHEMA-guided protein recombination. *Protein Sci.* **12**, 1686-1693
- 107 Meyer, M. M., Hochrein, L. & Arnold, F. H. (2006) Structure-guided SCHEMA recombination of distantly related  $\beta$ -lactamases. *Protein Eng. Des. Sel.* **19**, 563-570
- 108 Lineweaver, H. & Burk, D. (1934) The determination of enzyme dissociation constants. *J. Am. Chem. Soc.* **56**, 658-666
- 109 Henderson, P. J. F. (1992) Statistical analysis of enzyme kinetic data. Dans *Enzyme assays - A practical approach* (Rickwood, D. & Hames, B. D., eds.), Oxford University Press, Oxford
- 110 Bax, A. & Grzesiek, S. (1993) Methodological advances in protein NMR. *Acc. Chem. Res.* **26**, 131-138
- 111 Jarymowycz, V. A. & Stone, M. J. (2006) Fast time scale dynamics of protein backbones: NMR relaxation methods, applications, and functional consequences. *Chem. Rev.* **106**, 1624-1671
- 112 d'Auvergne, E. J. & Gooley, P. R. (2006) Model-free model elimination: A new step in the model-free dynamic analysis of NMR relaxation data. *J. Biomol. NMR* **35**, 117-135
- 113 Lipari, G. & Szabo, A. (1982) Model-free approach to the interpretation of nuclear magnetic resonance relaxation in macromolecules. 2. Analysis of experimental results. *J. Am. Chem. Soc.* **104**, 4559-4570
- 114 Lipari, G. & Szabo, A. (1982) Model-free approach to the interpretation of nuclear magnetic resonance relaxation in macromolecules. 1. Theory and range of validity. *J. Am. Chem. Soc.* **104**, 4546-4559

- 115 Krishnan, V. V. & Cosman, M. (1998) An empirical relationship between rotational correlation time and solvent accessible surface area. *J. Biomol. NMR* **12**, 177-182
- 116 Farmer, B. T., Constantine, K. L., Goldfarb, V., Friedrichs, M. S., Wittekind, M., Yanchunas, J., Jr., Robertson, J. G. & Mueller, L. (1996) Localizing the NADP<sup>+</sup> binding site on the MurB enzyme by NMR. *Nat. Struct. Biol.* **3**, 995-997
- 117 Branden, C. & Tooze, J. (1999) *Introduction to protein structure*. Garland Publishing, Taylor & Francis Group
- 118 Huang, W. Z., Petrosino, J., Hirsch, M., Shenkin, P. S. & Palzkill, T. (1996) Amino acid sequence determinants of β-lactamase structure and activity. *J. Mol. Biol.* **258**, 688-703

## Annexe 1 – Numérotation de la $\beta$ -lactamase TEM-1

La numérotation séquentielle de la forme mature de la  $\beta$ -lactamase TEM-1 exclut les premiers acides aminés de la séquence de localisation périplasmique et ne contient pas de numéro correspondant aux positions 239 et 253 en raison de la nomenclature des  $\beta$ -lactamases de classe A utilisée depuis le début des années 1990 [52]. Pour éviter toute confusion entre les différentes numérotations de TEM-1 utilisées tout au long de cette thèse, la correspondance entre les séquences génétique et protéique est ici présentée : a) séquence du gène *bla*, b) séquence protéique de la numérotation séquentielle utilisée pour la RMN au chapitre 4, c) séquence protéique suivant la nomenclature traditionnelle de Ambler [52]. Les sauts dans la numérotation séquentielle sont identifiés par des astérisques et les résidus ayant fait l'objet d'une mutagenèse semi-aléatoire au chapitre 6 sont soulignés.

1

a)	CAC	CCA	GAA	ACG	CTG	GTG	AAA	GTA	AAA	GAT	GCT	GAA	GAT	CAG
b)	H26	P27	E28	T29	L30	V31	K32	V33	K34	D35	A36	E37	D38	Q39
c)	H26	P27	E28	T29	L30	V31	K32	V33	K34	D35	A36	E37	D38	Q39

50

TTG	GGT	GCA	CGA	GTG	GGT	TAC	ATC	GAA	CTG	GAT	CTC	AAC	AGC
L40	G41	A42	R43	V44	G45	Y46	I47	E48	L49	D50	L51	N52	S53
L40	G41	A42	R43	V44	G45	Y46	I47	E48	L49	D50	L51	N52	S53

100

GGT	AAG	ATC	CTT	GAG	AGT	TTT	CGC	CCC	GAA	GAA	CGT	TTT	CCA
G54	K55	I56	L57	E58	S59	F60	R61	P62	E63	E64	R65	F66	P67
G54	K55	I56	L57	E58	S59	F60	R61	P62	E63	E64	R65	F66	P67

150

ATG	ATG	AGC	ACT	TTT	AAA	GTT	CTG	CTA	TGT	GGC	GCG	GTA	TTA
M68	M69	S70	T71	F72	K73	V74	L75	L76	C77	G78	A79	V80	L81
M68	M69	S70	T71	F72	K73	V74	L75	L76	C77	G78	A79	V80	L81

200

TCC	CGT	GTT	GAC	GCC	GGG	CAA	GAG	CAA	CTC	GGT	CGC	CGC	ATA
S82	R83	V84	D85	A86	G87	Q88	E89	Q90	L91	G92	R93	R94	I95
S82	R83	V84	D85	A86	G87	Q88	E89	Q90	L91	G92	R93	R94	I95

250

CAC	TAT	TCT	CAG	AAT	GAC	TTG	GTT	<u>GAG</u>	<u>TAC</u>	TCA	CCA	GTC	ACA
H96	Y97	S98	Q99	N100	D101	L102	V103	<u>E104</u>	<u>Y105</u>	S106	P107	V108	T109
H96	Y97	S98	Q99	N100	D101	L102	V103	<u>E104</u>	<u>Y105</u>	S106	P107	V108	T109

GAA	AAG	CAT	CTT	ACG	GAT	GGC	ATG	ACA	GTA	AGA	GAA	TTA	TGC
E110	K111	H112	L113	T114	D115	G116	M117	T118	V119	R120	E121	L122	C123
E110	K111	H112	L113	T114	D115	G116	M117	T118	V119	R120	E121	L122	C123

300

AGT	GCT	GCC	ATA	ACC	ATG	AGT	GAT	AAC	ACT	GCG	GCC	AAC	TTA
S124	A125	A126	I127	T128	M129	S130	D131	N132	T133	A134	A135	N136	L137
S124	A125	A126	I127	T128	M129	S130	D131	N132	T133	A134	A135	N136	L137

350

CTT	CTG	ACA	ACG	ATC	GGA	GGA	CCG	AAG	GAG	CTA	ACC	GCT	TTT
L138	L139	T140	T141	I142	G143	G144	P145	K146	E147	L148	T149	A150	F151
L138	L139	T140	T141	I142	G143	G144	P145	K146	E147	L148	T149	A150	F151

400

TTG	CAC	AAC	ATG	GGG	GAT	CAT	GTA	ACT	CGC	CTT	GAT	CGT	TGG
L152	H153	N154	M155	G156	D157	H158	V159	T160	R161	L162	D163	R164	W165
L152	H153	N154	M155	G156	D157	H158	V159	T160	R161	L162	D163	R164	W165

450

GAA CCG GAG CTG AAT GAA GCC ATA CCA AAC GAC GAG CGT GAC  
 E166 P167 E168 L169 N170 E171 A172 I173 P174 N175 D176 E177 R178 D179  
 E166 P167 E168 L169 N170 E171 A172 I173 P174 N175 D176 E177 R178 D179

500

ACC ACG ATG CCT GCA GCA ATG GCA ACA ACG TTG CGC AAA CTA  
 T180 T181 M182 P183 A184 A185 M186 A187 T188 T189 L190 R191 K192 L193  
 T180 T181 M182 P183 A184 A185 M186 A187 T188 T189 L190 R191 K192 L193

TTA ACT GGC GAA CTA CTT ACT CTA GCT TCC CGG CAA CAA TTA  
 L194 T195 G196 E197 L198 L199 T200 L201 A202 S203 R204 Q205 Q206 L207  
 L194 T195 G196 E197 L198 L199 T200 L201 A202 S203 R204 Q205 Q206 L207

550

ATA GAC TGG ATG GAG GCG GAT AAA GTT GCA GGA CCA CTT CTG  
 I208 D209 W210 M211 E212 A213 D214 K215 V216 A217 G218 P219 L220 L221  
 I208 D209 W210 M211 E212 A213 D214 K215 V216 A217 G218 P219 L220 L221

600

CGC TCG GCC CTT CCG GCT GGC TGG TTT ATT GCT GAT AAA TCT  
 R222 S223 A224 L225 P226 A227 G228 W229 F230 I231 A232 D233 K234 S235  
 R222 S223 A224 L225 P226 A227 G228 W229 F230 I231 A232 D233 K234 S235

\* 650

GGA GCC GGT GAG CGT GGG TCT CGC GGT ATC ATT GCA GCA CTG  
 G236 A237 G238 E239 R240 G241 S242 R243 G244 I245 I246 A247 A248 L249  
 G236 A237 G238 E240 R241 G242 S243 R244 G245 I246 I247 A248 A249 L250

\* 700

GGG CCA GAT GGT AAG CCC TCC CGT ATC GTA GTT ATC TAC ACG  
 G250 P251 D252 G253 K254 P255 S256 R257 I258 V259 V260 I261 Y262 T263  
 G251 P252 D254 G255 K256 P256 S258 R259 I260 V261 V262 I263 Y264 T265

750

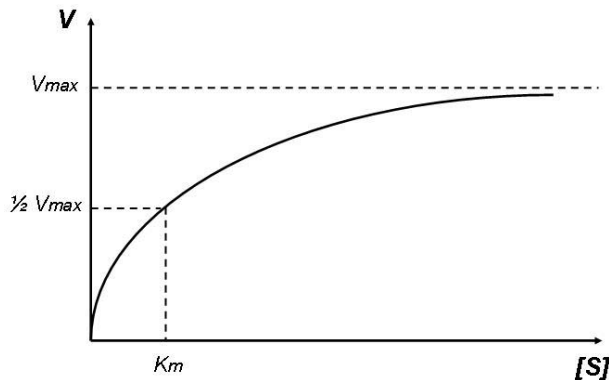
ACG GGG AGT CAG GCA ACT ATG GAT GAA CGA AAT AGA CAG ATC  
T264 G265 S266 Q267 A268 T269 M270 D271 E272 R273 N274 R275 Q276 I277  
T266 G267 S268 Q269 A270 T271 M272 D273 E274 R275 N276 R277 Q278 I279

GCT GAG ATA GGT GCC TCA CTG ATT AAG CAT TGG TAA  
A278 E279 I280 G281 A282 S283 L284 I285 K286 H287 W288 Ter  
A280 E281 I282 G283 A284 S285 L286 I287 K288 H289 W290 Ter

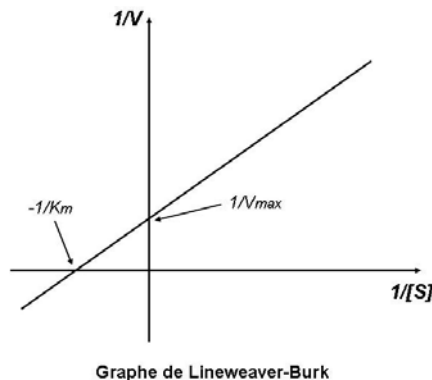
## Annexe 2 – Enzymologie : Détail des méthodes de régression employées

Il existe deux philosophies derrière le calcul des paramètres cinétiques  $V_{max}$  et  $K_m$  d'une enzyme d'intérêt. La première philosophie, dite non-linéaire, consiste en l'ajustement (le « *fitting* ») des données de concentration de substrat [S] et des vitesses obtenues expérimentalement ( $V$ ) dans l'équation hyperbolique de Michaelis-Menten :

$$V = \frac{V_{max}[S]}{K_m + [S]}$$



En revanche, la seconde philosophie consiste en l'utilisation de transformations mathématiques de l'équation de Michaelis-Menten de manière à en extraire les paramètres désirés à l'aide d'une régression linéaire appliquée sur les données expérimentales de vitesse ( $V$ ) et de concentration de substrat  $[S]$ . À titre d'exemple, la transformation classique de Lineweaver-Burk ( $1/V$  vs.  $1/[S]$ ) [108] permet de linéariser les valeurs expérimentales et d'extraire  $K_m$  et  $V_{max}$  à l'intersection des axes des abscisses ( $-1/K_m$ ) et des ordonnées ( $1/V_{max}$ ), respectivement :

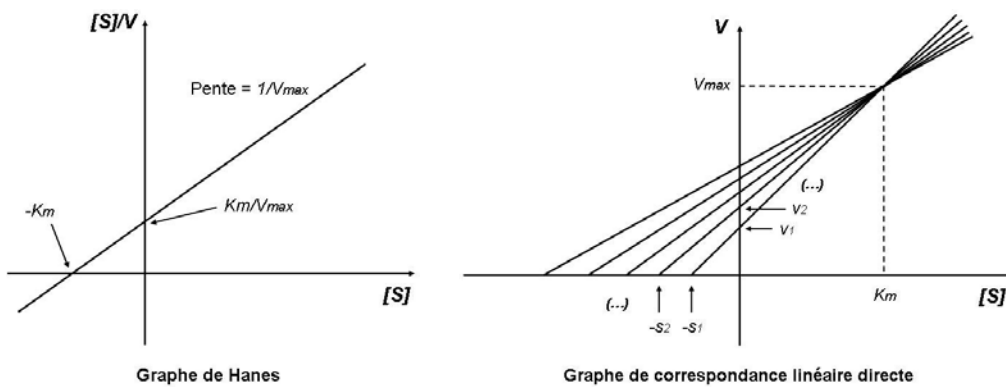


Graphe de Lineweaver-Burk

Avec l'avènement des logiciels informatiques permettant d'optimiser des calculs de régression non-linéaire, il est accepté que l'ajustement des valeurs expérimentales à l'équation de Michaelis-Menten est une méthode de calcul statistiquement plus fiable et plus précise que la régression linéaire de type Lineweaver-Burk, notamment en raison des erreurs importantes qui sont introduites dans cette droite aux faibles vitesses enzymatiques correspondant aux faibles concentrations de substrats testées (à l'extrême droite du quadrant I ci-haut).

En revanche, l'expérimentateur attentif aura tôt fait de se rendre compte qu'il est facile de se réfugier aveuglément derrière l'apparente « fiabilité » informatique de la régression non-linéaire. En effet, quelques essais expérimentaux suffisent à démontrer qu'il est simple de permettre l'ajustement d'à peu près n'importe quelle série de données à n'importe quelle équation non-linéaire d'intérêt. Il est toutefois important de demeurer critique devant les paramètres cinétiques obtenus à l'aide de telles régressions et de ne pas perdre de vue les incertitudes intrinsèques à chacune des valeurs expérimentales, car il est beaucoup plus difficile pour l'œil humain de juger de la fiabilité d'une régression non-linéaire que de celle d'une régression linéaire. Par exemple, le comportement biphasique d'une enzyme sera beaucoup plus simple à déceler par régression linéaire que par régression non-linéaire. Ainsi, les deux méthodes de calcul ne sont pas mutuellement exclusives, mais plus souvent qu'autrement complémentaires.

Sur ce, en raison des défauts intrinsèques à certaines méthodes de régression linéaire (notamment les faiblesses statistiques de la droite de type Lineweaver-Burk), il existe une forte tendance à considérer toutes les méthodes de régression linéaire comme étant moins fiables que celle de l'ajustement non-linéaire des données à l'équation de Michaelis-Menten. Or, en pratique, de multiples transformations linéaires sont reconnues pour donner des résultats statistiques similaires à la régression non-linéaire, notamment les graphes de Hanes ( $[S]/V$  vs.  $[S]$ ) ainsi que celui de la correspondance linéaire directe (« *direct linear plot* ») [109] :



Tout au long des études cinétiques entreprises dans cette thèse, les deux techniques de régression linéaire et non-linéaire furent ainsi utilisées de manière complémentaire pour juger de la fiabilité et de la pertinence des valeurs de  $K_m$  et  $V_{max}$  calculées. En revanche, il est à noter que certaines caractéristiques intrinsèques aux substrats  $\beta$ -lactames d'intérêt nous empêchent souvent d'utiliser une méthode particulière aux dépens d'une autre. À cet effet, pour calculer des valeurs statistiquement fiables de  $K_m$  et  $V_{max}$  en régression non-linéaire à l'aide de l'équation de Michaelis-Menten, il est suggéré d'utiliser une gamme de concentrations de substrat suffisamment vaste et dont les points expérimentaux flanquent la valeur de  $K_m$ . À cet effet, on suggère d'utiliser des  $[S]$  de  $K_m/2$  à  $10 \times K_m$  espacés de cette manière : 1) valeurs rapprochées les unes des autres à faible  $[S]$  et 2) évaluation d'au moins une  $[S]$  se rapprochant de la valeur de  $V_{max}$  [109]. Or, les substrats  $\beta$ -lactames utilisés (particulièrement les pénicillines) possèdent deux caractéristiques intrinsèques qui nous

empêchent bien souvent de calculer les paramètres  $V_{max}$  et  $K_m$  de manière efficace à l'aide cette méthode, *i.e.* un faible coefficient d'extinction molaire ( $\varepsilon$ ) et une inhibition de la réaction à de fortes [S].

La réaction catalysée par TEM-1 est l'hydrolyse du noyau  $\beta$ -lactame des substrats d'intérêt, dont la progression peut être suivie par spectrophotométrie UV aux alentours de 230-260 nm (voir chapitre 2). Or, le faible coefficient d'extinction molaire des pénicillines à cette longueur d'onde nous empêche bien souvent d'obtenir des droites d'hydrolyse reproductibles sous la barre des 50  $\mu\text{M}$  (très faible rapport signal/bruit des droites d'absorption *vs.* temps). Comme le  $K_m$  de TEM-1 pour les pénicillines se situe typiquement aux environs de cette [S], il nous est donc souvent impossible de calculer des vitesses de réaction inférieures aux valeurs de  $K_m$ , rendant ainsi la méthode de régression non-linéaire statistiquement invalide. De plus, il arrive régulièrement qu'une forte concentration de substrat ( $> 350 \mu\text{M}$ ) inhibe la vitesse de la réaction. Bien que cette [S] se rapproche de  $10K_m$  chez l'enzyme native pour certains substrats (notamment BZ, voir chapitre 2), elle s'avère insuffisante pour permettre une saturation de [S] satisfaisante pour la plupart des mutants de TEM-1 caractérisés dans la présente thèse. Ainsi, les vitesses réactionnelles de TEM-1 calculées avec les substrats  $\beta$ -lactames ne sont souvent linéaires, reproductibles et facilement caractérisables que dans un intervalle restreint de [S] (typiquement entre 50 et 350  $\mu\text{M}$  pour la plupart des  $\beta$ -lactames), nécessitant alors l'adoption d'une méthode de régression linéaire pour en extraire les valeurs de  $K_m$  et  $V_{max}$  désirées.

Lors des travaux de cinétique dont il est question ici (chapitres 2 et 6), il est à noter que le calcul des paramètres  $K_m$  et  $V_{max}$  par régression linéaire de type Lineweaver-Burk et Hanes donnèrent des résultats très similaires, dont les valeurs de  $K_m$  et  $V_{max}$  (et par extension  $k_{cat}$ ) s'avérèrent tout à fait comparables à celles retrouvées dans la littérature. De surcroît, il est important de garder en tête que les analyses enzymologiques effectuées dans le cadre de cette thèse ont comme objectif principal la comparaison des valeurs cinétiques de divers mutants entre eux (voir chapitres 2 et 6). Dans le but de limiter les erreurs qui

auraient pu être introduites par l'utilisation de diverses méthodes de calcul différentes, une attention particulière fut portée à l'utilisation constante et reproductible d'une seule méthode de régression particulière pour un essai donné (soit Lineweaver-Burk ou Hanes). Les valeurs cinétiques obtenues furent par la suite confirmées par une méthode de régression alternative (soit linéaire ou non-linéaire, lorsque possible). À cet effet, en aucun cas l'écart cinétique observé entre les divers mutants d'intérêt fut-il significativement différent d'une méthode de régression à une autre, confirmant ainsi la validité des valeurs calculées.

## Annexe 3 – Survol de la RMN des protéines

Le noyau atomique de certains éléments naturels et d'isotopes (notamment  $^1\text{H}$ ,  $^{13}\text{C}$  et  $^{15}\text{N}$ ) se comporte de manière similaire à un aimant qui effectue un mouvement de rotation sur lui même (une propriété nommée le « spin » nucléaire). Lorsque soumis à un fort champ magnétique, ces noyaux atomiques se réorientent et absorbent de l'énergie, obéissant à un phénomène nommé la résonance magnétique nucléaire (RMN). De manière similaire à une empreinte digitale unique, l'énergie ainsi absorbée produit un spectre caractéristique du composé à l'étude. En effet, en raison du blindage électronique et du phénomène de couplage de spins nucléaires entre noyaux avoisinants, l'environnement immédiat des noyaux atomiques affecte leur degré d'absorption énergétique de manière distincte, donnant ainsi lieu à l'apparition de spectres RMN tributaires des propriétés structurelles du composé à l'étude. L'analyse détaillée de ces spectres RMN permet ainsi l'obtention d'informations structurelles à propos de diverses molécules d'intérêt.

### 1.0 – RMN multidimensionnelle et attribution des résonances chez les macromolécules

La plupart des études RMN entreprises sur les petites molécules chimiques tirent profit de la RMN du proton ( $^1\text{H}$ ), permettant ainsi l'obtention d'un spectre RMN à une seule dimension dans laquelle les protons non-équivalents absorbent à des déplacements chimiques ( $\delta$ ) différents par rapport à une référence donnée. En revanche, plus la molécule chimique à l'étude est grosse, plus le spectre unidimensionnel du proton est chargé d'un nombre impressionnant de pics superposés, rendant ce spectre RMN unidimensionnel difficilement interprétable. Puisque les protéines contiennent une quantité importante d'atomes d'hydrogène, il est donc impossible d'entreprendre une analyse structurelle

détaillée de ces molécules en se basant uniquement sur leur spectre RMN du proton ( $^1\text{H}$ ) (Figure A3.1-A). C'est ainsi que la RMN multidimensionnelle tire profit de la corrélation existante entre le déplacement chimique d'un noyau (*e.g.*  $^1\text{H}$ ) et le déplacement chimique d'un noyau avoisinant possédant un moment magnétique (*e.g.*  $^{15}\text{N}$ ), sur la base du couplage dipolaire existant entre leurs moments magnétiques respectifs [110]. Pour observer une telle corrélation (*i.e.* le transfert de la magnétisation d'un noyau à l'autre), les deux atomes à l'étude doivent être situés à une faible distance l'un de l'autre à travers l'espace (typiquement  $< 5 \text{ \AA}$ ) ou encore à une distance maximale de 2 à 3 liens covalents sur la séquence primaire [110]. De plus, considérant la faible abondance de l'isotope  $^{15}\text{N}$  dans la nature (0,037 %), il est essentiel d'effectuer un marquage isotopique uniforme de la protéine d'intérêt en utilisant des techniques d'expression dans un système bactérien ne contenant que  $^{15}\text{N}$  comme source d'azote essentielle à la survie cellulaire.

L'expression d'une protéine uniformément marquée à l'azote-15 ( $^{15}\text{N}$ ) permet donc l'enregistrement d'un spectre  $^{15}\text{N}$ -HSQC bidimensionnel, dans lequel un axe correspond à  $^1\text{H}$  et l'autre axe correspond à  $^{15}\text{N}$  (Figure A3.1-B). Ainsi, puisque chaque résidu de la protéine contient un lien amide peptidique dans lequel un proton  $^1\text{H}$  est lié à un atome d'azote  $^{15}\text{N}$  (à l'exception de la proline), un pic correspondant à la corrélation de l'amide  $^1\text{H}$ - $^{15}\text{N}$  apparaîtra sur le spectre  $^{15}\text{N}$ -HSQC pour chacun des résidus de la séquence primaire de la protéine (à l'exception des prolines et du résidu situé en position *N*-terminale). Il est à noter que quelques pics supplémentaires seront également observés, correspondant aux résidus dont les chaînes latérales contiennent des liens amide  $^1\text{H}$ - $^{15}\text{N}$  (notamment Arg, Asn, Gln, His et Trp). Ainsi, le spectre  $^{15}\text{N}$ -HSQC tire profit du fait que tous les liens amide des résidus d'une protéine bien repliée possèderont des déplacements chimiques distincts en raison de leur environnement tridimensionnel particulier, donnant lieu à l'apparition d'un spectre bidimensionnel bien dispersé dans lequel chaque pic individuel sera normalement bien résolu (Figure A3.1-B).

En revanche, en fonction du nombre de résidus de la protéine à l'étude, il arrive parfois que la superposition de pics soit également un problème dans les spectres à deux dimensions. Par ailleurs, puisque le lien amide de chaque résidu  $i$  ne donne d'information que pour ce même résidu  $i$  et que la magnétisation du signal n'est pas transmise à d'autres noyaux avoisinants (*e.g.* au résidu  $i - 1$ , ou encore  $i + 1$ ), le spectre  $^{15}\text{N}$ -HSQC ne permet pas d'assigner chacun des pics à son résidu correspondant dans la séquence primaire de la protéine. Pour remédier à ces deux problèmes, il est essentiel d'introduire une troisième dimension, qui prend habituellement la forme d'un double marquage isotopique de la protéine au carbone-13 ( $^{13}\text{C}$ ) et à l'azote-15 ( $^{15}\text{N}$ ) (Figure A3.1-C). Ainsi, en tirant profit du transfert de la magnétisation entre noyaux avoisinants couplés, l'utilisation de diverses séquences d'impulsions de RMN à transformée de Fourier permet l'obtention de spectres tridimensionnels qui lient les atomes du résidu  $i$  à ceux du résidu  $i - 1$  (ou  $i + 1$ ) (Figure A3.2) [110]. De cette manière, la corrélation entre résidus voisins dans la séquence peut être observée et les structures primaire et secondaire de la protéine peuvent être déterminées. La RMN multidimensionnelle permet ainsi l'analyse de molécules beaucoup plus grosses et sert globalement à résoudre les problèmes de chevauchements de pics retrouvés dans les spectres à plus faibles dimensions [110].

## 1.1 – Relaxation

Suite à l'attribution des résonances des résidus de la séquence primaire de la protéine d'intérêt, l'un des avantages de la RMN est de tirer profit de l'information structurelle ainsi obtenue pour entreprendre des analyses dynamiques à propos des noyaux atomiques précédemment attribués. Possédant une structure tridimensionnelle maintenue par de faibles interactions non-covalentes, les protéines peuvent subir de larges fluctuations et adopter diverses conformations énergétiques en solution. Conséquemment, puisque les spins nucléaires sont sensibles aux mouvements des autres noyaux situés dans leur

environnement immédiat, ceux-ci possèdent des propriétés exceptionnelles en ce qui a trait à l'analyse du comportement dynamique des protéines en solution [90]. En effet, suite à l'absorption énergétique du noyau, la vitesse de retour à l'équilibre des spins nucléaires est dépendante du champ magnétique local qu'ils subissent et qui fluctue avec le temps en fonction des motions moléculaires locales [86]. Ainsi, l'analyse du retour à l'équilibre des spins nucléaires (un phénomène nommé « relaxation ») permet d'obtenir des informations importantes quant aux motions subies par les atomes sur diverses échelles de temps, donnant ainsi de précieux indices quant au rôle joué par la dynamique des changements conformationnels dans la structure et la fonction des protéines.

Chez les protéines, les études de relaxation sont habituellement entreprises sur les noyaux d'azote-15 ( $^{15}\text{N}$ ) du squelette peptidique en mesurant l'effet NOE (« *Nuclear Overhauser Effect* ») en plus de calculer les temps de relaxation longitudinale ( $T_1$ ) et transversale ( $T_2$ ) des spins nucléaires de cet atome [111]. Typiquement, le calcul de ces paramètres s'effectue à l'aide des spectres  $^{15}\text{N}$ -HSQC en mesurant la modulation d'intensité des pics en fonction d'un délai de temps inséré dans la séquence d'impulsion précédent l'enregistrement du signal [111]. Les données brutes correspondant aux variations d'intensités des pics sont ensuite insérées dans une équation exponentielle inverse, permettant de calculer les paramètres de relaxation susmentionnés.

Puisque les motions moléculaires sont des phénomènes stochastiques dont l'échelle de temps, l'amplitude et la direction ne peuvent être adéquatement décrits par de simples paramètres de relaxation, l'obtention d'une description complète et détaillée de toutes les motions moléculaires sur une échelle de temps d'intérêt s'avère être une tâche impossible à accomplir [111]. Une analyse brute des données de relaxation permet néanmoins de donner des indices grossiers quant à la dynamique observée à certains sites de la protéine à l'étude. Par exemple, puisque le taux de relaxation transversale ( $R_2$ ) peut être influencé par l'échange conformationnel de l'ordre de la  $\mu\text{s-ms}$  [111], des variations dans les valeurs de ce paramètre peuvent donner des indices quant à la possibilité d'échange entre deux

conformères distincts d'un résidu donné sur cette échelle de temps. En revanche, une analyse plus détaillée des données de relaxation expérimentales peut s'effectuer via l'utilisation de modèles physiques et mathématiques permettant d'extraire des informations précises à propos des mouvements globaux et internes observés chez la protéine d'intérêt.

## 1.2 – Analyse dynamique « Model-free »

L'interprétation dite « Model-free » consiste en une analyse théorique des données expérimentales de relaxation obtenues par RMN à l'aide d'équations mathématiques d'optimisation et de sélection statistique de modèles [112-114]. Au même titre que l'analyse structurelle *in silico* d'une protéine par dynamique moléculaire permet la création d'un modèle mimant le comportement de cette macromolécule en solution, l'analyse « Model-free » permet l'extraction de divers paramètres dynamiques simples qui décrivent le mouvement global ainsi que les motions internes de chaque résidu de la protéine sur diverses échelles de temps. Ainsi, sur la base des données expérimentales de relaxation longitudinale ( $R_1$ ), transversale ( $R_2$ ) et des effets NOE calculés par RMN, cette méthode permet d'extraire des informations sur l'amplitude et l'échelle de temps de mouvements d'intérêt, sans pour autant leur assigner de modèle physique de mouvement particulier (d'où l'appellation « Model-free ») [112-114]. Basée sur la prémissse voulant que les mouvements internes des vecteurs atomiques sont indépendants de la rotation diffusionnelle globale de la protéine en solution (liée à son temps de corrélation,  $\tau_m$ ), une analyse « Model-free » des données de relaxation permet notamment d'extraire les deux paramètres suivants, qui aident à la description de la dynamique interne de la protéine sur deux échelles de temps différentes :

- ***Le paramètre d'ordre ( $S^2$ )***. Le paramètre  $S^2$  caractérise l'amplitude des motions internes des vecteurs  $^{1}\text{H}$ - $^{15}\text{N}$  et donne ainsi une idée générale de leur rigidité en solution sur une

échelle de temps ps-ns. Il s'agit d'un paramètre sans unité dont les valeurs se situent entre 0 et 1 et qui décrit les restrictions spatiales du vecteur amide  $^1\text{H}-^{15}\text{N}$ . Ainsi, plus sa valeur est élevée (près de 1), plus les motions du vecteur amide  $^1\text{H}-^{15}\text{N}$  sont restreintes et plus celui-ci est rigide. À l'inverse, plus la valeur de  $S^2$  est faible (près de 0), plus le vecteur amide  $^1\text{H}-^{15}\text{N}$  est dynamique.

– ***Le paramètre d'échange conformationnel ( $R_{ex}$ )***. Variable intégrée à certains modèles dynamiques de l'analyse « Model-free » (voir chapitre 4), le paramètre  $R_{ex}$  peut servir d'indicateur de motions moléculaires plus lentes (de l'ordre de  $\mu\text{s-ms}$ ), bien que sa description physique demeure encore obscure [111]. En raison de l'échelle de temps dont il est question, ce paramètre décrit l'existence d'échanges conformationnels observés dans l'environnement local du résidu pour lequel il est calculé. Il donne ainsi un indice de la modification de la dynamique de certains résidus de l'enzyme sur une échelle de temps de l'ordre de  $\mu\text{s-ms}$ .

Les informations obtenues à l'aide de ces paramètres permettent la clarification d'événements dynamiques locaux sur la base du postulat voulant qu'ils soient indépendants du comportement dynamique global de la protéine d'intérêt en solution. À cet effet, à l'aide de modèles théoriques de diffusion rotationnelle [86], l'analyse « Model-free » permet également d'extraire un temps de corrélation global ( $\tau_m$ ) de la protéine en solution. Basé sur une estimation préalable de la forme structurelle de la protéine d'intérêt (isotrope ou anisotrope), ce paramètre correspond grossièrement au temps nécessaire pour que la protéine effectue une rotation de un radian en solution [115]. Puisque  $\tau_m$  peut notamment être affecté par la grosseur, la multimérisation, la forme et la concentration de la protéine ainsi que par le pH, la température et la viscosité du milieu [115], la comparaison directe de ce temps de corrélation nécessite l'étude de systèmes enzymatiques similaires analysés dans des conditions expérimentales identiques. En revanche, puisque le postulat de base de l'analyse « Model-free » permet de traiter la dynamique globale de manière indépendante à la dynamique interne des protéines et que cette dernière n'est théoriquement pas affectée

par les caractéristiques macromoléculaires susmentionnées, la comparaison des paramètres internes peut néanmoins être effectuée entre systèmes enzymatiques non-similaires.

## FIGURES

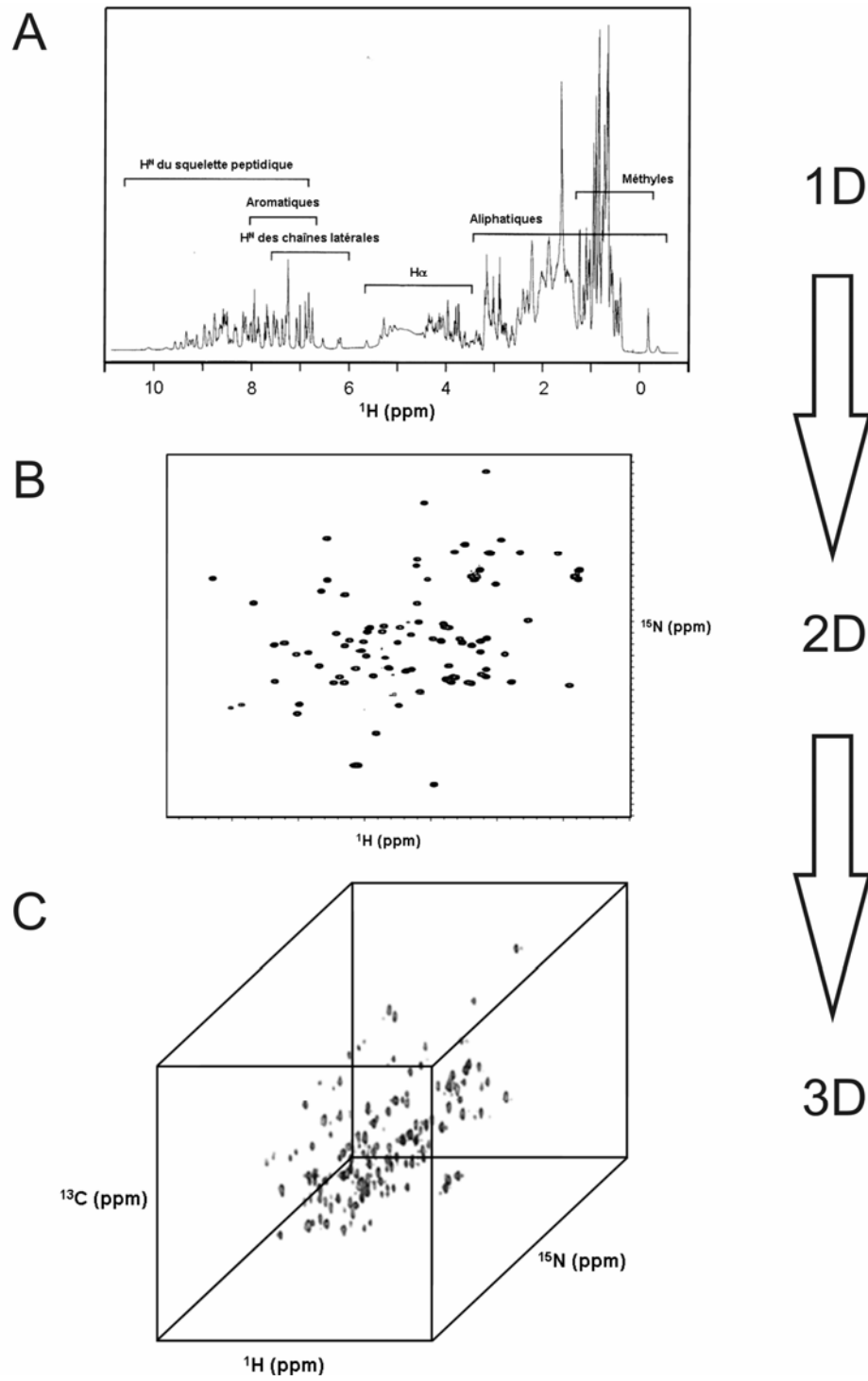


**Figure A3.1.** Spectroscopie RMN multidimensionnelle. A) Spectre unidimensionnel de l'atome d'hydrogène ( $^1\text{H}$ ) pour une protéine typique. Bien que chaque proton de la protéine possède un déplacement chimique unique, la trop grande quantité d'atomes d'hydrogène dans une protéine donne lieu à un nombre important de chevauchement des pics, rendant le spectre unidimensionnel impossible à résoudre. B) Spectre  $^{15}\text{N}$ -HSQC bidimensionnel. La corrélation entre  $^1\text{H}$  et  $^{15}\text{N}$  donne lieu à l'apparition d'un pic caractéristique pour chaque vecteur amide du squelette peptidique de la protéine. C) Spectre tridimensionnel typique de corrélation entre  $^1\text{H}$ ,  $^{13}\text{C}$  et  $^{15}\text{N}$ . Bien que la dispersion du spectre  $^{15}\text{N}$ -HSQC soit habituellement suffisante pour identifier les vecteurs amides du squelette peptidique, il arrive quand même que certains pics des spectres bidimensionnels soient chevauchés, nécessitant l'introduction d'une troisième dimension pour les résoudre. De plus, les spectres 3D sont nécessaires à l'attribution des séquences primaire et secondaire de la protéine via le transfert de la magnétisation vers les résidus avoisinants (voir Figure A3.2).

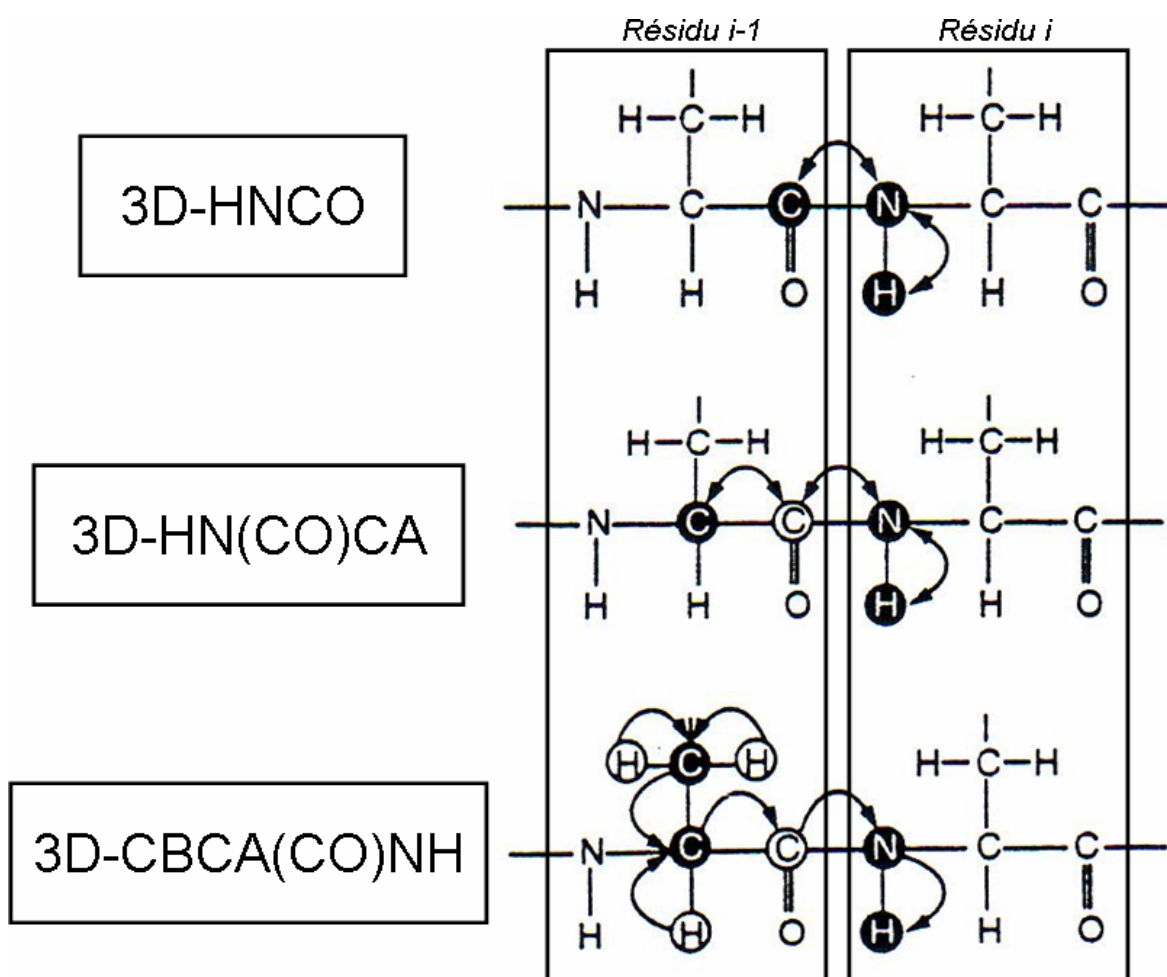


**Figure A3.2.** Représentation schématique de la corrélation entre les noyaux atomiques de trois spectres RMN tridimensionnels. Les noyaux avec un cercle noir correspondent à ceux pour lesquels le déplacement chimique est observé dans le spectre 3D. Les noyaux avec un cercle blanc correspondent à ceux qui participent au transfert de la magnétisation, mais dont le déplacement chimique n'est pas observé dans le spectre 3D. Image adaptée de [110].

## Annexe 4 – Matériel supplémentaire (chapitres 3 et 4)

### Chapitre 3

**Table S3.1.** Residue geometry of Glu104, Tyr105, Met129 and Asn132 analyzed by MolProbity for each minimized simulated annealing conformer obtained in the present study.

Conformer	Residue	MolProbity Parameters			Validation <sup>d</sup>
		ϕ, ψ Quality Values <sup>a</sup> (%)	Rotamer <sup>b</sup> (%)	Cβ Deviation <sup>c</sup> (Å)	
014	E104	Favored (29.88)	4.7	0.078	✓
	Y105	<b>OUTLIER (0.04)</b>	10	<b>0.44</b>	⊗
	M129	Favored (47.76)	23.5	<b>0.275</b>	⊗
	N132	Favored (13.1)	97.4	0.222	✓
027	E104	Favored (37.89)	1.3	0.194	✓
	Y105	Allowed (0.18)	12.2	<b>0.393</b>	⊗
	M129	Favored (48.29)	<b>0.2</b>	<b>0.262</b>	⊗
	N132	Favored (66.6)	13.6	0.091	✓
040	E104	Favored (52.13)	35	0.218	✓
	Y105	<b>OUTLIER (0.02)</b>	12.4	<b>0.331</b>	⊗
	M129	Favored (51.47)	<b>0.2</b>	0.172	⊗
	N132	Favored (18.58)	4.5	0.243	✓
<u>053<sup>e</sup></u>	E104	Favored (46.97)	<b>0.8</b>	0.156	⊗
	Y105	Allowed (0.15)	84.4	0.152	✓

	M129	Favored (13.31)	<b>1</b>	<b>0.287</b>	⊗
	N132	Favored (33.49)	10.1	0.194	√
066	E104	Favored (21.67)	7.8	0.183	√
	Y105	<b>OUTLIER (0.03)</b>	21.4	<b>0.315</b>	⊗
	M129	Favored (24.29)	2.1	0.121	√
	N132	Favored (13.97)	12.3	<b>0.313</b>	⊗
079	E104	Favored (54.2)	7.9	0.209	√
	Y105	Allowed (0.12)	19.2	<b>0.401</b>	⊗
	M129	Favored (37.02)	12.1	0.195	√
	N132	Favored (21.67)	4.7	<b>0.264</b>	⊗
092	E104	Allowed (0.22)	7.1	0.184	√
	Y105	Allowed (0.08)	49.5	<b>0.288</b>	⊗
	M129	Favored (32.88)	2.6	0.1	√
	N132	Favored (65.15)	17.6	0.07	√
105	E104	Favored (19.92)	2.5	0.161	√
	Y105	<b>OUTLIER (0.02)</b>	43.4	0.163	⊗
	M129	Favored (65.29)	15.7	0.097	√
	N132	Favored (32.47)	19	0.186	√
<u>118</u>	E104	Allowed (0.74)	<b>0.6</b>	<b>0.459</b>	⊗
	Y105	Favored (17.97)	23.7	0.111	√
	M129	Favored (35.9)	8.9	0.071	√
	N132	Favored (47.31)	91.8	0.04	√
<u>131</u>	E104	Allowed (0.66)	<b>0.1</b>	0.231	⊗
	Y105	Favored (6.88)	68.6	0.125	√
	M129	Favored (66.1)	13	0.165	√
	N132	Favored (26.89)	6.2	0.06	√

	E104	<b>OUTLIER (0)</b>	5.7	0.121	⊗
<u>014B</u>	Y105	Favored (25.59)	73.3	0.22	√
	M129	Favored (47.57)	31.4	0.167	√
	N132	Favored (63.75)	17.4	0.185	√
<u>027B</u>	E104	Allowed (0.21)	5.1	<b>0.468</b>	⊗
	Y105	Favored (14.26)	4.6	0.18	√
	M129	Favored (52.11)	4	0.082	√
<u>040B</u>	N132	Favored (27.8)	12.1	0.12	√
	E104	Favored (23.59)	9	0.067	√
	Y105	Allowed (0.73)	31.5	<b>0.305</b>	⊗
	M129	Allowed (0.23)	8.8	<b>0.312</b>	⊗
<u>053B</u>	N132	Favored (16.28)	77.5	0.161	√
	E104	Favored (16.76)	1.3	0.135	√
	Y105	Allowed (0.51)	6.6	0.192	√
	M129	Favored (41.06)	26.8	0.186	√
<u>066B</u>	N132	Favored (20.81)	73.8	0.06	√
	E104	Favored (2.32)	23.8	0.206	√
	Y105	Favored (3)	89.3	0.144	√
	M129	Favored (80.91)	13.4	0.18	√
<u>079B</u>	N132	Favored (50.36)	10.2	0.212	√
	E104	Allowed (0.09)	87	<b>0.356</b>	⊗
	Y105	Favored (31.45)	4	0.151	√
	M129	Favored (12.05)	33.6	0.191	√
<u>092B</u>	N132	Favored (22.21)	9.5	0.239	√
	E104	Favored (10.95)	26.4	0.106	√
	Y105	<b>OUTLIER (0.04)</b>	26	0.198	⊗

	M129	Allowed (0.46)	10.4	0.181	✓
	N132	Favored (81.85)	53.7	<b>0.294</b>	⊗
105B	E104	Favored (49.59)	29.1	0.037	✓
	Y105	Allowed (0.17)	1.9	<b>0.478</b>	⊗
	M129	Favored (12.86)	9.3	<b>0.256</b>	⊗
	N132	Favored (9.67)	7.4	<b>0.38</b>	⊗
118B	E104	Favored (46.49)	<b>0.5</b>	0.213	⊗
	Y105	<b>OUTLIER (0.03)</b>	21.1	<b>0.39</b>	⊗
	M129	Favored (54.03)	7.1	0.049	✓
	N132	Favored (29.17)	22.7	0.202	✓
131B	E104	Favored (47.29)	<b>0</b>	0.249	⊗
	Y105	Allowed (0.09)	10.1	<b>0.356</b>	⊗
	M129	Favored (40.72)	11.7	0.135	✓
	N132	Favored (37.16)	34.8	0.138	✓

<sup>a</sup>Ramachandran angle quality is estimated using a density-dependent smoothing function developed by Lovell *et al.* (2003)<sup>32</sup>. Values >2% are favored, values ranging from 0.02% to 2% are allowed and values <0.02% are Ramachandran outliers.

<sup>b</sup>The probability (% occurrence) of each rotamer is defined according to Lovell *et al.* (2000)<sup>25</sup>. Values <1.0% are considered as rotameric outliers.

<sup>c</sup>The C $\beta$  deviation is a measure of geometrical nonideality around the C $\alpha$  calculated as the distance of the observed C $\beta$  from the ideal one (according to Lovell *et al.* (2003)<sup>32</sup>). Values >0.25 Å are considered as outliers.

<sup>d</sup>A check mark (✓) indicates a validated residue with appropriate Ramachandran angles, a validated rotameric side chain and a C $\beta$  deviation <0.25 Å. Residues marked with “⊗” are outliers in either one of these three categories. Only conformers validated by MolProbity in all three categories for residue Tyr105 were analyzed in the present study.

<sup>e</sup>Underlined conformers were validated by MolProbity for Tyr105.

## Chapitre 4

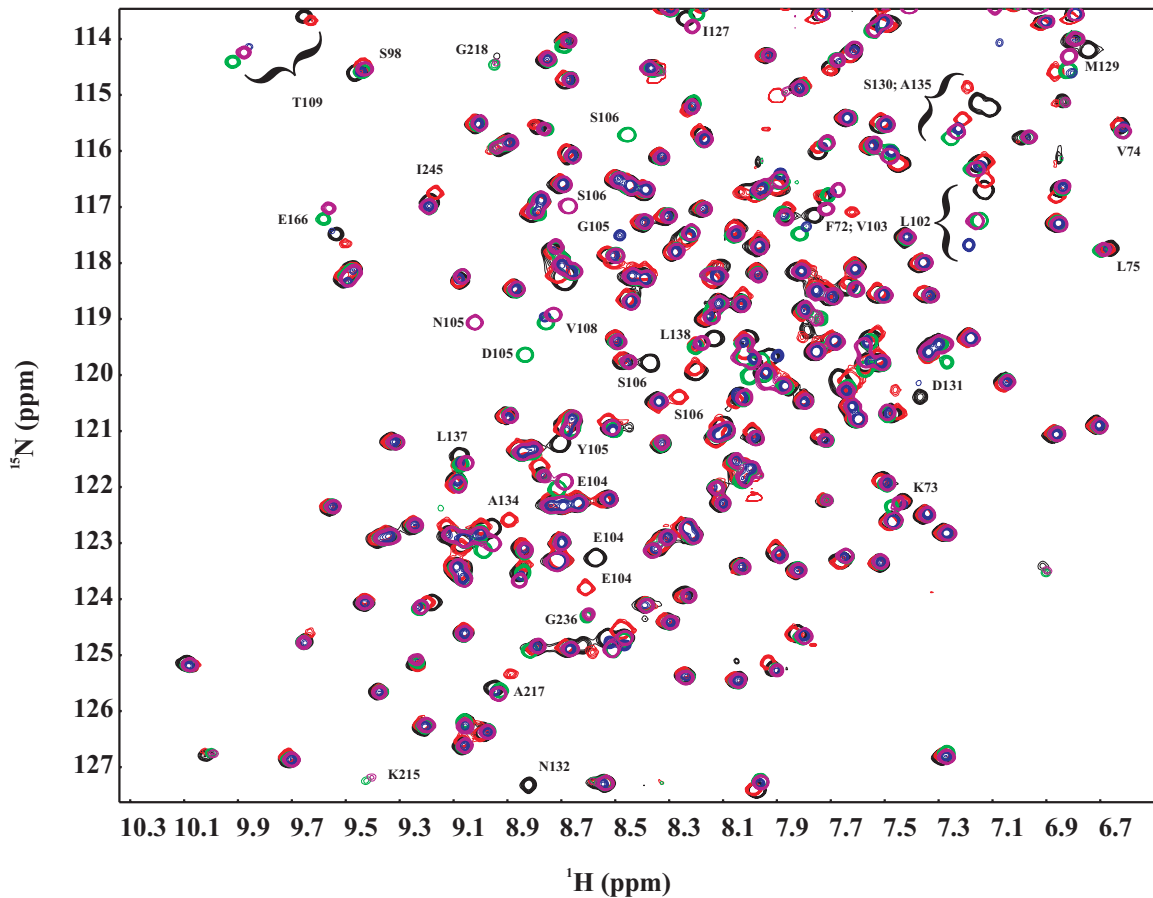


**Figure S4.1.** Main area of the 2D  $^1\text{H}$ - $^{15}\text{N}$  HSQC spectra of TEM-1 Y105X at pH 6.6, and 30°C. The WT is shown in black, Y105W in red, Y105D in green, Y105G in blue, and Y105N in magenta.

**Table S4.1.** R<sub>1</sub>, R<sub>2</sub>, and {<sup>1</sup>H}-<sup>15</sup>N NOE values for TEM-1 WT and the Y105D mutant at 600 MHz.

Residue	R <sub>1</sub> <sup>WT</sup> (s <sup>-1</sup> )		R <sub>1</sub> <sup>Y105D</sup> (s <sup>-1</sup> )		R <sub>2</sub> <sup>WT</sup> (s <sup>-1</sup> )		R <sub>2</sub> <sup>Y105D</sup> (s <sup>-1</sup> )		NOE <sup>WT</sup>		ΔNOE <sup>*</sup>		NOE <sup>Y105D</sup>		ΔNOE <sup>*</sup>		
	R <sub>1</sub> <sup>WT</sup>	ΔR <sub>1</sub> <sup>*</sup>	R <sub>1</sub> <sup>Y105D</sup>	ΔR <sub>1</sub> <sup>*</sup>	R <sub>2</sub> <sup>WT</sup>	ΔR <sub>2</sub> <sup>*</sup>	R <sub>2</sub> <sup>Y105D</sup>	ΔR <sub>2</sub> <sup>*</sup>	NOE <sup>WT</sup>	ΔNOE <sup>*</sup>	NOE <sup>Y105D</sup>	ΔNOE <sup>*</sup>	NOE <sup>WT</sup>	ΔNOE <sup>*</sup>	NOE <sup>Y105D</sup>	ΔNOE <sup>*</sup>	
His26																	
Pro27	#	#	#	#	#	#	#	#	#	#	#	#	#	#	#	#	
Gly28	0,99	0,01	0,96	0,01	18,22	0,46	17,89	0,45	0,78	0,03	0,81	0,04					
Thr29	1,01	0,01	1,00	0,01	19,72	0,54	18,88	0,47	0,78	0,02	0,89	0,04					
Leu30	1,01	0,02	0,99	0,01	19,86	0,50	19,67	0,49	0,86	0,03	0,89	0,04					
Val31	0,96	0,01	0,96	0,01	19,17	0,48	18,49	0,46	0,89	0,05	0,86	0,04					
Lys32	O	O	0,99	0,01	O	O	18,18	0,45	O	O	0,85	0,04					
Val33	O	O	0,99	0,01	O	O	19,26	0,48	O	O	0,84	0,04					
Lys34	0,96	0,01	0,98	0,01	19,09	0,48	18,21	0,46	0,86	0,03	0,80	0,04					
Asp35	1,01	0,01	1,02	0,01	18,87	0,47	18,49	0,46	0,80	0,03	0,76	0,03					
Ala36	1,03	0,01	0,99	0,01	19,19	0,48	18,79	0,47	0,88	0,03	0,89	0,04					
Glu37	0,99	0,01	1,01	0,01	20,36	1,43	18,71	0,47	0,80	0,03	0,83	0,04					
Asp38	0,98	0,00	0,98	0,01	19,09	0,48	18,44	0,46	0,81	0,02	0,82	0,04					
Gln39	1,01	0,01	0,99	0,01	18,50	0,46	17,90	0,45	0,77	0,03	0,80	0,04					
Leu40	0,97	0,02	0,98	0,02	19,15	0,48	18,62	0,60	0,79	0,03	0,80	0,04					
Gly41	0,98	0,01	0,99	0,01	19,43	0,49	19,35	0,48	0,83	0,03	0,88	0,04					
Ala42	0,94	0,00	0,93	0,01	18,32	0,46	17,43	0,44	0,80	0,02	0,79	0,03					
Arg43	0,88	0,01	0,85	0,01	13,97	0,35	13,28	0,33	0,60	0,03	0,57	0,03					
Val44	0,90	0,01	0,89	0,02	19,79	0,76	18,25	0,46	0,90	0,06	0,86	0,06					
Gly45	0,91	0,02	0,93	0,02	18,83	0,47	18,28	0,46	0,88	0,06	0,84	0,04					
Tyr46	0,96	0,01	0,99	0,01	18,17	0,45	18,82	0,53	0,79	0,04	0,82	0,04					
Ile47	0,99	0,01	0,96	0,02	17,16	0,43	17,17	0,43	0,85	0,03	0,87	0,04					
Glu48	0,96	0,01	0,95	0,02	20,51	0,59	19,41	0,49	0,86	0,04	0,84	0,04					
Leu49	0,98	0,01	0,98	0,01	17,99	0,45	18,04	0,45	0,83	0,03	0,82	0,04					
Asp50	1,00	0,01	1,00	0,02	17,83	0,62	17,70	0,44	0,81	0,03	0,81	0,04					
Leu51	1,02	0,02	1,02	0,01	17,69	0,68	17,75	0,44	0,81	0,04	0,82	0,04					
Asn52	0,98	0,03	0,97	0,04	17,38	0,66	16,87	0,42	0,65	0,03	0,62	0,03					
Ser53	1,01	0,03	0,99	0,02	17,37	0,43	17,00	0,43	0,77	0,02	0,76	0,03					
Gly54	1,07	0,01	1,04	0,02	19,16	0,53	19,06	0,75	0,75	0,02	0,78	0,03					
Lys55	1,00	0,01	1,01	0,01	18,26	0,46	17,61	0,44	0,77	0,02	0,77	0,03					
Ile56	1,00	0,01	0,98	0,01	17,34	0,43	16,10	0,40	0,80	0,03	0,77	0,03					
Leu57	0,94	0,02	0,92	0,01	19,16	0,48	18,20	0,73	0,89	0,05	0,88	0,06					
Glu58	0,88	0,01	0,89	0,01	19,00	0,60	18,18	0,45	0,83	0,03	0,73	0,03					
Ser59	0,90	0,00	0,88	0,01	19,00	0,47	18,67	0,47	0,77	0,02	0,79	0,03					
Phe60	0,91	0,01	0,89	0,02	20,18	0,50	19,49	0,49	0,82	0,03	0,81	0,04					
Arg61	0,94	0,02	0,93	0,01	20,01	0,50	20,38	0,51	0,82	0,03	0,85	0,04					
Pro62	#	#	#	#	#	#	#	#	#	#	#	#					



Val108	O	O	O	0,02	O	O	18,75	0,47	O	O	0,85	0,04
Thr109	0,91	0,02	0,89	0,02	18,50	0,46	18,82	0,47	0,75	0,10	0,76	0,06
Glu110	0,96	0,01	0,94	0,01	20,47	0,51	20,62	0,52	0,80	0,03	0,87	0,04
Lys111	0,97	0,01	0,94	0,01	18,63	0,47	17,97	0,45	0,85	0,02	0,82	0,04
His112	0,93	0,01	0,91	0,01	17,96	0,45	17,27	0,43	0,80	0,02	0,85	0,04
Leu113	1,00	0,01	1,01	0,01	18,95	0,47	18,13	0,45	0,84	0,02	0,80	0,04
Thr114	0,98	0,04	0,96	0,03	18,34	0,49	17,76	0,54	0,79	0,03	0,80	0,04
Asp115	1,05	0,05	1,02	0,04	18,59	0,46	18,45	0,46	0,74	0,03	0,74	0,04
Gly116	O	O	1,02	0,02	O	O	18,00	0,45	O	O	0,78	0,03
Met117	0,99	0,01	0,99	0,01	17,74	0,44	17,64	0,44	0,82	0,03	0,80	0,04
Thr118	1,01	0,01	0,97	0,01	18,41	0,81	18,08	0,45	0,79	0,03	0,80	0,04
Val119	0,97	0,01	0,92	0,02	19,53	0,49	19,22	0,48	0,81	0,04	0,78	0,04
Arg120	0,97	0,00	0,96	0,03	20,88	0,52	20,72	0,52	0,84	0,03	0,83	0,04
Glu121	0,94	0,01	0,94	0,01	19,97	0,50	19,47	0,49	0,91	0,04	0,86	0,04
Leu122	O	O	0,97	0,01	O	O	20,15	0,50	O	O	0,81	0,04
Cys123	0,96	0,01	O	O	20,21	0,51	O	O	0,83	0,03	O	O
Ser124	0,92	0,01	0,92	0,01	16,22	2,75	18,82	1,65	0,68	0,02	0,87	0,04
Ala125	O	O	O	O	O	O	O	O	O	O	O	O
Ala126	O	O	0,98	0,01	O	O	19,48	0,49	O	O	0,81	0,04
Ile127	0,94	0,01	0,93	0,02	19,34	0,67	18,24	0,46	0,84	0,06	0,81	0,04
Thr128	0,96	0,02	0,96	0,01	25,53	1,22	24,00	0,60	0,79	0,11	0,82	0,05
Met129	0,96	0,02	0,97	0,01	17,89	0,75	17,26	0,80	0,77	0,04	0,84	0,04
Ser130	W	W	0,99	0,02	W	W	22,26	4,06	W	W	0,62	0,05
Asp131	W	W	1,01	0,03	W	W	21,97	1,01	W	W	0,95	0,08
Asn132	1,06	0,03	1,03	0,01	18,63	0,67	17,56	0,44	0,81	0,07	0,82	0,05
Thr133	1,00	0,01	1,02	0,03	19,63	0,60	19,04	0,48	0,83	0,09	0,74	0,04
Ala134	O	O	1,02	0,01	O	O	18,41	0,46	O	O	0,82	0,04
Ala135	O	O	0,96	0,01	O	O	18,18	0,56	O	O	0,91	0,04
Asn136	0,98	0,01	1,00	0,01	19,47	0,50	18,45	0,46	0,92	0,04	0,81	0,04
Leu137	1,02	0,01	1,00	0,01	21,48	0,83	20,99	0,75	0,84	0,05	0,87	0,04
Leu138	0,98	0,02	0,99	0,02	19,63	0,49	19,33	0,48	0,71	0,03	0,86	0,04
Leu139	1,01	0,01	1,02	0,01	19,22	0,77	18,71	0,47	0,84	0,04	0,86	0,04
Thr140	O	O	O	O	O	O	O	O	O	O	O	O
Thr141	O	O	1,11	0,02	O	O	14,05	0,45	O	O	0,69	0,03
Ile142	0,97	0,02	1,00	0,02	18,97	0,47	19,10	0,48	0,83	0,03	0,79	0,03
Gly143	0,98	0,01	1,00	0,01	17,55	0,44	17,48	0,44	0,78	0,03	0,75	0,03
Gly144	1,00	0,02	1,01	0,01	17,42	0,44	17,64	0,44	0,79	0,03	0,76	0,03
Pro145	#	#	#	#	#	#	#	#	#	#	#	#
Lys146	1,02	0,02	1,01	0,04	19,15	0,76	18,02	0,45	0,81	0,03	0,81	0,04
Glu147	0,98	0,00	0,98	0,01	19,04	0,48	17,94	0,45	0,89	0,03	0,87	0,04
Leu148	0,99	0,01	1,01	0,01	18,89	0,47	18,62	0,47	0,81	0,03	0,85	0,04
Thr149	0,97	0,01	0,96	0,01	19,49	0,49	18,07	0,45	0,84	0,03	0,82	0,04
Ala150	0,97	0,00	0,95	0,01	20,53	0,51	20,39	0,96	0,83	0,03	0,84	0,04
Phe151	0,99	0,01	0,98	0,01	19,05	0,48	18,84	0,47	0,86	0,03	0,85	0,04
Leu152	O	O	0,98	0,02	O	O	19,76	0,65	O	O	0,78	0,04

His153	0,98	0,01	0,99	0,01	20,23	0,51	19,98	0,50	0,80	0,02	0,80	0,04
Asn154	0,96	0,01	0,96	0,01	19,06	0,48	18,50	0,46	0,86	0,06	0,87	0,04
Met155	0,97	0,00	0,94	0,01	17,25	0,43	16,60	0,41	0,84	0,03	0,80	0,04
Gly156	O	O	0,98	0,01	O	O	19,86	0,70	O	O	0,79	0,03
Asp157	O	O	0,93	0,01	O	O	20,32	0,51	O	O	0,81	0,04
His158	0,95	0,01	0,91	0,02	18,17	0,45	18,73	1,01	0,78	0,03	0,76	0,03
Val159	0,97	0,02	0,99	0,01	19,33	0,55	19,57	0,59	0,82	0,09	0,83	0,04
Thr160	0,97	0,01	0,97	0,02	18,18	0,45	17,90	0,45	0,88	0,04	0,80	0,04
Arg161	1,01	0,01	1,00	0,01	19,92	0,50	20,08	0,50	0,78	0,03	0,80	0,04
Leu162	0,96	0,03	0,96	0,02	19,64	0,49	18,80	0,47	0,85	0,04	0,83	0,04
Asp163	0,95	0,04	0,93	0,01	17,79	0,51	18,79	0,90	0,78	0,10	0,80	0,09
Arg164	0,87	0,01	0,84	0,01	18,73	0,47	18,21	0,46	0,87	0,04	0,82	0,04
Trp165	0,95	0,01	0,95	0,01	18,20	0,99	16,78	0,42	0,82	0,04	0,77	0,04
Glu166	0,99	0,02	0,97	0,03	19,77	0,49	19,20	0,48	0,85	0,06	0,87	0,05
Pro167	#	#	#	#	#	#	#	#	#	#	#	#
Glu168	0,97	0,01	0,97	0,01	19,52	0,49	18,77	0,47	0,83	0,04	0,75	0,03
Leu169	O	O	O	O	O	O	O	O	O	O	O	O
Asn170	0,97	0,01	0,97	0,01	21,08	0,53	20,54	0,51	0,81	0,06	0,89	0,04
Glu171	0,97	0,02	0,99	0,01	20,65	0,52	20,64	0,52	0,90	0,03	0,89	0,04
Ala172	1,02	0,02	O	O	19,89	0,50	O	O	0,77	0,06	O	O
Ile173	O	O	0,94	0,01	O	O	21,05	0,77	O	O	0,79	0,04
Pro174	#	#	#	#	#	#	#	#	#	#	#	#
Asn175	O	O	0,97	0,03	O	O	16,41	0,41	O	O	0,74	0,03
Asp176	0,96	0,01	0,96	0,01	17,58	0,44	17,61	0,44	0,81	0,02	0,79	0,03
Glu177	1,03	0,02	1,01	0,02	17,02	0,43	16,74	0,42	0,84	0,03	0,83	0,04
Arg178	1,02	0,01	1,01	0,01	18,65	0,47	18,38	0,46	0,85	0,03	0,74	0,03
Asp179	1,01	0,02	0,94	0,01	18,48	0,46	18,60	0,46	0,87	0,05	0,85	0,05
Thr180	0,98	0,02	0,98	0,01	18,54	0,46	18,24	0,46	0,82	0,02	0,84	0,04
Thr181	0,97	0,02	0,97	0,03	18,99	0,47	18,09	0,45	0,92	0,04	0,85	0,04
Met182	0,94	0,01	0,91	0,01	18,71	0,47	17,78	0,44	0,83	0,02	0,84	0,04
Pro183	#	#	#	#	#	#	#	#	#	#	#	#
Ala184	0,99	0,01	0,99	0,01	18,34	0,46	18,13	0,51	0,85	0,03	0,80	0,04
Ala185	0,91	0,01	0,90	0,01	17,90	0,45	17,51	0,44	0,83	0,02	0,81	0,04
Met186	0,97	0,01	0,98	0,02	18,86	0,47	18,52	0,46	0,82	0,03	0,81	0,04
Ala187	1,01	0,01	0,97	0,02	20,03	0,50	19,01	0,48	0,80	0,02	0,86	0,04
Thr188	0,99	0,01	0,99	0,01	18,41	1,31	18,27	0,74	0,82	0,03	0,77	0,03
Thr189	1,01	0,00	0,99	0,01	18,64	0,47	18,00	0,45	0,80	0,02	0,80	0,04
Leu190	1,01	0,02	1,00	0,01	19,79	0,49	20,15	0,50	0,80	0,04	0,81	0,04
Arg191	0,97	0,01	O	O	19,62	0,49	O	O	0,83	0,05	O	O
Lys192	1,01	0,01	1,00	0,01	19,65	0,50	19,72	0,49	0,83	0,04	0,76	0,04
Leu193	0,96	0,01	0,99	0,01	19,46	0,58	18,72	0,47	0,80	0,04	0,77	0,03
Leu194	0,94	0,01	0,99	0,01	19,12	0,48	18,39	0,46	0,83	0,03	0,79	0,03
Thr195	1,03	0,01	1,06	0,02	17,40	0,54	16,68	0,42	0,75	0,03	0,78	0,03
Gly196	O	O	O	O	O	O	O	O	O	O	O	O
Glu197	0,96	0,02	0,94	0,03	16,22	0,41	15,71	0,39	0,74	0,03	0,76	0,03

Leu198	0,87	0,01	0,86	0,01	15,18	0,38	14,95	0,37	0,44	0,02	0,44	0,02
Leu199	O	O	O	O	O	O	O	O	O	O	O	O
Thr200	0,93	0,01	0,92	0,02	18,88	0,53	18,41	0,46	0,82	0,03	0,81	0,04
Leu201	1,01	0,01	1,01	0,01	19,13	0,48	18,60	0,58	0,84	0,02	0,80	0,04
Ala202	0,99	0,01	0,99	0,02	18,78	0,47	18,50	0,46	0,84	0,02	0,82	0,04
Ser203	0,98	0,00	1,00	0,01	18,59	0,46	17,81	0,45	0,80	0,03	0,76	0,03
Arg204	O	O	1,02	0,01	O	O	18,44	0,46	O	O	0,81	0,04
Gln205	1,00	0,00	1,00	0,01	19,44	0,49	18,35	0,46	0,82	0,03	0,78	0,03
Gln206	0,99	0,01	1,00	0,01	18,93	0,47	18,24	0,46	0,83	0,03	0,84	0,04
Leu207	0,99	0,02	1,02	0,01	19,79	0,56	19,16	0,48	0,82	0,03	0,86	0,04
Ile208	1,01	0,01	1,00	0,01	18,81	0,47	18,57	0,46	0,86	0,03	0,83	0,04
Asp209	1,01	0,01	0,99	0,02	19,86	0,50	19,25	0,48	0,83	0,03	0,84	0,04
Trp210	1,01	0,02	1,00	0,02	19,60	0,49	19,07	0,48	0,85	0,02	0,81	0,04
Met211	0,97	0,01	0,97	0,01	19,51	0,80	17,41	0,44	0,80	0,04	0,83	0,04
Glu212	0,99	0,02	1,03	0,01	25,74	0,64	23,66	0,59	0,85	0,07	0,80	0,05
Ala213	O	O	0,98	0,01	O	O	18,56	0,46	O	O	0,79	0,04
Asp214	0,98	0,02	0,99	0,03	20,97	1,47	19,99	0,74	0,92	0,05	0,89	0,05
Lys215	W	W	1,02	0,03	W	W	26,78	2,45	W	W	0,84	0,09
Val216	0,98	0,04	1,03	0,03	49,84	7,71	30,59	1,41	0,90	0,14	0,94	0,07
Ala217	1,01	0,03	1,01	0,01	20,00	0,50	18,69	0,47	0,84	0,06	0,81	0,04
Gly218	1,02	0,05	1,05	0,05	36,50	4,21	25,96	1,25	0,74	0,09	0,82	0,06
Pro219	#	#	#	#	#	#	#	#	#	#	#	#
Leu220	0,95	0,02	0,92	0,02	24,54	2,95	21,60	2,82	0,81	0,05	0,81	0,04
Leu221	1,04	0,02	0,95	0,02	25,48	1,64	22,46	1,10	0,79	0,08	0,78	0,07
Arg222	O	O	O	O	O	O	O	O	O	O	O	O
Ser223	O	O	O	O	O	O	O	O	O	O	O	O
Ala224	0,98	0,01	0,96	0,01	18,72	0,47	18,18	0,45	0,80	0,02	0,75	0,03
Leu225	0,90	0,01	0,88	0,01	19,06	0,48	18,61	0,47	0,85	0,02	0,80	0,04
Pro226	#	#	#	#	#	#	#	#	#	#	#	#
Ala227	0,91	0,01	0,92	0,01	18,40	0,61	17,85	0,46	0,77	0,03	0,76	0,03
Gly228	0,91	0,04	0,89	0,03	16,51	0,57	16,86	0,42	0,78	0,03	0,78	0,04
Trp229	1,00	0,02	0,99	0,01	19,09	0,48	18,43	0,46	0,85	0,04	0,81	0,04
Phe230	O	O	O	O	O	O	O	O	O	O	O	O
Ile231	0,96	0,02	0,97	0,01	19,50	0,49	19,00	0,48	0,87	0,03	0,86	0,04
Ala232	0,94	0,02	0,96	0,01	18,74	0,47	18,12	0,45	0,84	0,04	0,79	0,04
Asp233	0,95	0,01	0,96	0,01	19,65	0,49	18,61	0,54	0,81	0,04	0,82	0,04
Lys234	0,92	0,01	0,93	0,01	23,16	0,58	20,79	0,52	0,73	0,07	0,75	0,07
Ser235	W	W	W	W	W	W	W	W	W	W	W	W
Gly236	O	O	0,89	0,01	O	O	22,26	0,56	O	O	0,77	0,06
Ala237	M	M	M	M	M	M	M	M	M	M	M	M
Gly238	O	O	0,89	0,02	O	O	17,96	0,45	O	O	0,80	0,04
Glu239	1,02	0,01	0,97	0,01	21,14	0,88	19,31	0,48	0,83	0,04	0,80	0,04
Arg240	1,02	0,01	O	O	19,07	0,48	O	O	0,86	0,09	O	O
Gly241	0,99	0,02	0,97	0,01	19,36	0,51	18,81	0,47	0,81	0,03	0,79	0,04
Ser242	1,01	0,01	0,99	0,01	22,01	0,55	20,51	0,51	0,80	0,03	0,84	0,04

Arg243	1,00	0,01	0,98	0,01	20,05	0,50	18,77	0,47	0,82	0,04	0,86	0,04
Gly244	0,99	0,02	0,97	0,01	21,41	0,54	19,52	0,49	0,87	0,05	0,84	0,04
Ile245	1,01	0,02	0,99	0,01	22,05	0,55	19,43	0,49	0,89	0,03	0,89	0,04
Ile246	O	O	O	O	O	O	O	O	O	O	O	O
Ala247	0,96	0,01	0,97	0,01	19,59	0,49	19,69	0,54	0,83	0,06	0,84	0,04
Ala248	O	O	O	O	O	O	O	O	O	O	O	O
Leu249	0,99	0,02	0,97	0,01	19,43	0,49	19,18	0,48	0,77	0,03	0,82	0,04
Gly250	1,02	0,02	0,99	0,01	21,20	0,67	20,43	0,54	0,81	0,03	0,83	0,04
Pro251	#	#	#	#	#	#	#	#	#	#	#	#
Asp252	0,91	0,02	0,93	0,01	21,43	0,54	20,97	0,58	0,75	0,03	0,76	0,04
Gly253	0,94	0,01	0,96	0,01	24,47	0,83	24,05	0,60	0,81	0,04	0,78	0,05
Lys254	0,90	0,01	0,91	0,01	20,37	0,51	19,66	0,49	0,80	0,02	0,82	0,04
Pro255	#	#	#	#	#	#	#	#	#	#	#	#
Ser256	0,95	0,02	0,94	0,02	19,16	0,48	20,06	0,78	0,79	0,05	0,80	0,06
Arg257	1,02	0,01	1,02	0,01	20,20	0,51	21,06	0,59	0,83	0,04	0,79	0,04
Ile258	0,96	0,01	0,97	0,01	19,79	0,49	19,81	0,82	0,86	0,03	0,82	0,04
Val259	0,93	0,02	0,94	0,01	19,10	0,48	18,84	0,47	0,86	0,03	0,84	0,04
Val260	0,93	0,01	0,89	0,01	18,13	0,45	17,61	0,50	0,84	0,04	0,85	0,04
Ile261	O	O	0,94	0,01	O	O	19,54	0,49	O	O	0,87	0,05
Tyr262	O	O	O	O	O	O	O	O	O	O	O	O
Thr263	0,92	0,02	0,91	0,01	19,24	0,48	19,16	0,48	0,82	0,05	0,85	0,04
Thr264	O	O	0,95	0,02	O	O	20,25	0,51	O	O	0,77	0,04
Gly265	0,95	0,02	0,93	0,01	21,32	0,53	20,78	0,57	0,88	0,06	0,81	0,04
Ser266	1,02	0,02	1,02	0,03	16,33	0,41	14,32	0,71	0,81	0,03	0,75	0,03
Gln267	0,99	0,04	0,96	0,02	19,40	0,49	18,57	0,46	0,85	0,04	0,83	0,04
Ala268	O	O	O	O	O	O	O	O	O	O	O	O
Thr269	0,96	0,02	0,93	0,01	18,96	0,47	18,90	0,47	0,78	0,03	0,77	0,03
Met270	1,05	0,02	1,02	0,04	22,24	0,86	23,56	2,33	0,90	0,11	0,82	0,06
Asp271	1,01	0,01	0,99	0,01	18,14	0,45	17,77	0,44	0,81	0,03	0,86	0,04
Glu272	0,99	0,01	0,98	0,01	19,53	0,54	18,91	0,47	0,86	0,05	0,84	0,04
Arg273	0,98	0,01	O	O	19,61	0,49	O	O	0,81	0,03	O	O
Asn274	0,98	0,02	0,98	0,01	19,13	0,72	17,94	0,45	0,84	0,03	0,82	0,04
Arg275	1,01	0,01	0,99	0,01	20,57	0,73	19,42	0,49		0,03	0,83	0,04
Gln276	0,97	0,01	0,98	0,01	19,42	0,79	18,24	0,46	0,84	0,03	0,80	0,04
Ile277	0,98	0,01	0,97	0,02	22,10	1,93	18,87	0,47	0,84	0,03	0,90	0,05
Ala278	O	O	O	O	O	O	O	O	O	O	O	O
Glu279	0,99	0,02	0,98	0,01	19,55	0,64	18,49	0,46	0,80	0,06	0,76	0,04
Ile280	0,97	0,01	0,95	0,01	17,99	0,47	19,08	0,48	0,77	0,03	0,82	0,04
Gly281	0,98	0,02	0,98	0,01	18,83	0,47	18,94	0,47	0,86	0,03	0,87	0,04
Ala282	1,01	0,01	1,01	0,01	19,41	0,49	18,96	0,47	0,85	0,03	0,86	0,04
Ser283	1,01	0,00	1,01	0,01	17,73	1,99	17,05	0,58	0,73	0,02	0,75	0,03
Leu284	O	O	O	O	O	O	O	O	O	O	O	O
Ile285	0,99	0,02	0,99	0,03	20,82	0,76	19,23	0,52	0,81	0,03	0,86	0,04
Lys286	1,01	0,01	0,99	0,01	19,50	0,49	19,38	0,48	0,78	0,03	0,80	0,04
His287	0,93	0,01	0,95	0,01	18,80	1,59	17,16	0,43	0,80	0,03	0,80	0,04

Trp288	0,97	0,01	0,99	0,01	15,69	0,48	16,28	0,41	0,73	0,03	0,76	0,03
--------	------	------	------	------	-------	------	-------	------	------	------	------	------

\*Δ correspond to errors coming from the Jackknife simulations for R<sub>1</sub> and R<sub>2</sub> and from the method described by Nicholson *et al.* (38) for NOEs.

O correspond to non-available data due to peaks overlapping.

W correspond to non-available data due to very weak peaks.

M correspond to missing attributions.

# correspond to Proline residues.

**Table S4.2.** Model-free Parameters.

Residue	Model		WT				Y105D							
	WT	Y105D	S <sup>2</sup>	ΔS <sup>2</sup>	τ <sub>e</sub> (ps)	Δτ <sub>e</sub>	R <sub>ex</sub> (s <sup>-1</sup> )	ΔR <sub>ex</sub>	S <sup>2</sup>	ΔS <sup>2</sup>	τ <sub>e</sub> (ps)	Δτ <sub>e</sub>	R <sub>ex</sub> (s <sup>-1</sup> )	ΔR <sub>ex</sub>
His26														
Pro27														
Gly28	1	1	0,93	0,01					0,90	0,02				
Thr29	1	1	0,95	0,01					0,94	0,02				
Leu30	1	1	0,97	0,02					0,95	0,02				
Val31	1	1	0,92	0,01					0,91	0,02				
Lys32		1							0,92	0,02				
Val33		1							0,94	0,02				
Lys34	1	2	0,93	0,01					0,91	0,02	19	12		
Asp35	1	1	0,95	0,01					0,95	0,02				
Ala36	1	1	0,96	0,02					0,93	0,02				
Glu37	1	1	0,94	0,02					0,95	0,02				
Asp38	1	1	0,93	0,01					0,93	0,02				
Gln39	2	2	0,93	0,02	36	18			0,91	0,02	13	10		
Leu40	1	1	0,93	0,02					0,92	0,02				
Gly41	1	1	0,95	0,02					0,96	0,02				
Ala42	1	2	0,90	0,02					0,87	0,02	14	7		
Arg43	0 <sup>a</sup>	0												
Val44	1	1	0,90	0,01					0,88	0,01				
Gly45	1	1	0,90	0,02					0,90	0,01				
Tyr46	2	1	0,90	0,02	21	11			0,94	0,02				
Ile47	1	1	0,93	0,01					0,89	0,02				
Glu48	1	1	0,95	0,02					0,93	0,02				
Leu49	1	1	0,93	0,02					0,93	0,02				
Asp50	1	1	0,94	0,02					0,93	0,01				
Leu51	1	1	0,95	0,02					0,94	0,02				
Asn52	2	2	0,88	0,02	63	14			0,84	0,02	52	9		
Ser53	1	1	0,89	0,02					0,89	0,02				
Gly54	2	1	0,97	0,01	342	259			0,96	0,02				
Lys55	2	1	0,92	0,02	37	15			0,92	0,02				
Ile56	1	1	0,92	0,02					0,88	0,02				
Leu57	1	1	0,92	0,02					0,90	0,02				
Glu58	1	1	0,89	0,01					0,88	0,02				
Ser59	2	1	0,89	0,01	21	9			0,88	0,01				
Phe60	1	1	0,92	0,01					0,90	0,02				
Arg61	1	1	0,94	0,02					0,94	0,02				
Pro62														
Glu63	2	1	0,91	0,02	12	10			0,89	0,01				

Glu64	1	1	0,91	0,01			0,90	0,02				
Arg65	2	1	0,89	0,02	10	7			0,87	0,01		
Phe66	1	2	0,94	0,02					0,90	0,02	19	12
Pro67												
Met68		1							0,96	0,02		
Met69	1	1	0,99	0,01					0,99	0,01		
Ser70												
Thr71	1	1	0,99	0,01					0,99	0,01		
Phe72	1	1	0,99	0,01					0,98	0,02		
Lys73	3	3	0,99	0,01			1,6	0,5	0,96	0,02		
Val74	1	1	0,97	0,02					0,96	0,02		
Leu75	1	1	0,94	0,02					0,94	0,02		
Leu76	1	1	0,94	0,02					0,89	0,02		
Cys77		1							0,90	0,02		
Gly78	1	1	0,96	0,02					0,94	0,02		
Ala79	1	1	0,97	0,01					0,96	0,02		
Val80	1	1	0,93	0,02					0,91	0,02		
Leu81	1	1	0,95	0,02					0,95	0,02		
Ser82	1	1	0,95	0,02					0,93	0,02		
Arg83	1	1	0,96	0,02					0,94	0,02		
Val84	1	2	0,93	0,02					0,90	0,02	15	10
Asp85		1							0,96	0,02		
Ala86	1	1	0,91	0,02					0,89	0,02		
Gly87	1	1	0,90	0,01					0,90	0,01		
Gln88	1	1	0,91	0,01					0,89	0,01		
Glu89	1	1	0,85	0,01					0,84	0,01		
Gln90	1	1	0,89	0,01					0,87	0,01		
Leu91	3	3	0,91	0,02			1,2	0,4	0,89	0,02		
Gly92	1	1	0,97	0,02					0,94	0,02		
Arg93	1	1	0,96	0,02					0,95	0,02		
Arg94	1	1	0,90	0,01					0,88	0,01		
Ile95	2	1	0,91	0,01	13	11			0,90	0,02		
His96												
Tyr97	1	2	0,87	0,01					0,84	0,01	18	6
Ser98	1	1	0,87	0,02					0,87	0,01		
Gln99	1	1	0,96	0,02					0,94	0,02		
Asn100	1	1	0,95	0,02					0,94	0,02		
Asp101	1	1	0,91	0,01					0,91	0,02		
Leu102	1	1	0,89	0,01					0,88	0,02		
Val103	1	1	0,90	0,02					0,87	0,02		
Glu104	1	1	0,94	0,01					0,92	0,02		
Tyr105	1	1	0,91	0,02					0,88	0,01		
Ser106	1	1	0,89	0,01					0,82	0,01		
Pro107												
Val108		1							0,95	0,02		

Thr109	1	1	0,89 0,02			0,89 0,02			
Glu110	1	1	0,97 0,02			0,95 0,02			
Lys111	1	1	0,93 0,02			0,90 0,02			
His112	1	1	0,89 0,01			0,86 0,01			
Leu113	1	1	0,95 0,01			0,94 0,02			
Thr114	1	1	0,92 0,02			0,90 0,02			
Asp115	1	1	0,92 0,02			0,92 0,02			
Gly116		1				0,93 0,02			
Met117	1	1	0,92 0,02	37	21		0,91 0,02		
Thr118	2	1	0,94 0,02				0,91 0,02		
Val119	1	1	0,95 0,02				0,91 0,02		
Arg120	1	1	0,97 0,02				0,97 0,02		
Glu121	1	1	0,94 0,02				0,94 0,02		
Leu122		1					0,95 0,02		
Cys123	1		0,94 0,02						
Ser124	2	1	0,87 0,02	50	9		0,91 0,02		
Ala125									
Ala126		1					0,95 0,02		
Ile127	1	1	0,93 0,02				0,90 0,02		
Thr128	3	3	0,96 0,02			5,3	1,0	0,96 0,02	3,8 0,5
Met129	1	1	0,92 0,02					0,92 0,02	
Ser130		1						0,91 0,02	
Asp131		1						0,98 0,02	
Asn132	1	1	0,97 0,02					0,93 0,02	
Thr133	1	1	0,95 0,02					0,96 0,02	
Ala134		1						0,95 0,02	
Ala135		1						0,91 0,02	
Asn136	3	1	0,93 0,02			1,1	0,4	0,93 0,02	
Leu137	3	3	0,96 0,02			2,3	0,7	0,94 0,02	2,5 0,6
Leu138	1	1	0,95 0,02					0,95 0,02	
Leu139	1	1	0,96 0,02					0,95 0,02	
Thr140									
Thr141		0							
Ile142	1	1	0,93 0,02					0,95 0,02	
Gly143	1	1	0,92 0,02					0,92 0,02	
Gly144	1	2	0,92 0,02					0,91 0,02	37 13
Pro145									
Lys146	1	1	0,98 0,02					0,91 0,02	
Glu147	1	1	0,94 0,02					0,92 0,02	
Leu148	1	1	0,94 0,02					0,94 0,02	
Thr149	1	1	0,93 0,02					0,91 0,02	
Ala150	1	1	0,96 0,02					0,93 0,02	
Phe151	1	1	0,94 0,01					0,93 0,02	
Leu152		1						0,94 0,02	
His153	1	1	0,96 0,02					0,96 0,02	



Leu199									
Thr200	1	2	0,91	0,01			0,89	0,02	12
Leu201	1	1	0,95	0,01			0,94	0,02	8
Ala202	1	1	0,94	0,02			0,93	0,02	
Ser203	1	2	0,93	0,01			0,91	0,02	36
Arg204		1					0,94	0,02	13
Gln205	1	1	0,96	0,02			0,94	0,02	
Gln206	1	1	0,94	0,01			0,93	0,02	
Leu207	1	1	0,95	0,02			0,96	0,02	
Ile208	1	1	0,95	0,02			0,94	0,02	
Asp209	1	1	0,97	0,02			0,94	0,02	
Trp210	1	1	0,96	0,02			0,94	0,02	
Met211	1	1	0,92	0,02			0,89	0,01	
Glu212	3	3	0,95	0,02		6,6	0,6	0,98	0,02
Ala213		1						0,93	0,02
Asp214	1	1	0,94	0,02			0,96	0,02	
Lys215		3						0,97	0,02
Val216	3	3	0,92	0,03		31,1	6,1	0,95	0,03
Ala217	1	1	0,98	0,02				0,95	0,02
Gly218	3	3	0,98	0,02		15,8	3,2	0,98	0,02
Pro219									
Leu220	1	1	0,95	0,02			0,91	0,02	
Leu221	3	3	0,99	0,01		4,9	1,4	0,92	0,02
Arg222									
Ser223		2						0,91	0,02
Ala224	2	2	0,93	0,02	23	16		0,90	0,02
Leu225	1	1	0,89	0,01				0,87	0,01
Pro226									
Ala227	2	2	0,88	0,02	20	8		0,87	0,02
Gly228	1	1	0,83	0,02				0,84	0,02
Trp229	1	1	0,95	0,02				0,93	0,02
Phe230									
Ile231	1	1	0,94	0,02			0,93	0,02	
Ala232	1	1	0,91	0,02			0,91	0,02	
Asp233	1	1	0,93	0,01			0,92	0,02	
Lys234	3	3	0,92	0,02		3,7	0,5	0,92	0,02
Ser235									
Gly236		3						0,89	0,02
Ala237									
Gly238		1						0,87	0,02
Glu239	1	1	0,99	0,01				0,94	0,02
Arg240	1		0,97	0,02					
Gly241	1	1	0,96	0,02				0,93	0,02
Ser242	3	3	0,98	0,02		2,0	0,5	0,95	0,02
Arg243	3	1	0,96	0,02		0,5	0,4	0,93	0,02

Gly244	3	1	0,96	0,02		1,8	0,5	0,94	0,02			
Ile245	3	1	0,98	0,02		2,1	0,5	0,95	0,02			
Ile246												
Ala247	1	1	0,93	0,01				0,93	0,02			
Ala248												
Leu249	1	1	0,96	0,02				0,93	0,02			
Gly250	3	3	0,97	0,02		1,9	0,6	0,93	0,02		2,0	0,5
Pro251												
Asp252	1	1	0,96	0,02				0,92	0,02			
Gly253	3	3	0,90	0,02		6,3	0,7	0,90	0,02		6,0	0,5
Lys254	1	1	0,91	0,01				0,92	0,02			
Pro255												
Ser256	3	3	0,89	0,02		1,4	0,5	0,88	0,02		2,7	0,7
Arg257	1	1	0,97	0,02				0,98	0,01			
Ile258	1	1	0,93	0,02				0,93	0,02			
Val259	1	1	0,92	0,02				0,92	0,02			
Val260	1	1	0,91	0,01				0,87	0,01			
Ile261		1						0,93	0,02			
Tyr262												
Thr263	1	1	0,92	0,01				0,91	0,02			
Thr264		1						0,95	0,02			
Gly265	3	3	0,95	0,02		1,4	0,5	0,92	0,02		1,5	0,5
Ser266	1	1	0,89	0,02				0,88	0,02			
Gln267	1	1	0,94	0,02				0,92	0,02			
Ala268												
Thr269	1	1	0,93	0,02				0,91	0,02			
Met270	1	1	0,99	0,01				0,99	0,02			
Asp271	1	1	0,94	0,01				0,91	0,02			
Glu272	1	1	0,95	0,02				0,94	0,02			
Arg273	1		0,95	0,01								
Asn274	1	1	0,93	0,02				0,92	0,02			
Arg275	3	3	0,95	0,02		1,8	0,6	0,92	0,02		1,5	0,5
Gln276	1	2	0,93	0,01				0,92	0,02	17	12	
Ile277	1	1	0,95	0,02				0,93	0,02			
Ala278												
Glu279	1	1	0,94	0,02				0,92	0,02			
Ile280	1	1	0,93	0,01				0,92	0,02			
Gly281	1	1	0,94	0,01				0,93	0,02			
Ala282	1	1	0,96	0,01				0,95	0,02			
Ser283	2	1	0,93	0,02	75	27		0,93	0,02			
Leu284												
Ile285	3	3	0,93	0,02		2,3	0,7	0,92	0,02		1,0	0,6
Lys286	1	1	0,96	0,02				0,94	0,02			
His287	1	1	0,89	0,01				0,89	0,02			
Trp288	1	1	0,88	0,01				0,89	0,02			

<sup>a</sup>model 0 means that the residue was not well fitted by any model

**Table S4.3.** Residues displaying significant variation<sup>a</sup> between wild-type TEM-1 and mutant Y105D.

R <sub>1</sub>	R <sub>2</sub>	{ <sup>1</sup> H}- <sup>15</sup> N NOE	S <sup>2</sup>	R <sub>ex</sub>
34	46	29	56	212
36	71	34	106	215*
37	72	41	146	216
43	76	58	221	218
45	83	65	239	234
46	103	71	260	
47	104	72		
54	106	75		
59	124	82		
64	158	83		
75	163	97		
76	211	98		
87	215*	103		
92	216	104		
100	218	106		
104	220	110		
106	221	112		
110	228	121		
111	234	124		
113	239	129		
118	244	133		
119	245	136		
132	256	138		
133	257	160		
136	266	165		
142	270	168		
143	277	170		

148	280	178		
158	287	181		
159	288	187		
164		192		
171		207		
179		218		
182		224		
186		243		
187		249		
193		265		
194		266		
195		270		
203		271		
207		277		
212		280		
216		285		
218				
220				
221				
232				
252				
253				
260				
269				
270				
287				
288				

<sup>a</sup> Variations in R<sub>1</sub>, R<sub>2</sub> and NOE were considered significant if the Y105D/WT ratio was larger than the average ratio  $\pm 1\sigma$ . Variations in S<sup>2</sup> were considered significant if the difference was larger than the sum of the errors + 0.01. Variations in R<sub>ex</sub> were considered

significant if the difference was larger than the sum of the errors + 1.0 s<sup>-1</sup>. Sequential numbering is used.

\* As residue Lys215 was significantly weaker for the wt than for Y105D, it was impossible to obtain relaxation data for the wt. We therefore conclude that R<sub>2</sub> value was significantly higher for the WT, reflecting significantly higher R<sub>ex</sub>.

## Annexe 5 – Réponse aux questions et commentaires des membres du jury

- Question : D'où proviennent les abréviations de TEM, SHV et OXA ? Quelle est la signification de chacun de ces termes ?

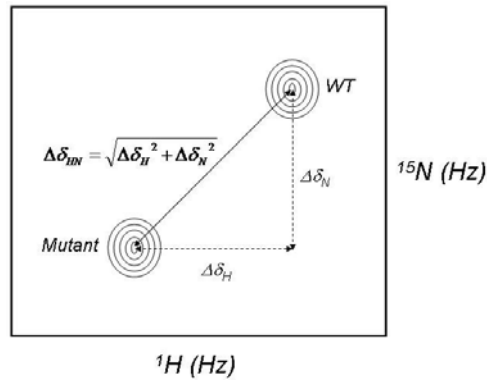
Réponse : Ces termes sont pour la plupart génériques ou historiques et ne servent qu'à définir des familles de  $\beta$ -lactamases originellement isolées à partir de patients infectés par des souches résistantes à certains antibiotiques particuliers. Par exemple, tel que discuté dans le texte, la  $\beta$ -lactamase TEM-1 fut isolée pour la première fois à partir d'une souche de *Escherichia coli* extraite d'une patiente grecque nommée Temoniera. Le terme « TEM » n'est en réalité que les trois premières lettres du prénom de cette patiente (« TEMoniera »). Ainsi, TEM-1 correspond à l'enzyme originale (native) retrouvée chez cette patiente, alors que les enzymes TEM-2, TEM-3, etc. correspondent à des variants légèrement mutés isolés subséquemment de diverses souches naturelles de *E. coli* et possédant un profil de résistance aux antibiotiques légèrement différent. De manière similaire, la  $\beta$ -lactamase SHV, dont le nom est une abréviation de « Sulphydryl Variable », est un homologue structurel de TEM-1 originellement isolé chez *E. coli* et chez *Klebsilla pneumoniae* [17]. SHV et TEM sont deux familles de  $\beta$ -lactamases faisant partie de la classe A des  $\beta$ -lactamases. Quant à OXA, il s'agit d'une famille de  $\beta$ -lactamases faisant partie de la classe D (également des hydrolases à sérine, mais structurellement distinctes). Le nom OXA provient de « *Oxacillin-resistant* », en raison de la forte activité que possède cette famille de  $\beta$ -lactamases pour ce substrat.

- Question : Les groupements carboxyliques sont parfois ionisés et parfois protonés. Quelle représentation est la bonne ?

Réponse : Le  $pK_a$  des acides carboxyliques se situe généralement aux alentours de 4-5, signifiant que ces groupements sont habituellement déprotonés à pH physiologique. Dans la littérature des  $\beta$ -lactames, il est toutefois commun de les représenter de manière protonée plutôt que déprotonée. Par souci de constance, tous les  $\beta$ -lactames présentés dans la thèse sont désormais représentés de manière protonée. En revanche, il est important de noter que les potentiels atomiques utilisés lors des études de modélisation furent fixés de manière à considérer ces acides carboxyliques déprotonés dans tous les calculs effectués.

- Commentaire : I would report the chemical shift change on a more general scale (ppm as opposed to Hz). This is just to help people who would like to use this data in another lab. The ppm scale is not dependent on the field strength of the magnet and the Hz scale is. This is the reason the ppm scale was developed.

Réponse : It is true that the ppm scale is independent of the field strength but the Hz scale was used here in order to normalize the weight of all chemical shifts differences observed for  $^1\text{H}$  and  $^{15}\text{N}$ . Knowing that 1 ppm ( $^1\text{H}$ ) = 599.739 Hz and 1 ppm ( $^{15}\text{N}$ ) = 60.778 Hz on the magnet we used, the transformation of all ppm values in Hz allows the direct comparison and addition of  $^1\text{H}$  and  $^{15}\text{N}$  chemical shift differences together, without the need to apply any subsequent scaling factor. The chemical shift differences of  $^1\text{H}+^{15}\text{N}$  ( $\Delta\delta_{\text{HN}}$ ) can thus be directly calculated on a  $^{15}\text{N}$ -HSQC spectrum as follows:



To allow anyone to perform the conversion between the two scales (ppm and Hz), we added the transformation factor for our magnet in the legend of Figure 4.1 [1 ppm ( $^1\text{H}$ ) = 599.739 Hz and 1 ppm ( $^{15}\text{N}$ ) = 60.778 Hz].

- Commentaire : You also could have included your carbonyl carbon chemical shifts in the analysis to make the analysis more complete. I am including a paper that discusses this for your information [116].

Réponse : This is a good suggestion and we originally thought about including the carbonyl carbons in our analysis. However, they were not included because their chemical shift variation was not significantly altered from one mutant to the other, therefore providing no further information to the analysis.

- Question : I would say looking at the data in chapter 4, the significant chemical shift changes are those that are > 40 Hz. The ones between 10-40 Hz are not that far above background and I would be inclined to say that this is not significant. What is the basis for claiming a chemical shift is significant? This should be discussed when choosing the value.

Réponse : The method used to calculate uncertainties was not explained in great detail in chapter 4 and the authors agree with the reviewer that they should have been discussed a bit more. Hopefully, the following explanation will clarify this point.

The legend in Table 4.1 states that the experimental error = 5.5 Hz and that only values greater than twice the experimental error were considered as significant (11 Hz). In order to define a threshold limit that separates the background values from the chemical shift differences considered as significant, the authors had to account for two particular error factors: 1) the digital resolution of the spectra recorded, and 2) the experimental error introduced in the preparation of the samples (pH, concentration, temperature, data acquisition).

In any case, the most important contribution to the global experimental error is the digital resolution of the  $^{15}\text{N}$ -HSQC spectra, which is defined as the spectral width (sw) divided by the number of points in each spectrum (n). In our experiments, all spectra were transformed in an identical fashion with  $^1\text{H}$  and  $^{15}\text{N}$  values recorded as follows:  $^1\text{H}$ : sw = 12000 Hz, n = 4096;  $^{15}\text{N}$ : sw = 1340 Hz, n = 512. As a result, the digital resolution of  $^1\text{H}$  is 2.9 Hz and that of  $^{15}\text{N}$  is 2.6 Hz. However, we considered the total digital resolution as a summation of these two error values (5.5 Hz). Although this digital resolution is the theoretical limit that separates background noise from significant values of chemical shift differences, it does not account for the various experimental errors introduced in the preparation of the samples.

Particular care was taken during preparation and handling of all samples in order to make sure that they were all precisely adjusted at the same pH and concentration. For instance, the pH was adjusted and monitored in the NMR  $^1\text{H}$  spectrum with the aid of 0.4 mM imidazole added to each sample. Moreover, the concentration was monitored both by UV absorbance at 280 nm and by peak integration in the NMR  $^1\text{H}$  spectrum to make sure that it was exactly the same in each sample. Finally, spectroscopic acquisition and transformation were performed in an identical fashion at the same temperature for all

Y105X mutants investigated. This careful sample handling allowed us to minimize the error factor attributed to the experimenter. To estimate the value of this experimental error, the perfect experiment remains the overlay of two  $^{15}\text{N}$ -HSQC spectra acquisitioned on two samples of the same protein prepared in parallel and in identical conditions. We performed visual inspection of  $^{15}\text{N}$ -HSQC spectra of WT TEM-1 recorded in such a fashion and the overlays always yielded perfect fits that were virtually indistinguishable. Moreover, to quantify the order of magnitude of the errors obtained from such an overlay, statistical analysis of a  $^{15}\text{N}$ -HSQC triplicate experiment performed on the same protein sample yielded an overall standard deviation of 0.240 Hz in peak position, with a minimum at 0.070 Hz and a maximum at 0.839 Hz (results from Sébastien Morin, Gagné lab). Although the comparison of two different samples is likely to give slightly higher error values, this experimental deviation nevertheless remains one order of magnitude lower than the digital resolution calculated above.

Consequently, to make sure that the variations in chemical shifts we observed were indeed significant when comparing two protein samples, we only considered values of  $\Delta\delta_{\text{HN}}$  greater than twice the digital resolution of the  $^{15}\text{N}$ -HSQC spectra recorded (*i.e.* 5.5 Hz  $\times 2 = 11$  Hz). This approximation is a reasonable assumption for the global error since it compensates for both spectral resolution and experimental error values. Enzyme catalysis can either be affected by a vast number of small effects on chemical shifts or a small number of important effects on chemical shifts (or both). As a result, the authors consider that every chemical shift variation higher than this threshold limit of 11 Hz is of importance to the current study.

Based on the reviewer's comment, the authors nevertheless agree that Figure 4.2 can be misleading because of the Y-axis scale used, which unfortunately biases the information by putting more weight on residues displaying high  $\Delta\delta_{\text{HN}}$  (rather than showing the total number of residues affected over background). We would like to emphasize that we consider significant both the number of residues affected in chemical shift as well as the

magnitude in the  $\Delta\delta_{\text{HN}}$  observed at each position. In order to adequately display the results presented in Table 4.1 and Figure 4.1, we provide a modified version of Figure 4.2 that clearly displays the aforementioned threshold value (see below). As a complement to the original Figure 4.2, the current version particularly emphasizes the amount of residues that display slight but nevertheless significant  $\Delta\delta_{\text{HN}}$  over background.

• Question : I also fail to see a real correlation between the enzymatic activity and the chemical shift changes. The Y105N and the Y105D mutants look to have virtually identical patterns of chemical shift changes. This would be expected given the chemical similarity between Asn and Asp. Yet they differ by an order of magnitude in terms of their activity ( $k_{\text{cat}}/K_M$ ). This difference is larger than the difference between the wild-type enzyme and the Y105N mutant (5 times). I really do not see that there is a correlation between chemical shift changes and activity. It would be interesting to compare the differences between the Y105N and Y105D mutants. If they are very similar, what does this say about a correlation between chemical shift change and enzymatic activity?

Réponse : It is important to keep in mind that the authors never suggested the existence of a ***proportional*** correlation between the changes in chemical shifts and enzyme activity. To that extent, the authors never wanted to imply that it is possible to quantitatively monitor differences in activities by quantitatively monitoring differences in chemical shifts. This assumption would be presumptuous since enzyme activity is an extremely complex process that can be affected in many ways which may or may not be linked to the chemical shift variations we observe here. In this chapter, the authors merely point out the existence of a negative trend existing between the number of residues affected in chemical shifts (as well as their magnitude) with the catalytic efficiency of each single mutant investigated. By ‘correlation’, we simply mean the following trend: the more the residues affected in chemical shifts and the higher the magnitude of these changes, the less

active is the mutant. This correlation may or may not be fortuitous, but we nevertheless consider it an honest observation worth mentioning.

*A priori*, it is impossible to predict how the activity of an enzyme will be affected by a mutation. The detrimental effects of a mutation on enzyme catalysis can either be localized in the immediate environment of this mutation, or they can spread throughout the structure to perturb interactions that are essential for catalysis. Table 4.1 demonstrates that there is an inverse trend between the activity of each mutant and the number of residues displaying significant chemical shift variations. Based on the significant limit discussed above ( $> 11$  Hz), there is no clear evidence to dismiss the importance of the residues that display variations lower than 40 Hz. Residues with  $\Delta\delta_{\text{HN}} = 11\text{-}40$  Hz display small but significant variations and their accumulation may be as important in affecting catalysis as the residues displaying higher  $\Delta\delta_{\text{HN}}$ .

The authors agree with the reviewer that mutants Y105N and Y105D both display very similar patterns of chemical shift changes. This result was expected given the chemical similarity between Asp and Asn. However, at the reviewer's request, we have compared the chemical shift variations of mutants Y105N and Y105D in order to highlight two important facts regarding these chemical shifts variations: 1) the magnitude in  $\Delta\delta_{\text{HN}}$  observed between Y105N and Y105D and 2) the functionally-relevant residues that are affected in both mutants. This information is now presented in Table A5.1 (see below).

To quantify variations in  $\Delta\delta_{\text{HN}}$  magnitude, we have highlighted residues that display a  $\Delta\Delta\delta_{\text{HN}} > 11$  Hz in both mutants ( $\Delta\Delta\delta_{\text{HN}} = |\Delta\delta_{\text{HN}}(\text{Y105N}) - \Delta\delta_{\text{HN}}(\text{Y105D})|$ ) (Table A5.1). While seven residues display a  $\Delta\Delta\delta_{\text{HN}}$  significantly higher in mutant Y105N when compared to Y105D, this number jumps to 29 residues in mutant Y105D when compared to Y105N. Moreover, while none of the seven residues displaying significant  $\Delta\Delta\delta_{\text{HN}}$  in Y105N are of particular importance with respect to mutational tolerance in TEM-1, six of the 29 residues displaying significant  $\Delta\Delta\delta_{\text{HN}}$  in Y105D cannot be mutated without

detrimental effects either on structure and/or activity in WT TEM-1 (Table A5.1). Modification in the environment of these six functionally-important residues may partly explain the differences in catalytic efficiencies observed between mutants Y105N and Y105D. Overall, these observations demonstrate that mutant Y105D is affected to a higher degree than mutant Y105N, which is in agreement with our original conclusion.

- **Commentaire :** I am not sure why a review article is included in the middle of any thesis. I also fail to see the connection between the review article and the work. I think the goal was to connect to chapter 6, and specifically the ‘semi-rational design’. This review is more or less a review of protein engineering. I failed to see any protein engineering in this thesis and the work in the thesis is not connected to the work described in this review. I see the thesis as trying to determine how the  $\beta$ -lactamase helps the bacteria hydrolyze penicillin and penicillin-like antibiotics. The design work that will be associated with the information in this thesis will be the design of new antibiotics that are resistant to  $\beta$ -lactamase. I think the chapter should be removed and part of it added to the discussion if this is a future direction. It is not part of the thesis in its current form.

Réponse : To effectively address this question, one needs to look at formal definitions of ‘protein engineering’ and ‘protein design’:

“We distinguish protein engineering, by which we mean mutating the gene of an existing protein in an attempt to alter its function in a predictable way, from protein design, which has the more ambitious goal of designing *de novo* a protein to fulfill a desired function [117].”

Applying these definitions to enzyme catalysis, enzyme engineering is the modification of an existing enzyme in an attempt to alter its catalytic activity in a predictable way (which was performed in the present thesis), while enzyme design is the ambitious goal of designing *de novo* an enzyme to catalyze a particular reaction (which was not performed in the present thesis).

Typically, there are two general experimental strategies to perform enzyme engineering: rational design and directed evolution. In order to modify enzyme catalysis, rational design implies the specific and targeted modification of residues to modify substrate specificity or activity without the use of combinatorial methods that do not rely on rational choices. To perform rational design, an in-depth knowledge of the structural features of the enzyme active site and their contribution to function are necessary. On the other hand, directed evolution is the low frequency introduction of randomly-distributed mutations in a gene of interest that can be performed without prior structural knowledge of the given enzyme. However, the main limitation of directed evolution is the necessity of developing a high-throughput screening methodology that allows identification of the desired property under relevant conditions.

In order to optimize library size as well as creating ‘smarter libraries’ that increase the probability of finding an active hit, chapter 5 describes a ‘semi-rational’ (or ‘semi-random’) approach that combines several advantages from both the rational design and directed evolution methodologies (summarized in Table 5.1). Based on prior structural knowledge, this semi-random approach to enzyme engineering was subsequently applied to modify the active-site of TEM-1 in a combinatorial fashion by simultaneously mutating several functionally-important active-site positions in order to select for CTX-resistant mutants of TEM-1. This study is presented in chapter 6 and the justification and advantages for choosing this semi-random methodology are summarized in the introduction as well as in the experimental sections of the review article presented in chapter 5 (particularly in section “*Targeted randomization of defined residues based on structural knowledge*”).

In addition, the author would like to draw attention to the fundamental difference between the works presented in chapters 2 and 6 of the present thesis. While both chapters make use of the saturation mutagenesis technique, chapter 2 is a straightforward structure/function study of single-site mutants obtained in a rational fashion and characterized individually. In contrast, chapter 6 introduces a combinatorial element

essential for the detection of cooperativity (additivity/synergy) or antagonism between active-site residues with respect to enzyme specificity and activity. As described in chapter 5, this technique uses prior structural and functional information to target the positions that are to be randomized and is a direct application of the semi-random methodology presented in this chapter. Consequently, the author considers chapter 5 an appropriate and relevant introduction to the experimental enzyme engineering work presented in chapter 6 and does not agree with the reviewer's comment "that the work described in the review is not connected to the work in chapter 6".

However, the reviewer is right in pointing out the ambiguity introduced with the use of the 'design' term. In fact, 'design semi-rationnel' was used here to describe the 'random design' of DNA libraries, which could easily be confused with the design term used in 'protein design' and 'computational design' (both of which were addressed in the review article but not performed in the work presented in the thesis). In agreement with the reviewer's suggestion, the 'design semi-rationnel' expression was replaced by 'mutagenèse semi-aléatoire' throughout the thesis, except in published articles. This expression eliminates the 'design' ambiguity and also uses the more appropriate 'semi-aléatoire' ('semi-random') term to replace the vague 'semi-rationnel' ('semi-rational') term. In addition, following a comment made by the reviewer to correct this problem, the title of the thesis was modified to "Mutagenèse semi-aléatoire et analyse dynamique de la  $\beta$ -lactamase TEM-1 de *Escherichia coli*". Finally, the 'préface au chapitre 5' and 'préface au chapitre 6' were extensively modified to clarify two important points regarding what is discussed here: a) the reader is encouraged to approach chapter 5 as an introduction to the methodology employed in chapter 6, specifically focusing on the introduction and the experimental sections of the review article, and b) the author specifically mentions that the 'protein design' and 'computational design' described at the end of this review article are not performed in the following chapter.

**Table A5.1.** Comparison of  $\Delta\delta_{\text{HN}}$  relative to WT for mutants Y105N and Y105D. For each mutant, only residues with  $\Delta\delta_{\text{HN}} > 11$  Hz are shown. Bold and underlined values represent residues that display a  $\Delta\Delta\delta_{\text{HN}} > 11$  Hz between mutants Y105N and Y105D ( $\Delta\Delta\delta_{\text{HN}} = |\Delta\delta_{\text{HN}}(\text{Y105N}) - \Delta\delta_{\text{HN}}(\text{Y105D})|$ ). Residues that do not tolerate any mutation in TEM-1  $\beta$ -lactamase are also presented (according to [118]).

Residue Number (Y105N)	$\Delta\delta_{\text{HN}}$ WT vs Y105N (Hz)	Residue Number (Y105D)	$\Delta\delta_{\text{HN}}$ WT vs Y105D (Hz)	Mutational tolerance in WT TEM-1
28	17,5	28	16,9	
34	12,7	34	12,8	
51	11,2	51	11,7	
		58	<b>11,4</b>	
		63	<b>11,5</b>	
65	11,4	65	11,4	
66	11,9	66	12,3	None
68	26,4	68	35,3	
69	16,0	69	<b>29,8</b>	
71	17,7	71	<b>33,5</b>	None
72	<b>32,4</b>	72	12,0	
		73	<b>23,4</b>	None
74	<b>11,6</b>			
75	12,1	75	16,1	
76	38,4	76	37,8	
77	19,5	77	<b>32,3</b>	
78	16,9	78	15,1	
79	17,3	79	15,6	
83	14,2	83	13,6	
86	15,9	86	15,7	
89	12,6	89	14,4	
		93	<b>11,4</b>	
98	17,4	98	14,4	
102	40,2	102	34,7	
103	28,7	103	35,1	
104	104,8	104	110,1	
105	229,8	105	121,8	
106	245,7	106	250,0	
108	43,8	108	<b>58,5</b>	
109	139,2	109	<b>163,8</b>	

110	123,4	110	<b><u>147,2</u></b>	
111	20,4	111	21,4	
		112	<b><u>12,8</u></b>	
		115	<b><u>15,6</u></b>	
117	12,0	117	13,9	
121	23,0	121	22,6	
123	16,2	123	19,4	
124	20,4	124	19,2	
125	17,8	125	20,9	None
126	12,4	126	16,9	
127	19,2	127	29,8	
128	17,5	128	23,2	
129	42,2	129	46,5	
130	107,4	130	<b><u>123,2</u></b>	None
131	76,7	131	71,9	None
132	55,2	132	<b><u>140,4</u></b>	None
133	159,0	133	<b><u>193,7</u></b>	
134	19,8	134	30,0	None
135	76,9	135	<b><u>89,8</u></b>	
136	61,8	136	55,2	
137	18,7	137	12,5	
138	25,8	138	<b><u>38,3</u></b>	
139	22,7	139	24,0	
141	15,8	141	15,7	
		143	<b><u>12,2</u></b>	
144	12,0	144	11,5	
		146	<b><u>11,7</u></b>	
147	13,5	147	14,5	
		148	<b><u>13,7</u></b>	
150	11,4	150	12,8	
		153	<b><u>11,4</u></b>	
155	13,5	155	13,9	
157	14,5	157	13,8	
161	13,6	161	14,0	
162	13,4	162	16,1	
163	16,8	163	13,3	
165	18,8	165	18,2	
166	31,3	166	30,8	None
168	<b><u>23,6</u></b>			
		169	<b><u>37,4</u></b>	
179	15,9	179	22,4	None
		180	<b><u>12,2</u></b>	None
181	15,5	181	16,4	None
182	16,4	182	17,4	

184	12,7	184	14,4	
		188	<b>12,0</b>	
191	12,1	191	14,1	
195	11,7	195	14,6	
196	13,6	196	15,4	
199	20,4	199	20,4	
200	14,0	200	15,6	
204	12,0	204	12,3	
205	13,9	205	14,5	
		208	<b>11,4</b>	
210	<b>12,8</b>			
211	21,7	211	19,7	
214	19,2	214	19,2	None
215	51,5	215	42,2	
216	64,5	216	70,8	None
217	12,9	217	15,2	None
		218	<b>11,3</b>	
220	15,0	220	15,0	None
		221	<b>11,3</b>	
223	16,8	223	18,6	
		225	<b>11,0</b>	
230	12,1	230	15,0	
232	11,2	232	11,9	None
233	14,7	233	15,7	None
		235	<b>12,8</b>	None
236	33,9	236	31,4	None
238	<b>41,3</b>	238	23,5	
242	<b>15,5</b>			
244	18,8	244	19,4	None
246	27,5	246	26,5	
248	11,6	248	11,4	
249	12,1	249	12,8	
250	11,4	250	11,4	None
257	11,8	257	12,2	
264	<b>11,7</b>			

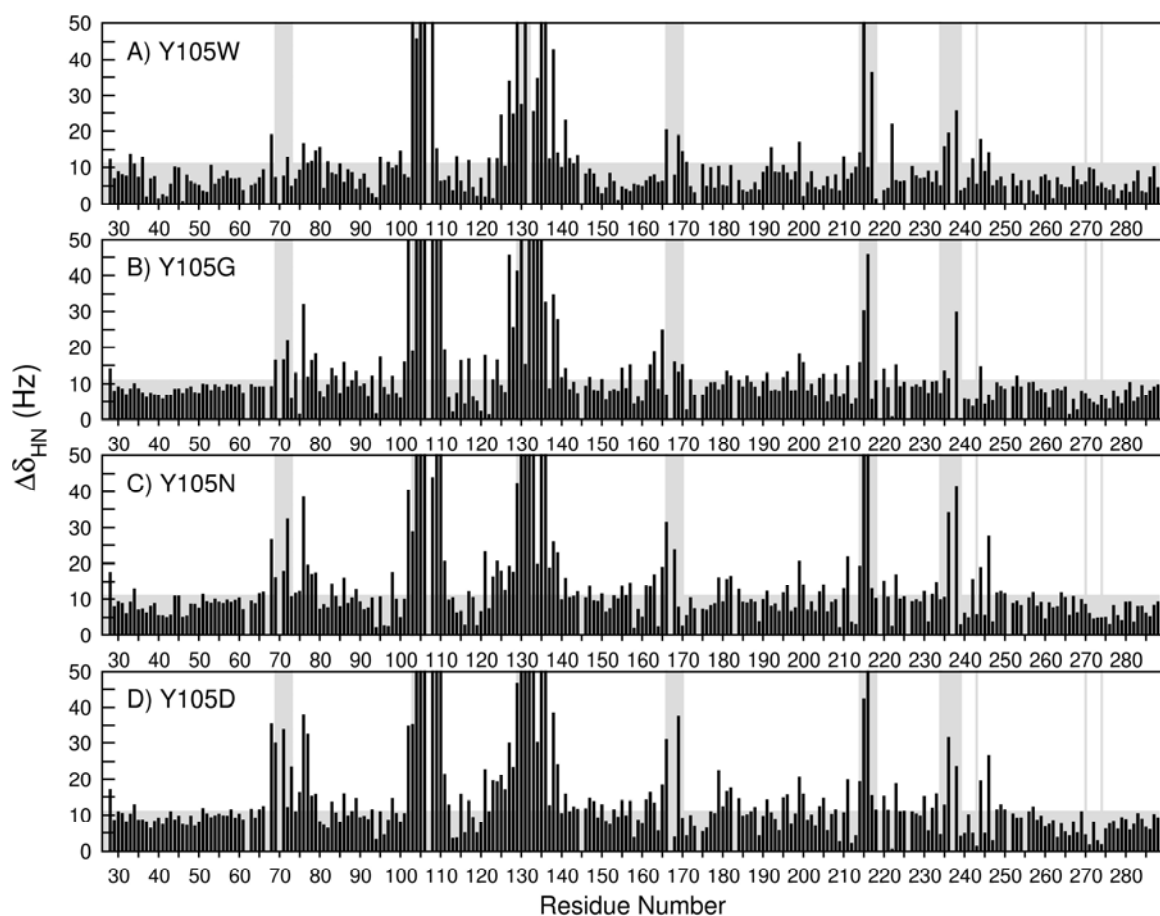


**Figure 4.2 (Alternate Version).** Sequence mapping of  $^1\text{H}$ - $^{15}\text{N}$  backbone chemical shift differences ( $\Delta\delta_{\text{HN}}$ ) (Hz) calculated between wild-type TEM-1 and mutants Y105W, Y105G, Y105N and Y105D. Residues that define active-site walls of TEM-1 are highlighted as grey vertical bars (see Figure 4.3). Grey horizontal bars represent the limit that separates background noise from significant chemical shift variations, and is defined as twice the digital resolution of the  $^{15}\text{N}$ -HSQC spectra (11 Hz).